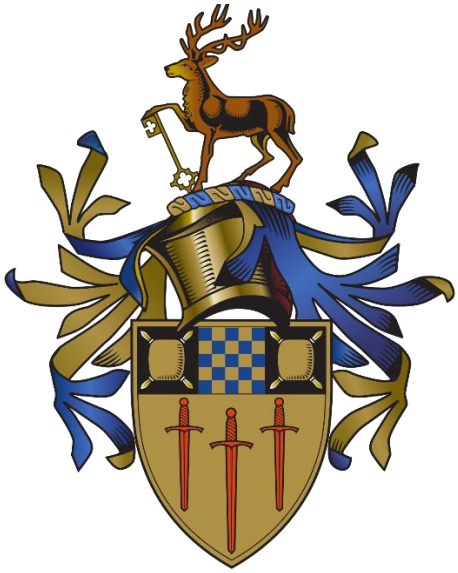

THE CHEMICAL SEPARATION OF TERBIUM FOR APPLICATIONS IN NUCLEAR MEDICINE

A thesis in fulfilment of the requirements of the University of Surrey
for the degree of Doctor of Philosophy

BEN WEBSTER

School of Chemistry and Chemical Engineering
Faculty of Engineering and Physical Sciences
University of Surrey, Guildford, GU2 7XH

Supervisors

Professor David Read (University of Surrey)
Dr Peter Ivanov (NPL)

AUGUST 2021

“I ate stones as a child”

Ben Webster *reflecting on how far he had come.*

Declaration of Originality

This thesis and the work to which it refers are the results of my own efforts. Any ideas, data, images or text resulting from the work of others (whether published or unpublished) are fully identified as such within the work and attributed to their originator in the text, bibliography or in footnotes. This thesis has not been submitted in whole or in part for any other academic degree or professional qualification. I agree that the University has the right to submit my work to the plagiarism detection service TurnitinUK for originality checks.

Ben Webster
University of Surrey
20 August 2021

Abstract

This research aimed to develop robust and thorough chemical separation procedures to support the development of novel diagnostic, therapeutic and/or theranostic nuclear medicine using several terbium isotopes, ^{149}Tb, ^{152}Tb, ^{155}Tb and ^{161}Tb. Little explored extraction chromatography resins were investigated for the separation of these terbium isotopes from other lanthanide impurities which are present after their production via various routes. Stable element standards and ICP-QQQ-MS analysis were used throughout method development experiments and, when possible, the developed methods were validated using radioactive terbium samples produced via the associated production route.

In a mass-separated, proton-induced spallation source of ^{155}Tb (t½ = 5.32 d), a significant polyatomic ^{139}Ce^{16}O impurity (t½ = 136.7 d) remained. Selective oxidation of cerium using $NaBrO_3$ was investigated and was shown to markedly change the chromatographic behaviour of cerium whilst leaving terbium unaffected. Separation of Tb(III) from Ce(IV) was studied separately on three extraction chromatography resins and an anion exchange resin. Through a series of batch separation and column separation experiments, UTEVA extraction chromatography resin (*Triskem International*) was shown to provide the best separation out of the four studied resins. A column-based UTEVA method was developed and formed an essential part of a larger processing procedure that was used to purify ^{155}Tb sources that are produced by proton-induced spallation. This procedure was shown to be capable of isolating high purity ^{155}Tb (>99% radiological purity) and subsequently facilitated SPECT imaging studies, nuclear data measurements and a world-first primary standardisation of ^{155}Tb.

Further study identified that this UTEVA method was not capable of isolating terbium from other lanthanide impurities present in mass-separated, proton induced spallation sources of ^{149}Tb, ^{152}Tb and ^{155}Tb. The presence of these other long-lived or stable impurities would reduce the specific activity of a radiopharmaceutical. This necessitated investigation into an alternative method which was capable of isolating terbium from all other lanthanide elements.

A series of batch and column separation experiments led to the development of a semi-automated, three-step column separation method which utilised the LN extraction chromatography resin (*Triskem International*). The method was capable of isolating terbium from trace quantities of all other lanthanide impurities. An ICP-QQQ-MS method, which utilised two quadrupole mass filters and an O_2 reaction cell, was used throughout the method

development process to ensure accurate percentage recovery and purity information could be derived by removing tailing and polyatomic measurement interferences. Using the developed LN resin method, high purity terbium fractions (>90% terbium recovery, >99% terbium purity) could be isolated in <120 minutes using a 200×7 mm LN resin column and a 0.5 mL/min mobile phase flowrate. This method results in a separation of comparable quality to the commonly used α-HIBA, cation exchange methods. Initial studies using a smaller LN resin column (50×5 mm) reduced the separation time significantly with minimal impact on the terbium recovery and purity (<15 mins). Use of these smaller columns should be considered for the shorter-lived terbium isotopes, ^{149}Tb (t½ = 4.12 h) and ^{152}Tb (t½ = 17.5 h) to reduce losses of the isotope due to radioactive decay.

The separation of trace quantities of terbium (µg) from bulk quantities of gadolinium and europium (≤100 mg) was then studied separately using the same stepwise LN resin method (200×7 mm column) to assess whether the method was also suitable for processing terbium produced in cyclotron or nuclear reactor facilities. The capacity of the resin was derived using a novel batch separation method (6.89 mg – 12.48mg Gd/mL of LN resin) and was shown to be a limiting factor for bulk-trace lanthanide separations. In all cases high terbium recovery (>80%) and significant removal of the bulk element was achieved (decontamination factor ~10^4), with separation quality decreasing at higher bulk element concentration.

The LN resin method was subsequently used as the third stage in a three-part separation for processing ^{155}Tb produced by the irradiation of gadolinium targets with protons at the ARRONAX cyclotron facility and performed in a comparable manner to the stable element studies (i.e., >80% ^{155}Tb recovery). The final ^{155}Tb preparations were of a high radionuclidic purity (<0.05 % ^{156}Tb impurity) and were successfully used in radiolabelling studies (>99% radiolabelling yield), SPECT imaging studies, and nuclear data measurements, all of which were conducted by other researchers.

This work has laid the foundations for using extraction chromatography resins for isolating radioactive terbium for applications in nuclear medicine. The developed LN resin method not only provided high quality lanthanide separation, but also showed itself to be an easier-to-use alternative to the commonly used cation exchange method.

Contents

Declaration of Originality ii

Abstract iii

List of Figures ix

List of Tables xii

List of Abbreviations xiv

Acknowledgements xvi

Chapter 1. Introduction 1

1.1 Rationale 2

1.2 Introduction to nuclear medicine 4

1.2.1 Radioactive isotopes 4

1.2.2 The use of radioactive isotopes in medicine 9

1.3 Production of radionuclides 17

1.3.1 Isotope production methods 18

1.3.2 Mass separation technology 23

1.3.3 Production routes for terbium isotopes 25

1.4 Chemistry of the lanthanide elements 27

1.4.1 Chromatography of the lanthanides 28

1.4.2 Chemical isolation of terbium 34

1.5 Requirements for the metrological and (pre)-clinical use of radioactive terbium sources 38

1.5.1 Determination of metrological information for radioactive isotopes 38

1.5.2 Purity requirements for radiolabelling and (pre)-clinical studies 41

1.6 Aims and objectives 43

Chapter 2. Materials and Methods 44

2.1 Isotope production 45

2.1.1 Proton-induced spallation at CERN-ISOLDE/MEDICIS and mass separation 45

2.1.2 Cyclotron production of terbium isotopes from lanthanide targets 47

2.2 Chemical purification methodology 51

2.2.1 Batch studies 51

2.2.2 Column studies 53

2.3 Measurement methodology 57

2.3.1 Inductively coupled plasma mass spectrometry overview 57

2.3.2 Gamma-ray spectrometry 62

2.4 Materials and reagents 64

Chapter 3. Removal of radioactive cerium impurities from ^{155}Tb sources produced by proton-induced spallation 66

3.1 Impurities present in ^{155}Tb sources produced by proton-induced spallation at CERN 67

3.2 Chemical separation of terbium from cerium impurities 68

3.2.1 Method development 68

3.2.3 Method validation 74

3.3 Discussion and summary 75

Chapter 4. Separation of terbium from trace stable and radioactive lanthanides 77

4.1 Production information and requirements for chemical separation 78

4.1.1 Characteristics of mass-separated terbium sources produced by proton-induced spallation at CERN-ISOLDE/MEDICIS 78

4.1.2 Requirement for the removal of stable impurities 79

4.1.3 Reasons for the chosen separation approach 80

4.2 Method development 81

4.2.1 Materials and reagents 81

4.2.2 Interference free measurement of trace lanthanides using ICP-QQQ-MS 82

4.2.3 Suitability of the UTEVA method for the separation of neighbouring lanthanides 83

4.2.4 Investigation of LN resin for the isolation of terbium from lanthanide impurities 84

4.3 Method validation and optimisation 91

4.3.1 Separation and measurement of 'simulant ^{xxx}Tb' solutions 91

4.3.2 Findings and areas for further optimisation 94

4.4 Fit-for purpose method and conclusions 100

Chapter 5. Isolation of radioactive terbium from bulk lanthanide target material 102

5.1 Alternative terbium production routes 103

5.2 Reagents and measurement methodology 105

5.2.1 Materials and reagents 105

5.2.2 Interference reduced measurement of trace-bulk lanthanide pairs using ICP-QQQ-MS 105

5.2.3 Measurement of radioactive isotopes using gamma-ray spectrometry 106

5.3 Chemical separation of terbium from bulk quantities of gadolinium 108

5.3.1 Experimental working capacity of LN resin 108

5.3.2 Assessment of column performance for the isolation of terbium from an increasing gadolinium excess 109

5.3.3 Behaviour of zinc on LN resin 111

5.3.4 Isolating mass-separated ^{155}Tb from remaining gadolinium target material 112

5.4 Chemical separation of terbium from bulk quantities of europium 117

5.5 Discussion and summary of results 119

5.5.1 Derivation of LN resin's working capacity 119

5.5.2 Suitability of the LN resin separation method 121

5.5.3 Assessment of the ICP-QQQ-MS measurement approach 122

5.6 Chapter conclusion 125

Chapter 6. Summary and concluding remarks 126

References 130

Appendix A – ICP-MS tune parameters and pass criteria 147

Appendix B – Data to accompany Figure 3.1 148

Appendix C – Data to accompany Figure 3.2 150

Appendix D – Data to accompany Figure 3.4 154

Appendix E – Data to accompany Figure 4.3 and Figure 4.4 162

Appendix F – Data to accompany Figure 4.11 165

Appendix G – Data to accompany 'simulant ^{xxx}Tb' separations 168

Appendix H – Data to accompany Table 4.5 174

Appendix I – Data to accompany Figure 4.16 177

Appendix J – Data to accompany Figure 5.1 178

Appendix K – Data to accompany Table 5.3 179

Appendix L – Data to accompany Table 5.8 191

Appendix M – ICP-QQQ-MS measurement interference at m/z 175 caused by high gadolinium concentration 199

Appendix N – Webster et.al. (2018) 200

Appendix O – Webster *et al.* (2019) 201

Appendix P – Russell *et al.* (2020) 210

Appendix Q – Trinder *et al.* (2020) 216

Appendix R – Duchemin *et al.* (2021) 222

List of Figures

Figure 1.1 - A graphical illustration of radioactive half-life. 4

Figure 1.2 - Illustration of the changes in number of protons (Z) and number of neutrons (N) as a result of the most common types of radioactive decay[37] 6

Figure 1.3 - An illustration of the competitive processes of x-ray emission and Auger electron emission which occurs after an electron vacancy is filled. 7

Figure 1.4 - The distribution of fission products and their fission yields from the fission reaction of ^{235}U induced by thermal neutrons[39] 7

Figure 1.5 - The decay scheme for ^{40}K; showing the possible decay routes and their branching ratios[6]. 8

Figure 1.6 - Comparison of a PET/CT scan and a SPECT/CT using International Electrotechnical Commission (IEC) standard body phantoms containing ^{18}F and ^{99m}Tc respectively (Taken from Bailey and Willowson)[43]. 9

Figure 1.7 - An illustration of positron-electron annihilation and the production of the resultant two characteristic gamma rays (E_γ = 511 keV). 12

*Figure 1.8 - Molecular structure of **(a)** [^{18}F]-FDG and **(b)** the PSMA-617 targeting molecule. 14*

Figure 1.9 - Fluka simulation[85] showing the incoming proton beam on an ISOLDE target (3.5 g/cm^2 UCx for the purpose of the simulation) and intercepting the MEDICIS target downstream (Courtesy of T. Stora, CERN)[86] 19

*Figure 1.10 - The internal view of the MC40 cyclotron (**left**) and the target set up on the beam line used for irradiations (**right**) at the Positron Imaging Centre at the University of Birmingham, UK (curtesy of R. Trinder, University of Birmingham) 20*

Figure 1.11 – A simplified schematic of the CERN-MEDICIS off-line mass separator. Ion beams are denoted in red. MELISSA ionisation laser is denoted in blue (Adapted from Gadelshin et al.)[109]. A/q = mass-to-charge ratio. 24

Figure 1.12 - Graphical representation of the trend of atomic and ionic radii for the lanthanide elements[122]. 28

Figure 1.13 - Comparison of the variations in the composition of mobile phase (%A) for different elution methods. These are often used in combination. 30

Figure 1.14 - Diagram showing an example of the macroporous cross-linking structure of a strong acid cation exchange resin and its sulphonic acid exchange sites[130]. 32

Figure 1.15 - Chemical structure of alpha-hydroxyisobutyric acid (α-HIBA). 32

Figure 1.16 - Illustration of an extraction chromatography bead. Adapted with reference to Horwitz (1998)[138]. 33

Figure 1.17 - The stationary phase extractants which are present in each of the three extraction chromatography resins used for lanthanide separations (LN, LN2 and LN3)[142]. 34

Figure 1.18 - A simplified measurement traceability hierarchy, illustrating the unbroken chain of measurements or calibrations required to ensure that a measurement it traceable to the International System of Units (SI). .. 40

*Figure 2.1 – (**top**) Screenshot taken with the beam scanner, located before the implantation chamber. Beams at A/q = 154,155,156 are seen (153, 157 partly visible). The collected beam is centred on A/q = 155, while isotopes present at other masses are physically removed from the implantation using mechanical slits located ahead of*

*the foil. The horizontal scale is in mm. (**bottom**) Two zinc-coated gold foils in the collection chamber seen from the rear[86]..... 46*
*Figure 2.2 - A simplified schematic of the target arrangement used at the ARRONAX facility (**left**) and an image of the deconstructed target prior to irradiation (**right**). (Figure courtesy of N. Michel et al.)..... 48*
*Figure 2.3 - A target holder used for the irradiation of gadolinium oxide powder with dimensions annotated (**left**). The preparation of a 1 g Gd_2O_3 target sealed with a thin titanium foil (**middle** and **right**) 50*
Figure 2.4 - positioning of a europium metal foil within the target holder (Image courtesy of Rebeckah Trinder, University of Birmingham)..... 50
Figure 2.5 - The trend of distribution coefficients of several actinide elements shown on UTEVA resin at varying acid concentrations[162]..... 52
Figure 2.6 - The process of packing a glass Econo-Column® Column with a chosen chromatography resin..... 54
Figure 2.7 - A schematic of the Agilent 8800 ICP-QQQ-MS. Arrows denote the direction of sample through the instrument when both quadrupoles and the collision/reaction cell is used (Agilent ICP-MS MassHunter Workstation software v. 3.7, Agilent Technologies)..... 58
Figure 2.8 - The tailing of a signal at 165 m/z, from a 10 µg/mL Ho solution, into the neighbouring masses (164-166 m/z) measured in SQ mode. The formation of a holmium hydride polyatomic (HoH+) could also be contributing to the signal at 166 m/z. 60
Figure 2.9 - The interference-free measurement of ^{166}Er in the presence of a bulk amount of ^{165}Ho using MS/MS mode with O_2 reaction gas[175,176]. 62
Figure 2.10 – the gamma-ray spectrometry set-up at the National Physical Laboratory showing the HPGe gamma-ray detector, sample holder, mounting plates, lead shielding and graded copper/cadmium lining. Sources measured for this work were placed in the mounting plate on the left, ~15cm from the detector. 63
Figure 3.1 - Distribution coefficients (K_d) of Tb(III), Ce(III) and Ce(IV) on UTEVA extraction chromatography resin across a range of HNO_3 concentrations. (Appendix B) 69
*Figure 3.2 - Distribution coefficients (K_d) of Tb (III) and Ce(IV) across a range of HNO_3 concentrations on **(a)** AGI ion exchange resin, **(b)** TEVA resin, **(c)** TK100 resin, **(d)** UTEVA resin. (Appendix C)..... 70*
*Figure 3.3 - Kinetics of the **(a)** adsorption of Tb (III) and Ce (IV) to UTEVA resin, and of the **(b)** oxidation of cerium in a 0.1 M $NaBrO_3$/10 M HNO_3 solution. Measured as the change in distribution coefficient (K_d) as a function of time. 71*
*Figure 3.4 - Elution profiles showing the separation of Tb from Ce impurities on a pre-conditioned 2 mL UTEVA resin cartridge **(left)** and pre-conditioned 2 mL TEVA resin cartridge **(right)**. (Flow rate ~ 0.3 mL/min, n=3)..... 72*
Figure 3.5 - Optimised method for the radiochemical separation and preparation of high radionuclidic purity ^{155}Tb. 73
Figure 3.6 - Gamma ray spectra of the ^{155}Tb source preparation before (grey) and after radiochemical separation (red) (reference time: 2017-09-29 12:00 UTC). 75
*Figure 4.1 - The chemical structure of two aminopolycarboxylic acid bifunctional chelators which can incorporate lanthanides (Ln^{3+}); (**left**) 1,4,7,10-Tetraazacyclododecane-1,4,7,10-tetraacetic acid (DOTA); (**right**) diethylenetriaminepentaacetic acid (DTPA)[124]. 80*

Figure 4.2 - Attempted separation of 'simulant ^{152}Tb' mixture using the UTEVA method (Chapter 3). 84
Figure 4.3 - Distubution coefficient (K_d) variation with nitric acid conentration of europium, gadolinium, terbium and dysprosium. 85
Figure 4.4 - Distribution coefficient (K_d) variation with nitric acid conentration of gadolinium, terbium and dysprosium – zoomed in to highlight conditions which were used in initial column-based separation studies. 86
Figure 4.5 - The apparatus set-up used for column-based separations. 86
Figure 4.6 - Initial column chromatography trial using a 200 × 7 mm glass Econo-Column® packed with LN resin (50-100 µm). Elution steps and conditions are summarised in the table (Flow rate ~1.0 mL/min). 88
Figure 4.7 - Column chromatography study using a 200 × 7 mm glass Econo-Column® packed with LN resin (50-100 µm). Differences in elution conditions are highlighted. (Flow rate ~1.0 mL/min) 88
Figure 4.8 - Column chromatography study using a 200 × 7 mm glass Econo-Column® packed with LN resin (50-100 µm). Changes to the wash conditions are highlighted. (Flow rate ~1.0 mL/min) 89
Figure 4.9 - Column chromatography study using a 200 × 7 mm glass Econo-Column® packed with LN resin (50-100 µm). Changes to the pre-conditioning, loading and elution conditions are highlighted. (Flow rate ~1.0 mL/min) 89
Figure 4.10 - Column chromatography study using a 200 × 7 mm glass Econo-Column® packed with LN resin (50-100 µm). Changes to the elution conditions are highlighted. (Flow rate ~1.0 mL/min). 90
*Figure 4.11 - Variation of the elution profiles of separations conducted at different mobile phase flow rates: ~1.0 mL/min **(left)** and ~0.5 mL/min **(right)**. Separations were conducted under identical chemical conditions (see also Appendix F).* 90
Figure 4.12 - Elution profile of the separation of a 'simulant ^{149}Tb' solution, containing Cs, Ba, Nd, Sm, Eu, Gd, Tb (1 mL fractions). 92
Figure 4.13 - Elution profile of the separation of a 'simulant ^{152}Tb' solution, containing Cs, Ba, Ce, Sm, Eu, Gd, Tb, Dy (1 mL fractions). 93
Figure 4.14 - Elution profile of the separation of a 'simulant ^{155}Tb' solution, containing La, Ce, Pr, Eu, Gd, Tb, Dy (1 mL fractions). 94
Figure 4.15 - The behaviour of cerium in absence of redox agents and in the presence of a reducing agent (KI) and an oxidising agent ($NaBrO_3$). The terbium elution in the absence of redox agents has been included here for comparison. 98
Figure 4.16 - The profile showing the elution behaviour of components of the 'simulant ^{155}Tb' solution on a shorter LN resin column and using smaller quantities of nitric acid (Table 4.6). 99
*Figure 5.1. - The variation of K_d with increasing excess of gadolinium (Gd, n=3, standard deviation) **(left)**. Physical change observed between samples suggesting that the working capacity had been exceeded. Left tube = 7.44 mg ± 0.54 mg Gd/mLresin, right tube = 11.35 mg ± 1.14 mg Gd/mL resin **(right)**.* 109
Figure 5.2 – Distribution coefficient (K_d) variation of zinc on LN resin across a nitric acid concentration range (50 – 100 µm particle size). 111

List of Tables

Table 1.1 - Commonly used and novel SPECT radionuclides[27,41]. [a] currently under pre-clinical assessment..... 11

Table 1.2 - Commonly used and novel PET tracers[27,41]. [a] currently under clinical assessment. 12

Table 1.3 - Commonly used and novel therapeutic radionuclides[27,41,60,61]. [a] currently under pre-clinical assessment. [b] currently under clinical assessment. 13

Table 1.4 - Commonly used and novel single entity theranostic radionuclides[27,41,60,61]. 15

Table 1.5 - The four terbium isotopes with clinical potential, their applications and radiopharmaceuticals synthesised and used in proof-of-concept and/or pre-clinical studies[73]. 16

Table 1.6 - Main classes of neutrons involved with or produced in nuclear reactions. 22

Table 1.7 - Studied production routes of the terbium isotopes with potential applications in nuclear medicine. 26

Table 2.1 - Table summarising the characteristics of the ion beams available at ARRONAX. Taken and adapted from Haddad et al. (2008)[159]. 47

Table 2.2 – A summary of the achievable energy ranges of the ion beams available at the University of Birmingham. Taken and adapted from the University of Birmingham's 'MC40 Cyclotron Facility' webpage (date accessed 21.04.2021)[92,117]. 49

Table 2.3 - The standard SQ mode operating parameters for ICP-MS measurement. 62

Table 2.4 - A summary of the chromatography resins used. 65

Table 3.1 - Radioisotope composition of a ^{155}Tb source received from CERN-ISOLDE before and after chemical separation (reference time: 2017-09-29 12:00 UTC). 74

*Table 4.1 - Potential impurities found in ^{149}Tb, ^{152}Tb and ^{155}Tb sources produced at by proton-induced spallation after mass separation[73,182]. (*radionuclides) 79*

Table 4.2 - Composition of 'simulant ^{149,152,155}Tb' solutions used to chemically mimic mass-separated, proton induced spallation produced, terbium sources (100 ng/mL in nitric acid solutions)[73,182]. 81

Table 4.3 – The Agilent 8800 series ICP-QQQ-MS operating parameters used for the interference minimised measurement of lanthanide element mixtures throughout the method development stages of Chapter 4 and Chapter 5. 83

Table 4.4 - The developed separation method and parameters for the isolation of terbium from lanthanide impurities 91

Table 4.5 – A summary of the terbium recovery and purity information achieved using the LN resin separation method developed in this study (Table 4.4). (see also Appendix H) 95

Table 4.6 - The downscaled separation method which used smaller nitric acid volumes and a smaller column to encourage faster isolation of terbium from trace lanthanide impurities (Figure 4.16) 99

*Table 4.7 - The proportion of terbium isotope that would be lost during chemical separation due to radioactive decay. A summary and comparison of two column sizes and associated separation times. *this assumes 100% chemical and therefore does not account for chemical losses during the separation. 100*

Table 5.1 - Established and proposed routes for the production of selected terbium isotopes from lanthanide target materials. The use of ^{nat}Gd targets with subsequent mass-separation is often a more obtainable route of production. 103

Table 5.2 - Preliminary gamma-ray emission intensities of ^{155}Tb determined at NPL (yet to be published) used to determine ^{155}Tb activity and purity of samples measured at NPL. 107

Table 5.3. - Summary of the achievable separation of trace quantities of terbium (Tb, 1 µg) from bulk quantities of Gd_2O_3 in 0.75 M HNO_3 solutions. Information related to fractions 41-50 unless otherwise stated. Decontamination factor is the degree to which the bulk Gd_2O_3 contaminant is removed. Reported uncertainties are the standard deviation between repeats (Appendix K). 110

Table 5.4 – Summary of the beam intensity and the ^{155}Tb activity at the 'end of bombardment' (EOB) in each source shipped to NPL..... 112

Table 5.5 – The first chemical separation step used at ARRONAX to process ^{155}Tb sources ahead of isotope separation at CERN-MEDICIS. 113

Table 5.6 - The second chemical separation step used at ARRONAX to process ^{155}Tb sources ahead of isotope separation at CERN-MEDICIS. 113

Table 5.7 – Characteristics of ^{155}Tb sources sent to, and chemically purified at NPL. $f_{Tb\text{-}156} = A_{Tb\text{-}156}/A_{Tb\text{-}155}$ post separation. N/A = not applicable. 116

Table 5.8. - Summary of the achievable separation of trace quantities of terbium (Tb, 1 µg) from bulk quantities of europium in 0.75 M HNO_3 solutions (see also Appendix L). Information related to fractions 41-50 unless otherwise stated. Decontamination factor is the degree to which the bulk europium contaminant is removed. 119

List of Abbreviations

ALARP – As Low as Reasonably Practicable

ARRONAX – Accelerator for Research in Radiochemistry and Oncology in Nantes Atlantique

BGO – Bismuth Germanate

CERN - European Organization for Nuclear Research

CPS – Counts Per Second (instrument response)

CT – Computed Tomography

CTN – Technological and Nuclear Campus, Portugal

DDEP – Decay Data Evaluation Project

DF – Decontamination Factor

DI – Deionised

DOTA – 1,4,7,10-Tetraazacyclododecane-1,4,7,10-tetraacetic acid

DOTAGA - 2,2′,2”-(10-(2,6-dioxotetrahydro-2H-pyran-3-yl)-1,4,7,10-tetraazacyclododecane-1,4,7-triyl)triacetic acid.

DTPA – 2-[Bis[2-[bis(carboxymethyl)amino]ethyl]amino]acetic acid

EC – Electron Capture

EDTA – Ethylenediaminetetraacetic acid

ENSDF – Evaluated Nuclear Structure Data File

EOB – End of Bombardment

FWHM - Full Width at Half Maximum

GMP – Good Manufacturing Practice

HAS – Human Serum Albumin

HDEHP - Di-(2-ethylhexyl)phosphoric acid

α-HIBA - alpha-hydroxyisobutyric acid

HPGe – High Purity Germanium

HPLC – High Performance Liquid Chromatography

IC – Internal Conversion

ICP – Inductively Coupled Plasma

IEC – International Electrotechnical Commission

ISO – International Organization for Standardization

ISOL- On-Line Isotope Separator

ISOLDE – Isotope Separator On-Line Device

iTLC – instant Thin Layer Chromatography

KU – Katholieke Universiteit, Leuven, Belgium

LET – Linear Energy Transfer

LN – referring to LN resin, a HDEHP based extraction chromatography resin
LYSO – Lutetium-yttrium oxyorthosilicate
mAb – monoclonal antibody
m/q – mass to charge ratio (relating to mass separation)
m/z – mass to charge ratio (relating to mass spectrometry)
MEDICIS – Medical Isotopes Collected from ISOLDE
MELISSA – MEDICIS Laser Ion Source for Separator Assembly
MIBG – metaiodobenzylguanidine
MS – Mass Spectrometer
NMI – National Measurement Institute
NPL – National Physical Laboratory, UK
PET – Positron Emission Tomography
ppb – parts per billion (1 ppb = 1 ng/mL)
ppm – parts per million (1 ppm = 1 µg/mL)
PSI – Paul Scherrer Institute, Switzerland
QQQ – triple quadrupole (pertaining to ICP-QQQ-MS)
RF – Radio Frequency
rpm – revolutions per minute
RSD – Relative Standard Deviation
S/C – Spray Chamber
SEC – Size Exclusion Chromatography
SF – Separation Factor
SPECT – Single Photon Emission Computed Tomography
SQ – Single Quadrupole
UTEVA – Uranium and Tetravalent Actinides
w/w – weight-to-weight ratio (%)

Acknowledgements

There are so many who have supported me in this research endeavour who need a mention of thanks. None should underestimate the value of having people around you who are patient, supportive and willing to offer a listening ear. Without supportive and collaborative working, PhD research doesn't have to be isolating. I have many to thank for their help, assistance, their encouraging and kind words, and their willingness to share their technical expertise. I am privileged to have had many around me that fit some or all of these descriptions.

Firstly, and most of all, I'd like to thank my wife, Sydney, for her faithful friendship, patience, encouragement and willingness to support me though whatever ups and downs that came my way through this PhD journey. I love you, Sydney. Without you, and all that you have done for me, I would not have completed this PhD.

I'd like to thank my supervisors, Professor David Read and Dr Peter Ivanov for their guidance, expertise, time and eagerness to give constructive feedback and support throughout the entirety of my PhD. I'd also like to give a special mention to Dr Ben Russell, who also gave a lot of his time and valuable feedback along the way and supported me with much of my experimental work. Thank you all for pushing me onwards and upwards.

I'd also like to especially thank Emma Braysher, my 'PhD buddy', who I am eternally grateful for. Thank you for your friendship, kind words and support. I would have struggled a lot more through the most difficult stages of this PhD if it weren't for your friendship.

I'd also like to thank, in particular, Sean Collins and Kelley Ferreira from NPL, Steffen Happel from Triskem International, Thierry Stora and Charlotte Duchemin from CERN, Ross Allen, Rebeckah Trinder and Tzany Kokalova Wheldon from the University of Birmingham, and Nathalie Michel from Arronax for their willingness to share resources and information that proved essential to this work. It made my life less complicated when writing papers, preparing presentations and writing this dissertation, so thank you all. You have all set a brilliant example of how collaborative work should be done.

Thank you to those who work, or have worked, in the PGI. You have encouraged me to develop in ways I wouldn't have done in my PhD. You have offered professional and personal support along the way which was above and beyond what you are paid to do. Leah Chapman, Debbie Meikle, Linden Fradet, Lauren Livingstone and Richard Burguete, thank you for all you do. I appreciate you all. It has been a pleasure learning from you, working with you and getting to know you.

I would also like to thank some of the many others who stuck with me and supported me along the way. Those who offered a listening ear, words of encouragement and faithful friendship: Ruth Cheah, Rebekah Cheah, Mike Jolley, Sam Jones, Theo Onumah, Dan Taylor.

And finally, but far from the least, I'd like to thank my family for being always so loving, dependable and patient. For always welcoming me home, no matter my mood, for loving me through the difficulties and for celebrating with me in the triumphs. Mum, Dad, Sam, I love you.

PAGE INTENTIONALLY LEFT BLANK.

Chapter 1. Introduction

1.1 Rationale

Nuclear medicine is a topic that has attracted interest ever since the discovery of radioactivity and radioactive elements in the late 19th century by Henri Becquerel. and Pierre and Marie Curie. The potential of using radiation and radioactive elements in therapeutic or diagnostic medicine was recognised as early as the 1890s and has developed over the past century into an essential medical tool, used as a standalone procedure, or to complement other medical procedures[1]. This can be achieved by the application of diagnostic and/or therapeutic nuclear medicine.

The development of computed X-ray tomography (CT), single photon emission computed tomography (SPECT) and positron emission tomography (PET) has contributed to the improvement in the diagnostic capabilities of radionuclides[2]. Rapid and accurate diagnostic procedures allow the identification of diseased areas (e.g., malignant tumours) and thus, facilitates the application of suitable therapeutic procedures. Currently ^{99m}Tc, a metastable gamma emitting radionuclide, is the most commonly used diagnostic radionuclide worldwide. Complexation of diagnostic isotopes to targeting moieties, such as monoclonal antibodies or molecular substrates, allows accurate targeted imaging of diseased tissue[3–5]. Due to its relatively short half-life ($t_{½}$= 6.0 h)[6], ^{99m}Tc can be produced from its parent isotope ^{99}Mo ($t_{½}$= 66.0 h) in a technetium generator at the hospital that is conducting the medical imaging procedure[7]. The ^{99}Mo required for the generator is isolated from other fission products following the induction of a fission reaction in ^{235}U targets with neutrons within a nuclear reactor. The global supply of ^{99}Mo is dependent on a very small number of facilities and has been disrupted in the past and is vulnerable to future disruption[8,9]. To endure lapses in the supply of ^{99m}Tc, novel methods for production of alternative diagnostic radionuclides are required to meet the current and increasing demand for accurate diagnostic imaging. These alternative diagnostic radionuclides also augment ^{99m}Tc by having different functionalities[10] (e.g. isotopes which decay by routes which could have diagnostic and therapeutic uses).

Therapeutic nuclear medicine, on the other hand, utilises the linear energy transfer (LET) of decay particles (i.e., Auger electrons, conversion electrons, β^- or α particles) into surrounding tissue to damage or kill diseased cells[11]. Therapeutic isotopes, which emit these decay particles, can also be bound to targeting molecules which allows the treatment of diseased areas with minimal effect on healthy tissue. The application of radioiodine (^{131}I) in the treatment of thyroid

diseases has been studied since the early 1950s and is commonly used around the world[12]. A number of therapeutic medicines which use ^{89}Sr, ^{153}Sm and, more recently, ^{223}Ra have been developed for palliative treatment of bone metastases[13,14]. These, and other therapeutic radionuclides, have been used for the treatment of many benign and malignant disorders[15].

The efficient combinative use of diagnostic and therapeutic radionuclides in clinical practice is referred to as *theranostic* nuclear medicine and has received increased interest over recent years[16–21]. Theranostic nuclear medicine has the potential to facilitate personalised medicine.

Recent developments in the production and isolation of some novel radioactive isotopes have made them available for medical related studies and highlighted their suitability as diagnostic or therapeutic radionuclides. Among these are various isotopes of the lanthanide series including ^{149}Pm, ^{166}Ho, ^{177}Lu and four terbium isotopes (^{149}Tb, ^{152}Tb, ^{155}Tb and ^{161}Tb)[22,23]. The production, isolation, and complexation of these isotopes, amongst others, is at the forefront of current radiopharmaceutical research. Both ^{166}Ho and ^{177}Lu-based radiopharmaceuticals have reached clinical use in several countries[24,25]. Pre-clinical studies and some initial clinical studies have also been conducted for the aforementioned terbium isotopes[4,26–33]. There is, however, a need for the establishment of robust production and chemical purification processes if these isotopes are to undergo comprehensive clinical study and for them to reach routine clinical application.

The four terbium isotopes are of particular interest due to their theranostic potential[16,23,27,30]. Each terbium isotope has identical chemical properties and different decay properties, meaning that a combination of two or more of these terbium isotopes could be used to give a procedure with excellent therapeutic and diagnostic capability. However, due to the production of these isotopes having not been studied to any great degree, and with the challenges associated with their chemical purification, the production of high purity single terbium isotopes in a large enough activity for medical application is a challenging task.

The aim of this study was to develop robust, efficient and reproducible chemical separation methods to allow the production of high purity and high specific activity terbium sources to enable further investigation towards the clinical use of these four terbium isotopes - ^{149}Tb, ^{152}Tb, ^{155}Tb and ^{161}Tb.

1.2 Introduction to nuclear medicine

1.2.1 Radioactive isotopes

1.2.1.1 Fundamentals of radioactivity

Radioactive nuclei are inherently unstable. In order to reach a more stable energy state, the nuclei undergo spontaneous radioactive decay through the emission of particles and/or electromagnetic radiation. The probability of radiative decay of a particular nucleus is defined by the decay constant, λ (s^{-1}). The decay constant reflects the rate of decay and is defined as:

$$\boldsymbol{\lambda = \frac{ln2}{t_{½}}} \qquad \textbf{(1.1)}$$

where, $t_{½}$ is the half-life of a particular radionuclide in seconds; the time in which it takes for the activity of a radionuclide to reduce by half (Figure 1.1).

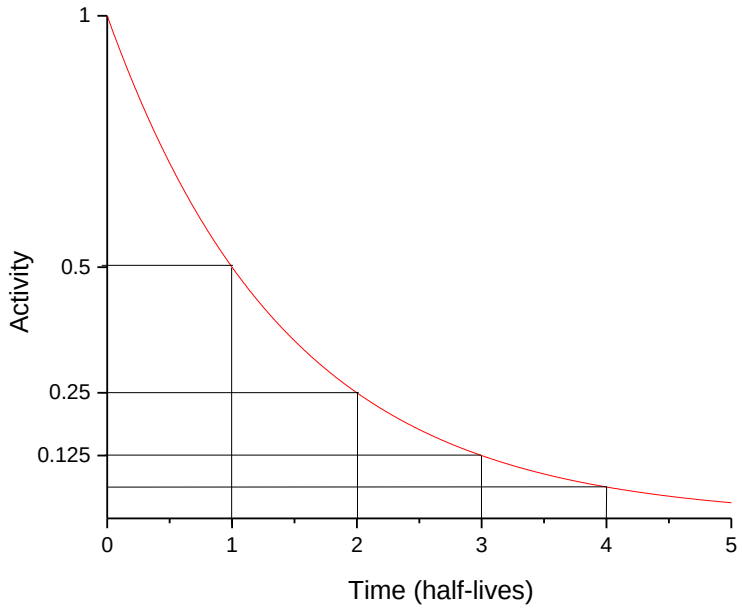

Figure 1.1 - A graphical illustration of radioactive half-life.

Common decay types are detailed below. In all cases, after radioactive decay, the resultant nucleus is closer to a physically stable state[34].

- *Alpha decay (α)* – involves the emission of a helium nucleus ($_2^4He^{2+}$) with kinetic energy (see example Equation 1.2). This type of decay typically occurs in nuclei which have an atomic number greater than 83; however, there are a few exceptions (e.g.,

^{149}Tb). Alpha particle energies are typically 4-8 MeV and have an inverse relationship to the parent nucleus' half-life (i.e., the shorter the half-life the higher the alpha energy)[35]. The energy of the emitted alpha particle is characteristic of the parent nucleus and can allow its identification. Alpha particles have a high linear energy transfer (LET), meaning that they deposit their energy in a very small volume of matter[36].

$$^{223}_{88}Ra \rightarrow {}^{219}_{86}Th + {}^{4}_{2}\alpha \qquad \textbf{(1.2)}$$

- *β^- (negatron) decay* – involves the emission of a nuclear electron with kinetic energy along with an antineutrino (see example Equation 1.3). The electron has a lower LET than an alpha particle and has a greater range on passing through matter. β^- decay occurs in neutron-rich nuclei. The total decay energy (E_{max}) released during the decay process is shared between the beta particle and the antineutrino.

$$^{131}_{53}I \rightarrow {}^{131}_{54}Xe + {}^{0}_{-1}\beta + \overline{\nu_e} \qquad \textbf{(1.3)}$$

- *β^+ (positron) decay* – involves the emission of a positron with kinetic energy along with a neutrino (see example Equation 1.4). After the positron loses enough of its kinetic energy, it annihilates with an electron, producing two 511 keV gamma rays which are emitted in opposite directions. β^+ decay occurs in neutron-poor nuclei.

$$^{18}_{9}F \rightarrow {}^{18}_{8}O + {}^{0}_{1}\beta + \nu_e \qquad \textbf{(1.4)}$$

- *Electron capture (EC)* – an decay route that competes with β^+ decay (see example Equation 1.5). The parent nucleus captures an inner orbital electron which combines with a proton, yielding a neutron. A neutrino and X-rays are also produced in this process. The daughter nucleus is the same as that which is produced as a result of β^+ decay from the same parent.

$$^{67}_{31}Ga + {}^{0}_{-1}e \rightarrow {}^{67}_{30}Zn + \nu_e \qquad \textbf{(1.5)}$$

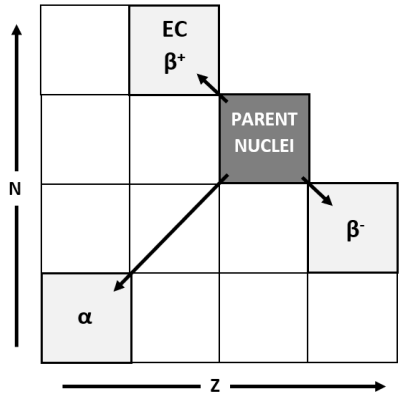

Figure 1.2 - Illustration of the changes in number of protons (Z) and number of neutrons (N) as a result of the most common types of radioactive decay[37].

- *Internal conversion (IC)* – the process competes with γ-ray emission during the de-excitation process within a nucleus. IC occurs when an orbital electron absorbs the energy released from an excited nucleus and is emitted from the atom with kinetic energy. In this process, vacancies in the electron shells are filled by outer shell electrons, which results in the emission of fluorescent X-rays (e.g., K_α) or an Auger electron. These X-rays are characteristic of the daughter nucleus (e.g., ^{109}Ag). As with β^- particles, IC electrons also dissipate energy and have therapeutic benefit if used *in-vivo*.

$$^{109}_{48}Cd \xrightarrow{EC(100\%)} {}^{109m}_{47}Ag \xrightarrow{IC\ (96\%),\ \gamma\ (4\%)} {}^{109}_{47}Ag \qquad \textbf{(1.6)}$$

- *Auger electrons* – as an electron from an outer shell fills an electron shell vacancy (caused by either electron capture or internal conversion), either an X-ray or an Auger electron can be emitted in order to release energy (Figure 1.3). As with β^- particles and IC electrons, Auger electrons also dissipate energy and have therapeutic benefit if used *in-vivo*.

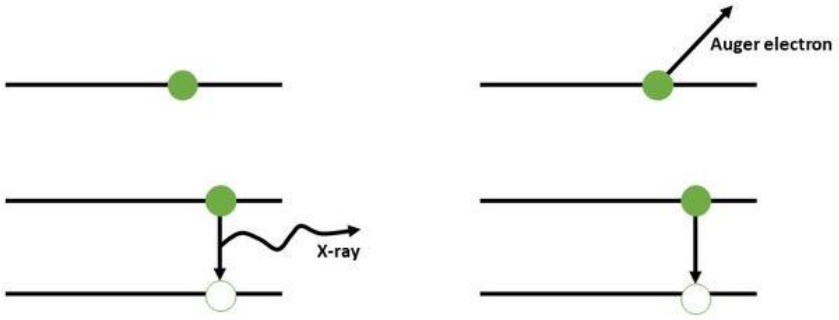

Figure 1.3 - An illustration of the competitive processes of x-ray emission and Auger electron emission which occurs after an electron vacancy is filled.

- *Fission* – either a spontaneous process or induced in an atomic nucleus through the interaction with a subatomic particle which has kinetic energy, typically neutrons. The nucleus splits into two fragments, releases a large amount of energy, and emits a number of fast neutrons. In nuclear reactors, fission is induced in enriched ^{235}U rods with thermalised neutrons and the energy release is used to generate power. Fission of other nuclides (e.g. ^{239}Pu) is also well understood[38]. A wide mass range of nuclides are produced as a result of fission and those with a high fission yield have the potential for being isolated and used for other purposes (Figure 1.4).

$$^{235}_{92}U + {}^{1}_{0}n \rightarrow {}^{236}_{92}U \rightarrow {}^{134}_{50}Sn + {}^{99}_{42}Mo + 3({}^{1}_{0}n) \qquad \textbf{(1.7)}$$

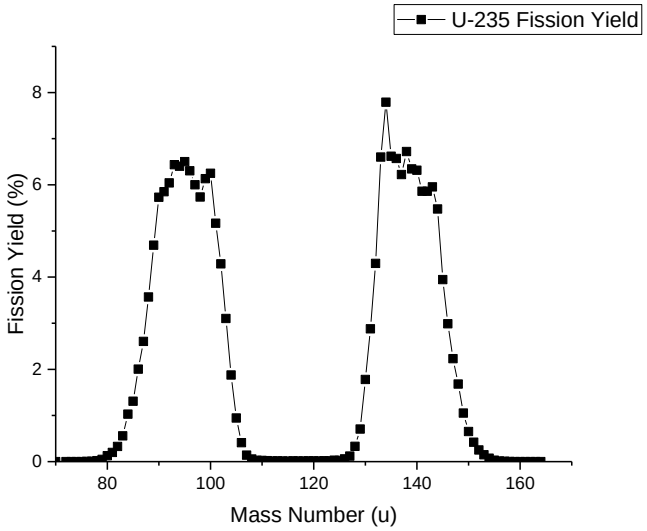

Figure 1.4 - The distribution of fission products and their fission yields from the fission reaction of ^{235}U induced by thermal neutrons[39]

- *Gamma radiation* – follows all of the aforementioned decay types if the initial decay leaves the daughter nucleus in an excited energy state. Gamma radiation is emitted as the nucleus falls from an excited energy state to a lower energy state. The energy of the gamma radiation is equal to the difference of the energy of the two energy states (i.e. $E_\gamma = E_1 - E_2$). Gamma radiation is a very low LET radiation type and therefore, experiences little attenuation as it passes through low density matter. Denser materials, such as lead blocks, are therefore required to provide sufficient shielding of gamma radiation.

In most cases, a radioactive nucleus can decay by more than one route. The probability of one of these routes taking place is given by the branching ratios (%). The example in Figure 1.5 shows how ^{40}K can decay by one of three routes, each with a different probability of occurrence.

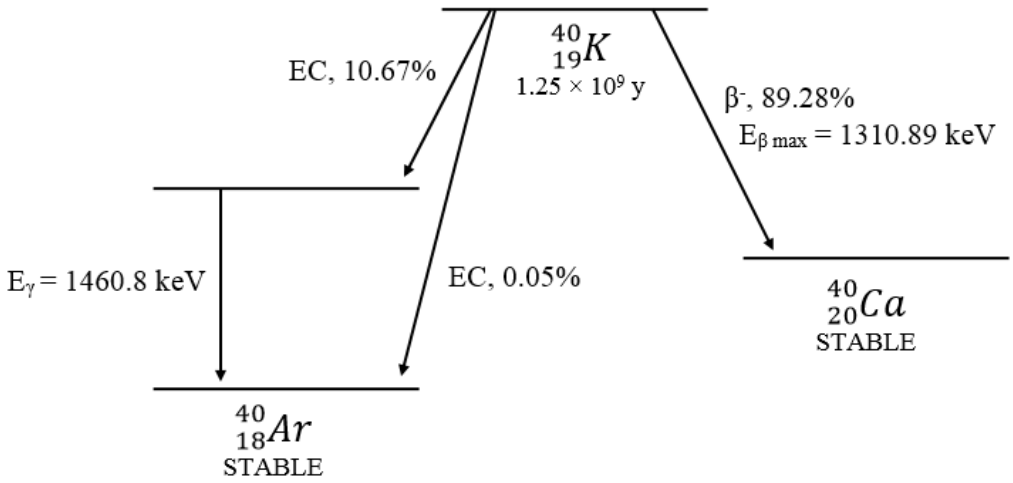

Figure 1.5 - The decay scheme for ^{40}K; showing the possible decay routes and their branching ratios[6].

1.2.1.2 Sources of radioactive elements

Radioactive isotopes can either be naturally occurring or anthropogenic. Naturally occurring radionuclides are either long-lived, part of a decay chain with a long-lived parent (e.g., ^{226}Ra) or are of cosmogenic origin (e.g. ^{14}C). Some industrial processes, such as those within the oil and gas industry, produce waste which is enhanced in naturally occurring radionuclides[40]. Anthropogenic radionuclides are artificial and are produced, typically, by the irradiation of a target material with charged particles or neutrons.

For nuclear medicine, radionuclides are most commonly obtained from anthropogenic sources. The processes which are used to produce artificial radionuclides are discussed in greater detail later (Section 1.3).

1.2.2 The use of radioactive isotopes in medicine

Nuclear medicine has become a fundamental tool in both diagnostic and therapeutic clinical procedures. The development of targeted diagnostic and therapeutic agents has increased the efficacy of nuclear medicines for a wide range of diseases, particularly cancers, neurological diseases and cardiac diseases[41].

Diagnostic imaging in nuclear medicine is achieved by using either positron emitting isotopes for positron emission tomography (PET) or gamma emitting isotopes for single photon emission computed tomography (SPECT). SPECT and PET procedures are functional imaging modalities which use radiotracers to visualise physiological processes. These are routinely coupled with anatomical imaging techniques, particularly computed tomography (CT), to provide spatial imagery to allow for accurate identification of diseased areas[42]. This is particularly useful for the identification of metastatic cancers and to improve the precision of surgical procedures.

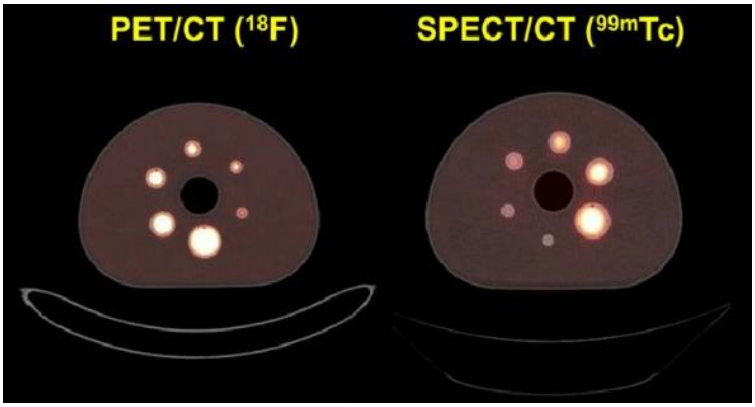

Figure 1.6 - Comparison of a PET/CT scan and a SPECT/CT using International Electrotechnical Commission (IEC) standard body phantoms containing ^{18}F and ^{99m}Tc respectively (Taken from Bailey and Willowson)[43].

Isotopes which emit alpha particles, beta particles, Auger electrons or conversion electrons can be used in therapeutic nuclear medicine. Here, energy transfer from the emitted particle to the diseased cells is exploited in order to kill or damage the cells (i.e., cytotoxicity)[44].

Accurate diagnosis and therapy are dependent on the effective use of targeting molecules, which direct the radionuclide to the diseased cells. A variety of targeting molecules have been developed including monoclonal antibodies, labelled glucose and small, receptor-specific, molecules[45].

The activity of a final radiopharmaceutical preparation must be accurately determined prior to its clinical use to ensure that an appropriate dose is administered to the patient for diagnostic investigation or for therapy. The activity can be determined using a radionuclide calibrator; an instrument typically incorporating a calibrated well-type ionisation chamber.

Henceforth, each diagnostic and therapeutic tool is briefly discussed before describing how they can be combined advantageously to provide a theranostic capability. The suitability of four terbium isotopes as theranostic candidates is then discussed.

1.2.2.1 Diagnostic nuclear medicine

Single photon emission computed tomography

Single photon emission computed tomography (SPECT) is the most frequently used diagnostic tool in nuclear medicine[46]. As previously mentioned, it uses radionuclides which emit gamma rays. Commonly used SPECT radionuclides include ^{99m}Tc, ^{111}In and ^{123}I, amongst others (Table 1.1).

Detection of the emitted gamma rays is typically achieved by two, or less commonly three, thallium doped sodium iodide (NaI(Tl)) crystal scintillation cameras. Signals are amplified and processed to give a functional image which is coupled with an anatomical image to allow accurate identification of diseased areas. NaI(Tl) crystals are nearly ideal scintillators for the detection of the 140 keV gamma photons emitted from ^{99m}Tc; however, the detectors function across a 40-960 keV energy range[47]. Therefore, novel SPECT tracers must emit gamma rays within this range, but ideally at an energy close to 140 keV to ensure high sensitivity and resolution.

Table 1.1 - Commonly used and novel SPECT radionuclides[27,41]. [a] *currently under pre-clinical assessment.*

Radionuclide	Half-life, $t_{½}$	Main energy (E_γ)	Example radiopharmaceutical
^{67}Ga	3.26 d	93.3 keV (38.8%)	[^{67}Ga]-citrate [48]
^{99m}Tc	6.01 h	141 keV (88.5%)	[^{99m}Tc]-MDP
^{111}In	2.80 d	245 keV (94.1%)	[^{111}In]-penteteoride [49]
^{123}I	13.2 h	159 keV (97.2%)	[^{123}I]-MIBG [50]
^{155}Tb	5.32 d	86.6 keV (32%) 105 keV (25%)	[a] ^{155}Tb-chCE7 [29]

MDP = methyl-diphosphonate, MIBG = meta-iodobenzylguanidine, chCE7= an anti-neuroblastoma monoclonal antibody. d = days, h = hours.

Positron emission tomography

Positron emission tomography (PET) is a technique that uses neutron deficient, positron emitting radionuclides to image diseased areas of the human body. As the radionuclide decays, positrons generally travel less than a few mm *in vivo* before they annihilate with an electron, producing two gamma rays (E_γ = 511 keV) that are emitted in opposite directions (Figure 1.7)[51]. These gamma rays are detected in coincidence by scintillator detectors positioned in a ring that fully surrounds the patient. Typically, bismuth germanate (BGO) or lutetium-yttrium oxyorthosilicate (LYSO) crystals are used as the scintillator, the latter being more common at present. These crystals are capable of providing highly sensitive images with good spatial resolution (~5 mm). Again, PET procedures are routinely coupled with computed tomography (CT) to provide anatomical imaging to allow for better identification of diseased areas.

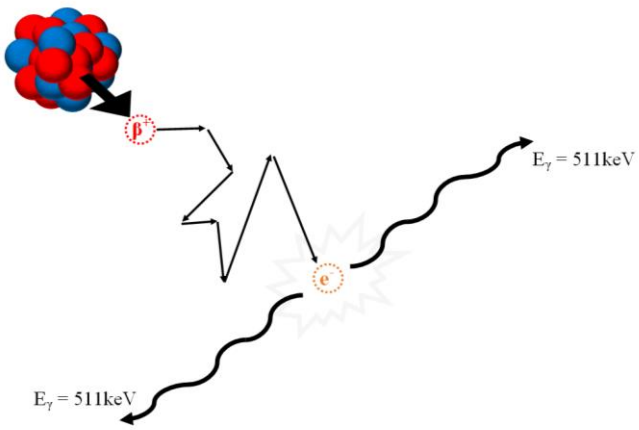

Figure 1.7 - An illustration of positron-electron annihilation and the production of the resultant two characteristic gamma rays (E_γ = 511 keV).

PET has gained particular interest due to its higher image resolution and sensitivity in comparison to SPECT. PET can be used as a dosimetric tool[52]. This is particularly useful for theranostic medicine as it provides an estimation of the dose to different areas of the body, in particular this is useful for assessing target and organ uptake of the administered radiopharmaceutical. Commonly used PET tracers include ^{18}F, most frequently in the form of fluorodeoxyglucose (^{18}F-FDG), and ^{68}Ga (Table 1.2). SPECT based dosimetry has been investigated; however, it currently is not as developed as with PET[53].

Table 1.2 - Commonly used and novel PET tracers[27,41]. [a] currently under clinical assessment.

Radionuclide	Half-life, $t_{½}$	Example radiopharmaceutical
^{11}C	20.4 m	[^{11}C]-Choline [54]
^{18}F	1.83 h	[^{18}F]-FDG [55]
^{64}Cu	12.7 h	[^{64}Cu]-ATSM [56]
^{68}Ga	67.8 m	[^{68}Ga]-DOTANOC [57]
^{152}Tb	17.5 h	[a] [^{152}Tb]-DOTATOC [31]

FDG = fluorodeoxyglucose, ATSM = diacetyl-bis[N4-methylthiosemicarbazone], DOTANOC = conjugate of 1,4,7,10-tetraazacyclododecane-N,N',N'',N'''-tetraacetic acid (DOTA) and the somatostatin analogue 1-Nal3-octreotide (NOC), DOTATOC = conjugate of 1,4,7,10-tetraazacyclododecane-N,N',N'',N'''-tetraacetic acid (DOTA) and [Tyr3]octreotide (TOC). h = hours, m = minutes.

1.2.2.2 Therapeutic nuclear medicine

Rather than using gamma rays, which pass through a large distance of tissue with minimal attenuation, therapeutic nuclear medicine utilises alpha particles or electrons (beta particles, Auger electrons and/or conversion electrons). These particles dissipate their kinetic energy as they interact with cells, resulting in damage or death of the affected cells. The linear energy transfer (LET) of a radiation particle is the measure of how efficiently it dissipates its energy. "LET describes the rate at which the energy is transferred per unit length (keV/μm)"[58]. Generally, alpha particles have an LET that is much greater than that of beta particles[59]. Table 1.3 details a variety of radionuclides which are used in routine treatment, as well as others which are being investigated in the literature.

Targeted radionuclide therapy involves using a therapeutic radionuclide bound to a targeting molecule that seeks out the diseased area. This allows for maximum efficiency in the treatment of particular diseases whilst also minimising unnecessary damage to healthy tissue.

Table 1.3 - Commonly used and novel therapeutic radionuclides[27,41,60,61]*. [a] currently under pre-clinical assessment. [b] currently under clinical assessment.*

Radionuclide	Half-life, $t_{½}$	Decay mode	Main energy	Example Radiopharmaceutical
^{67}Cu	2.58 d	β^-	577 keV	^{67}Cu-CPTA-mAb35 [62]
^{89}Sr	50.6 d	β^-	1.50 MeV (100%)	Strontium chloride ($^{89}SrCl_2$) [63]
^{90}Y	2.67 d	β-	2.28 MeV (100%)	[^{90}Y]-microspheres [64]
^{149}Tb	4.12 h	α	3.97 MeV (16.7%)	[a] [^{149}Tb]-rituximab [4]
^{223}Ra	11.4 d	α	5.98 MeV (100%)	Radium chloride ($^{223}RaCl_2$) [65]
^{225}Ac	10.0 d	α	5.83 MeV (100%)	[b] [^{225}Ac]-lintuzumab (HuM195) [66]

CPTA = Cu-4-(1,4,8,11-tetraazacyclotetradec-1-yl)-methyl benzoic acid tetrachloride. d = days, h = hours

1.2.2.3 Targeted nuclear medicine

Molecules which target disease specific proteins are commonly used to facilitate the accurate imaging or treatment of diseased areas using radioactive isotopes[16,45,67]. There are a wide range of targeting agents available for the diagnosis and treatment of a wide range of disorders and diseases. A radionuclide can be bonded covalently to the targeting molecule, as is the case with ^{18}F-FDG (Figure 1.8.a); or complexed to a targeting molecule using a chelator, as is the case with [^{177}Lu]-PSMA-617 (Figure 1.8.b)[68,69]. Monoclonal antibodies (mAbs), such as votumumab[70] or trastuzumab[71], can also be labelled by attaching radionuclides via a chelating ligand such as DOTA or DTPA.

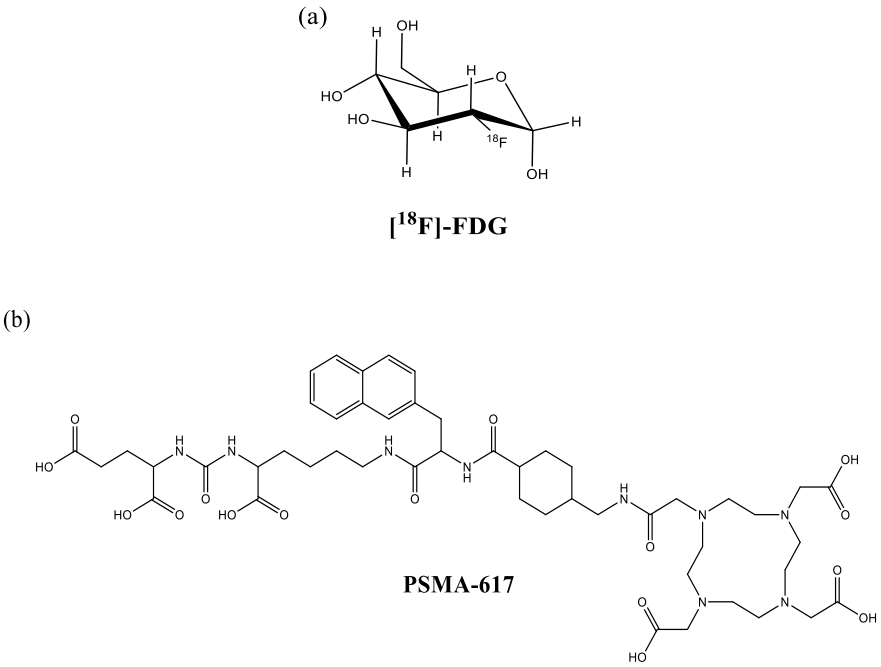

*Figure 1.8 - Molecular structure of **(a)** [^{18}F]-FDG and **(b)** the PSMA-617 targeting molecule.*

1.2.2.3 Theranostic nuclear medicine

Theranostic nuclear medicine is achieved by either **(i)**: the separate application of two radionuclides, one being diagnostic and the other being therapeutic (Table 1.1, Table 1.2 and Table 1.3), bound to the same molecule, or **(ii)**: the use of one radionuclide that produces radiation by two decay modes (Table 1.4), one diagnostic mode and the other therapeutic[16,17,23].

The former, **(i)**, has use in dosimetric measurement and facilitates the application of personalised medicine. The administration of a diagnostic radionuclide (e.g. ^{68}Ga) bound to a

molecule that targets a particular disease allows for toxicity and efficacy assessment of a particular radiopharmaceutical. If the resultant diagnostic image indicates that there is a high uptake of radioactivity in the diseased cells, then the use of a therapeutic radionuclide (e.g. ^{177}Lu) bound to the same, or a similar, targeting molecule should provide effective treatment for the patient. However, if the resultant diagnostic image indicates insufficient uptake of radioactivity in the diseased cells, or significant uptake in a particular organ, treatment using an alternative targeting molecule may afford better therapeutic results for the patient. Due to the PET dosimetric capability, PET tracers are currently better suited as the diagnostic component. SPECT tracers, however, would still provide valuable diagnostic information[52].

The latter **(ii)**, allows for monitoring of an administered therapeutic agent[72]. Isotopes used in this type of theranostic medicine have both a therapeutic and diagnostic decay mode. Use of ^{131}I conjugated to metaiodobenzylguanidine (MIBG) as a theranostic agent has been reported since then mid-1980s. Other radionuclides (Table 1.4) and targeting molecules have been identified as suitable single entity theranostic agents.

Table 1.4 - Commonly used and novel single entity theranostic radionuclides[27,41,60,61].

Radionuclide	Half-life, $t_{½}$	Decay modes	Main energy
^{64}Cu	12.7 h	β^-	579 keV (38.5%)
		β^+	653 keV (17.5%)
^{131}I	8.02 d	β^-	606 keV (89.4%)
		γ	364 keV (81.4%)
^{161}Tb	6.89 d	β-	154 keV (100%)
		γ	25.7 keV (23%)
^{177}Lu	6.65 d	β^-	498 keV (79.3%)
		γ	208 keV (10.4%)

1.2.2.4 Terbium in nuclear medicine

In recent years, terbium has gained particular interest in the field of nuclear medicine. Four terbium isotopes have been identified as therapeutic, diagnostic or theranostic agents (Table 1.5). Initial proof-of-concept and pre-clinical studies using these isotopes have highlighted their *in vivo* capability for theranostic nuclear medicine.

Table 1.5 - The four terbium isotopes with clinical potential, their applications and radiopharmaceuticals synthesised and used in proof-of-concept and/or pre-clinical studies[73].

Isotope	Half-life, $t_{½}$	Application	Proof-of concept/pre-clinical studies
^{149}Tb	4.12 h	Alpha therapy	^{149}Tb-cm09 [27]
		PET imaging	^{149}Tb-rituximab [4]
^{152}Tb	17.5 h	PET imaging	^{152}Tb-cm09 [27]
			^{152}Tb-DOTATOC [28]
^{155}Tb	5.32 d	SPECT imaging	^{155}Tb-cm09 [27,29]
		Auger therapy	^{155}Tb-DOTATATE [29]
			^{155}Tb-MD [29]
			^{155}Tb-chCE7 [29]
^{161}Tb	6.89 d	Beta therapy	^{161}Tb – octreotide [74]
		Auger therapy	^{161}Tb – DOTATATE [75]
		SPECT imaging	^{161}Tb – cm093 [27]
			^{161}Tb – PSMA-617 [30]

DOTATATE = conjugate of 1,4,7,10-tetraazacyclododecane-N,N',N'',N'''-tetraacetic acid (DOTA) and [Tyr3]-octreotate, MD = minigastrin analogue, PSMA = prostate-specific membrane antigen. d = day, h = hours

1.3 Production of radionuclides

In order to be able to use routine and novel radionuclides they need to be produced and isolated in quantities fit for their purpose; be it for clinical use, nuclear data measurements or primary standardisation (Section 1.5). Typically, low MBq to low GBq quantities of radionuclide are required for each nuclear medicine procedure[76]. This can be achieved by the exploitation of natural processes (i.e., spontaneous fission or radioactive decay) or, in most cases, by the induction of nuclear reactions (i.e., induced fission, induced spallation or activation reactions). There are some general concepts that apply to all artificial isotope production methods, as stated below[77].

1. An incident particle is required, with sufficient energy, to induce a nuclear reaction.
2. The energy of the incident particle has a direct impact on the type of nuclear reaction that occurs and therefore the product nucleus that is produced. The energy must be high enough in order to overcome any repulsive forces and activation barriers but low enough to minimise the co-production of unwanted isotopes.
3. Multiple reactions could occur on the same target, but the probability of a certain reaction occurring is dependent on the target nuclei and the energy of the incident particle.
4. The density of particles in the incident particle beam (i.e. beam current or flux) has a proportional effect on the yield of product.
5. The length of time of irradiation also has a proportional effect on the yield of product.
6. There is a maximum activity that can be achieved which is influenced by the production route and capability of the production facility. The maximum activity is reached at the point at which the rate of isotope production is equal to the rate at which that isotope is decaying[78,79].

The typical nomenclature for a nuclear reaction is demonstrated in the equation **below**[77]:

$$ {}^{A}_{Z}X\ (x_i, x_r)\ {}^{A'}_{Z'}X' \qquad \textbf{(1.8)} $$

where, *X* is the target nucleus with proton number, *Z*, and mass number, A; x_i is the incident particle; x_r is the released particle (or reaction type) and *X'* is the product nucleus with proton number, *Z'*, and mass number, *A'*.

When choosing a suitable production route, the lengthy processing and transit time between production and administration of the radionuclide must be considered as it can result in a significant loss in radiochemical yield when preparing a radiopharmaceutical. The radiochemical yield takes into account losses of the isotope during the transport, chemical separation and/or radiolabelling process, including any losses due to radioactive decay. This is particularly relevant to shorter lived radionuclides where time has a significant impact on the potential specific activity of the radiopharmaceutical. For the synthesis of short-lived radiopharmaceutical tracers, the use of radionuclide generators, such as ^{99}Mo/^{99m}Tc and ^{68}Ge/^{68}Ga, is common and advantageous[80]. They utilise suitable, longer-lived, parent nuclei to reduce the loss of radiochemical yield prior to administration of the agent. Shorter lived radionuclides can also be produced locally, using hospital-based cyclotrons. Longer-lived isotopes can be produced using less-accessible, more elaborate facilities and can be transported large distances without significant impact on the radiochemical yield.

This section describes methods used in the production of radioactive isotopes and concludes with a summary of studied production routes of the aforementioned terbium isotopes (^{149}Tb, ^{152}Tb, ^{155}Tb and ^{161}Tb).

1.3.1 Isotope production methods

1.3.1.1 Proton induced spallation

One method of isotope production involves the proton-induced spallation reaction, where a high energy proton beam is used to irradiate a target (e.g., high purity tantalum). As the protons interact with the target nucleus they induce a spallation reaction (*p*,*sp*) where atomic (or subatomic) fragments are ejected from the nucleus of the target[81,82]. This process produces a wide mass range of isotopes. To isolate a desired isotope, on-line or off-line mass separation can be applied.

The CERN-MEDICIS facility (Medical Isotopes Collected from ISODLE) is used for the production of radionuclides for medical applications[83,84] and is an extension of the Isotope Separator On-Line Device (ISOLDE). The facility utilises previously unused protons (E_p = 1.4 GeV) which have not interacted with the ISOLDE (primary) target to induce a spallation rection in a secondary target. As only approximately 15% of the protons from the proton synchrotron booster (PSB) interact with the primary target, a MEDICIS (secondary) target is placed at an optimum distance behind it (Figure 1.9). The secondary target must also have an

increased volume and density in comparison to the primary target (about 4 times the volume) in order to maximise the irradiation efficiency of reactions.

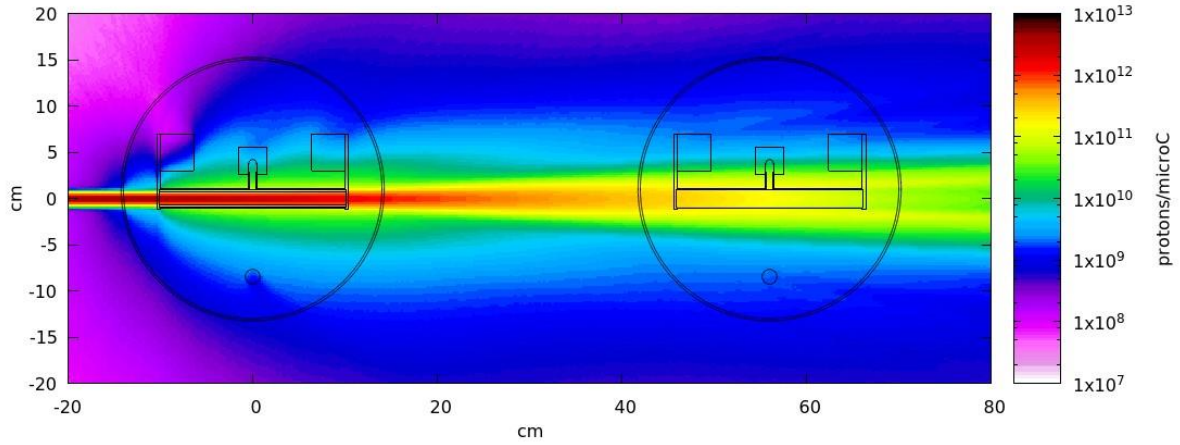

Figure 1.9 - Fluka simulation[85] showing the incoming proton beam on an ISOLDE target (3.5 g/cm^2 UCx for the purpose of the simulation) and intercepting the MEDICIS target downstream (Courtesy of T. Stora, CERN)[86].

The lower atomic number target materials, Ti and Y_2O_3, have been used to prepare similarly low atomic number isotopes including ^{44,47}Sc and ^{61,64}Cu respectively. More recently a tantalum target has been irradiated to produce three terbium isotopes, ^{149}Tb, ^{152}Tb, ^{155}Tb. Proof of concept studies have shown the promising therapeutic or diagnostic capabilities of these spallation-produced isotopes[17,27,87].

Future irradiations of a uranium carbide target, UC_x, have been planned in order to produce high mass isotopes by proton induced spallation. Uranium carbide spallation reactions have been previously studied at the ISOLDE facility for the production of noble gas isotopes[88,89].

As with all irradiation experiments, a high purity target must be used to minimise unexpected products. Subsequent on-line or off-line mass separation techniques and/or chemical separation techniques must be applied in order to obtain a chemically and isotopically pure source that would be suitable for application in nuclear medicine.

1.3.1.2 Cyclotron based nuclear reactions

Radionuclides for use in nuclear medicine can also be produced using a cyclotron. Hospital-based cyclotrons typically use protons (< 20 MeV) as the incident particle and are often used to produce short-lived radionuclides including ^{18}F and ^{64}Cu [90,91]. Research cyclotrons, such as

the MC40 cyclotron at the University of Birmingham[92] (Figure 1.10) or the C70 cyclotron at Arronax[93], are able to accelerate a range of incident particles across a wider energy range.

In general, the use of controllable energy particle beams (typically < 80 MeV) in a research cyclotron allows tailored irradiation of a specific target. Protons (p, $^{1}H^{+}$), deuterons (d, $^{2}H^{+}$), alpha particles (α, $^{4}He^{2+}$) and light helium nuclei ($^{3}He^{2+}$) are commonly used as incident particles[94]. Heavier ions, such as ^{12}C, can also be used as incident particles in suitable facilities. The charged particles are accelerated by applying an electric field between two hollow "D" shaped magnetic field regions (known as "dees"). The dees are separated by a small gap where the particle acceleration occurs. The path of the charged particle is circular and increases in radius with each time it passes the acceleration gap. The beam is then focused along a beam line where it irradiates a target.

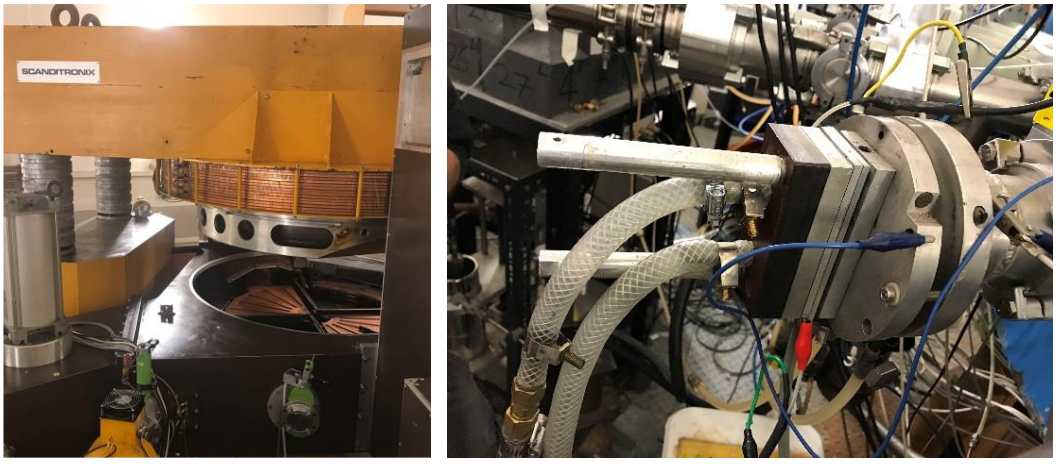

*Figure 1.10 - The internal view of the MC40 cyclotron (**left**) and the target set up on the beam line used for irradiations (**right**) at the Positron Imaging Centre at the University of Birmingham, UK (curtesy of R. Trinder, University of Birmingham)*

The lower and better controlled energy range of a cyclotron is an advantageous characteristic in comparison to using a synchrotron particle accelerator. Using a cyclotron, it is possible to alter the conditions (e.g. particle, particle beam energy, target material) of the isotope production experiment in order to optimise the production of the isotope of interest and to minimise the production of radionuclide impurities[95].

There are threshold energies required to induce a nuclear reaction; however, if the projectile energy is too high, a range of reactions will be observed (e.g. *(p, n)*, *(p, 2n)*, etc.). Therefore, there is an optimal projectile energy range which guarantees high production yield and low

impurity levels. Optimising the conditions, therefore, allows for methods for purification of the product nuclei from the target to be studied prior to irradiation whilst also minimising radioactive waste produced. In particular, the use of enriched, single isotope targets will result in fewer unwanted side-reactions occurring during production. These enriched targets, however, are much more expensive and are often harder to acquire.

The incident particle has to overcome energy barriers to induce a particular reaction: the Coulomb barrier and the Q value[96]. The Coulomb barrier is the energy required for the incident particle to overcome the electrostatic repulsion between itself and the target nucleus. This energy is often very high, but quantum tunnelling allows nuclear reactions to occur at energies much lower than the Coulomb barrier[78,79]. The Q value is the mass difference between the reactants and products in terms of their energy. The Q value is calculated using the following equations:

$$Q = 931.4\Delta M \qquad \textbf{(1.9)}$$

where,

$$\Delta M = (m_T + m_i) - (m_P + m_r) \qquad \textbf{(1.10)}$$

where, ΔM is the mass difference before and after the reaction; m_T is the mass of the target nucleus; m_i is the mass of the incident particle; m_r is the mass of the released particle; and m_P is the mass of the product nucleus.

If the Q value is positive (Q>0) then the nuclear reaction is exoergic, meaning there is a net release of energy. This means the Coulomb barrier is the highest energy barrier to overcome. If the Q value is negative (Q<0) then the reaction is endoergic and requires a net input of energy. In this case a greater amount of energy, in addition to the Coulomb barrier energy, must be supplied to the system for the nuclear reaction to proceed. Due to the effect of quantum tunnelling, the energy barrier in reality is still much lower than the Coulomb barrier.

The nuclear reaction cross-section (σ) is another factor that influences the type of nuclear reaction that occurs. The cross-section reflects the probability of a nuclear reaction occurring along a specific route (i.e., producing X' from X via route Y) at defined reaction parameters. The cross-section is measured in barns (1 b = 10^{-24} cm^2). Computational modelling programs, such as PACE4, TALYS 1.6 or ALICE/ASH, allow for predictions of cross-sections or production yields prior to experimental irradiations[97–99]. It is important to consider the isotopic

composition of the target and also the cross-sections of all possible nuclear reactions that could take place on that same target within the achievable incident particle energy range at the irradiation facility. This will allow an optimal particle energy to be chosen which will produce maximum yield of the desired radionuclide whilst minimising the occurrence of unwanted side reactions.

1.3.1.3 Neutron activation

Nuclear reactors are a source of neutrons that can be used to irradiate a target. The energy and flux (i.e. density of neutrons in a beam) of a neutron beam has a significant influence on the type and efficiency of a neutron-induced nuclear reaction (Table 1.6)[100].

Table 1.6 - Main classes of neutrons involved with or produced in nuclear reactions.

Neutron class	Energy range	Information
Thermal	0.025 eV	Induces fission reactions.
Epithermal	1 eV – 10 keV	More likely to induce neutron capture reactions.
Fast	≥ 10 keV	Released as a product of nuclear fission.

Typical neutron capture reactions include *(n,γ), (n,p)* and *(n,α)* reactions. The emitted particle, and the energy it is released with, are dependent on the neutron flux and the energy of the incident neutron[34]. Neutron capture reactions are typically induced by thermal or epithermal neutrons. Absorption of these neutrons causes an instability in the nucleus causing it to release energy in the form of gamma rays or particles with kinetic energy, such as protons or small nuclei. Hence, radioactive isotopes can be produced. An example of a neutron capture reaction is $^{176}Yb(n,\gamma)^{177}Yb$ which undergoes subsequent β^- decay to give the theranostic radionuclide, ^{177}Lu [101].

Fission *(n, f)* is another type of neutron induced reaction, caused by the absorption of thermal neutrons into the target which results in the split of the nucleus into two smaller nuclei[102]. Fast neutrons are released in this process. One of the products of the neutron induced fission of a ^{235}U target is ^{99}Mo, the radioactive precursor to ^{99m}Tc. Molybdenum-99 has a fission yield of approximately 6% [103].

Research reactors are currently the primary source of neutron capture and fission product radionuclides, but they are diminishing in number. The use of research reactors as a source of medical isotopes is therefore not sustainable and alternative sources are required. Alternative production routes for these isotopes, such as ^{99}Mo and ^{131}I, must be found to maintain the supply or alternative isotopes with sustainable production routes should be used[104].

1.3.2 Mass separation technology

Unwanted isotopes are often co-produced during production experiments. These additional isotopes are produced, either, as the particle beam interacts with other isotopes in the target material, or because different particle combinations are emitted from the nucleus during the reaction[77]. The former is dependent on the impurities present in the target material, the latter on the probability of a particular nuclear reaction taking place under specific reaction conditions (i.e. reaction cross section). Isotopes of the same element cannot be separated chemically due to their identical chemical properties. To isolate an isotope from other isotopes of the same element, mass separation techniques must be used.

There are several on-line isotope separation (ISOL) facilities around the world[82,105–107]. The ISOL technique uses an instrument which consists of a target, ion source and an electromagnetic mass analyser/separator coupled in series[108]. ISOL systems are often used to produce single A/q ion beams in order to induce reactions in other nuclear physics experiments, but these ions beams can be collected after mass separation, processed and used for other applications such as nuclear medicine studies.

Off-line mass separation, where isotope production and mass separation are conducted on separate systems, is also available but is less common. CERN-MEDICIS is one such facility and was used throughout this research (Figure 1.11)[109,110]. Details about the specific methods used are detailed in Chapter 2.

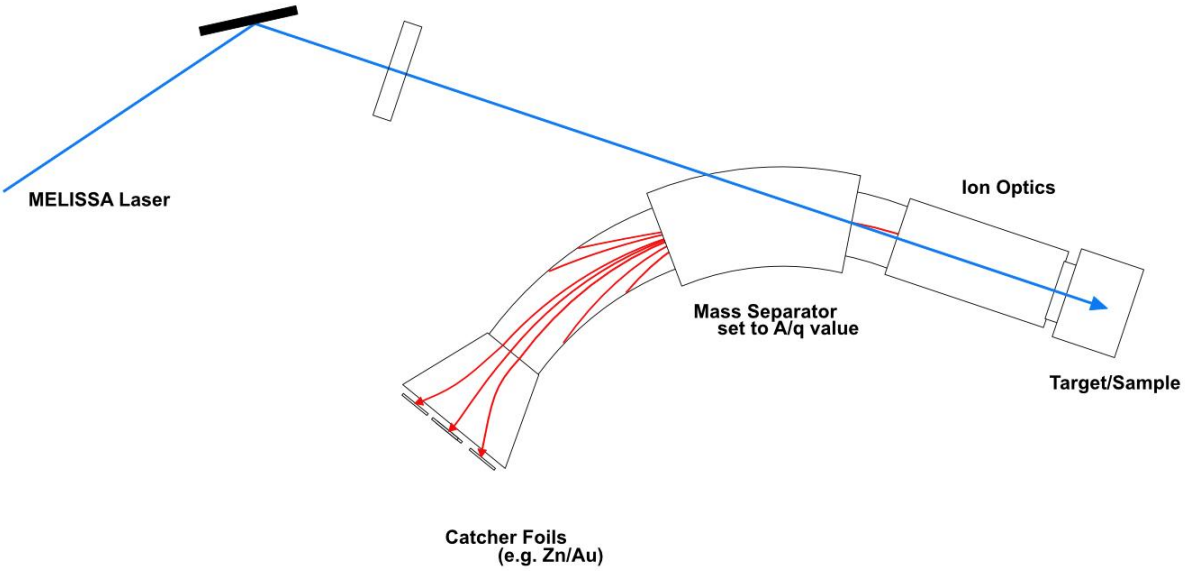

Figure 1.11 – A simplified schematic of the CERN-MEDICIS off-line mass separator. Ion beams are denoted in red. MELISSA ionisation laser is denoted in blue (Adapted from Gadelshin et al.*)*[109]*. A/q = mass-to-charge ratio.*

Typically, surface ionisation or plasma ionisation methods are used to extract ions from an irradiated target or sample by passing a voltage across the sample. The extracted ions are accelerated and directed towards the electromagnetic mass separator that is set to an optimal setting to separate ions of a particular A/q value. The resultant ion beams can then be implanted into catcher foils (e.g. a zinc coated gold foil). Surface ionisation offers limited selectivity, so isobaric and pseudo-isobaric impurities will contaminate the ion beam meaning that a single isotope cannot be isolated. In some cases, a combination of mass-separation and chemical separation techniques are required to isolate a high purity single isotope[27,86].

If available, the resonance ionisation laser ion source (RILIS) technique can be used to increase the selectivity of the ion extraction process[109,111]. A laser is used to induce a multi-step photoexcitation and ionisation of atoms of a desired chemical element before the mass separation step. At the CERN-MEDICIS facility, the MEDICIS Laser Ion Source for Separator Assembly (MELISSA) is used[109].

1.3.3 Production routes for terbium isotopes

The production of the four medically interesting terbium isotopes, ^{149}Tb, ^{152}Tb, ^{155}Tb and ^{161}Tb, has been studied using the aforementioned irradiation techniques. These terbium isotopes are not produced in significant quantities as a result of ^{235}U fission (<<1%). Therefore, it is not feasible to isolate the isotopes from the irradiated ^{235}U target. Table 1.7 details the studied production routes for the four isotopes.

Terbium-161 is regularly produced by the neutron irradiation of a ^{160}Gd target, which has facilitated pre-clinical and clinical investigation[23,27,30,32,75,101,112]. The other isotopes, ^{149}Tb, ^{152}Tb and ^{155}Tb, are currently only produced in significant quantities via the proton-induced spallation of a tantalum target. However, as this not a long-term sustainable method of production, the other methods of production are under investigation. More detail about some of these production routes is discussed in the relevant chapters (Chapters 2-5).

Table 1.7 - Studied production routes of the terbium isotopes with potential applications in nuclear medicine.

Isotope	Studied nuclear reactions	Production facility	Incident particle energy	References
^{149}Tb	$^{nat}Ta(p,sp)^{149}Tb$	Synchrotron	1.4 GeV (CERN-MEDICIS)	Allen *et al.*[113]
	$^{151}Eu(a,6n)^{149}Tb$	Cyclotron	65 MeV	Il'inskaya *et al.*[114]
	$^{141}Pr(^{12}C,4n)^{149}Tb$	Heavy ion cyclotron	65 MeV	Beyer *et al.* [115]
	$^{151}Eu(^{3}He, 5n)^{149}Tb$	Cyclotron	40-70 MeV	Zagryadskii *et al.*[116]
^{152}Tb	$^{nat}Ta(p,sp)^{152}Tb$	Synchrotron	1.4 GeV (CERN-MEDICIS)	Allen *et al.*[113]
	$^{151}Eu(a,3n)^{152}Tb$	Cyclotron	34 – 40 MeV	Trinder *et al.*[117]
	$^{155}Gd\ (p,4n)^{152}Tb$	Cyclotron	39 MeV	Steyn *et al.*[118]
^{155}Tb	$^{nat}Ta(p,sp)^{155}Tb$	Synchrotron	1.4 GeV (CERN-MEDICIS)	Müller *et al.*[27,119]
	$^{155}Gd(p,n)^{155}Tb$	Cyclotron	11 MeV	Vermeulen *et al.*[120]
	$^{153}Eu(a,2n)^{155}Tb$	Cyclotron	28 MeV	Kazakov *et al.*[121]
^{161}Tb	$^{160}Gd(n,\gamma)^{161}Gd \rightarrow {}^{161}Tb$	Nuclear reactor	(flux = 10^{13} - 10^{14} neutrons cm^{-2} s^{-1})	Lehenberger *et al.*[75]

1.4 Chemistry of the lanthanide elements

The four terbium isotopes (^{149}Tb, ^{152}Tb, ^{155}Tb and ^{161}Tb) can be produced by the irradiation of other lanthanide targets (e.g. production of ^{161}Tb by the neutron activation of gadolinium[75]) or via the proton-induced spallation of a tantalum target. The isolation of the desired isotope from the bulk target material, any daughter nuclei and any other trace impurities is required prior to clinical trials and use in order to minimise toxic and radiological side-effects, as well as to maximise the efficiency of the radiopharmaceutical preparation. For fundamental measurements to be made, such as nuclear data measurements and primary standardisations, the removal of radioactive impurities is essential. The removal of non-radioactive impurities is not required for this purpose (Section 1.5.1).

Currently, chemical separation is a necessary process in the preparation of high purity radionuclide sources for applications in nuclear medicine, even with the existence of preparative mass separation (i.e. ISOL techniques). The separation of lanthanides from other lanthanides, however, is challenging due to slight differences in chemical properties throughout the lanthanide series (La→Lu). Three main factors contribute to the similarity[122]:

1. *Oxidation states* – In aqueous conditions, all lanthanides readily lose three electrons from the 6s and 5p electron subshells and therefore lanthanides exist very stably in the III+ oxidation state. Due to the fact that empty ($4f^0$), half-filled ($4f^7$) or filled ($4f^{14}$) subshells are more stable, cerium can be easily oxidised to the IV+ oxidation state, and europium can be (less) easily reduced to the II+ oxidation state. A change in oxidation state significantly changes chemical behaviour and this can be used when trying to remove or isolate these elements from other lanthanide elements[123].
2. *Ionic size* – The 5s and 5p orbitals exist at a similar energy to the 4f sub-shell. The 4f orbital is therefore not shielded from an increasing nuclear charge. Hence, a gradual decrease in ionic radius is observed throughout the lanthanide series with increasing atomic number (La→Lu). This phenomenon is referred to the as *lanthanide contraction* (Figure 1.12)[122]. This, coupled with the III+ oxidation state, means that the lanthanides exhibit similar binding properties when interacting with organic chelators (e.g. EDTA or DTPA)[124].
3. *Coordination number* – Coordination numbers of the lanthanides range between eleven and two and there is a general reduction in coordination number with increasing atomic number; however, this is dependent on the coordinating species. Most commonly, early

lanthanides (La→Tb) exist with a coordination number of nine and the later lanthanides (Dy→Lu) have a coordination number of eight[125]. Steric effects, electrostatic interactions, hydrogen bonding and π-interactions between the ligands and other counter-ion species all have a significant impact on the coordination number. This makes predicting the coordination numbers difficult, particularly for complex systems.

Differences in these factors are not significant between neighbouring lanthanides which gives reason to the difficulties found in the literature with successfully purifying single lanthanides from neighbouring elements.

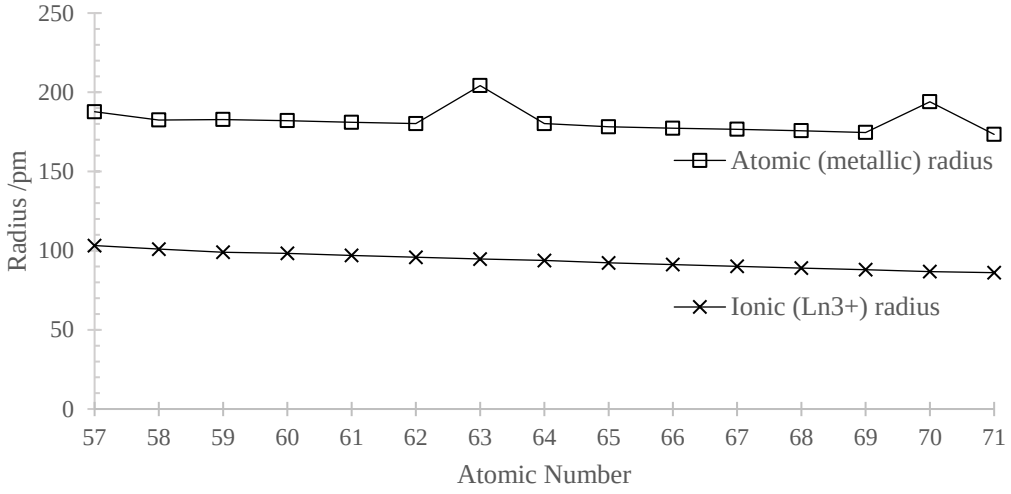

Figure 1.12 - Graphical representation of the trend of atomic and ionic radii for the lanthanide elements[122].

During the separation of lanthanide elements, slight changes in separation conditions often have a significant impact on separation efficiency. The optimisation of neighbouring lanthanide separation methods has been the focus of many studies over recent years, typically using chromatographic techniques. With the increased interest in radiolanthanide applications in nuclear medicine, the impact of research in this field has grown[23].

1.4.1 Chromatography of the lanthanides

Chromatography is a technique which aims to separate components of a mixture by taking advantage of the differences in affinity of the components to a stationary phase and a mobile phase[126]. In most scenarios, the mobile phase is an aqueous solution which is passed over or through a solid stationary phase. Chromatography techniques are commonly used as analytical tools, but as the identified radionuclides have an intended use after separation, namely nuclear

medicine procedures or as primary standards, preparative chromatography techniques have been the focus of the work reported here.

The chemical properties of the mobile and stationary phases influence how elements will behave during a chromatographic separation, so should be considered carefully. In particular, the pH and concentration of the mobile phase can cause changes to chemical form of the stationary phase as well as the elements undergoing the separation. These changes will affect how strongly each element will interact with the two phases, thus affecting the quality of separation that can be achieved. In addition to this, the chemical and physical structure of the phases can influence how elements will interact with them (i.e. steric hinderance and/or complex formation). These concepts can be explained further by example:

- the pH of the mobile phase will govern whether functional groups of a stationary phase will be protonated (e.g. amide, $R\text{-}NH_2$, or protonated amide, $R\text{-}NH_3^+$). The pH of the mobile phase, therefore, has a significant influence on the ionic interactions that will occur between the components of a sample and the stationary phase.
- the mobile phase may induce a redox reaction that will alter the oxidation state of the elements undergoing separation. This will change the ionic size and charge of the element, changing how it will interact with the two phases.
- chelating mobile phases, such as ethylenediaminetetraacetic acid (EDTA), can form complexes of varying strength with elements within a sample. The probability of forming complexes is influenced by the size and charge of the ion, and the pH of the chromatographic system. How these complexes interact with the stationary phase will also be influenced by chemical conditions of the chromatographic system (e.g. the pH or concentration of the mobile phase).

These chemical parameters can be tailored advantageously to selectively isolate single components of a specific elemental mixture. In addition to the chemical parameters of a system, other characteristics of the chromatographic system can affect the quality of separation. These are discussed in section 1.4.1.1.

When carrying out column-based separations, elution methods used in chromatography are typically isocratic, stepwise or gradient (Figure 1.13). Isocratic elution is where there is no change in the composition of the mobile phase during all or part of the analysis; the concentration and pH remain constant. Gradient elution is where there is a gradual change in

the composition of the mobile phase. A combination of isocratic and gradient conditions is often used to optimise separation time without compromising the quality of the separation[127,128].

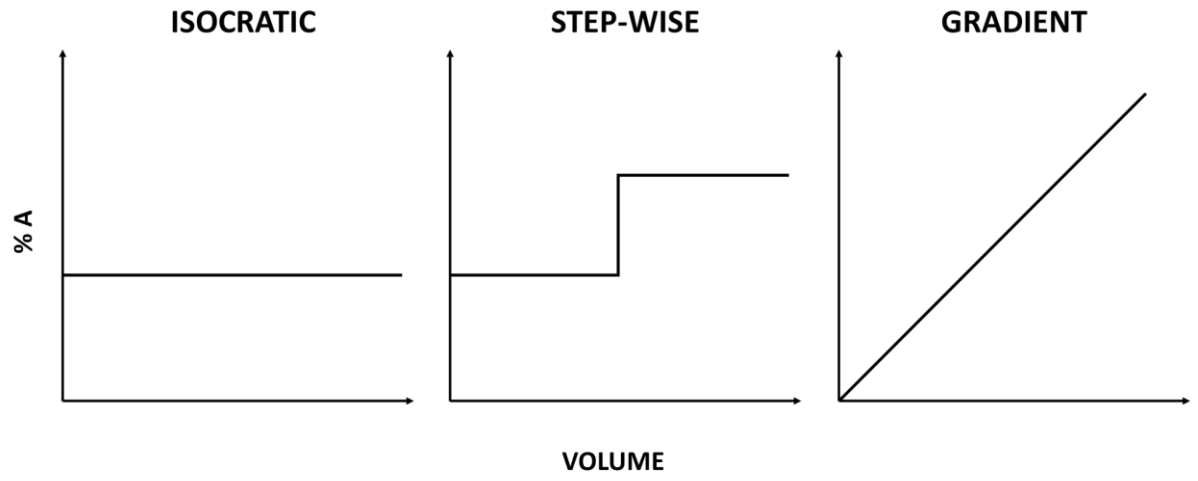

Figure 1.13 - Comparison of the variations in the composition of mobile phase (%A) for different elution methods. These are often used in combination.

1.4.1.1 Variable parameters in column chromatography

As components of a mixture pass through a column they behave differently, allowing for separation to be achieved. As they elute from the column, their peak shape, and thus the separation resolution between components, is governed by kinetic processes, such as the rate of mass transfer between the two phases, as well as the probability of interaction of each component under the defined chemical and physical conditions. Beyond changing the type of mobile phase and stationary phase used for a given separation, there are several parameters which can be varied to improve the separation resolution. These are described as follows[129,130]:

1. The *flow rate* of mobile phase through the packed column naturally affects the separation time, but also affects the magnitude of band spreading (i.e., the peak width on elution)[128]. At a slower flow rate, elution peaks sharpen and therefore improve the separation resolution. This is because the effect of the rate of mass transfer is minimised.
2. The *column length* also has an impact on the bandspreading. The longer the column the greater the bandspreading meaning that the analyte will elute in a greater volume. A longer column gives a greater resolution; however, larger volumes (mL) are required to ensure the elution of all analytes and thus results in an increased separation time.

3. A decrease in the *particle size* of the stationary phase results in a decrease in the height equivalent to the theoretical plate (HETP) value. This means that the degree of bandspreading reduces[131]. Using a chromatography resin with a smaller particle size results in the sharpening of elution peaks and therefore gives an improved separation resolution.
4. The *resin capacity* is another factor that will impact on the efficiency of separation. The total resin capacity describes the maximum amount of element that can be loaded on to the resin. This value is typically stated as the number of moles (mmol) of an element per unit volume of resin (mL). If this value is exceeded then the active sites of the resin will be saturated, resulting in breakthrough, loss of analytes and inadequate separation. The *operating resin capacity*, however, is dependent on the separation conditions and is the capacity at which the quality of separation becomes affected by the increasing concentration of analyte. This is a particularly important factor to consider when processing target material to isolate a produced isotope. As said by Stephen Heinitz: "*high column loading results in inferior lanthanide separation*"[132].
5. As mentioned previously, altering the *composition of the mobile phase* has a significant impact on the chromatographic behaviour. The concentration, pH and ionic strength of the mobile phase all influence the speciation of both the stationary phase functional groups and the analytes requiring separation. This heavily influences how the analytes interact with the two phases and therefore has a significant impact on the separation.

Ion-exchange chromatography and extraction chromatography techniques have been shown to be suitable methods for preparative separation of the lanthanides and are henceforth discussed in further detail.

1.4.1.2 Ion exchange chromatography

Ion exchange chromatography utilises the reversible interaction of ionic species between a stationary and a mobile phase in order to separate components of a mixture. A variety of ion exchange methods are commonly used for the separation of biomolecules, small molecules and/or elemental mixtures[133].

Ion exchange stationary phases are typically cross-linked polymeric chains with ionic functional groups. These ionic groups are fixed on the resin and are the sites at which ion-exchange takes place (see simplified diagram, Figure 1.14, where the sulphonate (SO_3^-) groups

are the site of ion-exchange). A range of mobile phases can be used including ionic solutions (e.g. NaOH) and chelating species (e.g. EDTA). The characteristics of solid stationary phase and the aqueous mobile phase both heavily influence the quality of separation.

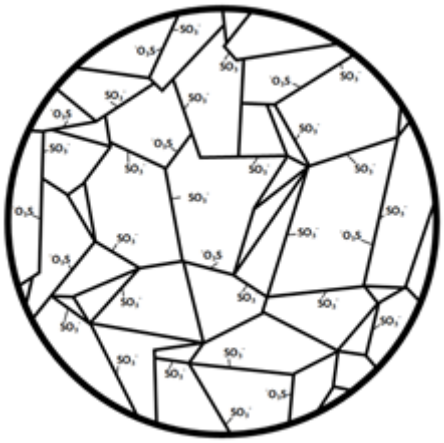

Figure 1.14 - Diagram showing an example of the macroporous cross-linking structure of a strong acid cation exchange resin and its sulphonic acid exchange sites[130].

Historically, ion exchange is the most commonly used tool for the separation of the lanthanide elements[23,134]. The use of a column packed with cation exchange resin and an α-HIBA mobile phase has been used for the preparation of the high purity lanthanides to ensure accurate analysis of geological and nuclear forensics samples, as well as for the preparation of radionuclides for nuclear medicine research[23,27,75,135]. Precise control of the concentration and pH of the α-HIBA solutions is required to ensure effective isolation of single lanthanide elements.

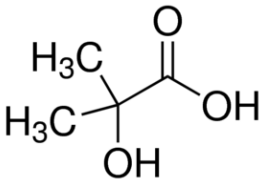

Figure 1.15 - Chemical structure of alpha-hydroxyisobutyric acid (α-HIBA).

It should be noted that the exposure of ion-exchange resins to high levels of ionising radiation can lead to resin breakdown, reducing the efficiency of the separations and the operating lifetime of a column[130,136]. This is a particularly important factor to consider when designing chemical separation methods capable of preparing the high activity sources of radioisotope required for nuclear medicine applications.

1.4.1.3 Extraction chromatography

Extraction chromatography combines the selectivity of solvent extraction techniques with the ease-of-use of solid-phase column chromatography techniques[137]. The stationary phase extractant, typically a hydrophobic organic molecule, is incorporated into a porous inert support, together forming a solid-phase extraction chromatography stationary phase (Figure 1.16). Mineral acids are typically used as the mobile phases in extraction chromatography separations (e.g., HCl or HNO_3).

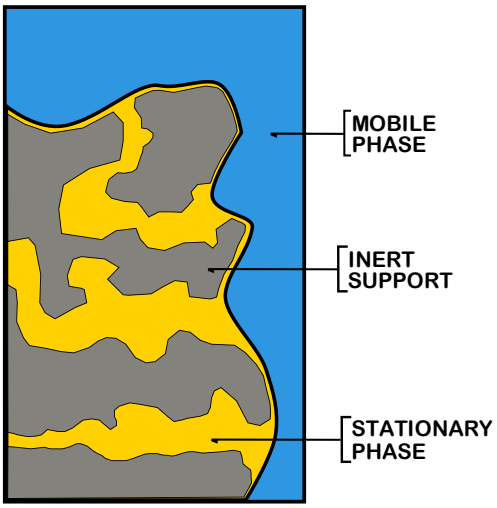

Figure 1.16 - Illustration of an extraction chromatography bead. Adapted with reference to Horwitz (1998)[138].

Extraction chromatography resins have been used for the preparation of environmental, geological, decommissioning and nuclear forensics samples for elemental characterisation, as well as for the purification of radioisotopes for use in nuclear medicine[139]. These resins exhibit high radiation and chemical resistance, being able to operate efficiently whilst using high acid concentrations and highly radioactive samples[140,141].

A series of extraction chromatography resins, (i.e. the LN resin series) using phosphorus-based extractants have been developed and designed for the separation of the lanthanide elements (Figure 1.17)[137,142]. In recent years, the use of these extraction chromatography resins to purify radioactive lanthanides for use in nuclear medicine has been studied, but research is in its infancy[23].

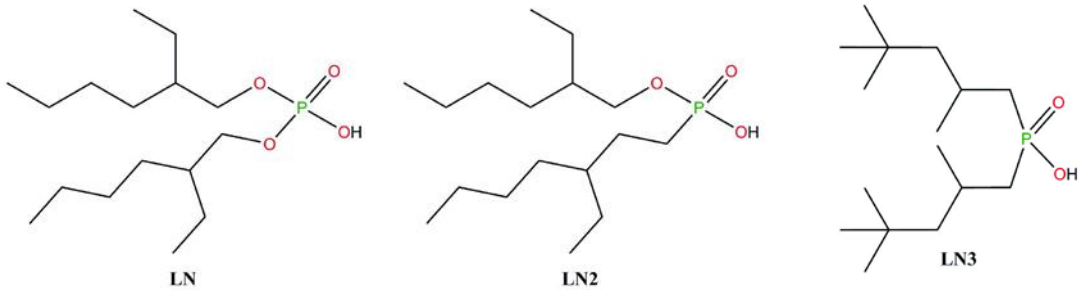

Figure 1.17 - The stationary phase extractants which are present in each of the three extraction chromatography resins used for lanthanide separations (LN, LN2 and LN3)[142].

1.4.2 Chemical isolation of terbium

Both ion-exchange and extraction chromatography techniques have been applied to situations requiring the isolation of terbium from matrices containing other lanthanide elements. The strict control of separation conditions is key to achieving high quality separations and this is clear in the methods reported in the literature. Here, a summary of some of the methods used in previous studies are presented allowing for comparison in later chapters.

1.4.2.1 Ion exchange chromatography

The α-HIBA/cation exchange method has been applied to isolate pure sources of terbium[27–29,143] produced by proton induced spallation, namely ^{149}Tb, ^{152}Tb and ^{155}Tb, and by neutron bombardment, namely ^{161}Tb.

Beyer *et al.* (2004)[115] reported the use of a step-wise α-HIBA/cation exchange method in order to isolate ^{149}Tb produced at CERN-ISOLDE by proton-induced spallation with subsequent mass separation. A small Aminex A5 column was used (NH_4^+ form, 3 × 60 mm) and notable terbium/gadolinium peak overlap was observed which resulted the isolation of a high purity, but moderate recovery (~80 %) ^{149}Tb source. The terbium fraction (~0.2 mL) was eluted in 0.25 M α-HIBA at a flow rate of 0.1 mL/min and was recovered within ~5 minutes.

A similar method was applied by Müller *et al.* (2012)[27] and involved the separation of terbium on a strong acid cation exchange column (50 × 5 mm) using ~0.15 M α-HIBA at pH 4.75. The exact resin, and the chemical purity and recovery of terbium post-separation, was not reported in this study. Reproducing this data would therefore be a challenge. The terbium sources produced here were of a suitable quality to radiolabel to a DOTA–folate conjugate cm09 and achieved a good radiochemical yield of >96%. Initial diagnostic and therapeutic pre-clinical trials were conducted using these ^{xxx}Tb-cm09 samples.

For the isolation of ^{161}Tb produced by neutron bombardment of an enriched ^{160}Gd target, the method reported by Lehenberger *et al.* (2012)[75] involved the separation of trace levels of terbium from a 40 mg ^{160}Gd target and 0.2 mg of dysprosium. A 150 × 7 mm Aminex A6 column (17.5 μm particle size, NH_4^+ form) was used. This method successfully recovered 90 % of the ^{161}Tb in 0.13 M α-HIBA (pH 4.5) whilst reducing the gadolinium content in this fraction by $>10^5$ and the dysprosium content by $>10^2$ (i.e., decontamination factors). It is a relatively slow method as it required the separation to be carried out at a low flowrate and using large volumes of mobile phase (~0.2 mL/min, ~90 mL, separation time ~ 450 minutes).

In a similar, more recent study by Gracheva *et al.* (2019)[143] a combination of different column properties (Sykam microporous cation exchange resin, 12-22 μm particle size, NH_4^+ form, 170 × 10 mm column) and a faster flowrate (~0.6 mL/min) were used to isolate high purity ^{161}Tb from gadolinium target material. The loading and terbium elution conditions were the same as reported in Lehenberger *et al.* (2012)[75]. The increased column volume and faster flowrate allowed for a high radionuclidic purity terbium (>99%) to be isolated from bulk quantities of Gd_2O_3 material (up to 140 mg) in a shorter time of ~100 minutes. Rapid concentration of the ^{161}Tb was achieved using LN3 extraction chromatography resin column (6 x 5 mm) and HCl elution (0.05 M, 500 μL). The purity of the terbium fraction was estimated using the radioactive tracers during method development steps, but no stable element analysis was conducted to quantify any gadolinium impurity remaining in the terbium fraction. Radiolabelling studies with DOTANOC (≥ 99% radiochemical yield, 180 MBq/nmol specific activity) showed that the terbium fractions were of a sufficient quality for further pre-clinical investigation.

1.4.2.2 Extraction chromatography

Monroy-Guzman *et al.* (2015)[144,145] investigated the use of LN extraction chromatography resin for the separation of lanthanide pairs. Their work describes the separation of micro/macro component systems of neighbouring lanthanide pairs, namely Pm/Nd, Tb/Gd, Ho/Dy and Lu/Yb, using 12 × 70 mm columns packed with Ln spec resin (50 – 100 μm, *Eichrom Industries*). The flow rate of solution through the column, and therefore separation time, is not defined in this study. The authors claim, and elution profiles suggest, effective separation of trace levels of terbium from bulk quantities of gadolinium (10 mg $Gd(NO)_3$) using a stepwise elution. The gadolinium was eluted in 0.8 M HNO_3 followed by the elution of terbium in 3 M HNO_3. The degree to which the bulk gadolinium target material is removed is unclear, as no stable element content analysis of the micro-component fractions is reported. No radiolabelling

studies were conducted, as per Gracheva *et al.* (2019)[143], which would have indicated whether a suitable quality had been achieved.

Jiang *et al.* (2015, 2017)[146,147] reported the successful isolation of ^{161}Tb from fission products using LN resin prior to its determination by liquid scintillation counting for nuclear forensics purposes. The reported method involved the isolation of the lanthanides, as well as some other chemically similar elements (e.g. yttrium), from a complex matrix using an anion exchange method and selective precipitation. The isolation of ^{161}Tb from other lanthanide fission products which remained was achieved using a column packed with LN resin (50 – 100 μm, *Triskem International*, 107 × 7 mm). Separation and collection of individual lanthanides was achieved using a stepwise elution profile (0.01 M - 8 M HNO_3). The ^{161}Tb fraction was further purified by passing the solution through another LN resin column (2.1 cm^3). There is no indication to the quantities of each element in the mixture used in this study, or to the flow rate and separation time required for efficient separation. Details regarding the stepwise elution method and are also absent, all of which making reproducing this method challenging.

Kazakov *et al.* (2018)[121] investigated the production of ^{155}Tb by alpha bombardment of Eu_2O_3 targets (~200 mg). They showed the removal of bulk europium material by means of chemical reduction using zinc chloride and subsequent sulphate (SO_4^{2-}) precipitation. Isolation of terbium from remaining gadolinium and europium impurities was carried out using an LN resin column (3 cm^3). A nitric acid stepwise elution was carried out at an unknown flowrate; 0.6 M HNO_3 (40mL) allowed the elution of europium and gadolinium from the column before the elution of terbium using a 3.0 M HNO_3 (15 mL) solution. Radiochemical yield of the ^{155}Tb was reported to be ~90 % with a radionuclide purity of >99 %. Column dimensions were not reported in this article.

Aziz *et al.* (2016, 2020)[148,149] reported the isolation of high radionuclide purity ^{161}Tb (>99 %) from small G_2O_3 targets (5 mg) using a similar method to the one reported by Monroy-Guzman *et al.* (2015)[144,145]. Details regarding the column dimensions, solution volumes, flow rate, terbium recovery and stable impurity profile are absent in this article.

These examples highlight the importance of precise control of separation parameters in order achieve reproducible results. Slight changes in separation parameters markedly change the time required for, and quality of separation. A thorough description of methods is essential in order to ensure reproducibility of the methods as well as to allow for a fair comparison of the method

with others. Gracheva *et al.* (2019)[143] is a good example of this. Some of the other manuscripts, however, were lacking in important information (e.g., column properties, separation time, purity and recovery of terbium post-separation).

In all these cases, a stable impurity profile of the purified terbium fractions is lacking. A complete understanding of the stable impurities would be helpful when it comes to radiolabelling and (pre)-clinical studies. Alternatively, as seen in Müller *et al.* (2012)[27] and Gracheva *et al.* (2019)[143], successful radiolabelling of bioconjugates with the purified terbium sources can be used to indicate a suitable chemical purity has been achieved.

Finally, self-evaluations of these reported methods mainly focus on beneficial aspects. A complete evaluation and discussion of the method would be helpful in informing the readers of potential applications and limitations of the reported methods as well as allowing for fair and comprehensive comparison to other methods.

1.5 Requirements for the metrological and (pre)-clinical use of radioactive terbium sources

The purity and specific activity requirements for applications post-separation need to be considered. The application of purified terbium sources can be split into two general categories that are to be considered within the remit of this study:

1. their use for the realisation of high-quality metrological information
2. their use in the development of novel nuclear medicine

The background to each of these applications and reasons behind purity requirements will be discussed in detail in this section.

1.5.1 Determination of metrological information for radioactive isotopes

1.5.1.1 The role of metrology and traceable measurement in nuclear medicine

Primary standardised radioactive sources are required to derive accurate metrological information. These include accurate nuclear data. Nuclear data measurements provide fundamental information about the decay of the studied isotopes. Half-life and energy level measurements can be conducted using these primary standards in order to validate or improve historic records. The derivation of ionisation chamber calibration factors (i.e., pA/MBq response), and SPECT or PET attenuation correction factors, is essential for carrying out safe and effective nuclear medicine procedures and this can also be achieved using primary standards. Accurate nuclear data are essential as they facilitate the qualitative and quantitative determination of the radionuclides present in more complex radionuclide mixtures when measured by decay counting techniques (e.g. gamma spectrometry, liquid scintillation counting and alpha spectrometry). The quality of nuclear data has significant implications on the accurate application nuclear medicine procedures.

A thorough characterisation of the radiological purity of the primary standards is of great importance. If any radiological impurities are present, they could have a significant impact on the accuracy of all metrological measurements and thus the safety and efficiency of nuclear medicine procedures.

In all clinical applications, the accurate determination of the activity of a radiopharmaceutical preparation ensures that a patient receives a suitable dose of targeted radiation. This facilitates

efficient, and in some cases quantitative, diagnostic imaging and/or efficient therapy and this minimises the probability of administering a harmful dose to a patient[150]. Typically, radionuclide calibrators that incorporate pressurised well-type ionisation chamber are used for this purpose.

Adherence to traceability procedures gives confidence to end-user measurements by ensuring that radionuclide calibrator measurements, which are made at a hospital, are accurate and are traceable to primary standards derived by national measurement institutes (NMI, e.g. NPL in the UK) and to the International System of Units (SI units, Figure 1.18).

1.5.1.2 Production of radioactivity standards

Primary standards of radioactivity are absolute activity sources which are made by NMIs, traceable to the SI units, and have a minimised but well-defined uncertainty budget[151]. Radioactive sources must first be produced (see section 1.3) and undergo chemical separation (see section 1.4) to remove radiological impurities before they can undergo primary standardisation.

The derived uncertainty of the radioactive primary standard is ideally independent of any other measurements (i.e., nuclear decay data). This independence would minimise the need for uncertainty propagation and thus lead to a greater confidence in the measurement (i.e., lower uncertainty). To achieve this, these primary standardisation measurements are typically made using high geometry counting methods (i.e., 4π or 2π geometry) such as liquid scintillation counting, or coincidence counting methods such as $4\pi\beta$-γ coincidence counting[151]. For radionuclides which undergo alpha decay, defined solid angle (DSA) counting is often used because it provides a significant improvement in the derived uncertainty of the measurement in comparison to other methods[151].

To guarantee traceability, these activity measurements – which are described using a derived SI unit, becquerel – should be directly traceable to the base SI units (Figure 1.18). Mass, time, frequency and length measurements are relevant here. For example, any mass measurement made in the primary standardisation process should be conducted using a high precision analytical balance which has been calibrated using a set of weights which are directly traceable to the fixed value of Planck constant (h)[152].

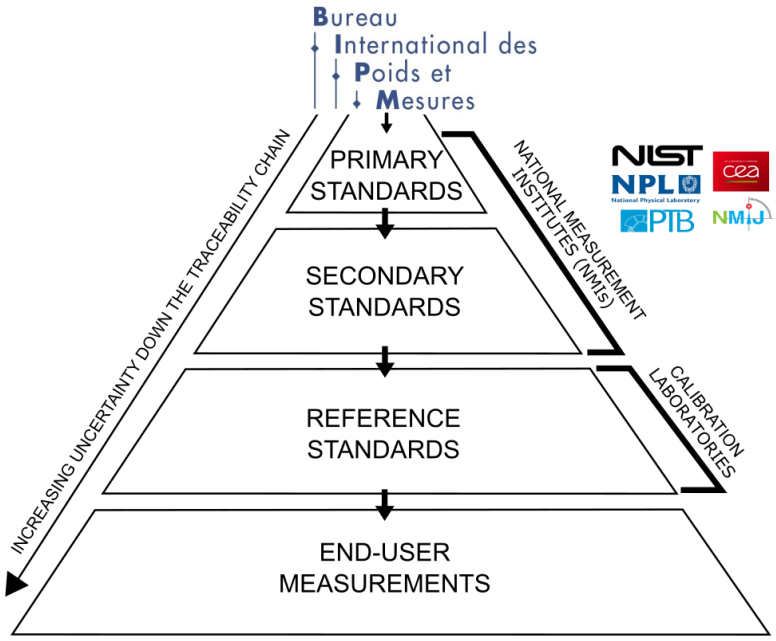

Figure 1.18 - A simplified measurement traceability hierarchy, illustrating the unbroken chain of measurements or calibrations required to ensure that a measurement it traceable to the International System of Units (SI).

Secondary standards are made with reference to a national primary standard and are, in some cases, used to provide a high-quality calibration of measurement instruments. Reference, or working, standards are in turn made by comparison to a secondary standard and are typically used to check the operating accuracy and precision of the relevant processes and analytical instruments (i.e., quality control/assurance). As alluded to before, traceability from the SI units to the end-user measurements ensures confidence in these measurements.

Throughout all steps of radioactive standard production, measures are taken to minimise the uncertainty introduced at each step, thus minimising the uncertainty on the end-user measurement.

1.5.1.2 Ideal characteristics of radioactive standards and their use in the field of nuclear medicine

The purity of a radioactive source which undergoes standardisation is an important factor to consider. The presence of radioactive impurities will result in inaccuracies in the activity, nuclear data and half-life measurements. In some cases, mathematical corrections can be implemented to account for any impurities present (e.g., ^{126}I impurities in ^{125}I), however this adds an additional uncertainty to the derived activity[153].

An absolute activity measurement value (i.e., primary standardisation measurement) of a standard pertains to a specific reference date and time due to the depreciating nature of radioactive isotopes. Therefore, for later measurements, corrections accounting for the radioactive decay over time must be applied. Hence, the half-life of the radionuclide needs to be well known for accurate corrections to be made when a standard is used for calibrations or for quality control measurements.

In the field of nuclear medicine, primary, secondary and reference standards are used for the calibration and quality assurance of ionisation chamber-based radionuclide calibrators. Standards also have the potential to be used for the establishment of quantitative imaging that is traceable to the SI units[154].

1.5.2 Purity requirements for radiolabelling and (pre)-clinical studies

To make the four terbium isotopes (^{149}Tb, ^{152}Tb ^{155}Tb and ^{161}Tb) isotopes available for large-scale clinical use, they first need to undergo (pre)-clinical study using sources of suitable purity. To enable targeted nuclear medicine, the terbium isotopes need to be chemically bound to a targeting molecule so that they can be used effectively in nuclear medicine procedures. Each isotope/molecule combination needs to undergo rigorous (pre)-clinical study in order to assess their efficacy and safety *in-vivo*.

Radioactive impurities, particularly those which emit high LET particles on decay, will introduce an unnecessary additional dose of radiation to the subject. The presence of radioactive impurities will also have an impact on the image quality for SPECT and PET studies. For dosimetric imaging studies, if the impurities are known and quantified then they could potentially be corrected for to allow for improved contrast and quantitative accuracy[155]. Generally, the presence of radioactive impurities should be minimised by means of chemical separation, to maintain patient welfare and to ensure effective application of the nuclear medicine procedures.

Requirements for commonly used radiopharmaceuticals are stated within monographs of the International Pharmacopoeia[156]. Requirements relevant in this study include:

- *Radionuclidic purity* – the minimum level of radionuclidic purity (%) as well as the maximum level of radionuclide impurities (%). Radionuclidic purity is commonly derived by means of gamma-ray spectrometry.

- *Radiochemical purity* – the amount of radionuclide that has been successfully labelled onto the molecule (%). Radiochemical purity is commonly assessed by means of paper or thin layer chromatography.
- *Chemical purity* – assessment of the presence of stable isotope impurities which could be present as a result of production, chemical separation and/or radiolabelling. This is sometimes implied by the radiochemical purity. Chemical purity is derived by comparison to standard solutions.

Requirements for the clinical use of *novel* radionuclides and radiopharmaceuticals are not defined within the International Pharmacopoeia and thus some assumptions must be made for the sake of this study. Monographs of similar radionuclides, in terms of their half-lives and decay type and energy, can be used as a guide to inform researchers of purity requirements for novel ones. It is important to only take this as a guide, as requirements stated in International Pharmacopoeia monographs are a result of thorough safety assessment through years of clinical trials and use. Defining these purity requirements for the terbium isotopes is beyond the scope of this project, so established monographs have been used throughout this study for the purpose of comparison (e.g. ^{67}Ga-citrate for ^{155}Tb)[157].

1.6 Aims and objectives

The production and subsequent purification of the terbium theranostic isotopes (^{149}Tb, ^{152}Tb, ^{155}Tb and ^{161}Tb) is currently in its infancy and is of fundamental importance if the scientific community is to fully explore their theranostic capability and clinical viability.

The primary aim of this study is to develop efficient radiochemical methods which are suitable for the processing of terbium sources post-irradiation. For this, extraction chromatography resins were studied. The aim was to acquire metrological information to quantify the quality of separation achieved using the studied extraction chromatography resins, allowing for a comparison to be made with the commonly used α-HIBA/cation-exchange method[143]. The aim was to develop and optimise methods capable of preparing high purity terbium sources from several of the production routes detailed in Table 1.7.

Method development was conducted using stable isotopes and quantified by mass spectrometry. Method validation was conducted when possible by applying the developed methods to ^{155}Tb sources produced within the remit of the CERN-MEDICIS collaboration[83,84].

This work aims to understand the suitability of extraction chromatography for the purification of terbium with the purpose of encouraging and facilitating further investigation into the metrological and medical use of the four terbium isotopes (i.e., production, (pre)-clinical applications, phantom imaging studies and primary standardisation).

Chapter 2. Materials and Methods

2.1 Isotope production

Isotope production experiments were an essential part of this research; however, these were not conducted by the author of this report. All isotope production experiments referred to in this report were carried out other researchers within the remit of the CERN-MEDICIS collaboration. This collaborative group brings together research institutes from across Europe and facilitates access to isotope production facilities (e.g., at CERN or Arronax), radiochemical expertise (e.g., at NPL or KU Leuven) and pre-clinal study capability (e.g., at PSI or CTN) to encourage the development of novel nuclear medicine[83,84].

Two production routes at the following facilities are particularly relevant to this study and thus are discussed in more detail here and in the relevant chapters.

2.1.1 Proton-induced spallation at CERN-ISOLDE/MEDICIS and mass separation

Information about the production and mass separation processes at CERN-MEDICIS was provided by Charlotte Duchemin, Thierry Stora and Reinhard Heinke at CERN on 04.09.2020 (European Organization for Nuclear Research, Esplanade des Particules 1, 1217 Meyrin, Switzerland).

This section expands on the content found in section 1.3.1.1. and is related to research reported in Chapter 3 and Chapter 4. Some of the previously mentioned terbium isotopes (^{149,152,155}Tb) are produced by the proton-induced spallation reaction on a tantalum target. An example irradiation scheduled from 27th September to 1st October 2018, which was conducted by researchers at CERN, is detailed herein:

High energy protons (1.4 GeV) from the proton synchrotron booster at CERN are focussed onto and interact with a secondary target containing multiple rolls of high purity tantalum foil which were arranged in a long tantalum tube coupled to a rhenium surface ion source (99.95% purity, 12 μm thick, 15 mm wide, 2 cm diameter, total mass 357 g).

After production, a wide range of elements and isotopes are present. To isolate isotopes of a selected mass (mass-to-charge ratio, A/q), off-line mass separation is available at the CERN-MEDICIS facility (see section 1.3.2)[83,84]. The separated isotopes are collected in a catcher material, often a zinc-coated gold foil (Figure 2.1). The mass separation of a ^{155}Tb produced

by proton irradiation of a gadolinium target is describe here as an example (see Chapter 5). Mass separation work was conducted by scientists at CERN.

In preparation for the collection of ^{155}Tb, the extraction voltage was set to 60 kV, and the extraction electrode positioned after an acceleration gap of 60 mm from the ion source's exit. This way the beam profile displays a gaussian shape of sigma = 0.8 mm at the position of the beam diagnostics before the implantation chamber. Respective currents of 400 A (1300 °C) and 290 A (2100 °C) were applied to heat the target and the line and to allow for preliminary optimization steps on a stable ^{159}Tb mass marker. Terbium-155 was extracted from targets that were heated up to 2200 °C (corresponding to a current of 750 A). The mass-separated ^{155}Tb beam was implanted into a solid catcher (zinc-coated gold foil, thickness: 0.1 mm, purity: 99.95%, Goodfellow Cambridge Ltd. Huntingdon, UK).

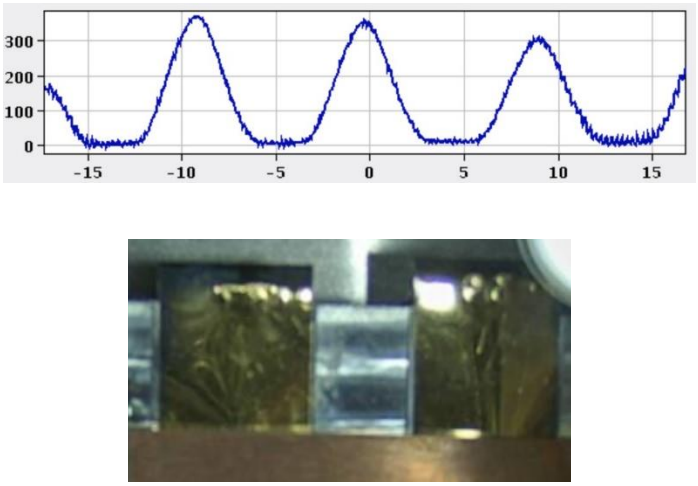

*Figure 2.1 – (**top**) Screenshot taken with the beam scanner, located before the implantation chamber. Beams at A/q = 154,155,156 are seen (153, 157 partly visible). The collected beam is centred on A/q = 155, while isotopes present at other masses are physically removed from the implantation using mechanical slits located ahead of the foil. The horizontal scale is in mm. (**bottom**) Two zinc-coated gold foils in the collection chamber seen from the rear*[86].

As of 2019, the use of a resonance ionisation laser ion source (MEDICIS's Laser Ion Source for Separator Assembly, MELISSA[110]) allowed the enhanced ionisation of a desired element through tuning the laser to the transitions between atomic energy levels and inducing stepwise excitation. This reduces the presence of isobaric and pseudo-isobaric impurities. MELISSA was not available at the CERN-MEDICIS facility for the study reported in Chapter 3[86]. In later studies (Chapter 5) MELISSA was used to selectively enhance the ionization of ^{155}Tb, using a two-step resonant excitation scheme with respective output powers of 0.8 and 1.2 W.

2.1.2 Cyclotron production of terbium isotopes from lanthanide targets

2.1.2.1 The ARRONAX facility

Information about the production at the ARRONAX facility was provided by Nathalie Michel, Ferid Haddad, Cyrille Alliot and Nadia Audouin at ARRONAX on 01.02.2021 (GIP-ARRONAX, Rue Arronax 1, 44800, Saint-Herblain, France).

Production of terbium isotopes by the irradiation of gadolinium target material was studied by researchers (stated above) using the cyclotron at the ARRONAX facility in Nantes, France[158]. The cyclotron routinely operates with hydrogen and helium beams of tuneable energy and current (Table 2.1).

Table 2.1 - Table summarising the characteristics of the ion beams available at ARRONAX. Taken and adapted from Haddad et al. (2008)[159].

Incident Particle	Beam energy range (MeV)	Intensity (μA)
$^{1}H^{-}$	30-70	< 350 (×2)
$^{1}H^{1}H^{+}$	17.5	< 50
$^{2}H^{-}$	15-35	50
$^{4}He^{2+}$	70	< 35

Gadolinium metal foil targets (>99.9% purity, 25 mm × 25 mm, 25 μm thickness, natural isotope abundance) were sandwiched between two graphite plates (500 μm thickness) and were inserted in between two copper plates (Figure 2.2). This package was then loaded into the target station for irradiation with protons (34 MeV $^{1}H^{-}$ on target).

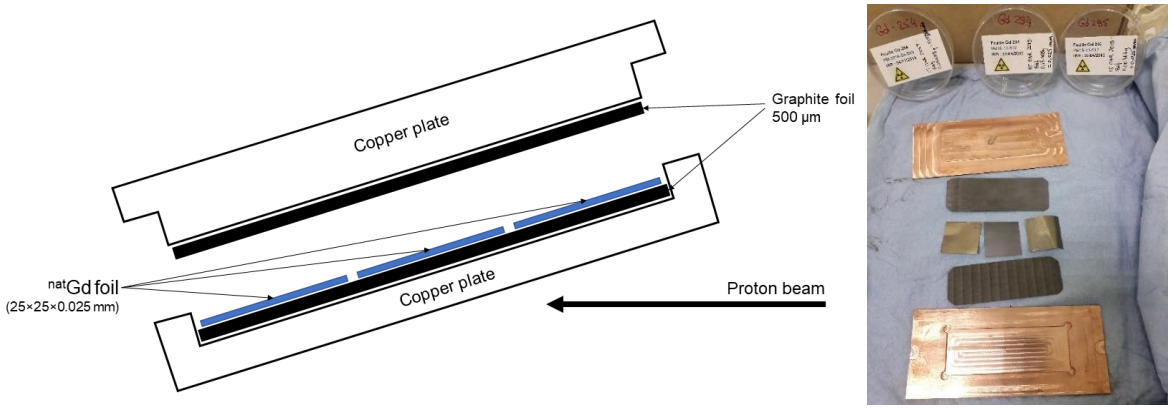

*Figure 2.2 - A simplified schematic of the target arrangement used at the ARRONAX facility (**left**) and an image of the deconstructed target prior to irradiation (**right**). (Figure courtesy of N. Michel et al.)*

After the production, an initial two-step chemical separation was conducted by researchers at the ARRONAX facility using an LN resin method. This significantly reduced the gadolinium excess prior to being sent to CERN-MEDICIS for mass-separation. Mass separation was carried out by scientists at CERN-MEDICIS as per the method reported in section 2.1.1. The samples were then sent to NPL for further chemical processing to isolate the ^{155}Tb from remaining isobaric and pseudo-isobaric impurities using the method developed in Chapter 4 of this study. Purified ^{155}Tb samples were then sent onto other laboratories for SPECT imaging (NPL and KU Leuven), radiolabelling (KU Leuven and Lausanne University Hospital) and metrological studies (NPL).

2.1.2.2 The MC40 cyclotron at the University of Birmingham, UK

Information about the production at the MC40 Cyclotron facility at the University of Birmingham was provided by Ross Allen, Rebeckah Trinder and Tzany Kokalova-Wheldon on 16.07.2021 (University of Birmingham, UK).

Production of terbium isotopes by the irradiation of either gadolinium or europium target material was also studied using the MC40 cyclotron at the University of Birmingham, UK[117]. This cyclotron also routinely operates with hydrogen and helium beams of tuneable energy and current (Table 2.1). This collaborative work is at an earlier stage, so does not feature heavily in this report but was important to consider when developing and optimising the chemical separation methods.

Table 2.2 – A summary of the achievable energy ranges of the ion beams available at the University of Birmingham. Taken and adapted from the University of Birmingham's 'MC40 Cyclotron Facility' webpage (date accessed 21.04.2021)[92,117].

Incident Particle	Beam energy range (MeV)	Intensity (μA)
$^{1}H^{-}$	2.7 - 40	< 20
$^{2}H^{-}$	15 - 35	< 20
$^{3}He^{2+}$	8 - 50	< 4
$^{4}He^{2+}$	10.8 - 40	< 4

Some initial investigation into two terbium production routes was conducted in collaboration with the University of Birmingham:

(i) the irradiation of gadolinium targets with protons - $^{nat}Gd(p,xn)$

(ii) the irradiation of europium targets with alpha particles - $^{nat}Eu(\alpha,xn)$

Two forms of high purity target material can be used at this facility: metal oxide powders and metal foils. When metal oxide targets with natural abundance isotope ratios were used, they were prepared using the following method (Figure 2.3) and secured in the irradiation position using a custom target holder.

1. A known mass of target material (>99.99% purity, oxide form) was added to the target holder
2. The powder was then lightly compressed unto the target holder using a spatula
3. A moulded circle of titanium foil (0.025 mm thickness, ~25 mm diameter) was added on top of the compressed powder and was secured using glue (Loctite ® Super Glue).
4. The targets were compressed further using a packing tool, before being labelled and packaged for shipping to the University of Birmingham.

*Figure 2.3 - A target holder used for the irradiation of gadolinium oxide powder with dimensions annotated (**left**). The preparation of a 1 g Gd_2O_3 target sealed with a thin titanium foil (**middle** and **right**)*

Metal foil targets were prepared by scientists at the MC40 Cyclotron Facility at the University of Birmingham. The larger foil was cut into nine smaller pieces (>99.9% purity, 0.5 mm thickness, natural isotope abundance, ~7 mm × 7 mm) and one piece was secured within a target holder (Figure 2.4). These targets were water-cooled from behind during the irradiation to reduce the chance of the foil melting due to the intensity of energy transfer during irradiation.

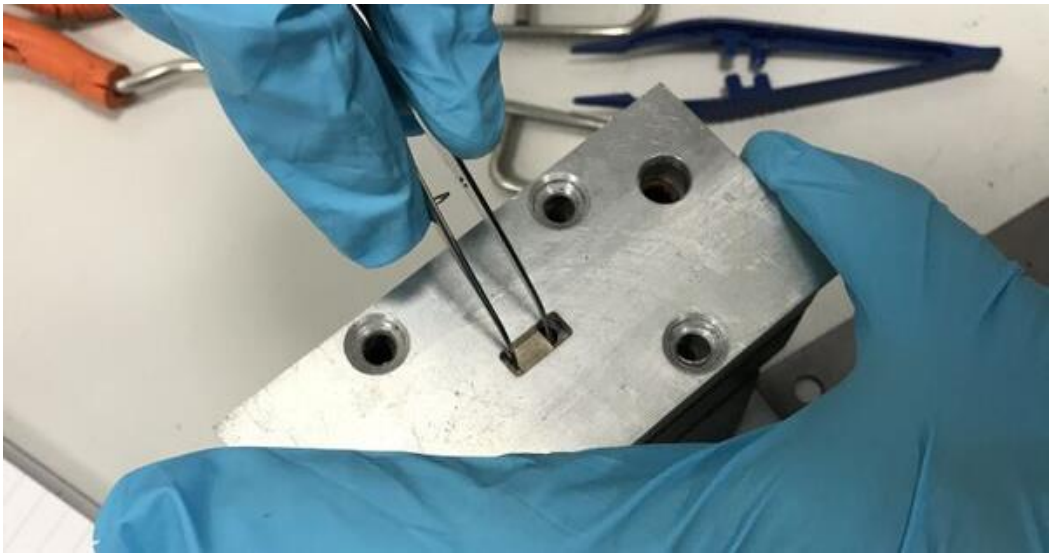

Figure 2.4 - positioning of a europium metal foil within the target holder (Image courtesy of Rebeckah Trinder, University of Birmingham)

2.2 Chemical purification methodology

In these studies, extraction chromatography methods were investigated for the separation of the lanthanide elements in order to prepare high purity radioactive terbium sources. Stable element standards were used throughout for method development and inductively coupled plasma mass spectrometry (ICP-MS) was used for subsequent quantitative analysis. A chemical separation method developed using stable mixtures will perform in the same way when applied to radioactive mixtures[160].

Chromatography-based studies were conducted under either batch or column conditions. Batch studies provide useful information about how each component behaves in a given chromatographic system (i.e., using certain stationary and mobile phases). Batch studies allow for the determination of suitable conditions for a column-based separation and thus, contribute to the development of an efficient column-based chromatographic separation method. Both concepts - batch and column studies - are conducted throughout this work and are henceforth discussed in more detail. An introduction to chromatography and its application to the lanthanide elements is discussed previously in section 1.4.

2.2.1 Batch studies

The distribution coefficients (K_d) can be derived by means of experimental batch separation and is used to illustrate how different elements behave in the presence of a chromatography resin. The K_d value reflects how likely an element is to be held by the studied resin; the higher the K_d value, the higher the probability of strong interaction and *vice versa*.

Batch studies were conducted across a range of acid concentrations in order to understand how the K_d value of an element varies when using a particular chromatography resin. For this, solutions of known elemental concentration, typically 100 ng/mL, were made up in a range of acid concentrations. An aliquot of each solution was taken and analysed by ICP-MS to derive the instrument response for analytes in the initial solutions (CPS_0). A larger aliquot (2 mL) of each solution was then added to separate 15 mL centrifuge tubes containing 0.100 g (± 0.005 g) of chromatography resin. The mixtures were shaken and left for approximately 24 h to ensure that system equilibrium had been reached[124,137,139,161]. The aqueous phase was isolated by passing the mixture though filter paper (Whatman 41 ashless filter paper, 20–25 μm pore size). An aliquot of each filtered solution was then taken and analysed by ICP-MS (CPS_t). Variations

from this method are detailed in the chapters where they arise. Distribution coefficients can then be calculated using the equation below:

$$K_d = \frac{(CPS_0 - CPS_t)}{CPS_t} \times \frac{V}{m} \qquad \textbf{(2.1)}$$

Where, $(CPS)_0$ and $(CPS)_t$ are the concentrations of analyte in the aqueous phase before and after equilibration, respectively, as measured by ICP-MS, V is the volume of solution added to the resin (mL) and m is the mass of resin used (g).

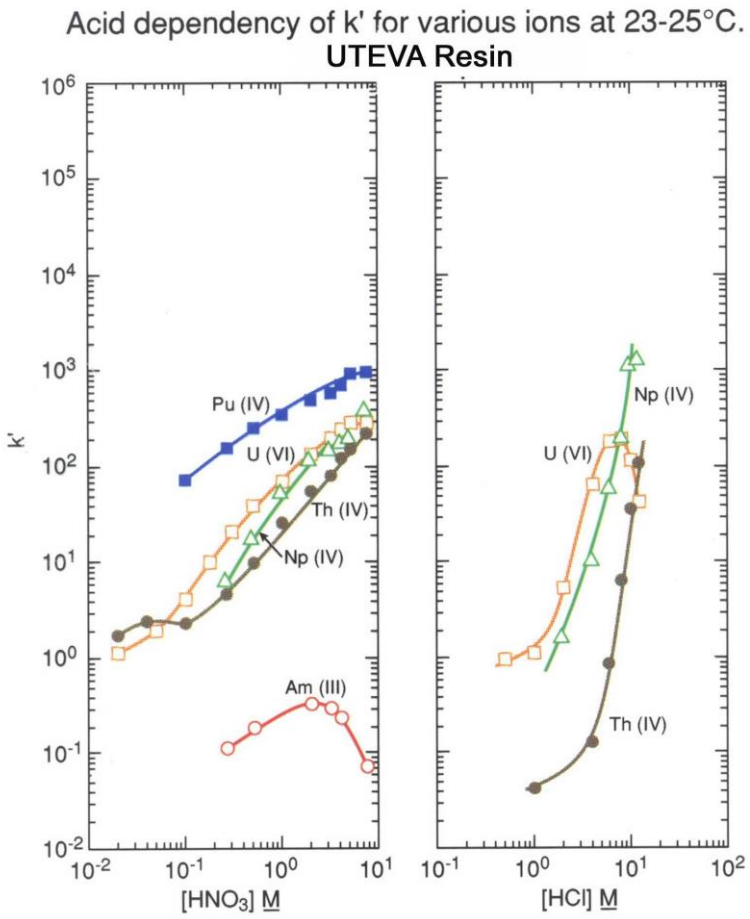

Figure 2.5 - The trend of distribution coefficients of several actinide elements shown on UTEVA resin at varying acid concentrations[162].

Between two different elements, the ratio of K_d values under the same separation conditions gives the separation factor (*SF*, equation **below**). This reflects the difference in affinity the elements have for the two chromatography phases and allows the identification of suitable

conditions for a column-based separation. The higher the separation factor between two elements, the more efficient the separation will be under column conditions.

$$SF = \frac{K_d(A)}{K_d(B)} \qquad (2.2)$$

2.2.2 Column studies

Column-based separations are required for lanthanide mixtures due to the similarities in chromatographic behaviour of the lanthanides. Separation can be achieved by loading the aqueous mixture onto either a commercially available, pre-packed column or a self-prepared column. Pre-packed extraction chromatography columns are available in a limited range of volumes and dimensions which limits the flexibility during method development and optimisation steps.

For situations where an efficient separation cannot be achieved using the commercially available columns, columns of suitable dimensions can be prepared using bulk chromatography resin and empty columns. Throughout this work, glass Econo-Column® columns (*BioRad*) were used which can be used in combination with a peristaltic pump allowing for flow rate control.

A slurry of the resin was prepared by mixing it with a weak acid solution. The slurried resin is then added to the empty column and allowed to settle under gravity to allow for uniform packing. Excess solution was removed from the column before more resin slurry was added to the column. This process was repeated until the column was full of resin and the resin was sealed into the column using a frit. The packed column was then ready to be used but, to ensure that the column does not dry out, it is capped at either end and filled with an excess of dilute acid solution whilst being stored in-between uses (Figure 2.6).

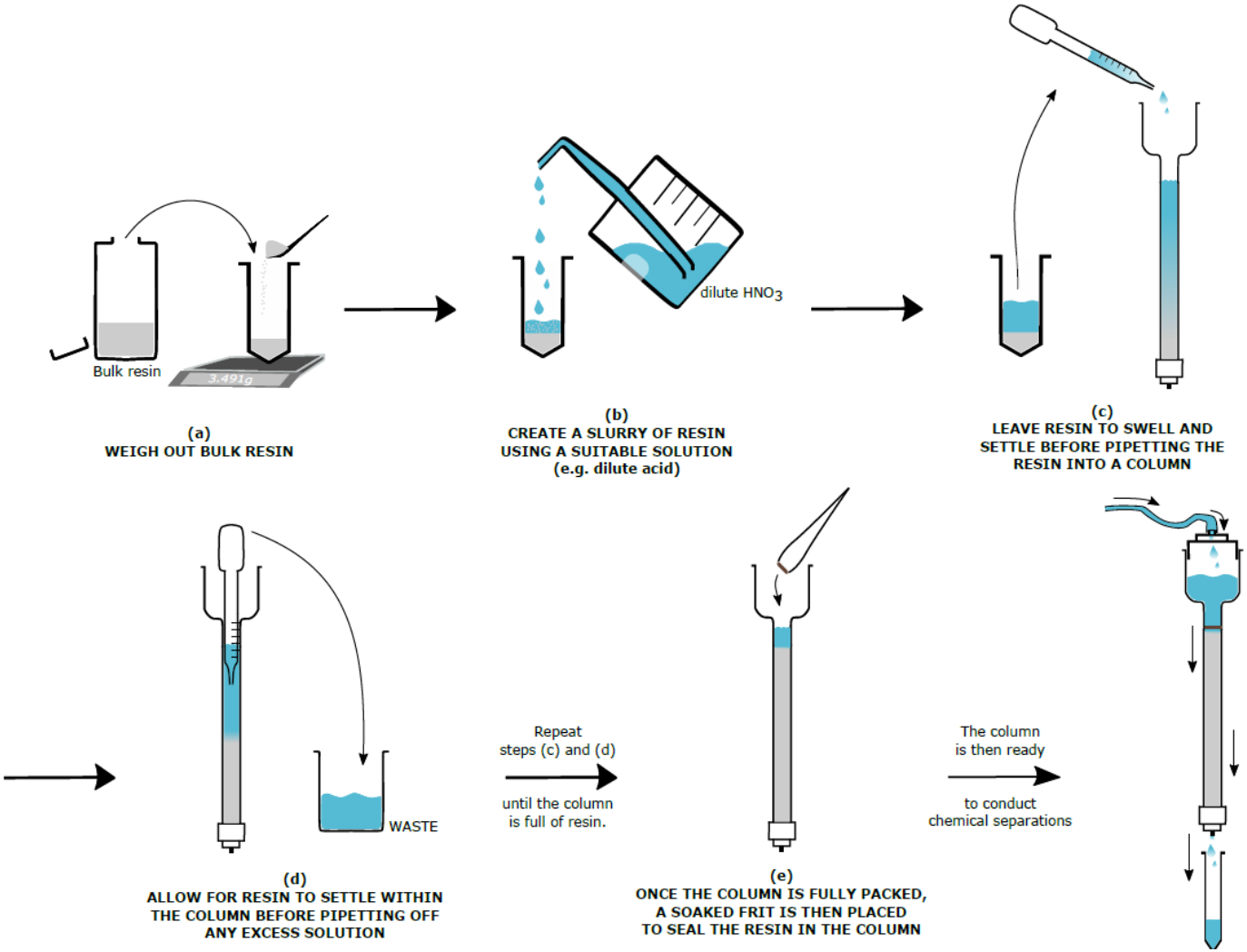

Figure 2.6 - The process of packing a glass Econo-Column® Column with a chosen chromatography resin.

The same generic steps tend to be used when conducting a column-based separation. An example from Carter (2012)[163] of the separation of uranium and thorium on UTEVA resin is used here to illustrate each step. The properties of the mobile phase can be chosen in order to maximise the separation factor based on information found from batch separation studies and the subsequent distribution coefficient calculation, or from previous column separation studies.

The steps are as follows:

- *Pre-condition* – the packed column is pre-conditioned with the same concentration of mobile phase that the element mixture will be loaded onto the column with (e.g., 2 M HNO_3).
- *Load* – the solution that contains the elements requiring separation is loaded on top of the pre-conditioned column (e.g., U and Th in 2 M HNO_3).
- *Wash* – a solution that ensures that elements which are not bound strongly to the column under the loading conditions are washed off the column (e.g., 2 M HNO_3).
- *Elution* – the solutions which are used to selectively elute the components remaining on the column (e.g., 5 M HCl to elute Th, then 0.02 M HCl to elute U). The order in which the solutions are passed through the column is of vital importance.
- *Regeneration* – a solution passed through the column to ensure all components have been stripped off the column to allow for its reuse (e.g., 0.02 M HCl).
- *Recondition* – a solution used to prepare the column for either storage in between uses (e.g., 0.01 M HNO_3) or to pre-condition the column for immediate reuse (e.g., 2 M HNO_3).

The fit-for-purpose concentration and volume of these solutions are derived through the method development. These separation method variables, as well as others, have a significant impact on the quality of separation. Flow rate, the column dimensions and the resin particle size are other characteristics which can be changed to optimise a separation procedure.

In this study, the flow rate of the mobile phase through the column was controlled using a Gilson Miniplus peristaltic pump and was set using the following method:

1. Attach tubing to the pump and fill (‘*prime*’) the tubing with DI water.
2. Weigh a 50 mL beaker.
3. Set pump to 1.00 rpm and pass DI water through the tubing for 5 minutes and collect in the weighed beaker.

4. Weigh beaker (+ DI water) and calculate '*mL/min*' flow rate at 1.00 rpm from the mass difference.
5. Calculate the '*rpm*' flow rate equivalent to the '*mL/min*' flow rate required for the separation
6. Repeat steps 2-4 at new '*rpm*' flow rate to check '*mL/min*' flow rate

To assess the quality of separation throughout all method development steps, fractions of the solutions which eluted from the column were collected and diluted with HNO_3 (2% v/v) prior to ICP-MS analysis. The instrument response for each fraction was then compared to the instrument response of the initial mixture to allow the calculation of the percentage recovery of each element after separation.

$$\boldsymbol{Element\ Recovery}\ (\%) = \frac{(\boldsymbol{CPS})_f}{(\boldsymbol{CPS})_0} \times \mathbf{100} \qquad \textbf{(2.3)}$$

where, $(CPS)_0$ and $(CPS)_f$ are the instrument's response for an element in the aqueous phase before separation and in an individual fraction after separation, respectively, as measured by ICP-MS.

If no sample was taken before the separation was conducted, the sum of the instrument responses of all fractions was used ($\sum(CPS)_f$), equation 2.4). Calculating the element recovery in this way assumed that all of the elements had been recovered from the column. This has been termed as the normalised elemental recovery.

$$\boldsymbol{Normalised\ Element\ Recovery}\ (\%) = \frac{(\boldsymbol{CPS})_f}{\sum((\boldsymbol{CPS})_f)} \times \mathbf{100} \qquad \textbf{(2.4)}$$

where, $(CPS)_f$ is the concentration of an element in an individual fraction after separation as measured by ICP-MS, and $\Sigma((CPS)_f)$ is the sum of the CPS values for that same element from all fractions.

The *(CPS)* values used in these calculations were blank, dilution and/or internal standard corrected. When necessary, the total element recovery of an element was calculated by the sum of multiple or all element recovery values.

2.3 Measurement methodology

2.3.1 Inductively coupled plasma mass spectrometry overview

An Agilent 8800 series inductively coupled plasma triple quad mass spectrometer (ICP-QQQ-MS, Figure 2.7) was used for the measurement of samples containing stable isotopes mixtures. The instrument is equipped with two quadrupole mass filters, one positioned either side of an octopole collision/reaction cell. The instrument was operated using Mass Hunter version 3.7[164].

An autosampler allows for multiple samples to be run in a single procedure. Aqueous samples are introduced into the instrument using a peristaltic pump. The aqueous solutions pass through a nebuliser which produces an aerosol of the sample that passes to a spray chamber (in this study a double pass spray chamber design). The spray chamber sorts droplets by size, allowing smaller droplets that are more easily ionised to pass into the plasma. Larger droplets are rejected and pumped out of the spray chamber as waste. The spray chamber is Peltier-cooled and maintained at a temperature of 2°C, so that droplets of a uniform size pass into the plasma, even if environmental conditions in the laboratory change during the course of a run. This is important as the ionisation efficiency in the plasma will vary if the droplet size fluctuates with spray chamber temperature. The amount of sample that passes through to the plasma varies with nebuliser and spray chamber design, but in this study is ~8-9 %.

The sample passes into the inductively coupled plasma (ICP). Argon gas flows into the quartz torch, and an electric spark introduces free electrons into the gas. An RF oscillating magnetic field is connected to an induction coil that accelerates the electrons at 27 MHz, causing electrons to combine with argon atoms to produce positive argon ions. These argon ions then combine with electrons to produce argon atoms, and this equilibrium produces an inductively coupled plasma, with a temperature of approximately 10,000 Kelvin. Ions in the sample are introduced to the ICP, where they are evaporated, atomised and ionised to produce a beam of singly charged positive ions.

The ion beam passes from atmospheric conditions during sample introduction to vacuum conditions, causing the ion beam to expand. Sample and skimmer cones positioned after the torch focus the central part of the ion beam, followed by an off-axis extraction lens at a negative voltage. Positive ions in the beam follow the path of the extraction lens, whilst photons and neutral species are removed, reducing instrument background.

A quadrupole mass analyser is used to separate ions by their mass-to-charge ratio. The quadrupole consists of two positive and two negative poles, across which a voltage is applied. The voltage is unique to each mass-to-charge ratio, with ions of the selected value passing between the poles to the detector. Ions at all other mass-to-charge ratios will collide with one of the poles, lose their charge and not reach the detector. Multiple mass-to-charge ratios can be measured within a single run. The instrument in this study has an additional quadrupole and a collision-reaction cell, the roles of which are explained later in this section.

The instrument is equipped with a dual-mode secondary electron multiplier detector. The output from the detector is in counts per second, with 'pulse mode' operating up to 1.5×10^6 CPS, and 'analogue mode' operating at higher count rates. The detector has a linear dynamic range of nine orders of magnitude and automatically switches between pulse and analogue modes[165,166].

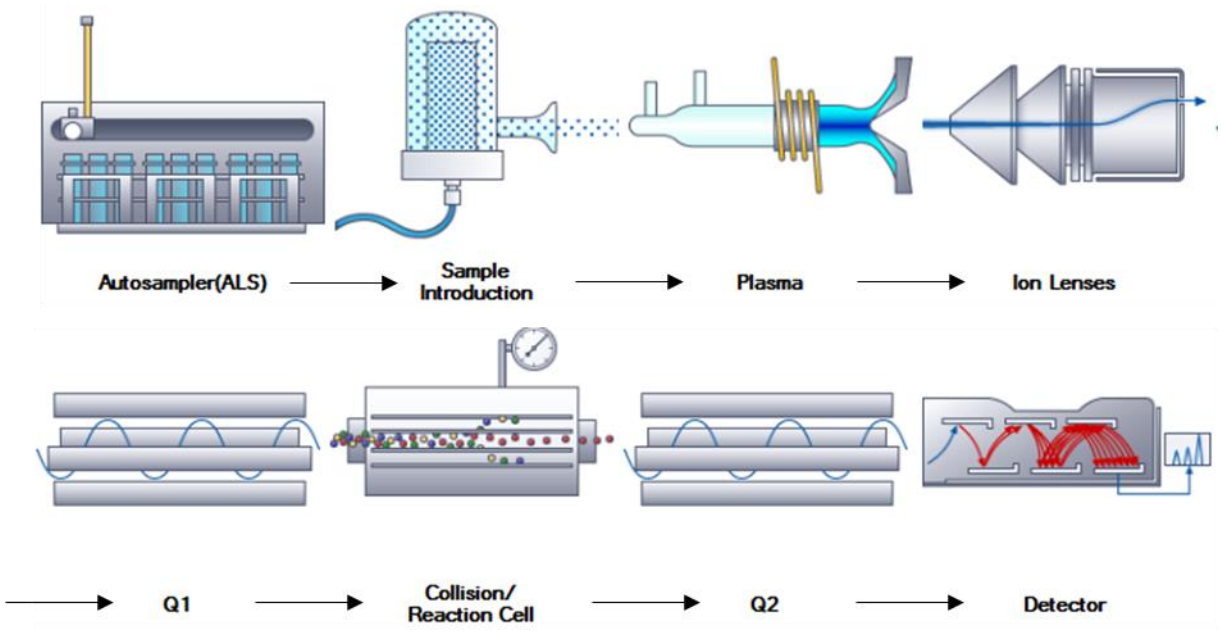

Figure 2.7 - A schematic of the Agilent 8800 ICP-QQQ-MS. Arrows denote the direction of sample through the instrument when both quadrupoles and the collision/reaction cell is used (Agilent ICP-MS MassHunter Workstation software v. 3.7, Agilent Technologies).

A daily tune procedure was run prior to analysis using a mixed element standard (1 ng/mL beryllium, yttrium, cerium and thallium in 2% v/v HNO_3). This method assesses the sensitivity of the instrument across a mass range (Be, Y and Tl) and identifies the degree to which oxide polyatomic species and doubly charged ions are formed within the plasma (Ce). The tune

procedure also assesses the uncertainty in the measurement at each mass, the peak mass, and the peak axis resolution. Threshold values for each parameter assessed in the tune procedure is summarised in Appendix A.

Instrument stability throughout analysis runs was monitored using an internal standard (e.g., 10 ng/mL ^{115}In, ^{209}Bi). The internal standard was introduced via a dedicated line positioned before the nebuliser. The tubing was loosely tied up to encourage a more turbulent flow. Corrections were made for any instrumental signal drift by comparing the change in internal standard signals to the first internal standard measurement.

A blank sample was run at the start of the procedure and throughout analysis runs. There was also an instrument wash cycle between each sample. All of this helped to minimise cross-contamination between samples.

Raw data from the ICP-MS were collected using ICP-MS MassHunter Workstation[164] and analysed using Microsoft Excel 2019[167] and OriginPro 2020[168]. Corrections were made to account for the background signal and any instrumental drift during analysis runs using the internal standard. Any sub-sampling and dilutions were also corrected.

2.3.2. Interferences

Interferences need to be removed in order to have confidence in the final measurement. The Agilent 8800 series ICP-QQQ-MS used in this study is capable of carrying out on-line spectral interference removal: namely, the removal of isobaric, polyatomic and tailing interferences[169–171]. These interferences are defined as follows:

- *Isobaric interferences* – components of the plasma gas or the sample which have a very similar mass as the analyte to be measured, which the detector cannot resolve. For example, ^{40}Ca and ^{40}Ar isotopes interfere with the detection of ^{40}K at m/z 40.
- *Polyatomic interferences* – a compound most commonly formed in the plasma with atoms present in the sample matrix (e.g., ^{1}H, ^{16}O) and/or plasma (e.g., ^{40}Ar). For example, $^{165}Ho^{1}H^{+}$ is a polyatomic species which interferes with the detection of erbium at m/z 166 (Figure 2.8)[172,173].
- *Tailing effects* – where an element of a neighbouring mass (one or two mass units on the high or low mass side) to the analyte is present, typically in larger quantity

compared to the analyte. The signal tails over into the m/z of the analyte and therefore interferes with the detection of the analyte (Figure 2.8). For example, a bulk quantity of ^{165}Ho may tail and interfere with the measurement of erbium at m/z 166 and dysprosium at m/z 164.

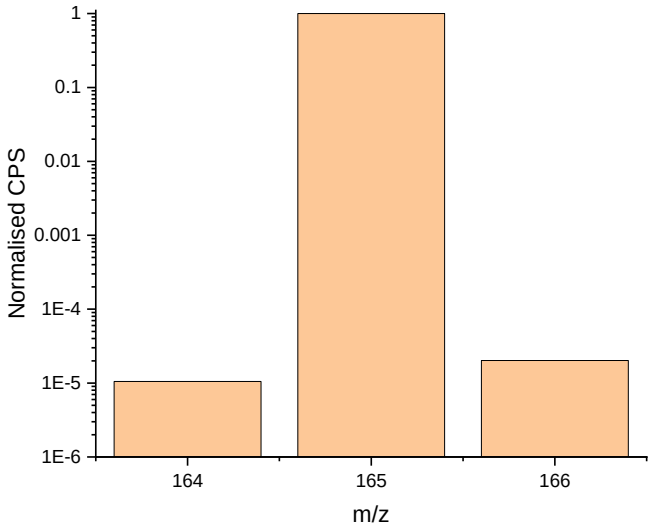

Figure 2.8 - The tailing of a signal at 165 m/z, from a 10 µg/mL Ho solution, into the neighbouring masses (164-166 m/z) measured in SQ mode. The formation of a holmium hydride polyatomic (HoH+) could also be contributing to the signal at 166 m/z.

2.3.3 ICP-QQQ-MS interference removal

The instrument can be operated in one of four modes: single quad mode (SQ), SQ gas mode, MS/MS mode and MS/MS gas mode. The gases can be used individually or in combination and can be either a reaction gas (O_2, NH_3/He, H_2) or a collision gas (He). Each mode can provide different degrees of interference removal and are these summarised below:

- *SQ mode* – only uses the second mass filter quadrupole (Q2) set to analyse at the optimal m/z of the elements of interest. This method is commonly used for analysis where the presence of polyatomic, isobaric, and tailing inferences is unlikely. For example, a mixture containing europium and terbium can be measured, simultaneously, in SQ mode at m/z 153 and m/z 159, respectively.
- *SQ gas mode* – Sample ions enter the reaction/collision cell and interact with a chosen gas before undergoing mass filtering.

- If a collision gas is chosen (e.g., He), polyatomic species will have a higher probability of interacting with the gas resulting in a loss of kinetic energy. The cell has kinetic energy discrimination at the exit, therefore, only ions with enough kinetic energy at the chosen mass-to-charge (m/z) ratios will be analysed. The analyte ion will lose some energy and transmission of analytes out of the collision cell will be slightly reduced, but this will happen to a greater extent for polyatomic species. This method is therefore efficient at reducing the measurement interference caused by polyatomic interferences.
- If a reaction gas is chosen (e.g., O_2), the ions will form polyatomic species in the cell to different degrees depending on formation probabilities. By example: SQ mode (no gas) is not be a suitable method[174] to quantify $^{90}Sr^+$ in samples also containing the isobaric interference, $^{90}Zr^+$. However, if the ions enter the reaction cell containing O_2 (i.e., using SQ gas mode), it is thermodynamically favourable for $^{90}Zr^+$ to form $^{90}Zr^{16}O^+$, whilst ^{90}Sr remains on mass. Therefore, ^{90}Sr can be measured at the mass-to-charge ratio of its ion (i.e., $^{90}Sr^+$ at m/z = 90) and, if required, ^{90}Zr can be measured at the mass-to-charge ratio of the polyatomic species formed (i.e. ZrO^+ at m/z = 106). However, if germanium is present in the sample, then the polyatomic species, $^{74}Ge^{16}O^+$, could form in the reaction cell, which would result in the formation of a new interference in the detection of $^{90}Sr^+$.

- *MS/MS mode* – Ions pass through both mass filters (Q1 and Q2) set at the optimal mass to detect the desired elements. This method is particularly effective at removing tailing interferences. By example: for the detection of trace quantities of $^{166}Er^+$ in the presence of a significant quantities of $^{165}Ho^+$, the use of only one quadrupole (i.e., SQ mode) would not get rid of tailing interferences when analysing the $^{166}Er^+$ at 166 m/z. It is therefore advantageous to run the instrument in MS/MS mode. It should be noted that this method would not remove any hydride polyatomic species (i.e., $^{165}Ho^1H^+$) that may have formed, and this still would result in inaccurate quantification of the $^{166}Er^+$ present. The abundance sensitivity in MS/MS mode is ~ 10^{-10}, compared to ~10^{-6} in SQ mode.
- *MS/MS gas mode* – Ions undergo mass filtering before they enter the collision/ reaction cell, such that ions of only one m/z value will interact with the reaction/collision gas. After passing through the cell, the ions will undergo a second level of mass filtering before detection. An example is shown in Figure 2.9**.**

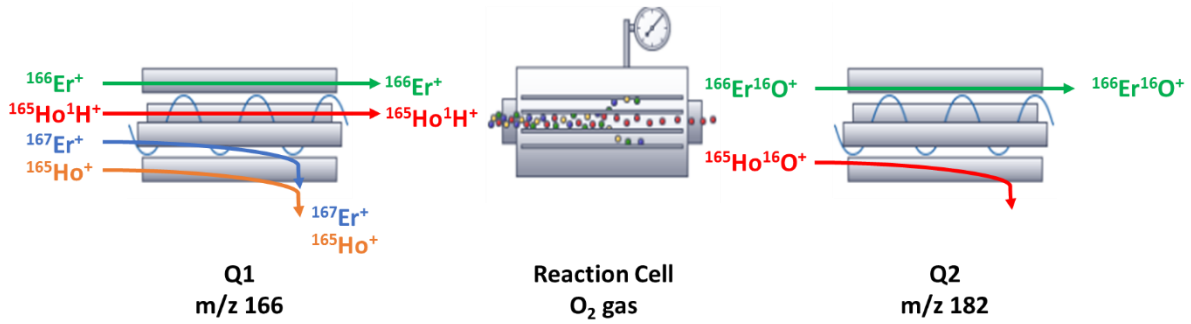

Figure 2.9 - The interference-free measurement of ^{166}Er in the presence of a bulk amount of ^{165}Ho using MS/MS mode with O_2 reaction gas[175,176].

In situations where measurement interferences were absent, the instrument was run in SQ mode (Table 2.3). When interferences remained, further instrumental tuning was required. These methods are described in detail in the relevant chapters.

Table 2.3 - The standard SQ mode operating parameters for ICP-MS measurement.

Parameter	Setting
Scan mode	SQ
Plasma conditions	Low Matrix
RF Power (W)	1550 W
Plasma gas flow rate (L/min)	15.0
Nebulizer gas flow rate (L/min)	1.0
S/C temperature (°C)	2
Extract 1 (V)	0.0
Extract 2 (V)	-200.0

2.3.2 Gamma-ray spectrometry

Gamma-ray spectrometry was used throughout this study to quantify the presence of radioactive isotopes in samples produced at isotope production facilities (see section 2.1). Gamma-ray spectrometry analysis was not conducted by the author of this paper, but by colleagues in the Nuclear Metrology Group at the National Physical Laboratory[86,177,178].

The detectors used in this work were placed within a 1.5 m × 1 m × 1 m lead shield container with 10 cm thick walls. The container was graded with a liner of 0.5 mm cadmium and 0.7 mm copper to reduce interferences from background radiation and lead fluorescence X-rays in

spectrum. Samples were mounted approximately 15 cm from the detector window along the horizontal axis using a kinematic mounting plate holding a precision engineered sample holder (Figure 2.10). This sample holder enabled highly reproducible geometric source positioning.

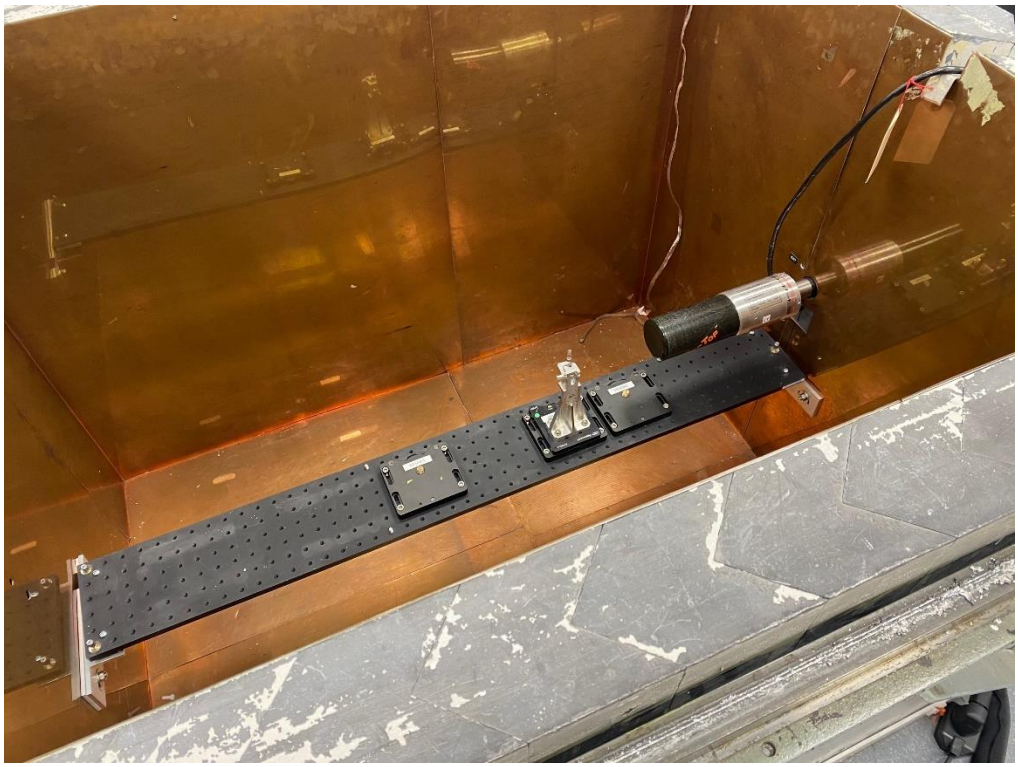

Figure 2.10 – the gamma-ray spectrometry set-up at the National Physical Laboratory showing the HPGe gamma-ray detector, sample holder, mounting plates, lead shielding and graded copper/cadmium lining. Sources measured for this work were placed in the mounting plate on the left, ~15cm from the detector.

For the work in Chapter 3 an n-type High Purity Germanium (HPGe) γ-ray spectrometer with a resolution (full width at half maximum, FWHM) of 1.79 keV at 1.33 MeV and relative efficiency 28% was used for the measurement of fractions before and after chemical separation. This allowed for the determination of the $^{139}Ce/^{155}Tb$ ratio (see section 3.2.3).

For the work reported in Chapter 5, the measurements that were conducted at NPL used a p-type HPGe gamma-ray spectrometer with a resolution (FWHM) of 585 eV and 1.8 keV at 122 keV and 1.33 MeV respectively and a relative efficiency of 9.5 % was used to determine the activity of the radionuclides present in the collected samples.

In both cases, the pulse signals from the pre-amplifier were processed using a CANBERRA LYNX digital signal analyser (DSA) and the spectrum recorded using the CANBERRA GENIE 2000 v3.4.1 spectrometry software[179]. The full-energy peak (FEP) detection efficiency

of each detector for a geometry of 1 g of H_2O in a 2 mL ISO ampoule had been previously determined across an energy range from 60 keV to 1836 keV using a suite of standards traceable to primary standards developed at NPL. The FEP detection efficiency curve was fitted using the CANBERRA GENIE 2000 v3.4.1 software using two polynomials to fit the region between 60 keV to 122 keV (quadratic) and 122 keV to 1836 keV (order 4) (see Collins et al.[177] for more details).

The nuclear data (half-lives and γ-ray emission intensities) used to determine the activities of detected radioisotopes were taken from the evaluated databases of ENSDF[6] and the DDEP[180], or using values derived at NPL which are yet to be published (see Table 5.2)

2.4 Materials and reagents

A range of HNO_3 (Trace Analysis Grade, Fisher Scientific) and HCl (Trace Analysis Grade, Fisher Scientific) solutions were prepared by diluting the concentrated acids with ultra-pure water (ELGA PURELAB Flex, Veolia Water, Marlow, UK, 18 MΩ cm, <5 ng/mL Total Organic Carbon). These solutions were used for both column and batch studies, and for ICP-MS analysis.

For the majority of the chemical separation method development and the ICP-MS detection method development processes, stable element standards were used. The starting concentrations of the standards were between 100 – 10 000 µg/mL (Ba → Lu, Fisher Chemical, Alfa Aesar SpecPure, Assurance SpexCertiprep and Johnson Matthey) and these were diluted down to the desired element concentration using HNO_3 or HCl solutions.

Solid reagents used for separation method development steps included: sodium bromate ($NaBrO_3$, Alfa Aesar), gadolinium oxide ($^{nat}Gd_2O_3$, Alfa Aesar, <10 µm powder, 99.999% purity), potassium chloride (KCl, Acros Organics, 99%+ purity) and zinc chloride ($ZnCl_2$, Aldrich, 99.995% purity).

All chromatography studies reported used extraction chromatography and/or ion-exchange chromatography resins. Used resins and their characteristics are summarised in Table 2.4.

Table 2.4 - A summary of the chromatography resins used.

Resin name	Resin type	Manufacturer	Active component	Bead size
UTEVA	Extraction	Triskem	DAAP	100-150 μm
TEVA	Extraction	Triskem	Aliquat® 336	100-150 μm
TK100	Extraction	Triskem	HDEHP and crown ether	100-150 μm
AG1-X8	Anion exchange	Bio-Rad	Quaternary amine, chloride form	106–180 μm
LN	Extraction	Triskem	HDEHP	50-100 μm
LN2	Extraction	Eichrom	HEH[EHP]	50-100 μm

DAAP = diamyl, amylphosphonate, HDEHP = di-(2-ethylhexyl)phosphoric acid, HEH[EHP] = 2-ethylhexylphosphonic acid mono-2-ethylhexyl ester

Commercially available 2 mL pre-packed cartridges (UTEVA and TEVA) or self-packed Bio-Rad glass Econo-columns (LN resin) were used for column-based separations. The mobile phase was introduced to the column using a peristaltic pump (Gilson Miniplus evolution) and connective tubing (Gilson PVC tubing), allowing for flow rate control. For less precise flow rate control, a vacuum box (Vacuum box, polycarbonate, 12 positions, *Triskem International*) was used.

Plastic centrifuge tubes (15 mL and 50 mL, Fisherbrand) were used throughout for batch studies, for collection of column fractions during chromatography method development and validation steps, as well as for ICP-MS method development and sample analysis.

Chapter 3. Removal of radioactive cerium impurities from ^{155}Tb sources produced by proton-induced spallation

This work was published in Nature Scientific Reports (Appendix O):

B. Webster, P. Ivanov, B. Russell, S. Collins, T. Stora, J. P. Ramos, U. Köster, A. P. Robinson and D. Read, Chemical Purification of Terbium-155 from Pseudo-Isobaric Impurities in a Mass Separated Source Produced at CERN, *Sci. Rep.*, 2019, **9**, 10884[86]

3.1 Impurities present in ^{155}Tb sources produced by proton-induced spallation at CERN

One of the routes for producing significant quantities (MBq) of ^{155}Tb is by proton-induced spallation on a tantalum target (sections 1.3 and 2.1)[83,84]. Subsequent mass separation can be used to provide some initial separation of the terbium from the target material and from some other co-produced isotopes, but it does not alleviate the need for further chemical separation as some isobaric (i.e., ^{155}Gd, ^{155}Eu and ^{155}Dy) and pseudo-isobaric (i.e., ^{139}Ce^{16}O, ^{139}La^{16}O) impurities, both stable and radioactive, remain. One substantial radioactive impurity, ^{139}Ce, was identified in a mass separated ^{155}Tb source supplied to NPL by CERN-ISOLDE in September 2017[181,182].

The isolation of individual lanthanide elements is challenging and requires well-defined separation procedures in order to be effective. Ordinarily, the application of preparative chromatography techniques is used to isolate a single lanthanide element, but these often are time and skills intensive (see section 1.4).

Cerium is an exception amongst the lanthanide series, as it can be easily oxidised from a III+ oxidation state to a IV+ state in relatively mild oxidising conditions[183]. This change in oxidation state has a significant effect on its chemical behaviour, particularly in terms of its speciation and coordination number in aqueous solution, and this can be utilised alongside chromatographic techniques to allow for its isolation from other lanthanide elements. Terbium, however, is very stable in a III+ oxidation state. Terbium can only be oxidised to the IV+ state using much stronger oxidising reagents and this has only been observed in concentrated carbonate solutions or in inorganic solids[184–186].

Therefore, the selective oxidation of cerium and subsequent chromatographic separation was investigated in the attempt to develop a quicker and easier-to-use alternative to the traditional lanthanide separation approaches. Extraction and ion exchange chromatography resins were chosen based on their affinity for IV+ species.

Currently, no purity requirements have been set for ^{155}Tb in the international pharmacopoeia due to the infancy of research into its clinical use. Therefore, the purity requirements for ^{67}Ga (t½ = 3.26 d[187]) have been used here as a guideline and comparison[157]. Gallium-67 was chosen due to its similar decay properties to ^{155}Tb (i.e., half-life, decay type, main gamma energy). The monograph for ^{67}Ga-citrate states that a radionuclidic purity ≥ 99% is required[157]. Thus, the separation method was designed to achieve a terbium purity ≥ 99% as well as to maximise terbium recovery.

3.2 Chemical separation of terbium from cerium impurities

All method development studies were conducted using stable element standards which have identical chemical properties to radioactive isotopes of the sample element. Measurement of samples throughout the method development process was achieved using ICP-MS analysis in SQ mode with no reaction/collision gas (Table 2.3).

3.2.1 Method development

3.2.1.1 Batch separation studies

The adsorption of terbium and cerium onto ion exchange (AG1) and extraction chromatography resins (TEVA, UTEVA and TK100) was studied over a range of nitric acid concentrations (2–10 M). Nitric acid solutions (2 mL), containing a mixture of 100 ng/mL stable cerium and terbium, were prepared by the dilution of standard element solutions (10 000 µg/mL Ce, Assurance SpexCertiprep and 1 000 µg/mL Tb, Johnson Matthey). An aliquot was taken from each solution for ICP-MS measurement. The remaining solution was added to 0.1 g of resin (UTEVA, TEVA, TK100 or AG1). Sodium bromate (0.1 M, 0.03 g, *Sigma Aldrich*) was added to identical samples to assess changes in adsorption to the resin as a result of selective oxidation of cerium. In all cases, the samples were shaken and left to equilibrate for 24h. After equilibration, the solutions were filtered to isolate the aqueous phase (Whatman 41 ashless filter paper, 20–25 µm pore size). An aliquot was taken from each sample, diluted with HNO_3 (2% v/v) and analysed by ICP-MS.

The adsorption of terbium and cerium onto each resin was quantified by calculating distribution coefficients (K_d) using the previously described method (equation 2.1). Separation factors (SF) between terbium and cerium in the same chemical environment were calculated using equation 2.2.

Pronounced cerium adsorption was observed in the presence of an oxidant (0.1 M $NaBrO_3$) on all of the studied chromatography resins. The adsorption behaviour of terbium was unchanged in the presence of the oxidant. This suggests that selective oxidation of Ce(III) to Ce(IV) was achieved, leaving terbium in its III+ oxidation state (Figure 3.1, Appendix B).

Significant cerium adsorption (K_d = 100-1000) was observed at high HNO_3 concentrations (8-10 M) on all four resins, whilst terbium adsorption remained minimal across the concentration range (K_d = 0.1-10). The highest separation factors (equation 2.2, SF > 100) were obtained on TEVA and UTEVA resins. Owing to the information obtained from these batch studies it was decided that only TEVA and UTEVA resins were to be investigated further (Figure 3.2).

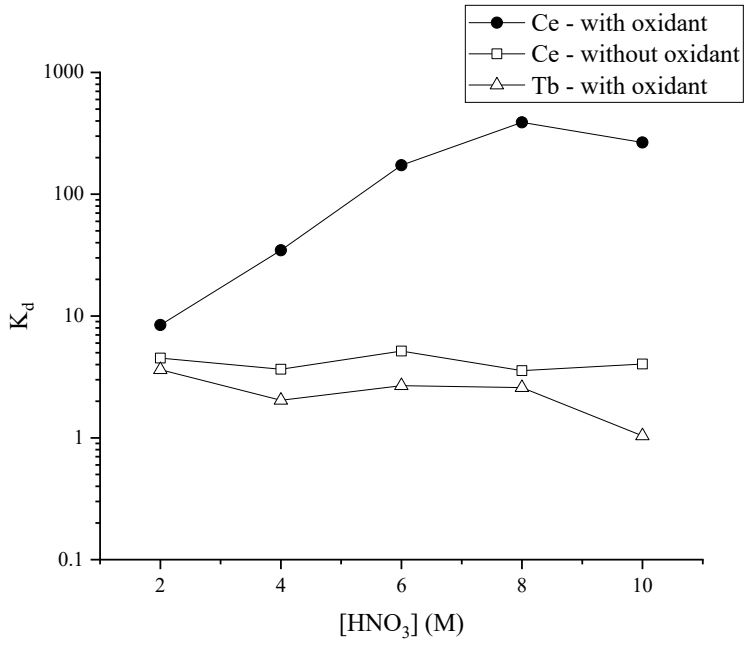

Figure 3.1 - Distribution coefficients (K_d) of Tb(III), Ce(III) and Ce(IV) on UTEVA extraction chromatography resin across a range of HNO_3 concentrations. (Appendix B)

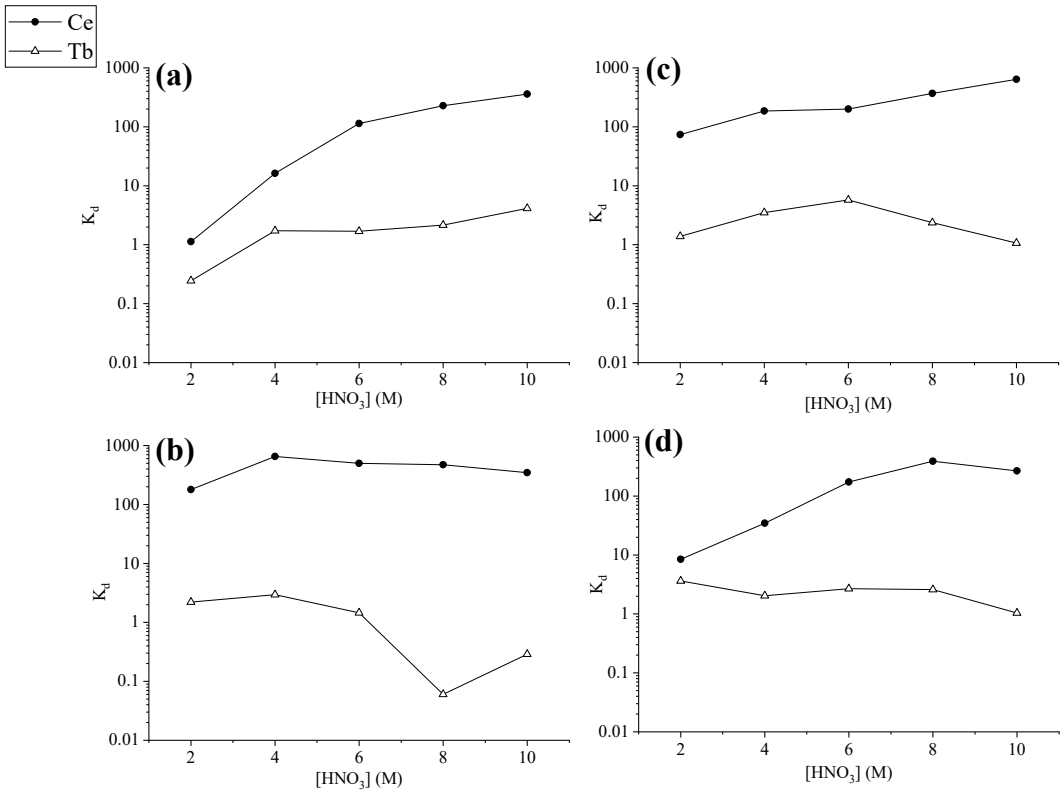

*Figure 3.2 - Distribution coefficients (K_d) of Tb (III) and Ce(IV) across a range of HNO_3 concentrations on **(a)** AGI ion exchange resin, **(b)** TEVA resin, **(c)** TK100 resin, **(d)** UTEVA resin. (Appendix C)*

3.2.1.2 Kinetic studies

Single experiments were conducted using UTEVA resin to demonstrate the kinetic behaviour of terbium and cerium. The rate of adsorption and the rate of cerium oxidation were studied by means of batch separation in order to identify any rate limiting factors of the separation method.

For the derivation of the rate of adsorption, a 10 M HNO_3/0.1 M $NaBrO_3$ solution containing 100 ng/mL of both cerium and terbium was prepared. The solution was left for 24 hours to allow for the oxidation of cerium. Aliquots (2 mL) were added to separate vials containing UTEVA resin (0.1 g) and these were left in static conditions before filtering at regular time intervals under vacuum (60 seconds – 180 minutes).

Similarly, to assess the rate of cerium oxidation, $NaBrO_3$ (0.1 M, 0.03 g) was added to a 10 M HNO_3 solution (2 mL) containing 100 ng/mL cerium, 100 ng/mL terbium and 0.1 g UTEVA resin. Repeat samples were left in static conditions before filtering at regular time intervals under vacuum to ensure rapid removal of the aqueous phase from the chromatographic material (90 seconds – 180 minutes).

Throughout both studies, aliquots of the solutions were taken before and after contact with the resin. These aliquots were diluted with HNO_3 (2% v/v) and analysed by ICP-MS. The distribution coefficients (K_d) were then calculated using equation 2.1 which allowed the rates of adsorption and oxidation to be estimated.

Both rapid cerium adsorption (<60 s, Figure 3.3.a) and rapid cerium oxidation (<90 s, Figure 3.3.b) were observed, which suggested that neither the rate of adsorption nor the rate of oxidation would be a limiting factor whilst carrying out column-based separations.

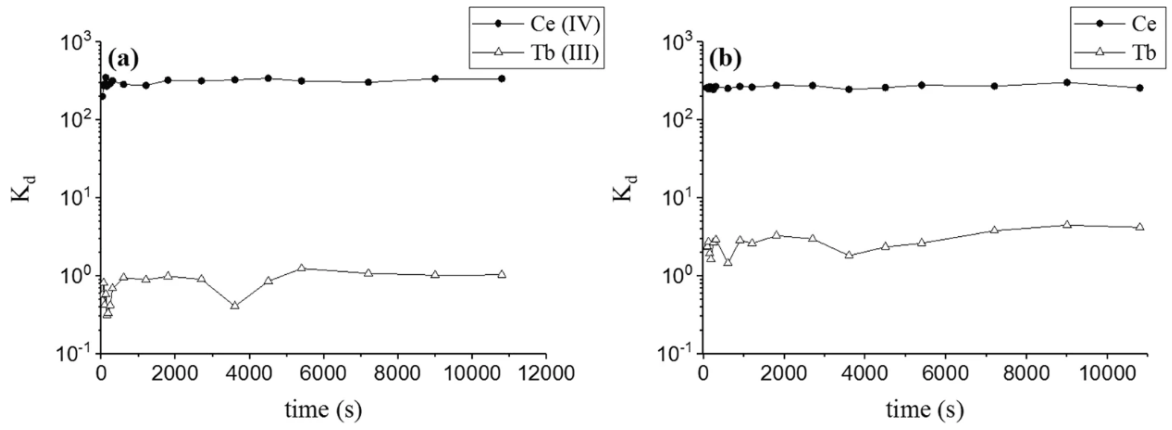

*Figure 3.3 - Kinetics of the **(a)** adsorption of Tb (III) and Ce (IV) to UTEVA resin, and of the **(b)** oxidation of cerium in a 0.1 M $NaBrO_3$/10 M HNO_3 solution. Measured as the change in distribution coefficient (K_d) as a function of time.*

3.2.1.3 Column separation studies

Owing to the favourable adsorption and kinetic behaviour, the column-based separation of terbium from cerium was subsequently studied using commercially available UTEVA and TEVA cartridges.

A pre-packed UTEVA cartridge (2 mL, 50-100 µm, *Triskem International*) was pre-conditioned with 8 M HNO_3. An 8 M HNO_3 solution (10 mL) containing 0.1 M $NaBrO_3$, 100 ng/mL cerium and terbium was introduced onto the resin. Nitric acid (8 M, 10 mL) was washed through the cartridge to ensure terbium elution. Elution of cerium was subsequently achieved using 0.1 M HCl (20 mL). A flow rate of approximately 0.3 mL/min was used throughout the separation. Fractions (1 mL) were collected and were diluted in HNO_3 (2% v/v) before analysis by ICP-MS. This separation procedure was also repeated using a conditioned pre-packed TEVA cartridge (2 ml, 50-100 µm, *Triskem International*). No measurements were taken of the initial terbium/cerium mixture. The terbium purity and recovery were estimated by the

comparison of the instrument response (CPS) of the terbium fractions to total instrument response of all fractions.

The column-based separation of terbium and cerium using a pre-packed 2 mL UTEVA cartridge provided excellent terbium purification (0.30 % ± 0.28 % cerium recovery) and recovery (98.25 % ± 1.00 % terbium recovery) in the initial load and subsequent wash solutions (20 mL, 8 M HNO_3). The cerium was also recovered from the column in a later elution step using 0.1 M HCl (<10 mL). Repeating the method using a TEVA cartridge afforded a less successful separation, with a significant cerium impurity (11.27 % ± 7.29 % cerium recovery) remaining in the terbium fraction (Figure 3.4, Appendix D). Elemental recovery values quoted here were calculated using equation 2.4 and refer to the proportion of the element present in fractions 1-15 and the standard deviation between repeats (*n=3*).

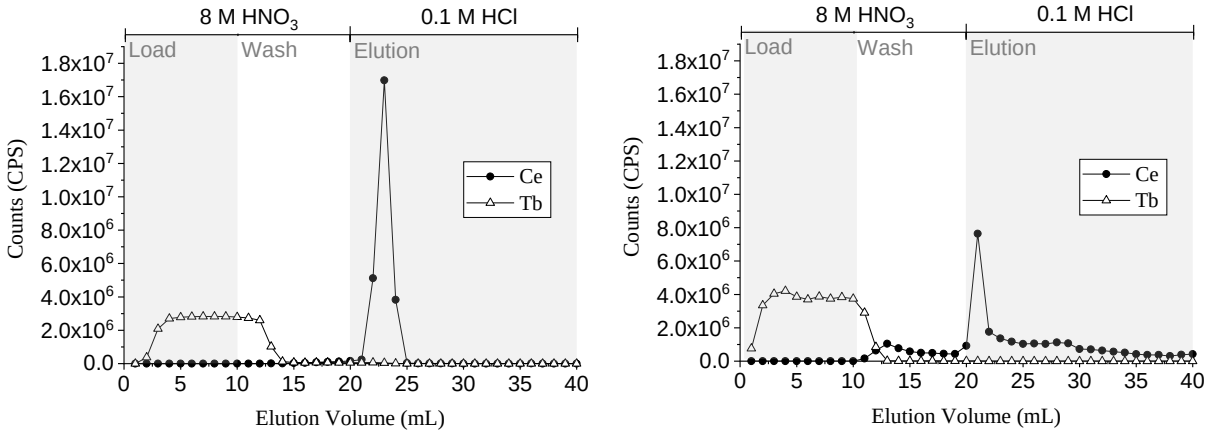

*Figure 3.4 - Elution profiles showing the separation of Tb from Ce impurities on a pre-conditioned 2 mL UTEVA resin cartridge **(left)** and pre-conditioned 2 mL TEVA resin cartridge **(right)**. (Flow rate ~ 0.3 mL/min, n=3)*

This separation contributed to a more complete method designed to process mass separated ^{155}Tb sources deposited onto a zinc-coated gold foil (Figure 3.5). A final chemical conversion of terbium into its chloride form is also reported to allow for further use in metrological and (pre)-clinical studies.

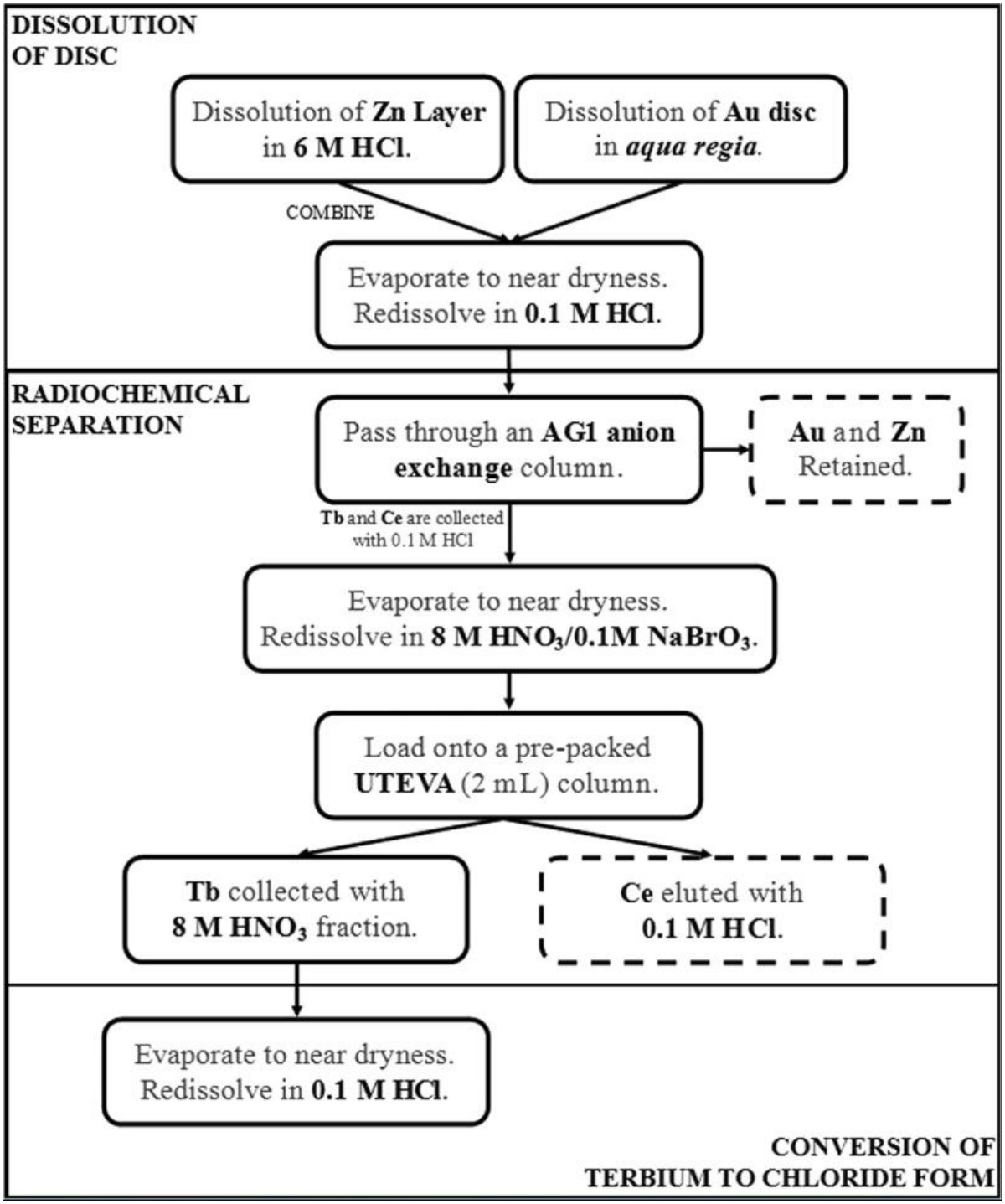

Figure 3.5 - Optimised method for the radiochemical separation and preparation of high radionuclidic purity ^{155}Tb.

3.2.3 Method validation

3.2.3.1 Measurement of ^{155}Tb prior to separation

Gamma spectrometry measurement was carried out by researchers in the Nuclear Metrology Group at NPL as per the method detailed in section 2.3.2. For a mass separated ^{155}Tb source received at the National Physical Laboratory (NPL), UK, from CERN-ISOLDE, Switzerland, gamma ray spectrometric analysis identified the presence of a significant ^{139}Ce impurity ($A_0(^{139}Ce)/A_0(^{155}Tb) = 0.30 \pm 0.02$, Table 3.1, where A_0 refers to the activity which has been decay corrected to the reference time: 2017-09-29 12:00 UTC).

3.2.3.2 Isolation of ^{155}Tb from ^{139}Ce impurities

The derived separation method (Figure 3.5) was applied to this ^{155}Tb source by scientists within the Nuclear Metrology Group at NPL and removed ^{139}Ce such that it was no longer observable above the Compton continuum background ($D_{L,0}(^{139}Ce)/A_0(^{155}Tb) = 0.00021$, Figure 3.6, where $D_{L,0}$ refers to the detection limit of the stated radionuclide above the Compton continuum background, decay corrected to the reference time: 2017-09-29 12:00 UTC). Total terbium recovery was 97.3% with a radiochemical purity > 99.9% (Table 3.1).

Table 3.1 - Radioisotope composition of a ^{155}Tb source received from CERN-ISOLDE before and after chemical separation (reference time: 2017-09-29 12:00 UTC).

Isotope	T½	Activity of material supplied (MBq)	Activity following separation
^{139}Ce	136.7 d	2.79 ± 0.068	≤ 1.90 kBq
^{155}Tb	5.32 d	9.28 ± 0.63	9.03 ± 0.049 MBq

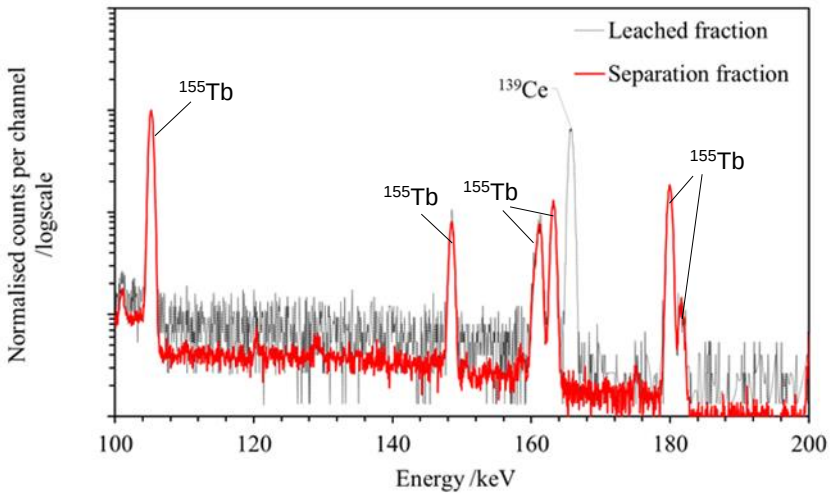

Figure 3.6 - Gamma ray spectra of the ^{155}Tb source preparation before (grey) and after radiochemical separation (red) (reference time: 2017-09-29 12:00 UTC).

3.3 Discussion and summary

A novel method (Figure 3.5) has been developed for the purification of ^{155}Tb sources from ^{139}Ce impurities produced by proton-induced spallation at CERN-ISOLDE and CERN-MEDICIS, one of the main producers of the isotope to date. The method was developed using stable analogues and ICP-MS elemental analysis which significantly reduces the amount of radiation that the researcher is exposed to. It also prevented radioactive waste being generated during the method development stages. These stable element experiments showed that the developed method, selective cerium oxidation and subsequent chromatographic separation using a UTEVA column, is capable of separating 100 ng/mL terbium and 100 ng/mL cerium from a 10 mL solution. This is equivalent to separating ~6 GBq ^{155}Tb from ~0.25 GBq ^{139}Ce.

This method was successfully applied to an active sample, producing a high radionuclide purity source (>99% ^{155}Tb purity, > 97 % ^{155}Tb recovery). Sources of this quality would be suitable for complexation to targeting molecules and for subsequent (pre)-clinical study as they meet the purity requirements[157] of the similar SPECT isotope, ^{67}Ga. Sources produced in this way were also of sufficient purity to allow other researchers at NPL to carry out nuclear data measurements and a world-first primary standardisation (results yet to be published)[188–190].

The terbium recovery and radionuclide purity achieved here was comparable to what can be achieved using the α-HIBA, cation exchange chromatography method as reported by Gracheva *et al.*[143]. The UTEVA method is also more rapid (~ 50 minutes vs. ~100 minutes). Use of faster

flowrates (>0.3 mL/min) was not studied here but would be worth considering in future studies in order to further minimise losses of isotope due to radioactive decay.

This method had not been validated for the removal of other stable (e.g., ^{139}La, ^{155}Gd) or longer-lived, radioactive (e.g., ^{155}Eu) isobaric impurities; as with ^{139}Ce^{16}O, they would not be removed by mass separation. The presence of stable impurities would not have a negative impact on the quality of nuclear data measurements or on the ability to produce a primary radioactive standard, but they could have an impact on the safe and efficient use of ^{155}Tb in nuclear medicine procedures.

These lanthanide impurities might not pose a significant toxicological risk if they were to enter the body[191–193] but they would also form stable complexes with DOTA (log K > 22)[124] and DOTA-containing targeting molecules[29,30]. This would result in competitive complexation with the ^{155}Tb meaning that an excess of targeting molecule would be required to ensure that all ^{155}Tb is incorporated into the molecule. The presence of stable impurities would therefore lead to a reduction in the specific activity and efficacy of the radiopharmaceutical. Further investigation into the comprehensive purification of the ^{155}Tb and the other terbium isotopes produced by proton-induced spallation, namely ^{149}Tb and ^{152}Tb was therefore required. These issues have been addressed in Chapter 4.

Chapter 4. Separation of terbium from trace stable and radioactive lanthanides

The method reported in Chapter 3 has shown that a high radionuclidic purity source of ^{155}Tb can be produced by proton-induced spallation, mass separation and the utilisation of a UTEVA cartridge-based chemical separation method[86]. This method was efficient for the removal of a major ^{139}Ce impurity; however, it was not validated for the removal of other lanthanides, which are produced in the same process. Owing to the similar chemical properties of neighbouring lanthanides, it is not expected that the method reported in Chapter 3 will be capable of producing chemically pure terbium sources. Therefore, the separation of trace terbium from neighbouring lanthanides was investigated and the 'fit-for-purpose' method was applied to simulant solutions which mimic mass-separated proton induced spallation sources of ^{149}Tb, ^{152}Tb and ^{155}Tb.

4.1 Production information and requirements for chemical separation

4.1.1 Characteristics of mass-separated terbium sources produced by proton-induced spallation at CERN-ISOLDE/MEDICIS

A number of stable, radioactive, isobaric and/or pseudo-isobaric lanthanide impurities are co-produced during the production of ^{149}Tb, ^{152}Tb and ^{155}Tb by proton-induced spallation and are not removed subsequent mass separation (Table 4.1). Regarding their quantities, Duchemin *et al.*[182] reports that ^{149}Tb, ^{152}Tb, ^{155}Tb and ^{133m}Ce are produced at a rate of >10^9 Bq/µAh, and ^{139}Ce is produced at a rate of >10^7 Bq/µAh. The significantly longer half-life of ^{139}Ce compared to the others means that the reported production yield activities indicate a similar mass quantity of each mentioned isotope (10-1000 ng/µAh). The production yields of other potential impurities (i.e., longer-lived, or stable isotopes) are not reported in the article.

In addition to the lanthanide impurities, the product ion beams can be captured on either $NaNO_3$ discs[194], zinc coated gold foils[27,86] or KNO_3 coated aluminium backings[4] during the mass separation process. The removal of the capture material must also be considered when developing the chemical separation method.

*Table 4.1 - Potential impurities found in ^{149}Tb, ^{152}Tb and ^{155}Tb sources produced at by proton-induced spallation after mass separation[73,182]. (*radionuclides)*

Sources of impurities	^{149}Tb	^{152}Tb	^{155}Tb
Isobaric (trace)	^{149}Gd*, ^{149}Eu*, ^{149}Sm, ^{149}Pm*	^{152}Dy*, ^{152}Gd, ^{152}Eu*, ^{152}Sm	^{155}Dy*, ^{155}Gd, ^{155}Eu*
Pseudo-isobaric (trace)	^{133}Ba*, ^{133}Cs	^{136}Ce, ^{136}Cs*, ^{136}Ba	^{139}Ce, ^{139}La*, ^{139}Pr*
Daughter products (trace)	^{145}Eu*, ^{145}Sm*, ^{145}Pm*, ^{145}Nd	^{152}Gd	^{155}Gd

4.1.2 Requirement for the removal of stable impurities

Regarding the stable impurities, the majority are lanthanide elements and these are generally of low to moderate toxicity when in their ionic form, with gadolinium and ytterbium being exceptions[191,195]. All lanthanide impurities, including gadolinium and ytterbium, do not pose a significant toxicological risk if they are present in trace quantities (~ng) and are administered with a DOTA or DTPA containing targeting molecule (Figure 4.1). These chelators display high complex stability with all lanthanide elements (i.e., high *logK*), ensuring that they will be held strongly within the targeting molecule complex, even under *in vivo* conditions[30,124,196–200]. In this scenario, most of the lanthanide impurities will be excreted, rather than accumulating within the body. Despite this, if substantial quantities of impurities are present, then the specific activity of the radiopharmaceutical preparation will be reduced significantly. An excess of targeting molecule will be needed to ensure all of the diagnostic or therapeutic radionuclide has been successfully chelated.

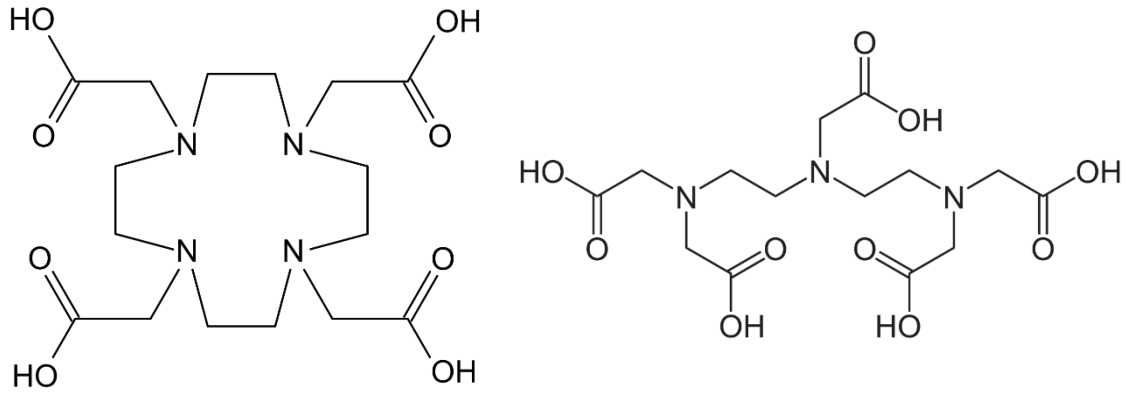

DOTA **DTPA**

*Figure 4.1 - The chemical structure of two aminopolycarboxylic acid bifunctional chelators which can incorporate lanthanides (Ln^{3+}); (**left**) 1,4,7,10-Tetraazacyclododecane-1,4,7,10-tetraacetic acid (DOTA); (**right**) diethylenetriaminepentaacetic acid (DTPA)*[124].

The removal of both radioactive and stable impurities is essential to maximise the efficiency of diagnostic or therapeutic medicine. The development of a fast and highly efficient method is therefore required for the recovery of these short-lived terbium radioactive isotopes.

4.1.3 Reasons for the chosen separation approach

Cation exchange methods have been the most commonly applied chromatography methods to purify proton-induced spallation terbium sources to date[27,29], however, the use of LN extraction chromatography resin methods have received little attention for this purpose.

Separation methods, incorporating LN resin steps, have been developed to process ^{161}Tb produced by neutron irradiation of ^{160}Gd targets[144,145,148,201] and have also been used in the purification of ^{155}Tb produced by the irradiation of europium targets with alpha particles[121]. There are no reports of using LN resin to process spallation-produced terbium.

In these previous studies, high quality information about radiochemical recoveries and purities are reported; however, details about the removal of stable impurities are vague (see section 1.4.2). In some cases, key details about the separation conditions are also not included. The impact of stable impurities is more significant when they are in bulk quantities (see Chapter 5); however, it is still important to understand how comprehensive the developed methods are. For these reasons the aim was to develop a well-defined and reproducible LN resin method that can process proton-induced spallation sources of terbium with well understood purity and recovery information.

4.2 Method development

4.2.1 Materials and reagents

Throughout this study, single element and multiple element solutions were prepared by diluting certified atomic spectrometry standards with a chosen concentration of nitric acid. For batch studies, bulk LN resin (50-100 µm, *Triskem International*) was used. For column studies, pre-packed UTEVA columns (2 mL, 50-100 µm) and glass Econo-Columns® (*BioRad*) packed with LN resin were used. General information about methods of packing and using chromatography columns are found in section 2.2. Specific details have been presented in text when necessary.

To mimic the radioactive mass-separated, proton induced spallation terbium sources, simulant solutions were prepared for each of the radioisotopes of interest (^{149}Tb, ^{152}Tb, ^{155}Tb). These simulant solutions (Table 4.2) contained stable element standards corresponding to the potential impurities present in the mass-separated ^{149,152,155}Tb sources (Table 4.1). These were prepared in acid concentrations suitable for the column-based separation.

Table 4.2 - Composition of 'simulant ^{149,152,155}Tb' solutions used to chemically mimic mass-separated, proton induced spallation produced, terbium sources (100 ng/mL in nitric acid solutions)[73,182].

Simulant solution	Components
^{149}Tb	Cs, Ba, Nd, Sm, Eu, Gd, Tb
^{152}Tb	Cs, Ba, Ce, Sm, Eu, Gd, Tb, Dy
^{155}Tb	La, Ce, Pr, Eu, Gd, Tb, Dy

4.2.2 Interference free measurement of trace lanthanides using ICP-QQQ-MS

Interference free measurement is an important factor to consider when developing chemical separation methods which can isolate one element from one or more other elements. This is because interference free measurement allows for the accurate assessment of the method through the derivation of highly accurate percentage recovery and purity information.

As implied in section 2.3.1, the lanthanide elements actively form hydride polyatomic species within the ICP (e.g.,$^{158}Gd^{1}H^{+}$) which interferes with the measurements of a neighbouring mass (e.g., ^{159}Tb)[202]. Most lanthanides will also form oxide (e.g., $^{156}Gd^{16}O^{+}$) and less commonly hydroxide (e.g., $^{158}Gd^{16}O^{1}H^{+}$) polyatomic species which can interfere with the measurement of other lanthanide elements (e.g., $^{172}Y^{+}$ and $^{175}Yb^{+}$, respectively)[170,203]. The near identical chemical properties of neighbouring lanthanide elements make the interference removal and accurate measurement of single lanthanides a challenge (e.g., ionisation potentials, likelihood of forming polyatomic species in the plasma etc.). Some of the lanthanide elements have several naturally occurring isotopes (e.g., $^{152,154,155,156,157,158,160}Gd$) and will potentially interfere with the detection of other lanthanide elements. The adjustment and optimisation of instrument parameters, as well as the tactical use of reaction/collision cell technology, can be used to minimise the presence of measurement interferences.

A method reported by Sugiyama[202] reports to be able to provide interference free measurement of the lanthanides using a MS/MS method with O_2 reaction cell gas. This method was used here to identify and quantify single lanthanide elements in lanthanide mixtures (Table 4.3). Accurate measurement was an essential part of the characterisation of the novel chemical separation method developed in this chapter[204].

Table 4.3 – The Agilent 8800 series ICP-QQQ-MS operating parameters used for the interference minimised measurement of lanthanide element mixtures throughout the method development stages of Chapter 4 and Chapter 5.

Parameter	Setting
Scan Mode	MS/MS
Plasma Conditions	Low Matrix
RF Power (W)	1550
Extract 1 (V)	0
Extract 2 (V)	-175
Reaction Cell Gas	Oxygen
Oxygen Flow Rate (mL/min)	0.3 (30% of full-scale)
Octopole Bias (V)	-5.0
Energy Discrimination (V)	-7.0
Octopole RF	200

4.2.3 Suitability of the UTEVA method for the separation of neighbouring lanthanides

Initially, to understand whether the method reported in Chapter 3 (Figure 3.5) was suitable for the isolation of terbium from lanthanide impurities other than cerium, the three simulant solutions (10 mL, 8 M HNO_3, Table 4.2) were exposed to the oxidant $NaBrO_3$ (0.15 g, 0.1 M) and passed through a pre-packed and pre-conditioned 2 mL UTEVA cartridge. The step-wise elution was carried out as per the reported method and the quality of the separations were assessed using ICP-MS analysis in MS/MS O_2 mode[202].

It was shown that using the UTEVA method to isolate terbium from more complex lanthanide mixtures was an ineffective approach. The separation between terbium and cerium occurred as previously reported; however, separation of terbium from other lanthanides did not occur (e.g., 'simulant ^{152}Tb solution', Figure 4.2). This reinforced the need for investigation into alternative separation methods.

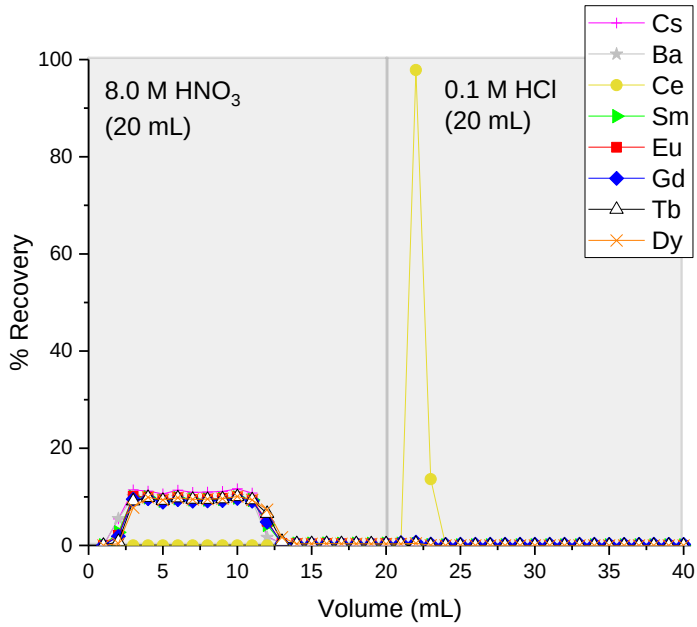

Figure 4.2 - Attempted separation of 'simulant ^{152}Tb' mixture using the UTEVA method (Chapter 3).

4.2.4 Investigation of LN resin for the isolation of terbium from lanthanide impurities

4.2.4.1 Batch studies

As previously ascertained, the LN extraction chromatography resin is suitable for lanthanide separations and investigation into its use for processing spallation produced terbium isotopes is justified.

The behaviour of lanthanide elements on LN resin was studied in batch conditions over a range of HNO_3 concentrations. Nitric acid solutions (2 mL) containing a mixture of 100 ng/mL stable europium, gadolinium, terbium and dysprosium were prepared. An aliquot was taken from each solution for ICP-MS measurement (CPS_0). The remaining solution was added to individual 15 mL centrifuge tubes containing LN resin (0.1 g, 50-100 µm, *Triskem International*). Each mixture was shaken and left to equilibrate for ~24 h before being filtered through filter paper in order to isolate the aqueous phase (Whatman 41 ashless filter paper, 20–25 µm pore size). An aliquot was taken from each filtered sample, diluted with HNO_3 (2% v/v) and analysed by ICP-MS (CPS_t) using the method summarised in Table 4.3.

The adsorption of the studied elements onto LN resin was quantified by the calculation of distribution coefficients (K_d) and separation factors (SF) using the methods described in section 2.2.1.

These batch separation experiments with LN resin indicated a minimal variation in separation factors (SF, < 5) between neighbouring lanthanides across a wide HNO_3 concentration range. This was expected due to the similar chemical properties of lanthanide elements. In general terms, strength of adsorption to the resin increased (i.e., K_d value) with increasing atomic number, but decreased with increasing HNO_3 concentration (Figure 4.3 and Figure 4.4, Appendix E). These findings agree with previously reported data[137,142] and allowed the estimation of appropriate column chromatography conditions for the isolation of terbium from lanthanide impurities.

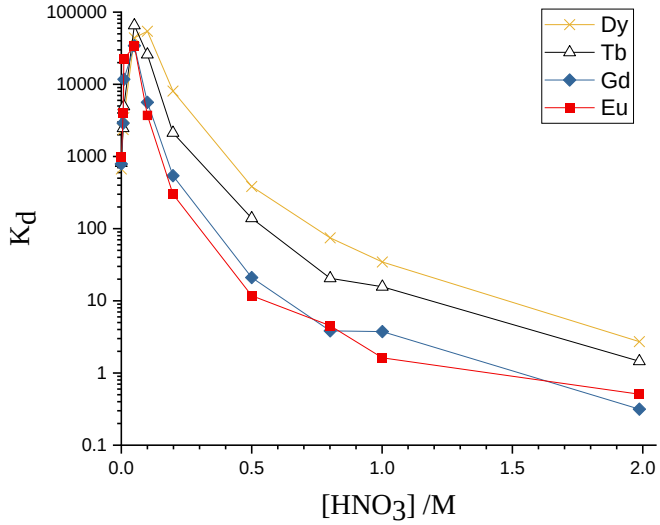

Figure 4.3 - Distubution coefficient (K_d) variation with nitric acid conentration of europium, gadolinium, terbium and dysprosium.

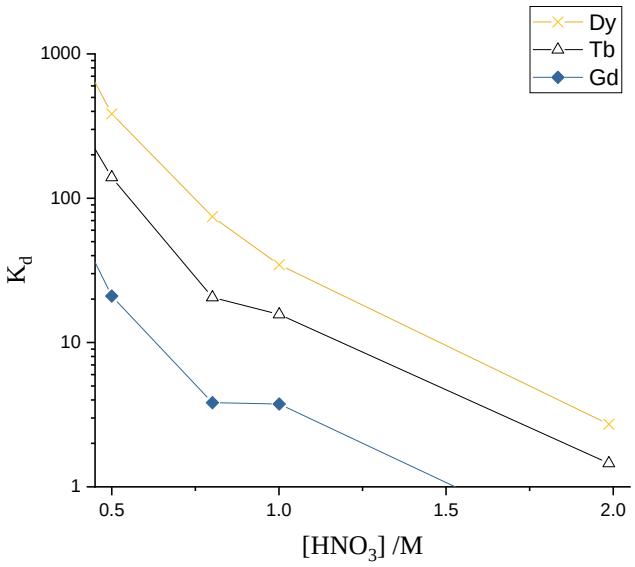

Figure 4.4 - Distribution coefficient (K_d) variation with nitric acid conentration of gadolinium, terbium and dysprosium – zoomed in to highlight conditions which were used in initial column-based separation studies.

4.2.4.2 Column separation studies

Column separation studies were conducted using self-packed 200 × 7 mm BioRad Econo-Columns® (see Figure 2.6). Mobile phase was introduced to the column at a defined flow rate using a Gilson Miniplus peristaltic pump and associated silicon tubing and connectors. The flow rate was controlled using the pump and was calculated before carrying out a separation (Section 2.2.2).

Figure 4.5 - The apparatus set-up used for column-based separations.

Nitric acid solutions containing 100 ng/mL of the investigated elements were used throughout the column-based separation method development process. An aliquot of the initial solution (1 mL) was taken, diluted with HNO_3 (2% v/v) and measured by ICP-MS in order to identify its starting concentration. Another aliquot of the solution (1 mL) was taken and added to the top of a pre-conditioned column to undergo separation.

A variety of acid concentrations and volumes were used in order to optimise the separation of terbium from gadolinium and dysprosium. Throughout, a stepwise elution was applied. As previously described (see section 2.2.1), 1 mL fractions were collected from the column in order to compile elution profiles and thus identify how each component of the mixture behaved on the column. In all cases, analysis of the fractions was conducted using ICP-MS in MS/MS O_2 mode (Table 4.3) and data was processed using the method described in section 2.2.2 in order to calculate elemental recovery (equation 2.3).

The increasing distribution coefficients (K_d) observed with increasing atomic number indicates that, when applied to a column-based system, the lanthanides will elute from an LN resin column in the order of increasing atomic number (i.e., lanthanum → lutetium). Due to the similarities in K_d between neighbouring lanthanides (low SF), a long column (200 × 7 mm, 7.70 mL) was initially used to ensure a sufficient separation resolution. Even though it would produce an excellent separation resolution, using a very long column would be impractical as it would result in a long separation time and larger volumes to elute components of the mixture.

The initial focus was to optimise the process of isolating terbium from gadolinium and dysprosium impurities on LN resin and was achieved through a series of single run separation experiments (Figures 4.6 – 4.11). Once optimised, this derived method would also be suitable for isolating terbium from all lanthanides.

Initial trials involved the use of 0.10 M HNO_3 (40 mL) to pre-condition the column and to load a mixture of terbium and gadolinium onto the column. These conditions ensured that both elements were retained on the column prior to the investigation of different elution conditions. A stepwise change in nitric acid concentration, at a flow rate of 1 mL/min, afforded moderate separation of terbium from gadolinium with a slight peak overlap being observed (Figure 4.6). It was concluded that larger volumes of each acid concentration (i.e., 0.75 M and 2.00 M) might improve peak resolution.

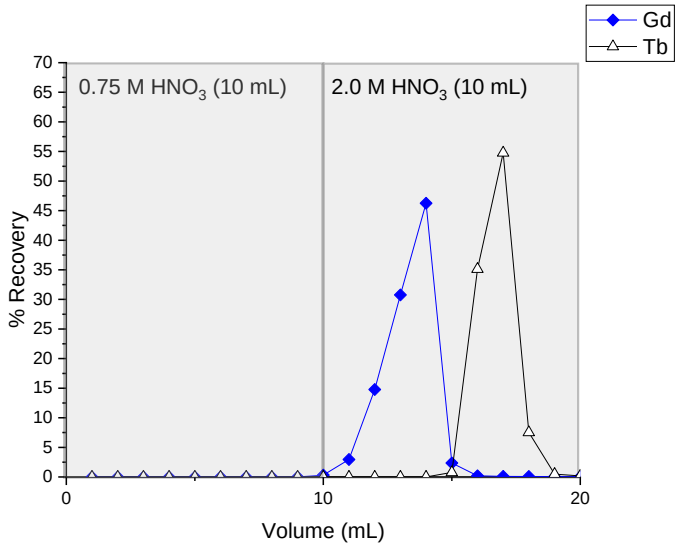

Separation step	Conditions
Pre-condition	0.10 M HNO_3 (40 mL)
Load	100 ppb Tb/Gd in 0.10 M HNO_3 (1 mL)
Wash	0.10 M HNO_3 (40 mL)
Elute 1	0.75 M HNO_3 (10 mL)
Elute 2	2.00 M HNO_3 (10 mL)

Figure 4.6 - Initial column chromatography trial using a 200 × 7 mm glass Econo-Column® packed with LN resin (50-100 μm). Elution steps and conditions are summarised in the table (Flow rate ~1.0 mL/min).

A slight change in the *wash* conditions, coupled with the increased *elute 1* and *elute 2* volumes gave an improved separation (Figure 4.7). Further investigation of different *pre-condition*, *wash* and *elute* conditions (Figure 4.8 and Figure 4.9) showed that the use of 0.75 M HNO_3 (20 mL) allowed the selective elution of gadolinium from the column. Terbium began to elute from the column after 25 mL of 0.75 M HNO_3. It was concluded that 0.75 M HNO_3 was suitable for both the *pre-condition* and *load* steps, as well as for the elution of gadolinium.

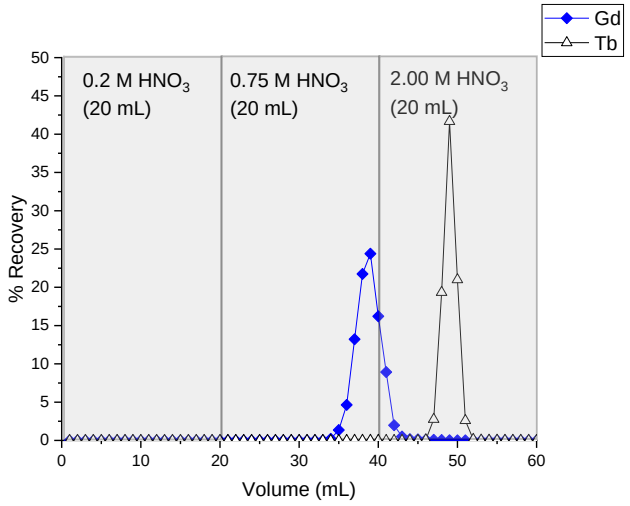

Separation step	Conditions
Pre-condition	0.10 M HNO_3 (40 mL)
Load	100 ppb Tb/Gd in 0.10 M HNO_3 (1 mL)
Wash	0.20 M HNO_3 (20 mL)
Elute 1	0.75 M HNO_3 (20 mL)
Elute 2	2.00 M HNO_3 (20 mL)

Figure 4.7 - Column chromatography study using a 200 × 7 mm glass Econo-Column® packed with LN resin (50-100 μm). Differences in elution conditions are highlighted. (Flow rate ~1.0 mL/min)

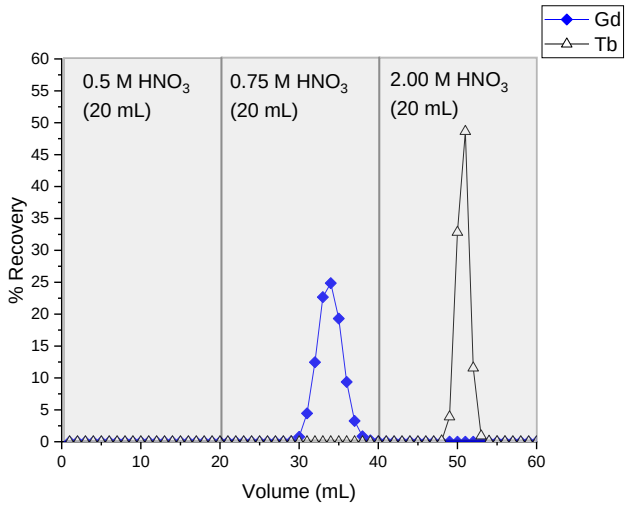

Separation step	Conditions
Pre-condition	0.10 M HNO_3 (40 mL)
Load	100 ppb Tb/Gd in 0.10 M HNO_3 (1 mL)
Wash	0.50 M HNO_3 (20 mL)
Elute 1	0.75 M HNO_3 (20 mL)
Elute 2	2.00 M HNO_3 (20 mL)

Figure 4.8 - Column chromatography study using a 200 × 7 mm glass Econo-Column® packed with LN resin (50-100 μm). Changes to the wash conditions are highlighted. (Flow rate ~1.0 mL/min)

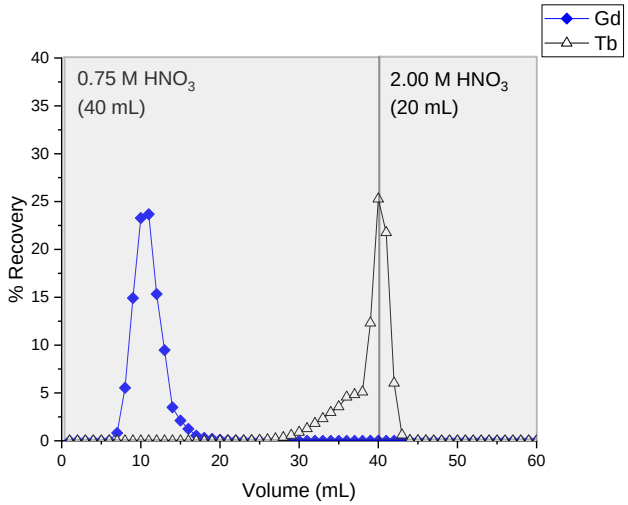

Separation step	Conditions
Pre-condition	0.75 M HNO_3 (40 mL)
Load	100 ppb Tb/Gd in 0.75 M HNO_3 (1 mL)
Elute 1	0.75 M HNO_3 (40 mL)
Elute 2	2.00 M HNO_3 (20 mL)

Figure 4.9 - Column chromatography study using a 200 × 7 mm glass Econo-Column® packed with LN resin (50-100 μm). Changes to the pre-conditioning, loading and elution conditions are highlighted. (Flow rate ~1.0 mL/min)

An intermediate *elute* solution (1.0 M HNO_3, 20 mL) was used to encourage faster elution of terbium from the column (Figure 4.10). This allowed the isolation of terbium from both dysprosium and gadolinium. Some peak overlap was still observed.

Separation at a decreased flow rate, 0.5 mL/min, resulted in an improved separation resolution (Figure 4.11). Using even slower flow rates would have provided little improvement in the separation resolution between peaks at the expense of the acheivable 'radiochemical' yield. Thus, it was decided that using a flowrate of 0.5 mL/min was sufficient for this application.

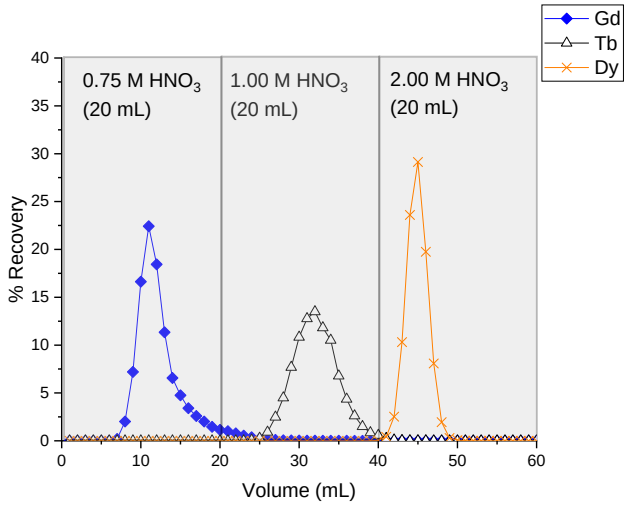

Separation step	Conditions
Pre-condition	0.75 M HNO_3 (40 mL)
Load	100 ppb Tb/Gd/Dy in 0.75 M HNO_3 (1 mL)
Elute 1	0.75 M HNO_3 (20 mL)
Elute 2	1.00 M HNO_3 (20 mL)
Elute 3	2.00 M HNO_3 (20 mL)

Figure 4.10 - Column chromatography study using a 200 × 7 mm glass Econo-Column® packed with LN resin (50-100 µm). Changes to the elution conditions are highlighted. (Flow rate ~1.0 mL/min)

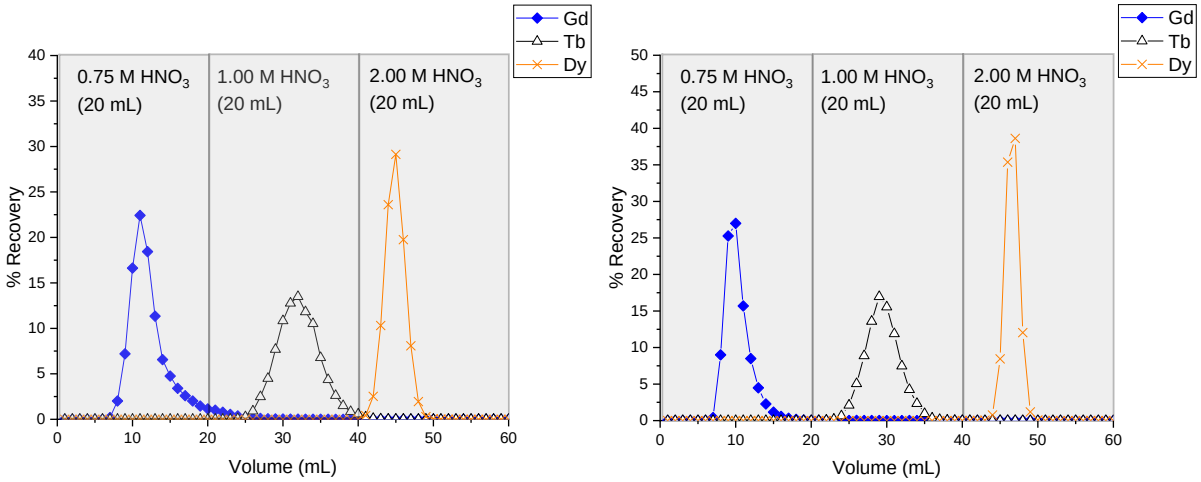

*Figure 4.11 - Variation of the elution profiles of separations conducted at different mobile phase flow rates: ~1.0 mL/min **(left)** and ~0.5 mL/min **(right)**. Separations were conducted under identical chemical conditions (see also Appendix F).*

4.2.4.3 Method Summary

The method summarised in Table 4.4 was shown to be suitable for the separation of terbium from neighbouring lanthanides. Even though the separation resolution could be improved upon further, a flow rate that is too slow would have a significant impact on the radiochemical yield of the short-lived radionuclides. Faster flow rates had a negative effect on the separation resolution and thus, on the purity of the terbium fraction. Results deemed that a separation using a flow rate of 0.5 mL/min was suitable for the separation of terbium from neighbouring

lanthanides. The isolation of high purity terbium (>95 % purity) was shown to be achievable in 80 minutes, with the majority of the terbium being isolated in fractions 25-40.

Table 4.4 - The developed separation method and parameters for the isolation of terbium from lanthanide impurities

Separation step	**Conditions**
Pre-condition	0.75 M HNO_3 (40 mL)
Load	0.75 M HNO_3 (1 mL)
Elute 1 (Gd)	0.75 M HNO_3 (20 mL)
Elute 2 (Tb)	1.00 M HNO_3 (20 mL)
Elute 3 (Dy)	2.00 M HNO_3 (20 mL)
Resin	LN resin (50 – 100 μm)
Column dimensions	200 mm × 7 mm
Flow rate	0.5 mL/min

4.3 Method validation and optimisation

For a large portion of this PhD project, a series of upgrades to CERN's facilities meant that proton-induced spallation produced terbium isotopes were not available to validate the method developed in this study. Therefore, to validate the chemical separation method, 'simulant ^{xxx}Tb' solutions were used to mimic active proton-induced spallation sources and they contained elements that might be present after production and mass-separation (Table 4.2).

4.3.1 Separation and measurement of 'simulant ^{xxx}Tb' solutions

These 'simulant ^{xxx}Tb' solutions underwent separation ('simulant ^{149}Tb, ^{152}Tb and ^{155}Tb', Table 4.2) using the developed LN resin method (Table 4.4). As with previous separations, 1 mL fractions were collected from the column and analysed using ICP-MS in order to compile elution profiles. A single separation run was conducted for each in order to demonstrate feasibility (see also Appendix G).

4.3.1.1 'Simulant ^{149}Tb'

The elution profile of the 'simulant ^{149}Tb' solution showed the successful isolation of high purity terbium (>99 %) with a high terbium recovery in fractions 25-40 (96.9 %, Figure 4.12).

Due to the short half-life of ^{149}Tb ($t_{½}$ = 4.118 h), the time required for separation will have a significant impact on the radiochemical recovery of ^{149}Tb when this method is applied to an active sample. A terbium recovery of 96.9% was achieved after 80 minutes using the reported separation process. This recovery would correspond to a ^{149}Tb *radiochemical recovery* of 77.4 %. This radiochemical recovery only takes into account losses of the isotope during the chemical separation process and not time required for any processing before or after the separation. Therefore, in practice, the radiochemical recovery would be significantly lower.

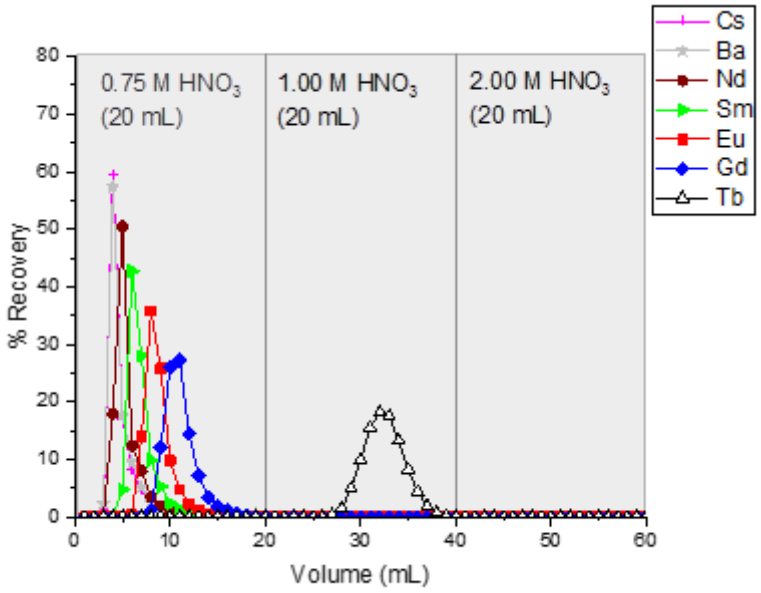

Figure 4.12 - Elution profile of the separation of a 'simulant ^{149}Tb' solution, containing Cs, Ba, Nd, Sm, Eu, Gd, Tb (1 mL fractions).

4.3.1.2 'Simulant ^{152}Tb'

The elution profile of the 'simulant ^{152}Tb' solution also showed a good level of terbium isolation (Figure 4.13). These data were inaccurate due to internal standard correction not being used during ICP-MS measurement. For this reason, an accurate terbium recovery could not be calculated at this stage. However, the elution profile still provided some qualitative insights; namely, identifying the presence of a minor cerium impurity which remained in the terbium fraction (~8 % cerium, ~92% terbium).

The elongated cerium elution observed in the profile is uncharacteristic of the lanthanides and suggests that the chemical behaviour of the cerium does not follow the trend under these conditions. It was thought that this was due to cerium existing in either its IV+ oxidation state in aqueous solution or it being present with a mixed oxidation state (i.e., Ce (III/IV)). Further investigation was required in order test this hypothesis and to alter the method so that it was able to remove the cerium impurities remaining in the terbium fraction.

As was the case for the 'simulant ^{149}Tb' separation, the relatively long separation time would also have an impact on the radiochemical recovery of the ^{152}Tb if this method was applied to an active sample. The time required for the isolation of the terbium fraction (i.e., 80 minutes), however, would have a less significant impact on the radiochemical recovery of ^{152}Tb ($t_{½}$ = 17.5 h) due to its longer half-life relative to ^{149}Tb. If a 95% terbium recovery could be achieved using this method, the corresponding *radiochemical recovery* of ^{152}Tb would be 90.2 %.

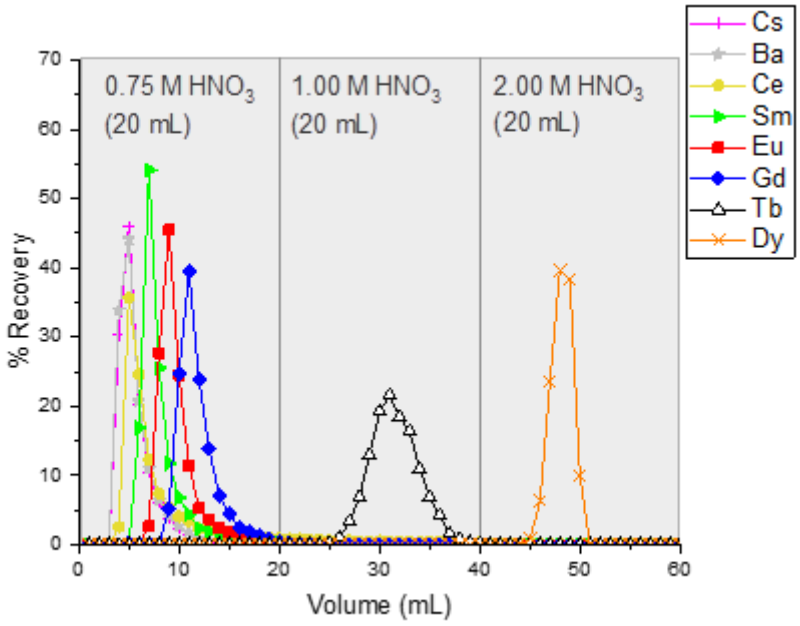

Figure 4.13 - Elution profile of the separation of a 'simulant ^{152}Tb' solution, containing Cs, Ba, Ce, Sm, Eu, Gd, Tb, Dy (1 mL fractions).

4.3.1.3 'Simulant ^{155}Tb'

A significant difference was observed when separating the 'simulant ^{155}Tb' solution (Figure 4.14). All elements eluted later than previously seen. Terbium even eluted in different conditions (2.00 M HNO_3). These observations were likely due to changes in the separation conditions, thus further investigation was required in order to identify the cause.

Due to the relatively long half-life of ^{155}Tb (t½ = 5.32 d), the 120 minutes separation required here would have a minimal impact on the radiochemical recovery of ^{155}Tb when applied to an active sample.

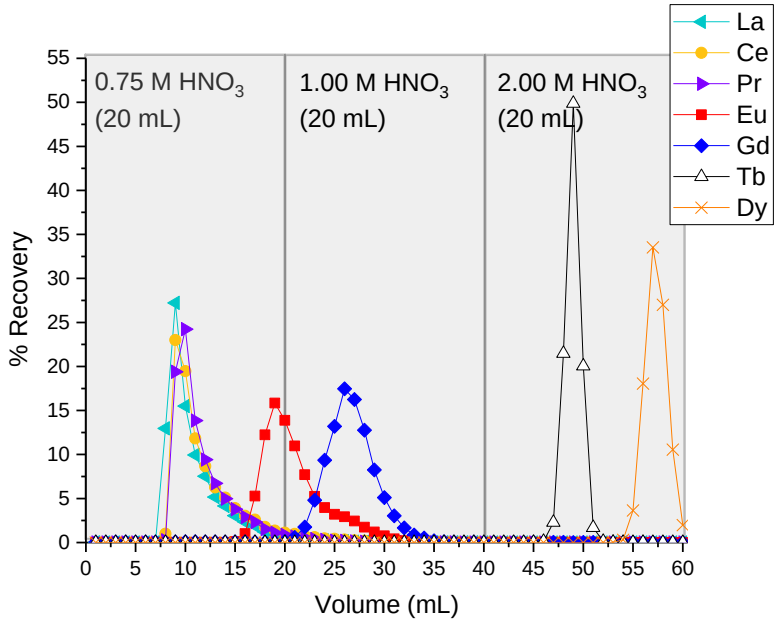

Figure 4.14 - Elution profile of the separation of a 'simulant ^{155}Tb' solution, containing La, Ce, Pr, Eu, Gd, Tb, Dy (1 mL fractions).

When the method was repeated using freshly made acid solutions and a freshly packed column, the same peak drift was observed. This suggested that there were differences in the resin composition between batches, as a new batch of resin was used for these separations.

4.3.2 Findings and areas for further optimisation

Several issues with the developed method (Table 4.4) were identified when separating the 'simulant ^{xxx}Tb' solutions. The issues were as follows:

- **Inaccuracies in the measurement of recoveries –** in some cases the raw data could not be processed to provide reliable percentage recovery and purity information due to a lack of internal standard correction to account for ICP-MS instrumental drift during measurement runs.
- **Shift in elution peaks between LN resin batches** – results suggested that there were differences in the composition of LN resin between batches that caused significant

changes in the elution behaviour of the lanthanide elements and thus impacted upon the isolation of the terbium fraction.

- **A remaining cerium impurity in terbium fraction** – elongated cerium elution indicated chemical behaviour that did not follow the lanthanide trend. This resulted in a small cerium impurity remaining in the terbium fraction.
- **Separation time causing a negative impact on radiochemical recovery –** due to the short half-lives of ^{149}Tb and ^{152}Tb in particular, a long separation time (>80 minutes) results in significant losses of the isotopes due to radioactive decay during separation.

Each of these issues were investigated and discussed further to correct for them and/or to provide further optimisation of the separation method to ensure that it was fit-for-purpose.

4.3.2.1 Correcting inaccuracies in the ICP-MS measurements

Further repeats were conducted allowing high quality metrological information to be calculated relating to the achievable terbium recovery and purity (Table 4.5). These values related to the elemental content of fractions 41-50 (see Figure 4.14). Stated uncertainties were calculated by the propagation of uncertainties from the ICP-MS counts per second measurement (*n=10*)[205]. This data assumes that instrumental drift was minimal throughout the analysis runs.

Table 4.5 – A summary of the terbium recovery and purity information achieved using the LN resin separation method developed in this study (Table 4.4). (see also Appendix H)

	Terbium recovery (%)	**Terbium purity (%)**
Simulant ^{149}Tb	100.58 ± 1.96	96.65 ± 2.82
Simulant ^{152}Tb	98.99 ± 2.96	97.31 ± 4.29
Simulant ^{155}Tb	93.83 ± 1.05	99.40 ± 1.14

Due to time constraints on this project, use of an internal standard was not implemented here Regular use of an internal standard (e.g., 10 ng/mL indium in 2% HNO_3) should be used in future studies to ensure that instrumental drift is corrected for in order to improve the reliability of the results. The internal standard can be introduced with each sample via a dedicated line positioned before the nebuliser (section 2.3.1).

4.3.2.2 Optimising method to account for resin batch variation

A shift in elution peaks was observed when a new batch of LN resin was used. Repeat separations with newly made columns and nitric acid solutions suggested that human error was not the cause of the variation between separation (see Chapter 5). This was supported by the generation of comparable results when the method was repeated by other users (section 5.3.4.3). The method is therefore both repeatable and reproducible, suggesting that the issue lies with the resin itself.

A private communication with *Triskem International* informed NPL that there was no significant difference recorded in the manufacture of the two batches of resin used in this study (e.g., quality of employed raw materials, fabrication process and quality control). Testing of a third batch of resin would be necessary to identify if variations between resin batches were the cause of the observed peak shift. This was not tested during this study due to time constraints, but it would provide a useful insight and should be tested in future work.

One advantage of this peak shift, however, was that the separation resolution between gadolinium and terbium was improved (Figure 4.14). This is of particular benefit to the separation of terbium from bulk quantities of gadolinium which is studied and discussed in Chapter 5.

The separation resolution between terbium and dysprosium was lower with the new resin batch, but a clear distinction between their elution peaks was still observed under the same elution conditions (Table 4.4). A high purity terbium fraction could therefore still be isolated. Should a dysprosium impurity be present after the chemical separation of a mass-separated terbium source, it would be in small quantities. This is because most of the dysprosium content would have been removed during chemical separation. The ^{149}Dy (t½ = 4.20 m), ^{152}Dy (t½ = 2.38 h) and ^{155}Dy (t½ = 9.9 h) decay into the medically interesting terbium isobars (^{149}Tb, ^{152}Tb, and ^{155}Tb respectively). The half-lives of these dysprosium isotopes are shorter than their daughter terbium isotopes, meaning that the relative activity of the terbium isotopes will increase over time whilst the activity of any remaining dysprosium impurity decreases.

The potential benefits of this peak shift could not be relied upon until the reason for it could be identified. Both batches of LN resin were still capable of isolating high purity terbium (Table 4.5), but, to account for the potential difference in elution behaviour between batches, analysis of fractions would be essential when the method is applied to active sources. For active

samples, HPGe gamma spectrometry can be used. For stable element samples, mass spectrometry methods can be used.

Most of the future separations in chapters 4 and 5, used the second batch of resin and the method summarised in Table 4.4. Elution patterns were comparable to that shown in Figure 4.14 (Appendix K and L).

4.3.2.3 Optimising cerium removal from the terbium fraction

Significant tailing of the cerium elution peak was observed during separation. This suggested that cerium exists in a mixed oxidation state when in the HNO_3 load solution (0.75 M). To test this hypothesis, the method (Table 4.4) was repeated with the addition of an oxidant, sodium bromate ($NaBrO_3$, 0.1 M), in an attempt to improve cerium removal in a similar manner to the method reported in Chapter 3 by its oxidation to Ce(IV).

The addition of the oxidant caused an even broader cerium elution which resulted in an increased contamination of the terbium fraction (Figure 4.15). These findings suggested that the cerium had successfully been oxidised to Ce(IV) but caused a negative impact on the separation.

Potassium iodide (KI, 0.1 M) was used as a reducing agent in a similar manner and resulted in the elution of most of the cerium in a smaller volume compared to when no redox agent was used. This suggested that more of the cerium was present in the III+ form. Removal of cerium from the terbium fraction was not significantly improved with the addition of KI. The elution of all other lanthanides remained unaffected. In particular, the elution of europium was unaffected, suggesting minimal europium reduction. This was expected as strong reducing conditions are required to reduced europium to its II+ state[121].

In conclusion, the use of an oxidising agent resulted in an increased cerium contamination within the terbium fraction. It also introduced a small bromine contamination into the terbium fraction. The addition of mM quantities of KI also introduces a significant quantity of iodine contamination into the terbium fractions which nullifies the slight improvement in cerium removal (Figure 4.15). It was decided that no redox agents should be used due to insignificant improvement in the separation.

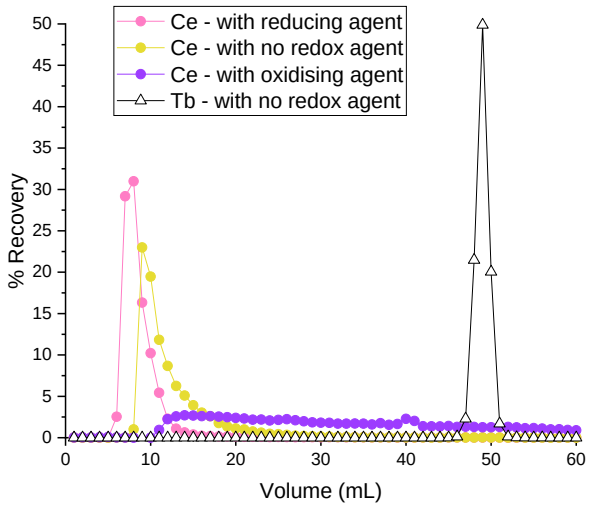

Figure 4.15 - The behaviour of cerium in absence of redox agents and in the presence of a reducing agent (KI) and an oxidising agent ($NaBrO_3$). The terbium elution in the absence of redox agents has been included here for comparison.

4.3.2.4 Reducing separation time to minimise losses in radiochemical recovery

The time taken to isolate terbium using this method (i.e., 80 – 120 minutes, Table 4.4) will have significant impact on the radiochemical yield when it is applied to active samples containing the shorter-lived terbium isotopes. A smaller column and use of smaller acid volumes at the same flow rate can be used to downscale a method, reduce the separation time and improve the radiochemical yield post-separation[206].

Initial trails using a smaller, 5 × 50 mm, glass Econo-Column showed similar elution patterns with reduced peak resolution compared to longer column studies ('Simulant ^{155}Tb', Figure 4.16, Table 4.6, Appendix I). The reduced resolution between elution peaks is also due to the smaller number of fractions taken throughout the duration of the separation (i.e., fifteen, 0.5 mL fractions, Figure 4.16, compared to sixty, 1 mL fractions, Figure 4.14). In future separations, the collection of smaller fractions should improve the resolution

Good terbium recovery was achieved (94.96 %) when using this downscaled method. Good separation of terbium from gadolinium impurities was observed, whereas increased overlap of terbium and dysprosium elution peaks was observed (21.72% dysprosium impurity). For reasons previously discussed, this is not a significant issue (see section 4.3.2.2).

Table 4.6 - The downscaled separation method which used smaller nitric acid volumes and a smaller column to encourage faster isolation of terbium from trace lanthanide impurities (Figure 4.16)

Separation step	**Conditions**
Pre-condition	0.75 M HNO_3 (5 mL)
Load	0.75 M HNO_3 (1 mL)
Elute 1	0.75 M HNO_3 (2.5 mL)
Elute 2	1.00 M HNO_3 (2.5 mL)
Elute 3	2.00 M HNO_3 (2.5 mL)
Resin	LN resin (50 – 100 μm)
Column dimensions	50 mm × 5 mm
Flow rate	0.5 mL/min

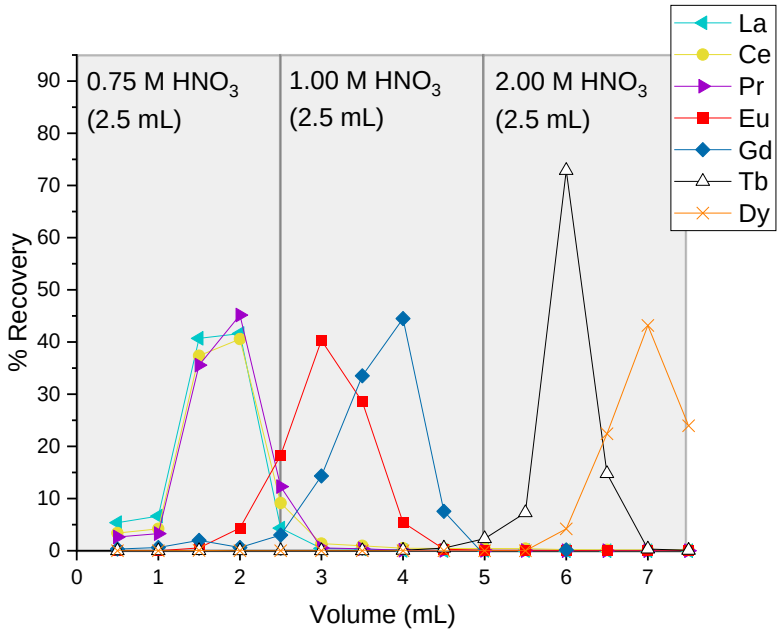

Figure 4.16 - The profile showing the elution behaviour of components of the 'simulant ^{155}Tb' solution on a shorter LN resin column and using smaller quantities of nitric acid (Table 4.6).

Isolation of the terbium fraction was achieved in < 15 minutes, eight times faster than the previously reported method. The quicker separation would significantly reduce the losses of isotope during the separation process due to radioactive decay when the method is applied to active samples (Table 4.7).

*Table 4.7 - The proportion of terbium isotope that would be lost during chemical separation due to radioactive decay. A summary and comparison of two column sizes and associated separation times. *this assumes 100% chemical and therefore does not account for chemical losses during the separation.*

	Proportion of activity, relative initial activity, lost during separation due to radioactive decay (%)*		
	^{149}Tb	^{152}Tb	^{155}Tb
Using a 50 × 5 mm column (Separation time ~ 900 s)	4.2	1.0	0.1
Using a 200 × 7 mm column (Separation time ~ 7200 s)	28.6	7.6	1.1

4.4 Fit-for purpose method and conclusions

A fit-for-purpose LN resin extraction chromatography method has been developed to isolate terbium from impurities present in mass-separated proton-induced spallation sources of ^{149}Tb, ^{152}Tb and ^{155}Tb (Table 4.4). High terbium recovery (> 90 %) and high terbium purity (> 95 %) was repeatedly achieved within 120 minutes when using a 200 × 7 mm column packed with LN resin (50-100 μm). This method presents itself as an easy-to-use alternative to the commonly used α-HIBA/cation exchange method due to the use of simple nitric acid solutions and lack of pH control. The quality of terbium sources produced using this method are comparable to those produced using the α-HIBA/cation exchange method[4,27–29,143].

An initial trial showed that shorter columns (50 × 5 mm) can be used to reduce the separation time's effect on radiochemical yield (Table 4.6) suggesting that it should be considered for the purification of the shorter-lived terbium isotopes, ^{149}Tb and ^{152}Tb. Despite recovering a high proportion of the terbium (> 90 %), use of a shorter column had negative impact on the purity of the terbium fraction. The remaining dysprosium impurity would have a minimal impact on the achievable radiolabelling yield, a minimal impact on the efficacy of therapeutic (^{149}Tb) studies and a reducing impact on the image quality during PET or SPECT imaging studies (^{152}Tb and ^{155}Tb, respectively) due to previously discussed reasons. The co-collection of the dysprosium and terbium isobars, alongside a suitable decay period, has been used to enhance the terbium isotope activity post-production in the past and is reported in the literature[110,207,208].

Further optimisation of the method is not essential but could contribute towards greater separation resolution and, therefore, terbium purity and recovery. Optimisation will also improve the reproducibility and repeatability of the method. Some suggestions for method optimisation are as follows:

- Use of LN resin with finer particle size (e.g., 20 – 50 μm, *Triskem International*). Peak shape and separation resolution could be improved further by using a smaller particle size chromatography resin if needed (see section 1.4.1.1). Finer particle size resins are more expensive, and therefore the benefit-to-cost ratio should be considered.
- Testing of a third batch of LN resin (50-100 μm, *Triskem International*). This would be advisable to confirm whether variations in composition of different batches is the cause of the shift in elution peaks that was observed between the two batches of LN resin used in this study.
- Consistent use of an internal standard during ICP-MS measurements in order to correct for any instrumental drift during measurement runs. This would improve the reliability of the reported metrological information.
- Automation of the method, for example, by its adaptation for use in a HPLC system. This would reduce the impact of human error and increase the repeatability and reliability of this method. This would be an important future step in developing an LN resin method capable of preparing terbium isotopes for regular clinical study or use under Good Manufacturing Practice (GMP).

Chapter 5. Isolation of radioactive terbium from bulk lanthanide target material

5.1 Alternative terbium production routes

So far, only the purification of terbium sources produced by proton induced spallation and subsequent mass separation has been investigated (Chapters 3 and 4). In these cases, the isolation of trace quantities of terbium (~μg) from trace quantities of lanthanide impurities was achieved. The purification of terbium sources produced via other production routes, which make use of lanthanide targets, were not investigated in these earlier chapters (Table 5.1). These alternative routes of production have the potential of producing the terbium isotopes in quantities sufficient for clinical use at localised facilities, thus making the isotopes more accessible for general use. Further investigation into the production and purification of theranostic terbium isotopes is therefore warranted.

Table 5.1 - Established and proposed routes for the production of selected terbium isotopes from lanthanide target materials. The use of ^{nat}Gd targets with subsequent mass-separation is often a more obtainable route of production.

Isotope	Facility	Reaction	Particle characteristics	References
^{152}Tb	Research Cyclotron	^{155}Gd(p,4n)^{152}Tb	~ 39 MeV protons ($^{1}H^{+}$)	Steyn *et al.*[118]
	Research Cyclotron	^{151}Eu(α,3n)^{152}Tb	34 – 40 MeV alphas ($^{4}He^{2+}$)	Trinder *et al.* [117] Moiseeva e*t al.* [209]
^{155}Tb	Research/ Medical Cyclotron	^{155}Gd(p,n)^{155}Tb	~11 MeV protons ($^{1}H^{+}$)	Vermeulen *et al.*[120]
	Research Cyclotron	^{153}Eu(α,2n)^{155}Tb	~29 MeV alphas ($^{4}He^{2+}$)	Kazakov *et al.*[121]
^{161}Tb	Nuclear Reactor	^{160}Gd(n,γ)^{161}Gd → ^{161}Tb + β^{-}	Neutron flux 10^{13} – 10^{14} ncm^{-2}s^{-1}	Lehenberger *et al.*[75] Gracheva *et al.*[143]

Of these examples summarised in Table 5.1, the production, purification and (pre)-clinical use of ^{161}Tb has received the most attention due the relative accessibility and ease of its production route compared to other terbium isotopes. As a result, initial pre-clinical and clinical studies have shown its suitability as a theranostic agent (β-/Auger therapy and SPECT diagnostics),

with results showing that it has the potential to be a more efficient theranostic agent than ^{177}Lu[30,210]. The chemical isolation of the trace quantities of ^{161}Tb (~μg) from the bulk quantities of the enriched ^{160}Gd target (10-100 mg) has commonly been achieved using cation-exchange methods with elution in α-HIBA solutions (Section 1.4.2)[23,29,30,75,143,211]. More recently, an additional step using a small LN3 extraction chromatography column was used with dilute HCl (0.05 M) to provide further purification, concentration of the isotope and conversion into the chloride form, all of which is useful for the labelling process[143]. Other studies have investigated the use of LN extraction chromatography resin for the purification of ^{161}Tb sources (Aziz *et al.*[148,149], and Monray-Guzman *et al.*[144,145]), however these studies often lack detail, making the methods difficult to reproduce (see Section 1.4.3).

The production of ^{155}Tb, by irradiation of ^{155}Gd targets with protons, has received little attention beyond initial cross-section and theoretical yield studies[120]. Another study has investigated the production of ^{155}Tb by the irradiation of europium oxide targets (~200 mg) with alpha particles[121]. The isolation of the terbium from the remaining trace lanthanide impurities involved the use of an LN resin method, which afforded a high terbium recovery and radiopurity. The production yield, however, was low (~kBq ^{155}Tb).

The production of ^{149}Tb and ^{152}Tb from lanthanide targets has not been studied beyond initial cross-section and theoretical yield studies[120,182,208,209].

For all these proposed production routes, the use of enriched single isotope targets would be advantageous as it minimises the production of unwanted isotopes, but production of the desired isotopes from natural abundance targets is also a viable option. Natural abundance target materials are cheaper than enriched ones and are easier to acquire. Terbium isotopes produced using natural abundance targets would require mass separation to remove unwanted terbium isotopes which are co-produced during irradiation. Chemical processing before and after mass separation would also be required to produce a high purity single terbium isotope suitable for medical applications[84].

The LN resin method reported in Chapter 4 (Table 4.4) was shown to be capable of separating trace quantities of terbium from lanthanide mixtures, but further study of the method was required to assess its suitability for isolating terbium produced from bulk gadolinium targets and/or bulk europium targets (Table 5.1).

This work was conducted in collaboration with CERN-MEDICIS (Geneva, Switzerland), ARRONAX (Nantes, France), Lausanne University Hospital (Lausanne, Switzerland) and KU Leuven (Belgium).

5.2 Reagents and measurement methodology

5.2.1 Materials and reagents

Mixed element solutions were used throughout the method development process and were prepared in HNO_3 (Trace Analysis Grade, Fisher Scientific) and diluted to the required concentration with ultrapure water (ELGA PURELAB Flex, Veolia Water, Marlow, UK, 18 MΩ cm, <5 ng/mL Total Organic Carbon). For lower concentration solutions, 1000 µg/mL element standards of europium, gadolinium and terbium were used as the starting solutions (*Johnson Matthey* or *Assurance CertiPrep*, in 5% HNO_3). For higher element concentration solutions, high purity oxide powders (Gd_2O_3, 99.99% REO, *Alfa Aesar* and Eu_2O_3, 99.9%, *Aldrich*) were dissolved in concentrated HNO_3, evaporated to dryness and redissolved in a suitable concentration and volume of HNO_3 to give the desired element concentration.

As per Chapter 4, glass EconoColumns® (*BioRad*, 200 × 7 mm) were packed with LN extraction chromatography resin (*Triskem International*, 50 – 100 µm particle size). Flow rate of solutions through the column were controlled using a Gilson Miniplus Evolution peristaltic pump with associated PVC tubing and connectors.

Active samples of ^{155}Tb, used for method validation, were prepared and delivered to NPL as part of the CERN-MEDICIS collaboration. Details of the production process are included in section 2.1.2 and later in this chapter (Section 5.3.4).

5.2.2 Interference reduced measurement of trace-bulk lanthanide pairs using ICP-QQQ-MS

ICP-MS methods have been used in previous chapters because of their ability to accurately determine ng/mL quantities of a single element in complex element mixtures. Again, ICP-MS methods were used for the stable element analysis during the method development section of this chapter.

Bulk-trace pairs were the subject of analysis in this chapter meaning that the presence and impact of measurement interference is larger (see section 2.3.1). In the case of measuring trace

quantities of terbium in the presence of bulk quantities of gadolinium, it is particularly difficult to achieve interference free measurement due to their neighbouring mass to charge ratios (m/z) and their near identical chemical behaviour[202–204]. As previously discussed, the lanthanide elements actively forms hydride, oxide and hydroxide polyatomic species within the ICP which results in measurement inferences across the lanthanide series (section 4.3.2). When measuring mixed element solutions, tailing of measurement signals into neighbouring masses are more apparent when one element is in large excess, and it can cause significant measurement interference. This is the case when measuring terbium in the presence of bulk quantities of gadolinium.

The ICP-MS measurement method detailed in Chapter 4 was used throughout this chapter in the attempt to accurately measure terbium whilst in the presence of large excesses of gadolinium or europium. This method is summarised in Table 4.3 and is based on the work of Sugiyami and Woods[202,203]. The ability of this method in the detection of bulk-trace lanthanide pairs is discussed later in this chapter (section 5.5.3).

Blank and internal standard corrections were carried out using 2% v/v HNO_3 and 10 ng/mL indium solutions, respectively, to correct for environmental variations throughout analysis runs (see section 2.3.1).

5.2.3 Measurement of radioactive isotopes using gamma-ray spectrometry

Measurement and analysis of radioactive components in solutions was carried out by researchers at NPL using the p-type HPGe gamma-ray spectrometer set up described in section 2.3.2.

The activities of individual radioactive isotopes which were present in samples before and after chemical separation were determined using the GENIE 2000 v3.4.1 software[179] and an in-house developed software package (GAMMANAL v2.1). Net peak areas were calculated, modifying the peak fits using the GENIE 2000 interactive peak fitting application where required, and the activity determined using GAMMANAL. The gamma-ray emission intensities used to determine the activities of ^{155}Tb are given in Table 5.2, along with the emission intensities taken from preliminary determinations made at NPL, which is going to be published shortly. The half-life of ^{155}Tb is taken from preliminary determination made at NPL, with a value of 5.237(10) d. Using these new values resolves a number of discrepancies found in the current

literature[212]. These values have a significantly improved precision. The half-life and gamma-ray intensities of ^{156}Tb have been taken from the evaluation of Reich (2012)[213].

Table 5.2 - Preliminary gamma-ray emission intensities of ^{155}Tb determined at NPL (yet to be published) used to determine ^{155}Tb activity and purity of samples measured at NPL.

Energy /keV	Gamma-ray emissions per 100 decays
86.6	30.71 ± 0.25
105.3	25.57 ± 0.13
148.6	2.504 ± 0.015
161.3	2.609 ± 0.018
163.3	4.310 ± 0.029
180.1	7.003 ± 0.046
262.3	4.802 ± 0.032

5.3 Chemical separation of terbium from bulk quantities of gadolinium

5.3.1 Experimental working capacity of LN resin

Initially it was important to understand the working capacity of the chromatography resin before then assessing the quality of separation that could be achieved with increasing excesses of gadolinium.

The variation in the distribution coefficients (K_d) of terbium with increasing gadolinium excess was studied in order to derive the working capacity of LN resin (50-100 μm). This was done by means of batch separation and was studied in 0.1 M HNO_3 solutions due to the high affinity of gadolinium to the resin at this concentration.

A series of 0.1 M HNO_3 solutions containing increasing quantities of gadolinium (0.5 – 10000 μg/mL) were prepared. An aliquot was taken from each solution (CPS_0, 1 mL) for ICP-MS measurement. Another aliquot from each solution (1 mL) was added to separate centrifuge tubes containing 0.10 ± 0.01g of LN resin. Mixtures were shaken and left for 3 h to reach equilibrium before isolating the aqueous phase by filtration (Whatman 41 ashless filter paper, 20-25 μm pore size). An aliquot was taken from each filtered sample (CPS_t), diluted with 2% v/v HNO_3 and analysed by ICP-MS. The K_d values were calculated using the method detailed in section 2.2.1. This experiment was carried out in triplicate ($n=3$). ICP-MS measurement was conducted in SQ mode (Table 2.3)

A notable reduction in K_d value was observed between ~2 mg Gd/mL LN resin and ~20 mg Gd/mL LN resin. Further investigation identified a working capacity of 6.89 mg – 12.48mg Gd/mL of LN resin (Figure 5.1, $n=3$, standard deviation; Appendix J). A physical change in the HNO_3/LN resin mixtures supported this finding, where in resin particles were seen to coalesce at higher gadolinium content.

Glass Econo-Columns (*BioRad*, 200 mm × 7 mm) packed with LN resin (*Triskem International*, 50 μm -100 μm) were used throughout this study. The working capacity of the column was estimated to be within the range of 53.07 mg – 96.11 mg Gd (equivalent to 61.16 mg – 110.78 mg Gd_2O_3).

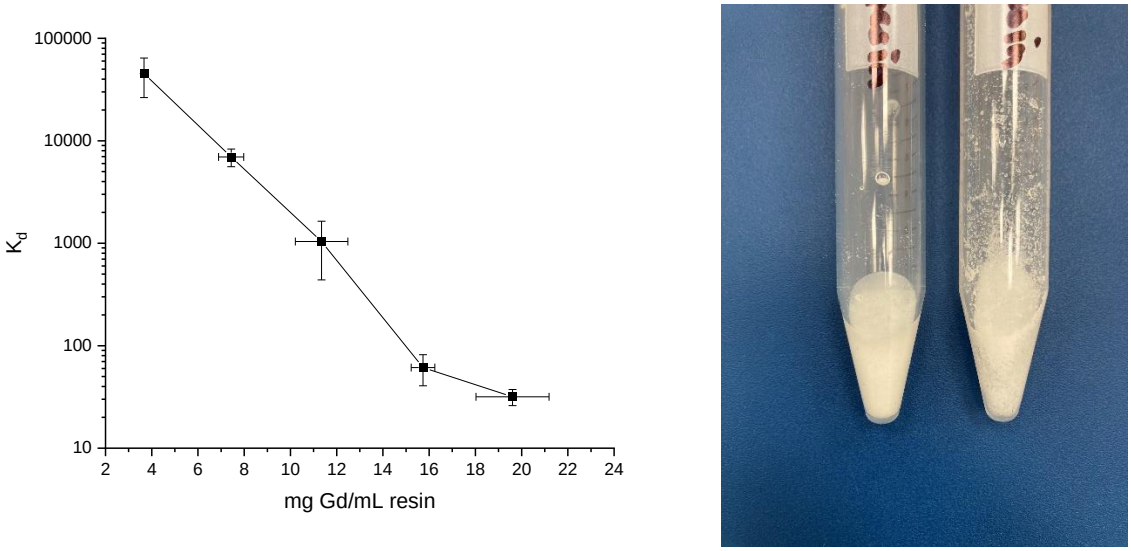

Figure 5.1. - The variation of K_d with increasing excess of gadolinium (Gd, n=3, standard deviation) ***(left)****. Physical change observed between samples suggesting that the working capacity had been exceeded. Left tube = 7.44 mg ± 0.54 mg Gd/mLresin, right tube = 11.35 mg ± 1.14 mg Gd/mL resin* ***(right)****.*

5.3.2 Assessment of column performance for the isolation of terbium from an increasing gadolinium excess

Stable element mixtures containing trace quantities of terbium and bulk quantities of gadolinium were subjected to separation using the method described in Chapter 4 (Table 4.4) in order to assess its suitability for processing terbium isotopes produced by the irradiation of gadolinium targets (e.g., ^{155}Gd(*p*,*n*)^{155}Tb or ^{160}Gd(n,γ)^{160}Tb → ^{161}Tb). The quantities of Gd_2O_3 were chosen based the experimental working capacity of the column and target masses found in the literature (7.3 – 94.9 mg Gd_2O_3 from Gracheva *et al.* 2019)[143].

Three nitric acid solutions (0.75 M, HNO_3) containing 10 000 µg dissolved Gd_2O_3/mL, 50 000 µg dissolved Gd_2O_3/mL and 100 000 µg dissolved Gd_2O_3/mL were prepared. Each solution was spiked with a small volume of terbium standard solution to give 1 µg/mL terbium, whilst minimising the dilution of the gadolinium.

An aliquot of each of these three solutions were taken, diluted with 2% HNO_3 (up to 10000× dilution) and analysed using the previously described ICP-QQQ-MS method (Table 4.3). In separate experiments, another aliquot of each solution was added to the top of a pre-conditioned LN resin column (200 × 7 mm column, 50 – 100 µm resin particle size). The stepwise elution was carried out as previously described with the collection of 1 mL fractions throughout. Some

of these 1 mL fractions underwent sequential dilution to afford a maximum gadolinium concentration of 10 µg/mL (Fractions 1-40, up to 10000× dilution). Knowledge of the elution behaviour of the studied elements from previous studies, allowed the remaining fractions to undergo lesser dilution (Fractions 41-60, 10× dilution). These diluted fractions were then analysed using the same ICP-QQQ-MS analysis method.

The degree to which the bulk gadolinium contaminant was removed from the terbium fraction was quantified by the calculation of the decontamination factor (DF, Equation 5.1)[214].

$$\boldsymbol{DF} = \frac{\boldsymbol{CPS_i(A)}}{\boldsymbol{CPS_{Tb}(A)}} \qquad \textbf{(5.1)}$$

where $CPS_i(A)$ is the concentration of analyte, *A*, in this case gadolinium, in the initial solution and $CPS_{Tb}(A)$ is the concentration of the analyte, *A*, in the terbium fractions post-separation (Fractions 41-50).

Measurement interference in the terbium measurement, significant dilution factors (up to 10000×) and sampling error contributed to inaccurate terbium recovery information being calculated when using equation 2.3. Therefore, element recovery data was normalised using equation 2.4 in order to provide a more realistic estimation of terbium recovery. The benefits and drawbacks of using this method are discussed in section 5.5.3.

Table 5.3. - Summary of the achievable separation of trace quantities of terbium (Tb, 1 µg) from bulk quantities of Gd_2O_3 in 0.75 M HNO_3 solutions. Information related to fractions 41-50 unless otherwise stated. Decontamination factor is the degree to which the bulk Gd_2O_3 contaminant is removed. Reported uncertainties are the standard deviation between repeats (Appendix K).

	10 mg Gd_2O_3 (*n=3*)	**50 mg Gd_2O_3 (*n=1*)**	**100 mg Gd_2O_3 (*n=1*)**
Decontamination Factor	$1.18 \pm 0.13 \times 10^4$	1.20×10^4	5.16×10^3
Tb recovery	104.69 ± 18.19 %	100.65 %	87.42 %
Normalised Tb recovery	98.34 % ± 0.05 %	90.54 %	83.86 %
Tb purity	53.59 % ± 2.76 %	9.82 %	4.15 %
Gd/Tb ratio (after separation)	0.87 ± 0.01	9.18	23.12
Gd recovery (fractions 1-40)	94.52 ± 1.57 %	91.24 %	93.45 %

5.3.3 Behaviour of zinc on LN resin

During the mass-separation process conducted at CERN-MEDICIS, the ion beam, A/q 155 in this study, is implanted into a zinc-coated gold foil. Understanding the chemical behaviour of zinc across a nitric acid concentration range is important to ensure that it will be removed from the terbium fraction during chemical separation.

Separate HNO_3 solutions containing 100 ng/mL Zn were prepared by dilution of a zinc standard elemental standard (1 000 µg/mL Zn, *Trace*CERT®) with HNO_3 solutions (0.005 – 2.0 M). Batch separation studies were conducted as per the method described in section 2.2.1 to derive distribution coefficient information across the HNO_3 concentration range (Figure 5.2).

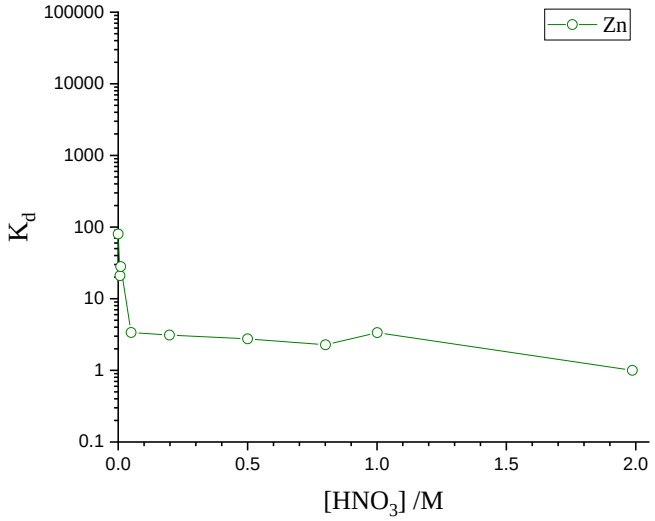

Figure 5.2 – Distribution coefficient (K_d) variation of zinc on LN resin across a nitric acid concentration range (50 – 100 µm particle size).

This study showed that zinc is not retained strongly by LN resin in nitric acid conditions (Figure 5.2, K_d <10, >0.05 M HNO_3) suggesting that zinc is unlikely to cause contamination of the terbium fraction if present in a solution processed using the LN resin column separation method (Table 4.4).

5.3.4 Isolating mass-separated ^{155}Tb from remaining gadolinium target material

Information about the production and initial chemical separation was provided by Nathalie Michel, Ferid Haddad, Cyrille Alliot and Nadia Audouin at ARRONAX (GIP-ARRONAX, Rue Arronax 1, 44800, Saint-Herblain, France).

5.3.4.1 Production of ^{155}Tb source by proton irradiation at cyclotron facilities and initial processing

Three ^{155}Tb sources were produced by researchers at ARRONAX using the proton activation method described in section 2.1.2.1 (i.e., ^{nat}Gd(p,xn) using protons with an ingoing energy of 34 MeV). After irradiation, targets were dissolved in 2 M HNO_3. An aliquot was taken to measure 'end of bombardment' (EOB) activity of ^{155}Tb and radioactive contaminants by gamma spectrometry (Table 5.4). All samples were measured using the same high-purity germanium (HPGe) detector at ARRONAX which had been calibrated previously with standard liquid source from Eckert & Ziegler, Germany.

Table 5.4 – Summary of the beam intensity and the ^{155}Tb activity at the 'end of bombardment' (EOB) in each source shipped to NPL.

Production Date	**Cumulated beam intensity (µAh)**	**^{155}Tb EOB activity (MBq)**
08.06.2020	392	831 ± 41
29.07.2020	360	692 ± 34
27.10.2020	362	751 ± 37

These ^{155}Tb sources underwent an initial chemical separation conducted by researchers at the ARRONAX facility to reduce the gadolinium content ahead of offline mass separation conducted at the CERN-MEDICIS facility.

A two-step chemical separation method using LN resin was used, similar to the one developed in this study (Table 4.4). The first step in this separation was conducted (Table 5.5) and all terbium fractions were combined, evaporated to dryness at 125 °C and then recovered with 0.75 M HNO_3 ahead of the second separation step (Table 5.6).

Table 5.5 – The first chemical separation step used at ARRONAX to process ^{155}Tb sources ahead of isotope separation at CERN-MEDICIS.

Separation step	**Conditions**
Precondition	0.75 M HNO_3
Load	Target residue in 0.75 M HNO_3 (12 mL)
Gd elution (Step 1)	0.75 M HNO_3 (32 mL)
Gd elution (Step 2)	1.00 M HNO_3 (60 mL)
Tb elution (Step 1)	1.00 M HNO_3 (20 mL)
Tb elution (Step 2)	2.00 M HNO_3 (85 mL)
Resin	LN resin (100 - 150 μm)
Column volume	36.9 mL
Flow rate	1 mL/min

Table 5.6 - The second chemical separation step used at ARRONAX to process ^{155}Tb sources ahead of isotope separation at CERN-MEDICIS.

Separation step	**Conditions**
Precondition	0.75 M HNO_3
Load	Target residue in 0.75 M HNO_3 (12 mL)
Gd elution	1.00 M HNO_3 (15 mL)
Tb elution (Step 1)	1.00 M HNO_3 (10 mL)
Tb elution (Step 2)	2.00 M HNO_3 (20 mL)
Resin	LN resin (100 - 150 μm)
Column volume	8.6 mL
Flow rate	1 mL/min

After the second separation step was conducted, fractions containing >1% of the initial ^{155}Tb activity were combined and evaporated to dryness at 175°C. The residue was recovered in 0.01 M HNO_3 (3 mL) and transferred to a dedicated sample holder developed at CERN. The final solution was evaporated to dryness at 175°C in the sample holder. High terbium recovery was achieved (>80%) using this method, with the ^{155}Tb:Gd ratio being reduced from ~1:1 000 000 to <1:100. The method used to calculate the ^{155}Tb:Gd ratio was not shared, and no detailed radioactive or stable impurity information was provided for these sources.

These ^{155}Tb sources were then sent to CERN-MEDICIS for offline mass separation to remove other co-produced terbium isotopes which were not removed in the chemical separation (section 2.1.3). The mass separated ^{155}Tb source was then shipped to NPL for further chemical processing in order to prepare the ^{155}Tb for radiolabelling studies, SPECT imaging studies and for fundamental measurements.

5.3.4.2 Measurement of ^{155}Tb source prior to separation

One ^{155}Tb source (production date: 27.10.2020) was measured by gamma spectrometry by researchers at NPL prior to chemical separation in order to identify any major radioactive impurities and to allow for the calculation of percentage recovery information post-separation (Table 5.7).

For this source, the zinc layer of the foil was dissolved in approximately 10 mL of 6 M HCl. An aliquot (~0.2 g) was taken from this solution, made up to 1 mL with 6 M HCl, and measured by HPGe gamma-ray spectrometry using the previously described method (see section 2.3.2). The remainder of the dissolved zinc layer was processed using the separation procedure presented in this work (Table 4.4).

5.3.4.3 Isolation of ^{155}Tb from remaining gadolinium target material

The application of the LN resin method to the mass-separated ^{155}Tb sources aimed to remove the zinc collection material as well as to remove any remaining gadolinium impurities. The method was not capable of removing any remaining ^{156}Tb impurities from the ^{155}Tb due to the fact that different isotopes of the same element have identical chemical behaviour.

The chemical separation was carried out as previously reported (Table 4.4) and afforded high terbium recovery (> 80%) akin to the stable element separations (Table 5.7). These results were comparable to those achieved in the initial chemical separations conducted by ARRONAX (section 5.3.3.1). Due to time constraints, stable element analysis was not conducted to quantify the presence of gadolinium and zinc impurities present in the final source.

Significant differences in the activity reported at EOB and post-chemical separation were observed. Significant processing times and long transport times did contribute to this difference. Information about other possible contributors, such as the recovery yield when using mass-separation techniques, were not available from the supplied information.

Table 5.7 – Characteristics of ^{155}Tb sources sent to, and chemically purified at NPL. $f_{Tb\text{-}156} = A_{Tb\text{-}156}/A_{Tb\text{-}155}$ post separation. N/A = not applicable.

Reference time (UTC)	**Activity of ^{155}Tb pre-separation (MBq)**	**Activity of ^{155}Tb post-separation (MBq)**	**Yield (A_{Post}/A_{Pre})**	**Detected gamma-ray emitting radionuclide impurity**	**Post-separation application**
2020-07-20 12:00	*Not measured at NPL*	0.981(11)	*N/A*	$f_{Tb\text{-}156}$ = 0.000359(36)	Radiolabelling studies with Trastuzumab at Lausanne University Hospital
2020-08-05 12:00	*Not measured at NPL*	2.198(20)	*N/A*	$f_{Tb\text{-}156}$ = 0.000381(57)	Radiolabelling studies with DOTAGA-HGA at KU Leuven
2020-11-03 12:00	18.45(14)	15.31(10)	0.8298(63)	$f_{Tb\text{-}156}$ = 0.000454(75)	SPECT imaging studies at NPL and KU Leuven. Nuclear data measurements at NPL (primary standardisation and half-life measurement)

5.3.4.4 Post-separation use of ^{155}Tb sources

The first of the three sources (production date: 08.06.2020, 0.981MBq ^{155}Tb) was sent to Lausanne University Hospital, Switzerland, on 24.07.2020 for radiolabelling studies with Trastuzumab, a monoclonal antibody. Researchers at Lausanne University Hospital prepared CHX-A″-DTPA-Trastuzumab, which was added to a buffered ^{155}Tb solution and incubated for 60 min at 38°C. A >99% radiolabelling yield of CHX-A″-DTPA-Trastuzumab with ^{155}Tb was reported and confirmed by instant thin-layer chromatography (iTLC) with no free ^{155}Tb being observed.

The second ^{155}Tb source (production date: 29.07.2020, 2.198 (20) MBq ^{155}Tb) was sent to KU Leuven on 07.08.2020 for radiolabelling studies with DOTAGA-HSA. Researchers at KU Leuven directly labelled DOTAGE-HSA with ^{155}Tb from a buffered HCl solution (0.005 M HCl, pH 4.7, $^{155}TbCl_3$) by incubation at 40°C for 60 min. A >99% radiolabelling yield of DOTAGA-HSA with ^{155}Tb was reported and confirmed by iTLC and radio-size exclusion chromatography (radio-SEC).

These successful radiolabelling studies showed that the post-separation ^{155}Tb fractions were of suitable purity. Even though remaining gadolinium and zinc impurities were not quantified, they were sufficiently low to allow efficient labelling of two different biomolecule compounds with ^{155}Tb.

In addition to these radiolabelling studies, half of the final ^{155}Tb source (production date: 27.10.2020, ~7.5 MBq ^{155}Tb) was sent to KU Leuven on 05.11.2020 for radiolabelling studies. The remaining activity (~7.5 MBq ^{155}Tb) remained at NPL for SPECT imaging studies and nuclear data measurements (i.e., a primary standardisation and a new half-life measurement).

5.4 Chemical separation of terbium from bulk quantities of europium

The method has been shown to be capable of separating terbium from bulk quantities of gadolinium, but terbium radioisotopes (^{152,155}Tb) can also be produced by the irradiation of europium targets with alpha particles at suitably equipped cyclotron facilities (i.e., ^{151,153}Eu(α, xn) nuclear reactions)[117,209]. The use of the method developed in this work (Table 4.4) for the isolation of terbium from bulk europium material was therefore investigated. Research into this alternative production method is only in its infancy and at present only one initial study has

reported experimental data for the production of ^{155}Tb in this way[121]. Poor production yields were achieved (~kBq) from large targets (~200 mg europium metal).

In this previous study, Kazakov *et al.* used a LN resin method, similar to the one described in this report, to isolate the produced ^{155}Tb from the remaining trace quantities of europium target material. Most of the europium target material had already been removed in a selective reduction and precipitation step. This study showed the resin to be capable of isolating ^{155}Tb from trace europium. To build on this work, here the separation of bulk europium and trace terbium was investigated.

The quantities of Eu_2O_3 used in this section were based on the derived experimental working capacity of the column and target masses found in the literature for the production of ^{161}Tb by neutron irradiation of a ^{160}Gd target (7.3 – 94.9 mg Gd_2O_3 from Gracheva *et al.* 2019)[143]. Kazakov et al. used a 200 mg europium metal target in their initial study, however, as it is unlikely that the size of column used in these studies (7.7 mL, 200 x 7 mm) would have been capable of efficiently isolating trace quantities of terbium, solutions containing ≤100 mg dissolved Eu_2O_3 were used in these initial studies. Using the same quantities of Eu_2O_3 as used for the bulk Gd experiments (section 5.3.2) also allowed for direct comparison between the two.

Solutions containing bulk quantities of europium were prepared by the dissolution of Eu_2O_3 in concentrated HNO_3, evaporation to near dryness and redissolution of the residue in 0.75 M HNO_3 to give the desired europium concentration. A low volume (100 µL) of a terbium standard solution was added to give 1 µg/mL terbium whilst minimising the dilution of the europium. An aliquot of each of these solutions were taken for ICP-MS analysis. Separately, another aliquot of each solution (1 mL) was added to the top of a pre-conditioned column and the separation procedure was carried as described in Table 4.4. Fractions (1 mL) were collected throughout, diluted with 2% v/v HNO_3 and analysed by ICP-MS. Decontamination factors were calculated as per Equation 5.1.

As with the bulk gadolinium separation, significant dilution factors (up to 10000×) and sampling error may have contributed to inaccurate terbium recovery information. Data was therefore normalised using equation 5.2 to provide an estimation of terbium recovery. This also allowed comparison to be made between the bulk europium and bulk gadolinium separations.

Table 5.8. - Summary of the achievable separation of trace quantities of terbium (Tb, 1 μg) from bulk quantities of europium in 0.75 M HNO_3 solutions (see also Appendix L). Information related to fractions 41-50 unless otherwise stated. Decontamination factor is the degree to which the bulk europium contaminant is removed.

	10 mg Eu_2O_3 (*n=1*)	**50 mg Eu_2O_3 (*n=1*)**
Decontamination Factor	2.45×10^4	1.93×10^4
Tb recovery	102.49 %	111.71 %
Normalised Tb recovery	99.92 %	99.92%
Tb purity	71.02 %	27.86 %
Eu/Tb ratio (after separation)	0.41	2.59
Eu recovery (fractions 1-40)	90.16 %	87.74 %

5.5 Discussion and summary of results

5.5.1 Derivation of LN resin's working capacity

The working capacity of a resin is a useful and important piece of information to be aware of when designing or assessing the suitability of a chromatography resin for different separation challenges. Exceeding the column capacity may give reason to sub-optimal separation.

A novel batch separation approach was developed in this study to derive resin capacity information (section 5.3.1). This approach produced results of adequate precision for LN resin (~10% relative standard deviation, RSD). The calculated capacity range was supported by a change in physical appearance in the resin-solution mixture (see Figure 5.1), and a fall in column separation performance at higher gadolinium content (Table 5.3). The column capacity was derived to be in the range of 6.89 mg – 12.48mg Gd/mL of LN resin from 0.1 M HNO_3 solutions. This capacity range is inflated due to the inclusion of the variation between repeats (± 1σ). The working capacity of the resin was identified as being the main limiting factor for the column separation method used in this chapter. Importantly, significant co-elution of terbium with the bulk element was not observed in the column separation. A drop in column performance was observed however at increased bulk element concentrations (~100 mg) causing an increased contamination of the terbium fraction.

In a recent study, Smith and Dietz[215] investigated the impact of HDEHP support loading on column performance. As part of this, they derived a method for the determination of resin capacity information. Noting that the LN resin used in this study has a HDEHP support loading of 40 % (w/w), the value derived here is comparable to the value reported by Smith and Dietz for a different HDEHP-based extraction chromatography resin (11.04 mg Eu/mL bed at 40% w/w).

The resin's manufacturer, *Triskem International*, however, states a capacity of 0.16 mmol/mL LN resin for lanthanides and trivalent actinides and this was taken from the original Eichrom data. This equates to 25.2 mg Gd/mL LN resin which is significantly higher than the range derived in this study. The method used to derive this value is unknown, so no comment can be made on its accuracy.

Here, the capacity of LN resin was studied for gadolinium from 0.1 M HNO_3 solutions only. These conditions were chosen due to gadolinium being the initial focus of this chapter, and because lanthanides have the highest affinity at this HNO_3 concentration. For this reason, the derived capacity range likely reflects the maximum working capacity of the resin for all other lanthanides. The results of column separation studies (Table 5.8) and the values reported by Smith and Dietz[215] supported this hypothesis.

Repeats of the experiment, studying the behaviour of a range of elements under different mobile phase compositions, would prove useful in further assessing the ability of this novel batch separation approach for deriving useful capacity information. It will also contribute to a greater understanding of the characteristics and limits of the resin. This should be considered in future studies.

Comparison to other capacity deriving methods, such as the column-based approach reported by Horwitz *et al.*[216] for resins based on tetraalkyldiglycolamides, would also be helpful assessing the accuracy and reproducibility of this novel batch separation approach.

5.5.2 Suitability of the LN resin separation method

The separation method developed in Chapter 4 was shown to be capable of isolating terbium from a bulk amount of either gadolinium or europium (Table 5.3 and Table 5.8, respectively, decontamination factor ~10^4, terbium recovery >80%). This extraction chromatography method is comparable to the commonly used α-HIBA/cation exchange method for isolation of terbium from bulk lanthanide impurities (<100 mg)[143].

As was expected, better separation of terbium from bulk europium was achieved compared to separation of terbium from bulk gadolinium. This is due to the larger terbium-europium separation factor (Figure 4.3, Appendix L).

The method was used to process radioactive ^{155}Tb sources produced from gadolinium foil targets. Post-separation, these sources were used in radiolabelling studies conducted at KU Leuven, Belgium and Lausanne University Hospital, Switzerland. These radiolabelling experiments were successful, with both laboratories reporting a radiolabelling yield of >99% and this highlighted the potential of this chemical separation method to enable pre-clinical studies. This method was, however, only applied to the ^{155}Tb sources once two separation steps and a mass separation step had already been applied. Further testing of this method would be required to fully assess its ability to isolate terbium from bulk impurities and thus its ability to produce high quality terbium sources for nuclear medicine applications. Stable element analysis of the terbium fraction would also be useful to better understand the quality of separation.

In order to isolate radioactive terbium from greater quantities of target material (>100 mg), further method development work would be required to scale up the method by means of an increased column length or volume. This would result in an increase in processing time and its impact on the radiochemical yield should be evaluated in further studies.

In a private communication, researchers at ARRONAX, informed NPL of a similar stepwise LN resin method that they used to isolate radioactive terbium from bulk quantities of gadolinium target material (>100 mg gadolinium metal, see section 5.3.3.1). As expected, larger columns and mobile phase volumes were used. Their results suggest a reduction in gadolinium excess by >10^4, however their findings are yet to be published and the details provided in this private communication are limited. This limits the comparison that can be made to the method developed in this study.

Terbium recoveries and decontamination factors could be improved upon by using a smaller particle size LN resin. This would result in sharper peaks due to a reduced effect of mass transfer of elements between the two phases[217]. Batches of LN resin with smaller particle size are more expensive and this increased cost should be considered against the degree to which the smaller particle size improves the separation outcomes. A resin with increased HDEHP loading would also provide a higher capacity resin, capable of processing larger targets[215]. This is something which is being investigated by the manufacturer.

Stable-element method development studies suggested that ~90% of the original target material could be recovered post-chemical separation (in fractions 1 – 40). Recovery of the gadolinium or europium fractions and further processing (e.g., calcination to oxide form) would allow the target material to be used for additional production runs. This would be of particular benefit if enriched single isotope targets are used as it would make them a more affordable option[101].

5.5.3 Assessment of the ICP-QQQ-MS measurement approach

ICP-QQQ-MS techniques are renowned for high resolution, high sensitivity measurement across a wide linear dynamic range (~10^9) and has an impressive measurement interference removal capability. In Chapter 4, an efficient method was used to enable the interference-free measurement of trace quantities of neighbouring lanthanides (section 4.3.2). In this chapter, the same ICP-QQQ-MS method was used in the attempt of providing interference-free measurement of trace lanthanide/bulk lanthanide pairs.

The generation of useful qualitative data was relatively unaffected despite the large gadolinium or europium excess present in these studies (e.g., understanding how each element behaves on the column/building of elution profiles). When generating quantitative data, several factors shed uncertainty on the results, particularly regarding the precision and accuracy of the calculated decontamination factor and percentage terbium recovery values.

Because of the high concentration of the bulk element in the starting mixtures, up to 100 mg/mL, sequential dilution was required to bring the concentration down to a level that could be accurately quantified by ICP-QQQ-MS (<10 µg/mL, up to 10,000× dilution for the starting solution and fractions 1-40). This significant dilution allowed the determination of the bulk element in the starting solutions and in individual fractions, and therefore allowed an estimation of the amount of target material that could be recycled after separation. The quantification of the trace elements, however, was more challenging when such a high dilution factor was used

(1 µg/mL in starting solution, < 0.1 ng/mL terbium after dilution). In particular, for trace terbium/bulk europium separation, the measurement of trace gadolinium in fractions 1-40 was not achievable using the ICP-QQQ-MS method.

Knowledge of the elution behaviour of europium, gadolinium, and terbium from the previous studies in chapter 4 allowed for smaller dilutions to be made for the later fractions (fractions 41-60, 10× dilution). This increased the counting statistics of the trace element measurements and allowed a more realistic estimation of percentage terbium purity and recovery information.

Repeat experiments would improve the precision of the calculated data and would allow the calculation of the standard deviation of data points. Repeat experiments were only conducted for Gd_2O_3:Tb, 10000:1, but should be conducted for the others in future studies. Repeats, however, will not highlight the presence of any systematic error that may arise from the measurement itself. Two sources of systematic error were identified: the presence of polyatomic interferences and high/low mass tailing.

Polyatomic interferences and high/low mass tailing interference are more apparent when isotopes of neighbouring masses are at a large excess. These measurement inferences, although greatly reduced when using the ICP-QQQ-MS method (Table 4.3), are still observed when measuring terbium as $^{159}Tb^{16}O$ at m/z 175. When gadolinium is in a large excess, up to 100000× in the case of this study, tailing interference from $^{158}Gd^{16}O$ and $^{160}Gd^{16}O$, and polyatomic interference from $^{158}Gd^{16}O^{1}H$ will contribute to the signal detected at m/z 175. This was observed when separating ~100 mg gadolinium from 1 µg terbium where co-elution seemed to appear on the elution profile (100000× excess, Appendix K, Figure K.3). Total terbium recovery values exceeded 100% when calculated using equation 2.3, which suggested that the cause was not co-elution but rather measurement interference. Terbium recovery for the other bulk gadolinium, trace terbium experiments at lower gadolinium content (10 mg and 50 mg Gd_2O_3) also exceeded 100%, although this was not as obvious on the elution profiles. On average 0.00141 % ± 0.00022% of the gadolinium signal at m/z 173 was showing up in the instrument response at m/z 175 (based of fractions 11-30, see Appendix M, $n=5$), supporting the hypothesis that measurement interferences were contributing to the inaccurate terbium recovery information.

To provide a more realistic estimate of the terbium recoveries, the data were normalised by assuming that exactly 100% of the terbium was recovered during separation (see equation 2.4).

This corrected for sampling error between the aliquots taken and added to the column, and those taken for the $(CPS)_0$ measurement (see equation 2.3). It did not correct for any measurement interference, however. Therefore, the normalised terbium recovery will be more accurate for the lower bulk element excess experiments (e.g., 10 mg Gd_2O_3, 1 μg terbium separations), where polyatomic and tailing interferences were less apparent. The low standard deviation between repeats supports this statement (98.34 % ± 0.05 %, n=3). In all cases, the normalised terbium recovery values are likely to be an under-estimation due to them not correcting for increased CPS input from the polyatomic and tailing of gadolinium into the terbium measurement. Consistently using this approach, despite its obvious drawbacks, allowed the identification of trends in the quality of separation with increasing bulk element excess and allowed for comparison between different bulk elements experiments.

An alternative measurement approach to improve the accuracy of the trace element measurements could involve spiking bulk element solutions with moderately long-lived isotopes of the trace elements (e.g., ^{160}Tb, $t_{½}$=72.3 (2) d) and then measuring them by gamma spectrometry. This approach is used frequently in the literature[27,143,144,147,214]. The bulk gadolinium or europium content could still be measured by ICP-QQQ-MS methods. This alternative approach would avoid the error imposed by polyatomic interferences, tailing interferences and significant dilution. It would also improve the accuracy of the trace element measurements within each fraction, thus improving the accuracy of calculated terbium recovery and purity information as well as providing a better understanding of the elution behaviour of all elements under these extreme conditions.

5.6 Chapter conclusion

The LN extraction chromatography method developed in chapter 4 was shown to be capable of isolating trace quantities of terbium from bulk quantities of either gadolinium or europium (≤ 100 mg). Bulk element content was reduced by about four orders of magnitude whilst still recovering a high proportion of the terbium (>80 % recovery). Repeat experiments and use of alternative method development approaches should be a priority in future studies to improve the reliability of the metrological information reported in this chapter (i.e., decontamination factor, terbium recovery and terbium purity).

This method was successfully applied to mass-separated ^{155}Tb sources produced from the irradiation of large gadolinium targets. Resultant ^{155}Tb sources were used for radiolabelling studies, SPECT imaging studies and nuclear data measurements conducted by various leading European research institutions, all of which suggesting that a suitable ^{155}Tb purity had been achieved as a result of the chemical separation.

Chapter 6. Summary and concluding remarks

Four terbium isotopes, ^{149}Tb, ^{152}Tb, ^{155}Tb and ^{161}Tb have been identified as excellent candidates for use in all aspects of nuclear medicine. Therapeutic ^{149}Tb or ^{161}Tb nuclides used in combination with the diagnostic ^{152}Tb or ^{155}Tb have the potential to facilitate theranostic, and therefore, personalised medicine. Even though interest in these isotopes has grown considerably over recent years, research into the use of these isotopes in medicine is still in its infancy and, therefore, a pipeline for their production, purification and radiopharmaceutical preparation is yet to be put in place. To enable investigation into the pre-clinical use of these isotopes, this project investigated the suitability of extraction chromatography methods for the chemical separation and preparation of high quality terbium sources. Methods were developed using stable element standards and ICP-MS measurement and, where possible, procedures were validated using active samples provided to NPL by members of the CERN-MEDICIS collaboration. This work enabled further radiolabelling studies, medical imaging studies and the taking of fundamental measurements.

Initially, a separation method was developed, capable of isolating ^{155}Tb from the significant ^{139}Ce impurities present in mass-separated proton-induced spallation ^{155}Tb sources. High radiological purity ^{155}Tb sources (>99 %) were isolated by the selective oxidation of cerium, using sodium bromate, and subsequent separation on a UTEVA extraction chromatography column (Figure 3.5). The resultant ^{155}Tb sources were used for a world-first primary standardisation, nuclear data measurements, radiolabelling studies and SPECT imaging studies, all conducted by other researchers as part of the CERN-MEDICIS collaboration.

This UTEVA extraction chromatography method, however, was unable to isolate terbium from any other long-lived or stable lanthanides isotopes present in proton-induced spallation ^{149}Tb, ^{152}Tb and ^{155}Tb sources. Any significant contamination that remains impacts negatively upon the efficiency of radiolabelling studies and, depending on the contaminant, introduces an unnecessary dose of radiation to a patient. This necessitated further study into alternative extraction chromatography methods.

As a result, a new semi-automated method using LN extraction chromatography resin (Table 4.4) was developed to isolate trace quantities of terbium from trace quantities of other lanthanides. An ICP-QQQ-MS method (Table 4.3) using two quadrupole mass filters and an O_2 reaction cell was successfully applied in this study to achieve interference free measurement.

Midway through the separation method development process, an unexplained shift in elution peaks was observed between the two batches of LN resin used in this study. Further study would be required to understand the cause of this difference and thus improve the trustworthiness of the developed method. Both batches of resin, however, were still capable of isolating high purity terbium fractions, so the study continued. This method was then tested using 'simulant ^{149}Tb, ^{152}Tb or ^{155}Tb' which contained stable analogues of other lanthanide isotopes expected to be found in mass-separated proton-induced spallation terbium sources. This method was shown to capable of isolating a high proportion of terbium (>90% terbium recovery) from all lanthanide impurities (>99% terbium purity).

To develop this study further, it was important to assess the suitability of this LN resin method for isolating the terbium isotopes produced by other production methods, namely by the irradiation of gadolinium or europium targets at cyclotron or nuclear reactor facilities. Initially the working capacity of the resin was calculated in order to understand the limitations of the method. A capacity range of 6.89 mg – 12.48mg Gd/mL of LN resin was determined using a novel batch separation method. This value agreed with one other found in the literature[218], but disagreed with the value reported by the manufacturer[142]. Column separation studies with bulk quantities of gadolinium also supported the value derived in this work.

Column experiments studying the separation of trace amounts of terbium from bulk quantities of gadolinium or europium (≤100 mg Gd_2O_3 or Eu_2O_3) recovered a high proportion of terbium (>80% terbium recovery) whilst removing a significant proportion of the bulk element (decontamination faction ~10^4). Bulk element contamination of the terbium fraction increased with the excess, suggesting that the column capacity had been exceeded and column performance had reduced at the higher concentrations (e.g., 100 mg Gd_2O_3).

Although it was shown to be capable of achieving interference-free measurement of trace quantities of neighbouring lanthanides, the ICP-QQQ-MS method (Table 4.3) did not achieve interference-free measurement for the bulk gadolinium experiments. This resulted in inaccurate terbium recoveries being calculated. Unquantified error in the sampling and dilution also contributed to inaccuracies. Normalisation of the terbium recovery allowed for a more realistic estimation of the terbium recovery by correcting for sampling error but would likely be an underestimation due to it not correcting for measurement interferences. Despite the measurement challenges, the method was fit-for-purpose.

Researchers at NPL subsequently applied the LN resin method to three mass-separated ^{155}Tb sources produced by the irradiation of gadolinium targets. As per the stable element studies, good terbium recovery was achieved (>80%) with resultant solutions being of suitable purity to facilitate successful radiolabelling studies (>99% radiolabelling yield), SPECT imaging phantom studies and nuclear data measurements.

Further improvement of this method by testing other HDEHP-based resins which have increased capacity (higher HDEHP %w/w) and finer particle size (sharper peaks, reduced mass-transfer effects) would improve the removal of bulk element from the terbium fractions. Investigation into the use of larger columns would also allow for larger targets to be processed without negatively impacting the chemical recovery. Repeats are essential in future studies in order to improve reliability and reproducibility of the methods.

Converting this method into an automated system would also be of interest in future studies. Automation would result in improved ease of use, increased reliability and reproducibility, and would result in reduced exposure to radiation due to minimised human interaction during the separation (e.g., by adaptation of the method for HPLC).

In summary, this work has laid the groundwork for using LN extraction chromatography resin for isolating radioactive terbium from trace and bulk lanthanide impurities which are present after isotope production. This work has found the use of LN extraction chromatography methods comparable to the commonly used α-HIBA/cation exchange chromatography methods[143].

This project has also contributed to the larger aim of making the medically interesting terbium isotopes, ^{149,152,155,161}Tb, more widely accessible to the research community, by assessing alternative routes of radiochemical processing. As a result of this work, radiolabelling studies, SPECT imaging studies, nuclear data measurements and a world first primary standardisation have been conducted for ^{155}Tb. The methods reported here are capable of providing radiochemical purification of all of the aforementioned terbium isotopes for various cyclotron, nuclear reactor and synchrotron-based production methods.

References

1 A. Kułakowski, The contribution of Marie Skłodowska-Curie to the development of modern oncology., *Anal. Bioanal. Chem.*, 2011, **400**, 1583–6.

2 C. Schiepers and M. Allen-Auerbach, *Diagnostic nuclear medicine*, Springer, 2006.

3 M. K. Yu, J. Park and S. Jon, Targeting strategies for multifunctional nanoparticles in cancer imaging and therapy., *Theranostics*, 2012, **2**, 3–44.

4 G.-J. Beyer, M. Miederer, S. Vranješ-Đurić, J. J. Čomor, G. Künzi, O. Hartley, R. Senekowitsch-Schmidtke, D. Soloviev and F. Buchegger, Targeted alpha therapy in vivo: direct evidence for single cancer cell kill using 149Tb-rituximab, *Eur. J. Nucl. Med. Mol. Imaging*, 2004, **31**, 547–554.

5 A. Boschi, L. Uccelli and P. Martini, A Picture of Modern Tc-99m Radiopharmaceuticals: Production, Chemistry, and Applications in Molecular Imaging, *Appl. Sci.*, 2019, **9**, 1–16.

6 Brookhaven National Laboratory, National Nuclear Data Center, http://www.nndc.bnl.gov/, (accessed 20 August 2021).

7 National Research Council, in *Medical Isotope Production Without Highly Enriched Uranium*, National Academies Press, Washington, D.C., 2009.

8 Nuclear Energy Agency, *The Supply of Medical Radioisotopes - Review of potential molybdenum-99/technetium-99m production technologies*, 2010.

9 L. M. Filzen, L. R. Ellingson, A. M. Paulsen and J. C. Hung, Potential ways to address shortage situations of 99Mo/99mTc, *J. Nucl. Med. Technol.*, 2017, **45**, 273–277.

10 S. C. Vaz, F. Oliveira, K. Herrmann and P. Veit-Haibach, Nuclear medicine and molecular imaging advances in the 21st century, *Br. J. Radiol.*, 2020, **93**, 1–12.

11 R. Baskar, J. Dai, N. Wenlong, R. Yeo and K.-W. Yeoh, Biological response of cancer cells to radiation treatment., *Front. Mol. Biosci.*, 2014, **1**, 1–9.

12 M. Schlumberger, C. Challeton, F. De Vathaire, J. P. Travagli, P. Gardet, J. D. Lumbroso, C. Francese, F. Fontaine, M. Ricard and C. Parmentier, Radioactive iodine treatment and external radiotherapy for lung and bone metastases from thyroid carcinoma., *J. Nucl. Med.*, 1996, **37**, 598–605.

13 C. Parker, S. Nilsson, D. Heinrich, S. I. Helle, J. M. O 'sullivan, S. D. Fosså, A. Chodacki, P. Wiechno, J. Logue, M. Seke, A. Widmark, D. C. Johannessen, P. Hoskin, D. Bottomley, N. D. James, A. Solberg, I. Syndikus, J. Kliment, S. Wedel, S. Boehmer, M. Dall 'oglio, L. Franzén, R. Coleman, N. J. Vogelzang, C. G. O 'bryan-Tear, K. Staudacher, J. Garcia-Vargas, M. Shan, Ø. S. Bruland and O. Sartor, Alpha Emitter Radium-223 and Survival in Metastatic Prostate Cancer, *N. Engl. J. Med.*, 2013, **369**,

213–223.

14 I. G. Finlay, M. D. Mason and M. Shelley, Radioisotopes for the palliation of metastatic bone cancer: a systematic review, *Lancet Oncol.*, 2005, **6**, 392–400.

15 C.-H. Yeong, M.-H. Cheng and K.-H. Ng, Therapeutic radionuclides in nuclear medicine: current and future prospects, *J Zhejiang Univ-Sci B (Biomed Biotechnol)*, 2014, **15**, 845–863.

16 A. Yordanova, E. Eppard, S. Kürpig, R. A. Bundschuh, S. Schönberger, M. Gonzalez-Carmona, G. Feldmann, H. Ahmadzadehfar and M. Essler, Theranostics in nuclear medicine practice., *Onco. Targets. Ther.*, 2017, **10**, 4821–4828.

17 S. M. Qaim, Theranostic radionuclides: recent advances in production methodologies, *J. Radioanal. Nucl. Chem.*, 2019, **322**, 1257–1266.

18 F. Rösch, H. Herzog and S. M. Qaim, The beginning and development of the theranostic approach in nuclear medicine, as exemplified by the radionuclide pair 86Y and 90Y, *Pharmaceuticals*, 2017, **10**, 1–28.

19 L. Filippi, A. Chiaravalloti, O. Schillaci, R. Cianni and O. Bagni, *Expert Rev. Med. Devices*, 2020, 17, 331–343.

20 J. F. G. Marin, R. F. Nunes, A. M. Coutinho, E. C. Zaniboni, L. B. Costa, F. G. Barbosa, M. A. Queiroz, G. G. Cerri and C. A. Buchpiguel, Theranostics in nuclear medicine: Emerging and re-emerging integrated imaging and therapies in the era of precision oncology, *Radiographics*, 2020, **40**, 1715–1740.

21 N. Jokar, M. Assadi, A. Yordanova and H. Ahmadzadehfar, Bench-to-Bedside Theranostics in Nuclear Medicine, *Curr. Pharm. Des.*, 2020, **26**, 3804–3811.

22 F. Rösch and E. Forssell-Aronsson, in *Metal ions in biological systems: Volume 42: Metal complexes in tumor diagnosis and as anticancer agents*, Marcel Dekker, 2004, pp. 78–101.

23 M. Van de Voorde, K. Van Hecke, T. Cardinaels and K. Binnemans, Radiochemical processing of nuclear-reactor-produced radiolanthanides for medical applications, *Coord. Chem. Rev.*, 2019, **382**, 103–125.

24 L. Emmett, K. Willowson, J. Violet, J. Shin, A. Blanksby and J. Lee, Lutetium 177 PSMA radionuclide therapy for men with prostate cancer: a review of the current literature and discussion of practical aspects of therapy, *J. Med. Radiat. Sci.*, 2017, **64**, 52–60.

25 M. L. Smits, J. F. Nijsen, M. A. van den Bosch, M. G. Lam, M. A. Vente, J. E. Huijbregts, A. D. van het Schip, M. Elschot, W. Bult, H. W. de Jong, P. C. Meulenhoff and B. A. Zonnenberg, Holmium-166 radioembolization for the treatment of patients with liver metastases: design of the phase I HEPAR trial, *J. Exp. Clin. Cancer Res.*, 2010, **29**, 1–11.

26 C. Müller, A. Singh, C. A. Umbricht, H. R. Kulkarni, K. Johnston, M. Benešová, S. Senftleben, D. Müller, C. Vermeulen, R. Schibli, U. Köster, N. P. van der Meulen and R. P. Baum, Preclinical investigations and first-in-human application of 152Tb-PSMA-617 for PET/CT imaging of prostate cancer, *EJNMMI Res.*, 2019, **9**, 1–10.

27 C. Muller, K. Zhernosekov, U. Koster, K. Johnston, H. Dorrer, A. Hohn, N. T. van der Walt, A. Turler and R. Schibli, A Unique Matched Quadruplet of Terbium Radioisotopes for PET and SPECT and for alpha and beta- Radionuclide Therapy: An In Vivo Proof-of-Concept Study with a New Receptor-Targeted Folate Derivative, *J. Nucl. Med.*, 2012, **53**, 1951–1959.

28 C. Müller, C. Vermeulen, K. Johnston, U. Köster, R. Schmid, A. Türler and N. P. van der Meulen, Preclinical in vivo application of 152Tb-DOTANOC: a radiolanthanide for PET imaging, *EJNMMI Res.*, 2016, **6**, 1–10.

29 C. Müller, E. Fischer, M. Behe, U. Köster, H. Dorrer, J. Reber, S. Haller, S. Cohrs, A. Blanc, J. Grünberg, M. Bunka, K. Zhernosekov, N. van der Meulen, K. Johnston, A. Türler and R. Schibli, Future prospects for SPECT imaging using the radiolanthanide terbium-155 — production and preclinical evaluation in tumor-bearing mice, *Nucl. Med. Biol.*, 2014, **41**, 58–65.

30 C. Müller, C. A. Umbricht, N. Gracheva, V. J. Tschan, G. Pellegrini, P. Bernhardt, J. R. Zeevaart, U. Köster, R. Schibli and N. P. van der Meulen, Terbium-161 for PSMA-targeted radionuclide therapy of prostate cancer, *Eur. J. Nucl. Med. Mol. Imaging*, 2019, **46**, 1919–1930.

31 R. P. Baum, A. Singh, M. Benešová, C. Vermeulen, S. Gnesin, U. Köster, K. Johnston, D. Müller, S. Senftleben, H. R. Kulkarni, A. Türler, R. Schibli, J. O. Prior, N. P. van der Meulen and C. Müller, Clinical evaluation of the radiolanthanide terbium-152: first-in-human PET/CT with 152Tb-DOTATOC, *Dalt. Trans.*, 2017, **46**, 14638–14646.

32 J. Grünberg, D. Lindenblatt, H. Dorrer, S. Cohrs, K. Zhernosekov, U. Köster, A. Türler, E. Fischer and R. Schibli, Anti-L1CAM radioimmunotherapy is more effective with the radiolanthanide terbium-161 compared to lutetium-177 in an ovarian cancer model, *Eur. J. Nucl. Med. Mol. Imaging*, 2014, **41**, 1907–1915.

33 U. Jakobsson, E. Mäkilä, A. Rahikkala, S. Imlimthan, J. Lampuoti, S. Ranjan, J. Heino, P. Jalkanen, U. Köster, K. Mizohata, H. A. Santos, J. Salonen, A. J. Airaksinen, M. Sarparanta and K. Helariutta, Preparation and in vivo evaluation of red blood cell membrane coated porous silicon nanoparticles implanted with 155Tb, *Nucl. Med. Biol.*, 2020, **84**–**85**, 102–110.

34 M. F. L'Annunziata, *Handbook of Radioactivity Analysis*, Elsevier Science Ltd, 3rd edn., 2012.

35 M. G. Stabin, *Radiation Protection and Dosimetry - An Introduction to Health Physics*, Springer, New York, 2007.

36 M. Donya, M. Radford, A. El Guindy, D. Firmin and M. H. Yacoub, Radiation in medicine: Origins, risks and aspirations, *Glob. Cardiol. Sci. Pract.*, 2014, **2014**, 437–

448.

37 Z. Sóti, J. Magill and R. Dreher, Karlsruhe Nuclide Chart – New 10th edition 2018, *EPJ Nucl. Sci. Technol.*, 2019, **5**, 1–11.

38 J. E. Gindler, L. E. Glendenin, D. J. Henderson and J. W. Meadows, Mass distributions in monoenergetic-neutron-induced fission of 239Pu, *Phys. Rev. C*, 1983, **27**, 2058–2062.

39 IAEA, Nuclear Data for Safeguards - Chain Fission Yields, https://www-nds.iaea.org/sgnucdat/c1.htm#92-U-235, (accessed 19 March 2018).

40 DEFRA, *UK Statutory Instruments No. 1075: The Ionising Radiations Regulations 2017*, 2017.

41 C. Grupen, *Introduction to radiation protection : practical knowledge for handling radioactive sources*, Springer, 2010.

42 M. K. O'Connor and B. J. Kemp, Single-Photon Emission Computed Tomography/Computed Tomography: Basic Instrumentation and Innovations, *Semin. Nucl. Med.*, 2006, **36**, 258–266.

43 D. L. Bailey and K. P. Willowson, An evidence-based review of quantitative SPECT imaging and potential clinical applications, *J. Nucl. Med.*, 2013, **54**, 83–89.

44 R. Zimmermann, in *Nuclear medicine : radioactivity for diagnosis and therapy*, EDP Sciences, 2007, pp. 82–107.

45 W. J. G. Oyen, L. Bodei, F. Giammarile, H. R. Maecke, J. Tennvall, M. Luster and B. Brans, Targeted therapy in nuclear medicine current status and future prospects, *Ann. Oncol.*, 2007, **18**, 1782–1792.

46 M. K. O'Connor and B. J. Kemp, Single-Photon Emission Computed Tomography/Computed Tomography: Basic Instrumentation and Innovations, *Semin. Nucl. Med.*, 2006, **36**, 258–266.

47 T. E. Peterson and L. R. Furenlid, SPECT detectors: the Anger Camera and beyond., *Phys. Med. Biol.*, 2011, **56**, 145–182.

48 M. F. bin Othman, N. R. Mitry, V. J. Lewington, P. J. Blower and S. Y. A. Terry, Re-assessing gallium-67 as a therapeutic radionuclide, *Nucl. Med. Biol.*, 2017, **46**, 12–18.

49 J. O. Olsen, R. V. Pozderac, G. Hinkle, T. Hill, T. M. O'Dorisio, W. J. Schirmer, E. C. Ellison and M. S. O'Dorisio, Somatostatin receptor imaging of neuroendocrine tumors with indium-111 pentetreotide (Octreoscan), *Semin. Nucl. Med.*, 1995, **25**, 251–261.

50 M. H. Bourguignon, E. K. J. Pauwels, C. Loc'h and B. Mazière, Iodine-123 labelled radiopharmaceuticals and single-photon emission tomography: a natural liaison, *Eur J Nucl Med*, 1997, **24**, 331–344.

51 M. N. Lonsdale and T. Beyer, Dual-modality PET/CT instrumentation—Today and

tomorrow, *Eur. J. Radiol.*, 2010, **73**, 452–460.

52 G. Flux, M. Bardies, M. Monsieurs, S. Savolainen, S.-E. Strand and M. Lassmann, The Impact of PET and SPECT on Dosimetry for Targeted Radionuclide Therapy, *Z. Med. Phys.*, 2006, **16**, 47–59.

53 J. Dickson, J. Ross and S. Vöö, Quantitative SPECT: the time is now, *EJNMMI Phys.*, 2019, **6**, 1–7.

54 Z. Tu and R. H. Mach, C-11 radiochemistry in cancer imaging applications., *Curr. Top. Med. Chem.*, 2010, **10**, 1060–95.

55 D. Le Bars, Fluorine-18 and medical imaging: Radiopharmaceuticals for positron emission tomography, *J. Fluor. Chem.*, 2006, **127**, 1488–1493.

56 C. J. Anderson and R. Ferdani, Copper-64 radiopharmaceuticals for PET imaging of cancer: advances in preclinical and clinical research., *Cancer Biother. Radiopharm.*, 2009, **24**, 379–93.

57 S. R. Banerjee and M. G. Pomper, Clinical applications of Gallium-68., *Appl. Radiat. Isot.*, 2013, **76**, 2–13.

58 H. Murshed, in *Fundamentals of Radiation Oncology*, Academic Press, 3rd edn., 2019, pp. 57–87.

59 G. D. Flux, Imaging and dosimetry for radium-223: The potential for personalized treatment, *Br. J. Radiol.*, 2017, **90**, 1–9.

60 S. M. Qaim and I. Spahn, Development of novel radionuclides for medical applications, *J. Label. Compd. Radiopharm.*, 2018, **61**, 126–140.

61 Laboratoire National Henri Becquerel, Nucléide – Lara Application, http://www.lnhb.fr/nuclear-data/module-lara/, (accessed 8 August 2018).

62 I. Novak-Hofer and A. P. Schubiger, Copper-67 as a therapeutic nuclide for radioimmunotherapy, *Eur. J. Nucl. Med. Mol. Imaging*, 2002, **29**, 821–830.

63 M. Fischer and W. U. Kampen, Radionuclide Therapy of Bone Metastases., *Breast care*, 2012, **7**, 100–107.

64 R. Salem and R. D. Hunter, Yttrium-90 microspheres for the treatment of hepatocellular carcinoma: A review, *Int. J. Radiat. Oncol.*, 2006, **66**, 83–88.

65 M. R. Harrison, T. Z. Wong, A. J. Armstrong and D. J. George, Radium-223 chloride: a potential new treatment for castration-resistant prostate cancer patients with metastatic bone disease., *Cancer Manag. Res.*, 2013, **5**, 1–14.

66 D. A. Scheinberg and M. R. McDevitt, Actinium-225 in targeted alpha-particle therapeutic applications., *Curr. Radiopharm.*, 2011, **4**, 306–20.

67 S. Lheureux, C. Denoyelle, P. S. Ohashi, J. S. De Bono and F. M. Mottaghy, Molecularly targeted therapies in cancer: a guide for the nuclear medicine physician, *Eur. J. Nucl. Med. Mol. Imaging*, 2017, **44**, 41–54.

68 F. Dammacco, G. Rubini, C. Ferrari, A. Vacca and V. Racanelli, 18F-FDG PET/CT: a review of diagnostic and prognostic features in multiple myeloma and related disorders, *Clin. Exp. Med.*, 2015, **15**, 1–18.

69 M. Benešová, M. Schäfer, U. Bauder-Wüst, A. Afshar-Oromieh, C. Kratochwil, W. Mier, U. Haberkorn, K. Kopka and M. Eder, Preclinical Evaluation of a Tailor-Made DOTA-Conjugated PSMA Inhibitor with Optimized Linker Moiety for Imaging and Endoradiotherapy of Prostate Cancer., *J. Nucl. Med.*, 2015, **56**, 914–20.

70 B. G. Wolff, J. Bolton, R. Baum, A. Chetanneau, A. Pecking, A. N. Serafini, A. J. Fischman, H. C. Hoover, J. L. Klein, G. E. Wynant, R. Subramanian, D. K. Goroff and M. G. Hanna, Radioimmunoscintigraphy of recurrent, metastatic, or occult colorectal cancer with technetium Tc 99m 88BV59H21-2V67-66 (HumaSPECT®-Tc), a totally human monoclonal antibody, *Dis. Colon Rectum*, 1998, **41**, 953–962.

71 A. V. F. Massicano, B. V. Marquez-Nostra and S. E. Lapi, Targeting HER2 in Nuclear Medicine for Imaging and Therapy, *Mol. Imaging*, 2018, **17**, 1–11.

72 D. Y. Lee and K. C. P. Li, Molecular theranostics: a primer for the imaging professional., *AJR. Am. J. Roentgenol.*, 2011, **197**, 318–24.

73 B. Pritychenko, R. Arcilla, M. W. Herman, P. Obložinský, D. Rochman, A. A. Sonzogni, J. K. Tuli and D. F. Winchell, in *AIP Conference Proceedings*, American Institute of PhysicsAIP, 2006, vol. 819, pp. 589–590.

74 M. de Jong, W. A. P. Breeman, B. F. Bernard, E. J. Rolleman, L. J. Hoflande, T. J. Visser, B. Setyono-Han, W. H. Bakker, M. E. van der Pluijm and E. P. Krenning, Evaluation in vitro and in rats of161Tb-DTPA-octreotide, a somatostatin analogue with potential for intraoperative scanning and radiotherapy, *Eur. J. Nucl. Med.*, 1995, **22**, 608–616.

75 S. Lehenberger, C. Barkhausen, S. Cohrs, E. Fischer, J. Grünberg, A. Hohn, U. Köster, R. Schibli, A. Türler and K. Zhernosekov, The low-energy β− and electron emitter 161Tb as an alternative to 177Lu for targeted radionuclide therapy, *Nucl. Med. Biol.*, 2011, **38**, 917–924.

76 F. Jacobs, H. Thierens, A. Piepsz, K. Bacher, C. Van De Wiele, H. Ham and R. A. Dierckx, Optimised tracer-dependent dosage cards to obtain weight-independent effective doses, *Eur. J. Nucl. Med. Mol. Imaging*, 2005, **32**, 581–588.

77 J. Lilley, in *Nuclear Physics : Principles and Applications.*, Wiley, 2013, pp. 93–126.

78 G. B. Saha, in *Fundamentals of Nuclear Pharmacy*, Springer New York, New York, NY, 1984, pp. 35–52.

79 S. M. Qaim, in *Medical Radionuclide Production*, De Gruyter, 2020, pp. 71–94.

80 F. Rösch and F. F. Knapp, in *Handbook of Nuclear Chemistry*, Springer US, Boston, MA, 2011, pp. 1935–1976.

81 A. Kowalczyk, Proton induced spallation reactions in the energy range 0.1 - 10 GeV, https://arxiv.org/pdf/0801.0700.pdf, (accessed 12 February 2018).

82 M. Lindroos, Review of ISOL-type Radioactive Beam Facilities, *Proc. EPAC*, 2004, 45–49.

83 R. Manuel, S. Augusto, L. Buehler, Z. Lawson, S. Marzari, M. Stachura, T. Stora and C.-M. Collaboration, CERN-MEDICIS (Medical Isotopes Collected from ISOLDE): A New Facility, *Appl. Sci*, 2015, **4**, 265–281.

84 C. Duchemin, J. P. Ramos, T. Stora, E. Aubert, N. Audouin, E. Barbero, V. Barozier, A. P. Bernardes, P. Bertreix and A. Boscher, in *Conference: 11th International Particle Accelerator Conference (IPAC2020)*, 2020, pp. 75–79.

85 T. T. Böhlen, F. Cerutti, M. P. W. Chin, A. Fassò, A. Ferrari, P. G. Ortega, A. Mairani, P. R. Sala, G. Smirnov and V. Vlachoudis, The FLUKA Code: Developments and challenges for high energy and medical applications, *Nucl. Data Sheets*, 2014, **120**, 211–214.

86 B. Webster, P. Ivanov, B. Russell, S. Collins, T. Stora, J. P. Ramos, U. Köster, A. P. Robinson and D. Read, Chemical Purification of Terbium-155 from Pseudo-Isobaric Impurities in a Mass Separated Source Produced at CERN, *Sci. Rep.*, 2019, **9**, 1–9.

87 L. Deilami-nezhad, L. Moghaddam-Banaem, M. Sadeghi and M. Asgari, Production and purification of Scandium-47: A potential radioisotope for cancer theranostics, *Appl. Radiat. Isot.*, 2016, **118**, 124–130.

88 U. C. Bergmann, G. Auböck, R. Catherall, J. Cederkäll, C. A. Diget, L. Fraile, S. Franchoo, H. Fynbo, H. Gausemel, U. Georg, T. Giles, H. Jeppesen, O. C. Jonsson, U. Köster, J. Lettry, T. Nilsson, K. Peräjärvi, H. Ravn, K. Riisager, L. Weissman and J. Äystö, Production yields of noble-gas isotopes from ISOLDE UCx/graphite targets, *Nucl. Instruments Methods Phys. Res. Sect. B Beam Interact. with Mater. Atoms*, 2003, **204**, 220–224.

89 D. Neidherr, G. Audi, D. Beck, K. Blaum, C. Böhm, M. Breitenfeldt, R. B. Cakirli, R. F. Casten, S. George, F. Herfurth, A. Herlert, A. Kellerbauer, M. Kowalska, D. Lunney, E. Minaya-Ramirez, S. Naimi, E. Noah, L. Penescu, M. Rosenbusch, S. Schwarz, L. Schweikhard and T. Stora, Discovery of ^{229}Rn and the Structure of the Heaviest Rn and Ra Isotopes from Penning-Trap Mass Measurements, *Phys. Rev. Lett.*, 2009, **102**, 112501.

90 M. A. Synowiecki, L. R. Perk and J. F. W. Nijsen, Production of novel diagnostic radionuclides in small medical cyclotrons., *EJNMMI Radiopharm. Chem.*, 2018, **3**, 1–25.

91 IAEA, *Directory of Cyclotrons used for Radionuclide Production in Member States*, 2006.

92 University of Birmingham, MC40 Cyclotron Facility - The Birmingham Centre for Nuclear Education and Research - University of Birmingham, https://www.birmingham.ac.uk/research/activity/nuclear/about-us/facilities/mc40-cyclotron-facility.aspx, (accessed 2 December 2020).

93 Équipements - Production des radionucléides - Arronax Nantes, https://www.arronax-nantes.fr/en/radionuclide-production/equipment/cyclotron-c70/, (accessed 2 December 2020).

94 W. Scharf, E. Lepa, F. T. Cole and J. P. Blewett, *Particle accelerators and their uses: Part 1 Accelerator Design*, Harwood Academic Publishers, 1986.

95 C. A. Bertulani, P. Danielewicz and Institute of Physics (Great Britain), *Introduction to Nuclear Reactions*, Institute of Physics, 2004.

96 International Atomic Energy Agency, *Cyclotron Produced Radionuclides: Physical Characteristics and Production Methods*, 2009.

97 C. Duchemin, A. Guertin, F. Haddad, N. Michel and V. Métivier, Deuteron induced Tb-155 production, a theranostic isotope for SPECT imaging and auger therapy, *Appl. Radiat. Isot.*, 2016, **118**, 281–289.

98 M. Yiğit and A. Kara, Model-based predictions for nuclear excitation functions of neutron-induced reactions on 64,66−68Zn targets, *Nucl. Eng. Technol.*, 2017, **49**, 996–1005.

99 O. B. Tarasov and D. Bazin, Development of the program LISE: application to fusion–evaporation, *Nucl. Instruments Methods Phys. Res. Sect. B Beam Interact. with Mater. Atoms*, 2003, **204**, 174–178.

100 International Atomic Energy Agency, *Manual for reactor produced radioisotopes*, 2003.

101 Z. Talip, C. Favaretto, S. Geistlich and N. P. van der Meulen, A Step-by-Step Guide for the Novel Radiometal Production for Medical Applications: Case Studies with 68Ga, 44Sc, 177Lu and 161Tb, *Molecules*, 2020, **25**, 1–29.

102 World Nuclear Association, Physics of Uranium and Nuclear Energy, http://www.world-nuclear.org/information-library/nuclear-fuel-cycle/introduction/physics-of-nuclear-energy.aspx#ECSArticleLink1, (accessed 12 February 2018).

103 National Academies of Science, Engineering and Medicine, *Molybdenum-99 for Medical Imaging*, National Academies Press, Washington, D.C., 2016.

104 World Nuclear Association, Research Reactors, http://www.world-nuclear.org/information-library/non-power-nuclear-applications/radioisotopes-research/research-reactors.aspx, (accessed 12 February 2018).

105 G. Prete, A. Andrighetto, L. Biasetto, M. Manzolaro, F. Gramegna, A. Lombardi, A.

Pisent, J. Esposito, E. Fagotti, M. Cinausero, P. Mastinu and L. Calabretta, The SPES project: An ISOL facility for exotic beams, *J. Phys. Conf. Ser.*, 2009, **168**, 9–11.

106 M. Ashford, L. Popescu, D. Houngbo, M. Dierckx and H. Aït Abderrahim, Exploratory study for the production of Sc beams at the ISOL facility of MYRRHA preliminary thermal investigations, *Nucl. Instruments Methods Phys. Res. Sect. B Beam Interact. with Mater. Atoms*, 2020, **463**, 244–247.

107 J. Dilling, R. Krücken and L. Merminga, *ISAC and ARIEL: The TRIUMF radioactive beam facilities and the scientific program*, Springer Netherlands, 2014.

108 H. L. Ravn and B. W. Allardyce, in *Treatise on Heavy Ion Science*, Springer US, 1989, pp. 363–439.

109 V. M. Gadelshin, V. Barozier, T. E. Cocolios, V. N. Fedosseev, R. Formento-Cavaier, F. Haddad, B. Marsh, S. Marzari, S. Rothe, T. Stora, D. Studer, F. Weber and K. Wendt, MELISSA: Laser ion source setup at CERN-MEDICIS facility. Blueprint, *Nucl. Instruments Methods Phys. Res. Sect. B Beam Interact. with Mater. Atoms*, 2020, **463**, 460–463.

110 V. M. Gadelshin, S. Wilkins, V. N. Fedosseev, E. Barbero, V. Barozier, A. P. Bernardes, E. Chevallay, T. E. Cocolios, B. Crepieux, K. Dockx, M. Eck, P. Fernier, R. F. Cavaier, F. Haddad, J. Jakobi, L. Lambert, B. A. Marsh, S. Marzari, J. P. Ramos, A. R. Moberg, S. Rothe, T. Stora, D. Studer, A. V. Suarez, F. Weber and K. Wendt, First laser ions at the CERN-MEDICIS facility, *Hyperfine Interact.*, 2020, **241**, 1–9.

111 V. N. Fedosseev, B. A. Marsh, D. V. Fedorov, U. Köster and E. Tengborn, in *Laser 2004*, Springer-Verlag, 2006, pp. 15–27.

112 S. Haller, G. Pellegrini, C. Vermeulen, N. P. van der Meulen, U. Köster, P. Bernhardt, R. Schibli and C. Müller, Contribution of Auger/conversion electrons to renal side effects after radionuclide therapy: preclinical comparison of 161Tb-folate and 177Lu-folate, *EJNMMI Res.*, 2016, **6**, 1–11.

113 B. J. Allen, G. Goozee, S. Sarkar, G. Beyer, C. Morel and A. P. Byrne, Production of terbium-152 by heavy ion reactions and proton induced spallation, *Appl. Radiat. Isot.*, 2001, **54**, 53–58.

114 N. N. Il'inskaya, T. Y. Malamut and A. A. Ogloblin, Production of 149 Tb in Alpha-Particle-Induced Nuclear Reactions 1, *JETP Lett.*, 2018, **108**, 1–4.

115 G. J. Beyer, J. J. Čomor, M. Daković, D. Soloviev, C. Tamburella, E. Hagebø, B. Allan, S. N. Dmitriev, N. G. Zaitseva and null null, Production routes of the alpha emitting 149Tb for medical application, *Radiochim. Acta*, 2002, **90**, 247–252.

116 V. A. Zagryadskii, S. T. Latushkin, T. Y. Malamut, V. I. Novikov, A. A. Ogloblin, V. N. Unezhev and D. Y. Chuvilin, Measurement of Terbium Isotopes Yield in Irradiation of 151Eu Targets by 3He Nuclei, *At. Energy*, 2017, **123**, 55–58.

117 R. R. Trinder, T. Kokalova, D. J. Parker, C. Wheldon, B. Phoenix, P. Ivanov, B. Russel,

B. Webster, P. Regan, A. Robinson, D. Cullen, S. Pells, R. Allen, S. Pirrie, A. Turner and P. Santa Rita, in *Journal of Physics: Conference Series*, IOP Publishing Ltd, 2020, vol. 1643, p. 12209.

118 G. F. Steyn, C. Vermeulen, F. Szelecsényi, Z. Kovács, A. Hohn, N. P. Van Der Meulen, R. Schibli and T. N. Van Der Walt, Cross sections of proton-induced reactions on 152 Gd, 155 Gd and 159 Tb with emphasis on the production of selected Tb radionuclides, *Nucl. Instruments Methods Phys. Res. Sect. B Beam Interact. with Mater. Atoms*, 2014, **319**, 128–140.

119 U. Köster and ISOLDE Collaboration, ISOLDE target and ion source chemistry, *Radiochim. Acta*, 2001, **89**, 749–756.

120 C. Vermeulen, G. F. Steyn, F. Szelecsényi, Z. Kovács, K. Suzuki, K. Nagatsu, T. Fukumura, A. Hohn and T. N. van der Walt, Cross sections of proton-induced reactions on natGd with special emphasis on the production possibilities of 152Tb and 155Tb, *Nucl. Instruments Methods Phys. Res. Sect. B Beam Interact. with Mater. Atoms*, 2012, **275**, 24–32.

121 A. G. Kazakov, R. A. Aliev, A. Y. Bodrov, A. B. Priselkova and S. N. Kalmykov, Separation of radioisotopes of terbium from a europium target irradiated by 27 MeV α-particles, *Radiochim. Acta*, 2017, **106**, 135–140.

122 S. Cotton, *Lanthanide and actinide chemistry*, Wiley, 2006.

123 N. E. Topp, *The chemistry of the rare-earth elements*, Elsevier Pub. Co., 1965.

124 W. P. Cacheris, S. K. Nickle and A. D. Sherry, Thermodynamic Study of Lanthanide Complexes of 1,4,7-Triazacyclononane-N,N′,N″-triacetic Acid and 1,4,7,10-tetraazacyclododecane-N,N′,N″,N″-tetraacetic Acid, *Inorg. Chem.*, 1987, **26**, 958–960.

125 S. A. Cotton, Establishing coordination numbers for the lanthanides in simple complexes, *Comptes Rendus Chim.*, 2005, **8**, 129–145.

126 E. Heftmann, in *Chromatography: Fundamentals and Applications of Chromatographic and Electrophoretic Methods- part A: fundamentals and techniques*, 1983, pp. A1–A16.

127 A. Braithwaite and F. J. Smith, *Chromatographic Methods*, Blackie Academic and Professional, Fifth., 1999.

128 C. Horvath and W. R. Melander, in *Chromatography: Fundamentals and Applications of Chromatographic and Eectrophoretic Methods- part A: fundamentals and techniques*, 1983, pp. A28–A130.

129 E. Heftmann, *Chromatography: Fundamentals and Applications of Chromatographic and electrophoretic methods- part A: fundamentals and techniques*, 1983.

130 C. E. Harland, *Ion Exchange: Theory and Practice*, Royal Society of Chemistry, Cambridge, 2nd edn., 2007.

131 G. S. Katykhin, in *Extraction Chromatograrphy*, eds. T. Braun and G. Ghersini, 1975, pp. 134–174.

132 S. Heinitz, N. Kivel, D. Schumann, U. Köster, M. Balata, M. Biasotti, V. Ceriale, M. De Gerone, M. Faverzani, E. Ferri, G. Gallucci, F. Gatti, A. Giachero, S. Nisi, A. Nucciotti, A. Orlando, G. Pessina, A. Puiu and S. Ragazzi, Production and separation of 163Ho for nuclear physics experiments, *PLoS One*, 2018, **13**, 1–12.

133 G. R. Chatwal, in *Analytical Chromatography*, ed. M. Arora, Himalaya Publishing House, 2nd edn., 2006, pp. 136–146.

134 G. R. Choppin and R. J. Silva, *Separation of the lanthanides by ion exchange with alpha-hydroxyisobutyric acid*, Lawrence Berkeley National Laboratory, 1956.

135 S. Z. Islami-Rad, M. Shamsaei, R. Gholipour-Peyvandi and M. Ghannadi-Maragheh, Reactor production and purification of 153Sm radioisotope via natSm target irradiation, *Radiochemistry*, 2011, **53**, 642–645.

136 R. Chiarizia and E. P. Horwitz, Radiolytic stability of some recently developed ion exchange and extraction chromatography resins containing diphosphonic acid groups, *Solvent Extr. Ion Exch.*, 2000, **18**, 109–132.

137 E. Philip Horwitz, D. R. McAlister and M. L. Dietz, Extraction Chromatography Versus Solvent Extraction: How Similar are They?, *Sep. Sci. Technol.*, 2006, **41**, 2163–2182.

138 E. P. Horwitz, in *International Workshop on the Application of Extraction Chromatography in Radionuclide Measurement*, Institute for Reference Materials and Measurements (IRMM), 1998, pp. 1–11.

139 E. A. Erin, V. N. Momotov, A. A. Baranov, L. V. Nagaitseva, Y. S. Konovalova and Y. A. Galina, Extraction-chromatographic properties and radiation resistance of a solid extractant based on di-2-ethylhexyl hydrogen phosphate, *Radiochemistry*, 2017, **59**, 58–64.

140 M. L. Dietz and E. Philip Horwitz, Applications of extraction chromatography in the development of radionuclide generator systems for nuclear medicine, *Ind. Eng. Chem. Res.*, 2000, **39**, 3181–3188.

141 M. L. Dietz and E. P. Horwitz, Improved chemistry for the production of yttrium-90 for medical applications, *Int. J. Radiat. Appl. Instrumentation. Part A. Appl. Radiat. Isot.*, 1992, **43**, 1093–1101.

142 Triskem International, *Product Sheet - LN/LN2/LN3 resins*, 2015.

143 N. Gracheva, C. Müller, Z. Talip, S. Heinitz, U. Köster, J. R. Zeevaart, A. Vögele, R. Schibli and N. P. van der Meulen, Production and characterization of no-carrier-added 161Tb as an alternative to the clinically-applied 177Lu for radionuclide therapy, *EJNMMI Radiopharm. Chem.*, 2019, **4**, 1–16.

144 F. Monroy-Guzman and E. J. Salinas, Separation of Micro-Macrocomponent Systems:

Ho-Dy and Lu-Yb by Extraction Chromatography, *J. Mex. Chem. Soc.*, 2015, **59**, 143–150.

145 F. Monroy-Guzman, F. Jimenez Barreiro, E. Jaime Salinas and A. L. Vera Trevino, Radiolanthanide device production, *World J. Nucl. Sci. Technol.*, 2015, **5**, 111–119.

146 J. Jiang, A. V. Davies and R. E. Britton, Measurement of 160Tb and 161Tb in nuclear forensics samples, *J. Radioanal. Nucl. Chem.*, 2017, **314**, 727–736.

147 J. Jiang, A. Davies, L. Arrigo, J. Friese, B. N. Seiner, L. Greenwood and Z. Finch, Analysis of 161Tb by radiochemical separation and liquid scintillation counting, *Appl. Radiat. Isot.*, 2015, **170**, 1–6.

148 A. Aziz and W. T. Artha, Radiochemical Separation of 161Tb from Gd/Tb Matrix Using Ln Resin Column, *Indones. J. Chem.*, 2018, **16**, 283–288.

149 A. Aziz, Physico-chemical characterization of the terbium-161 radioisotope through separation based on cartridge LN resin column from irradiated of enriched Gd2O3 target, *J. Phys. Conf. Ser.*, 2020, **1436**, 1–10.

150 S. M. Judge, D. Arnold, B. Chauvenet, R. Collé, P. De Felice, E. García-Toraño and U. Wätjen, 100 Years of radionuclide metrology, *Appl. Radiat. Isot.*, 2013, **87**, 27–31.

151 S. Pommé, Methods for primary standardization of activity, *Metrologia*, 2007, **44**, S17-26.

152 T. C. Liebisch, J. Stenger and J. Ullrich, Understanding the Revised SI: Background, Consequences, and Perspectives, *Ann. Phys.*, 2019, **531**, 1800339.

153 R. Gadd, M. Baker, K. S. Nijran, S. Owens, W. Thomson, M. J. Woods and F. Zananiri, *Measurement Good Practice Guide No. 93 - Protocol for Establishing and Maintaining the Calibration of Medical Radionuclide Calibrators and their Quality Control*, 2006.

154 M. Bauwens, I. Pooters, R. Cobben, M. Visser, R. Schnerr, F. Mottaghy, J. Wildberger and R. Wierts, A comparison of four radionuclide dose calibrators using various radionuclides and measurement geometries clinically used in nuclear medicine, *Phys. Medica*, 2019, **60**, 14–21.

155 S. Staelens, S. Deleye and I. Lemahieu, Energy window based correction for septal penetration effects caused by impurities in cyclotron-produced Thallium-201, *J. Nucl. Med.*, 2008, **49**, 1–24.

156 *The International Pharmacopoeia*, World Health Organisation, Geneva, 8th Editio., 2018.

157 World Health Organisation, in *The International Pharmacopoeia*, Ninth., 2019.

158 A. Vidal, C. Bourdeau, M. Frindel, T. Garcia, F. Haddad, A. Faivre-Chauvet and M. Bourgeois, ARRONAX Cyclotron: Setting up of In-House Hospital Radiopharmacy, *Biomed Res. Int.*, 2020, 1–6.

159 F. Haddad, L. Ferrer, A. Guertin, T. Carlier, N. Michel, J. Barbet and J. F. Chatal, ARRONAX, a high-energy and high-intensity cyclotron for nuclear medicine, *Eur. J. Nucl. Med. Mol. Imaging*, 2008, **35**, 1377–1387.

160 M. Thoennessen, in *The discovery of isotopes: A complete compilation*, Springer International Publishing, 2016, pp. 1–4.

161 E. Philip Horwitz, R. Chiarizia and M. L. Dietz, A novel strontium selective extraction chromatographic resin., *Solvent Extr. Ion Exch.*, 1992, **10**, 313–336.

162 Triskem International, *Product Sheet - UTEVA resin*, 2015.

163 H. Carter, *Uranium separations using extraction chromatography*, Loughborough University, 2012.

164 Agilent Technologies, 2017.

165 M. Wiedenbeck, R. Bugoi, M. J. M. Duke, T. Dunai, J. Enzweiler, M. Horan, K. P. Jochum, K. Linge, J. Košler, S. Merchel, L. F. G. Morales, L. Nasdala, R. Stalder, P. Sylvester, U. Weis and A. Zoubir, GGR Biennial Critical Review: Analytical Developments Since 2010, *Geostand. Geoanalytical Res.*, 2012, **36**, 337–398.

166 Agilent Technologies, *Agilent 8800 ICP-QQQ Application Handbook 2ND Edition*, 2019.

167 Microsoft Corporation, 2019.

168 OriginLab Corporation, 2020.

169 S. C. Wilschefski and M. Baxter, Inductively Coupled Plasma Mass Spectrometry: Introduction to Analytical Aspects, *Clin Biochem Rev*, 2019, **40**, 115–133.

170 A. Vesterlund and H. Ramebäck, Avoiding polyatomic interferences in measurements of lanthanides in uranium material for nuclear forensic purposes, *J. Radioanal. Nucl. Chem.*, 2019, **321**, 723–731.

171 N. I. Rousis and N. S. Thomaidis, Reduction of interferences in the determination of lanthanides, actinides and transition metals by an octopole collision/reaction cell inductively coupled plasma mass spectrometer – Application to the analysis of Chios mastic, *Talanta*, 2017, **175**, 69–76.

172 D. Burney and C. R. Neal, Method for quantifying and removing polyatomic interferences on a suite of moderately volatile elements (Zn, Se, Rb, Ag, Cd, In, Sb, Tl, Pb, and Bi) during solution-mode ICP-MS, *J. Anal. At. Spectrom.*, 2019, **34**, 1856–1864.

173 T. W. May and R. H. Wiedmeyer, A table of polyatomic interferences in ICP-MS, *At. Spectrosc.*, 1998, **19**, 150–155.

174 Y. Takagai, M. Furukawa, Y. Kameo and K. Suzuki, Sequential inductively coupled plasma quadrupole mass-spectrometric quantification of radioactive strontium-90

incorporating cascade separation steps for radioactive contamination rapid survey, *Anal. Methods*, 2014, **6**, 355–362.

175 A. Y. Leikin, V. K. Karandashev, S. V. Lisovskii and I. A. Volkov, The Application of Collision/Reaction Cell for Detection of Impurity Elements in Rare Earth Metals by ICPMS Analysis, *Inorg. Mater.*, 2015, **51**, 1389–1393.

176 I. Wysocka, Determination of rare earth elements concentrations in natural waters – A review of ICP-MS measurement approaches, *Talanta*, 2021, **221**, 121636.

177 S. M. Collins, J. D. Keightley, P. Ivanov, A. Arinc, A. J. Fenwick and A. K. Pearce, The potential radio-immunotherapeutic α-emitter 227 Th – part II: Absolute γ-ray emission intensities from the excited levels of 223 Ra, *Appl. Radiat. Isot.*, 2019, **145**, 251–257.

178 G. R. Gilmore, *Practical Gamma-Ray Spectrometry: Second Edition*, John Wiley and Sons, 2008.

179 Mirion Technologies, 2016.

180 BIPM, *Monographie BIPM-5 – Table of Radionuclides, Seven Volumes, CEA/ LNE-LNHB, 91191 Gif-sur-Yvette, France and BIPM, Pavillon de Breteuil, 92312 Sèvres,France*, 2004.

181 H. Verhoeven, T. E. Cocolios, K. Dockx, G. J. Farooq-Smith, O. Felden, R. Formento-Cavaier, R. Gebel, U. Köster, B. Neumaier, B. Scholten, I. Spahn, S. Spellerberg, M. E. Stamati and S. Stegemann, Measurement of spallation cross sections for the production of terbium radioisotopes for medical applications from tantalum targets, *Nucl. Instruments Methods Phys. Res. Sect. B Beam Interact. with Mater. Atoms*, 2020, **463**, 327–329.

182 C. Duchemin, T. E. Cocolios, K. Dockx, G. J. Farooq-Smith, O. Felden, R. Formento-Cavaier, R. Gebel, U. Köster, B. Neumaier, B. Scholten, I. Spahn, S. Spellerberg, M. E. Stamati, S. Stegemann and H. Verhoeven, Production Cross-Section Measurements for Terbium Radionuclides of Medical Interest Produced in Tantalum Targets Irradiated by 0.3 to 1.7 GeV Protons and Corresponding Thick Target Yield Calculations, *Front. Med.*, 2021, **8**, 625561.

183 R. Marsac, F. Réal, N. L. Banik, M. Pédrot, O. Pourret and V. Vallet, Aqueous chemistry of Ce(IV): Estimations using actinide analogues, *Dalt. Trans.*, 2017, **46**, 13553–13561.

184 C. T. Palumbo, I. Zivkovic, R. Scopelliti and M. Mazzanti, Molecular Complex of Tb in the +4 Oxidation State, *J. Am. Chem. Soc.*, 2019, **141**, 9827–9831.

185 D. E. Hobart, K. Samhoun, J. P. Young, V. E. Norvell, G. Mamantov and J. R. Peterson, Stabilization of praseodymium(IV) and terbium(IV) in aqueous carbonate solution, *Inorg. Nucl. Chem. Lett.*, 1980, **16**, 321–328.

186 T. Moeller, *The Chemistry of the Lanthanides*, Pergamon Press, 1st edn., 1973.

187 H. Junde, H. Xiaolong and J. K. Tuli, *Nuclear Data Sheets - 67 Ga*, 2005.

188 S. Pommé, Methods for primary standardization of activity, *Metrologia*, 2007, **44**, S17-26.

189 Y. Nedjadi, P. Spring, C. Bailat, P. Froidevaux, C. Wastiel and F. Bochud, Purification and activity standardisation of a 166mHo solution, *Appl. Radiat. Isot.*, 2008, **66**, 900–904.

190 W. B. Mann, A. Rytz, A. Spernol and W. L. McLaughlin, Radioactivity measurements. Principles and practice, *Appl. Radiat. Isot.*, 1988, **39**, 717–937.

191 K. T. Rim, K. H. Koo and J. S. Park, Toxicological evaluations of rare earths and their health impacts to workers: a literature review., *Saf. Health Work*, 2013, **4**, 12–26.

192 S. A. Cotton, *Scandium, Yttrium and the Lanthanides: Inorganic and Coordination Chemistry in Encyclopedia of Inorganic Chemistry*, John Wiley & Sons, Ltd, Chichester, UK, 2006.

193 S. Hirano and K. T. Suzuki, Exposure, Metabolism, and Toxicity of Rare Earths and Related Compounds, *Env. Heal. Perspect*, 1996, **1**, 85–95.

194 A. Andrighetto, · M Tosato, · M Ballan, · S Corradetti, · F Borgna, · V Di Marco, · G Marzaro and · N Realdon, The ISOLPHARM project: ISOL-based production of radionuclides for medical applications, *J. Radioanal. Nucl. Chem.*, 2019, **322**, 73–77.

195 International Atomic Energy Agency (IAEA), *Quality Assurance for Radioactivity Measurement in Nuclear Medicine - Technical Reports Series no. 454*, 2006.

196 J. C. Bousquet, S. Saini, D. D. Stark, P. F. Hahn, M. Nigam, J. Wittenberg and J. T. Ferrucci, Gd-DOTA: Characterization of a new paramagnetic complex, *Radiology*, 1988, **166**, 693–698.

197 N. Alexander, R. Vali, H. Ahmadzadehfar, A. Shammas and S. Baruchel, Review: The Role of Radiolabeled DOTA-Conjugated Peptides for Imaging and Treatment of Childhood Neuroblastoma, *Curr. Radiopharm.*, 2017, **11**, 14–21.

198 C. Müller, C. Vermeulen, U. Köster, K. Johnston, A. Türler, R. Schibli and N. P. van der Meulen, Alpha-PET with terbium-149: evidence and perspectives for radiotheragnostics, *EJNMMI Radiopharm. Chem.*, 2016, **1**, 1–5.

199 J. B. Stimmel and F. C. Kull, Samarium-153 and Lutetium-177 chelation properties of selected macrocyclic and acyclic ligands, *Nucl. Med. Biol.*, 1998, **25**, 117–125.

200 N. J. M. Klaassen, M. J. Arntz, A. Gil Arranja, J. Roosen and J. F. W. Nijsen, The various therapeutic applications of the medical isotope holmium-166: a narrative review, *EJNMMI Radiopharm. Chem.*, 2019, **4**, 1–26.

201 A. Aziz, Physico-chemical characterization of the terbium-161 radioisotope through separation based on cartridge LN resin column from irradiated of enriched Gd2O3 target Physico-chemical characterization of the terbium-161 radioisotope through separation based, *J. Phys. Conf. Ser.*, 2020, **1436**, 1–10.

202 N. Sugiyama, *Removal of hydride ion interferences (MH+) on Rare Earth Elements using the Agilent 8800 Triple Quadrupole ICP-MS*, 2012.

203 N. Sugiyama and G. Woods, *Direct measurement of trace rare earth elements (REEs) in high-purity REE oxide using the Agilent 8800 Triple Quadrupole ICP-MS with MS/MS mode*, 2012.

204 B. Russell, P. Ivanov, B. Webster and D. Read, *Agilent Application Note: Characterization of Rare Earth Elements used for Radiolabeling Applications by ICP-QQQ*, 2020.

205 Havard University, *A Summary of Error Propagation*, 2007.

206 C. M. Riley, in *High Performance Liquid Chromatography: Fundamental Principles and Practice*, eds. I. W. Wainer and W. . Lough, Taylor & Francis, 1st edn., 1995, pp. 15–35.

207 A. Brown, *Design of the CERN MEDICIS Collection and Sample Extraction System*, University of Manchester, 2015.

208 A. K. M. R. Rahman and · Abdul Awal, Production of 149 Tb, 152 Tb, 155 Tb and 161 Tb from gadolinium using different light-particle beams, *J. Radioanal. Nucl. Chem.*, 2020, **323**, 731–740.

209 A. N. Moiseeva, R. A. Aliev, V. N. Unezhev, V. A. Zagryadskiy, S. T. Latushkin, N. V. Aksenov, N. S. Gustova, M. G. Voronuk, G. Y. Starodub and A. A. Ogloblin, Cross section measurements of 151Eu(3He,5n) reaction: new opportunities for medical alpha emitter 149Tb production, *Sci. Rep.*, 2020, **10**, 1–7.

210 R. P. Baum, A. Singh, H. R. Kulkarni, P. Bernhardt, T. Rydén, C. Schuchardt, N. Gracheva, P. V. Grundler, U. Köster, D. Müller, M. Pröhl, J. R. Zeevaart, R. Schibli, N. P. Van der Meulen and C. Müller, First-in-Human Application of Terbium-161: A Feasibility Study Using 161 Tb-DOTATOC, *J. Nucl. Med.*, 2021, **62**, 1391–1397.

211 M. T. Durán, F. Juget, Y. Nedjadi, F. Bochud, P. V. Grundler, N. Gracheva, C. Müller, Z. Talip, N. P. van der Meulen and C. Bailat, Determination of 161Tb half-life by three measurement methods, *Appl. Radiat. Isot.*, 2020, **159**, 109085.

212 N. Nica, Nuclear Data Sheets for A=155, *Nucl. Data Sheets*, 2019, **160**, 1–404.

213 C. W. Reich, Nuclear Data Sheets for A = 156, *Nucl. Data Sheets*, 2012, **113**, 2537–2840.

214 L. M. Arrigo, J. Jiang, Z. S. Finch, J. M. Bowen, C. L. Beck, J. I. Friese, L. R. Greenwood and B. N. Seiner, Development of a separation method for rare earth elements using LN resin, *J. Radioanal. Nucl. Chem.*, 2021, **327**, 457–463.

215 C. D. Smith and M. L. Dietz, Support loading effects on the performance of an extraction chromatographic resin: Toward improved separation of trivalent lanthanides, *Talanta*, 2021, **222**, 121541.

216 E. P. Horwitz, D. R. McAlister, A. H. Bond and J. E. Barrans, Novel extraction of chromatographic resins based on tetraalkyldiglycolamides: Characterization and potential applications, *Solvent Extr. Ion Exch.*, 2005, **23**, 319–344.

217 P. Markl and E. R. Schmid, in *Extraction Chromatograrphy*, eds. T. Braun and G. Ghersini, Elsevier Scientific Publishing Company, 1975, pp. 45–67.

218 C. D. Smith and M. L. Dietz, Support loading effects on the performance of an extraction chromatographic resin: Toward improved separation of trivalent lanthanides, *Talanta*, 2021, **222**, 121541.

219 C. Duchemin, J. P. Ramos, T. Stora, E. Ahmed, E. Aubert, N. Audouin, E. Barbero, V. Barozier, A.-P. Bernardes, P. Bertreix, A. Boscher, F. Bruchertseifer, R. Catherall, E. Chevallay, P. Christodoulou, K. Chrysalidis, T. E. Cocolios, J. Comte, B. Crepieux, M. Deschamps, K. Dockx, A. Dorsival, V. N. Fedosseev, P. Fernier, R. Formento-Cavaier, S. El Idrissi, P. Ivanov, V. M. Gadelshin, S. Gilardoni, J.-L. Grenard, F. Haddad, R. Heinke, B. Juif, U. Khalid, M. Khan, U. Köster, L. Lambert, G. Lilli, G. Lunghi, B. A. Marsh, Y. M. Palenzuela, R. Martins, S. Marzari, N. Menaa, N. Michel, M. Munos, F. Pozzi, F. Riccardi, J. Riegert, N. Riggaz, J.-Y. Rinchet, S. Rothe, B. Russell, C. Saury, T. Schneider, S. Stegemann, Z. Talip, C. Theis, J. Thiboud, N. P. van der Meulen, M. van Stenis, H. Vincke, J. Vollaire, N.-T. Vuong, B. Webster, K. Wendt, S. G. Wilkins and the C.-M. Collaboration, CERN-MEDICIS: A Review Since Commissioning in 2017, *Front. Med.*, 2021, **0**, 1068.

Appendix A – ICP-MS tune parameters and pass criteria

Table A.1 - Summary of the pass criteria for the ICP-MS quality control tune process.

Tune parameter	Elements measured	Pass criteria
Low mass	$^{9}Be^{+}$	> 1500 CPS at 9 m/z
Medium mass	$^{89}Y^{+}$	> 20000 CPS at 89 m/z
High mass	$^{205}Tl^{+}$	> 13000 CPS at 205 m/z
Oxide formation	$^{140}Ce^{16}O^{+}/^{140}Ce^{+}$	< 2 % ratio between signals at 156 m/z and 140 m/z
Formation of doubly charged ions	$^{140}Ce^{++}/^{140}Ce^{+}$	< 2 % ratio between signals at 70 m/z and 140 m/z

Appendix B – Data to accompany Figure 3.1

The 'Mean K_d' data within these tables (Table B.1 - B.3) were used to compile Figure 3.1. * denotes samples for which the K_d value could not be calculated. In these cases, the aqueous phase was not successfully isolated at the end of the batch separation due to it being absorbed by the filter paper. In future studies, larger volumes of aqueous phase (>2mL) or alternative ways of isolating the aqueous phase should be considered in order to avoid this.

Table B.1 – Distribution coefficient values (K_d) for cerium on UTEVA resin across a nitric acid concentration range (Ce – without oxidant).

HNO_3 (M)	*Repeat 1 (K_d)*	*Repeat 2 (K_d)*	*Mean K_d*
2	4.29	4.74	4.51
4	*	3.66	3.66
6	7.70	2.61	5.16
8	4.61	2.51	3.56
10	6.89	1.17	4.03

Table B.2 – Distribution coefficient values (K_d) for cerium on UTEVA resin across a nitric acid concentration range in the presence of an oxidising agent, $NaBrO_3$ (Ce – with oxidant).

HNO_3 (M)	*Repeat 1 (K_d)*	*Repeat 2 (K_d)*	*Repeat 3 (K_d)*	*Mean K_d*
2	14.71	6.78	3.81	8.43
4	36.52	32.30	35.12	34.66
6	158.50	190.71	170.52	173.24
8	452.79	356.29	357.72	388.93
10	253.94	*	278.34	266.14

Table B.3 – Distribution coefficient values (K_d) for terbium on UTEVA resin across a nitric acid concentration range in the presence of an oxidising agent, $NaBrO_3$ (Tb – with oxidant).

HNO_3 (M)	*Repeat 1 (K_d)*	*Repeat 2 (K_d)*	*Repeat 3 (K_d)*	*Mean K_d*
2	4.74	4.35	1.80	3.63
4	3.66	2.33	0.12	2.04
6	2.61	1.38	4.06	2.68
8	2.51	3.62	1.63	2.58
10	1.17	*	0.91	1.04

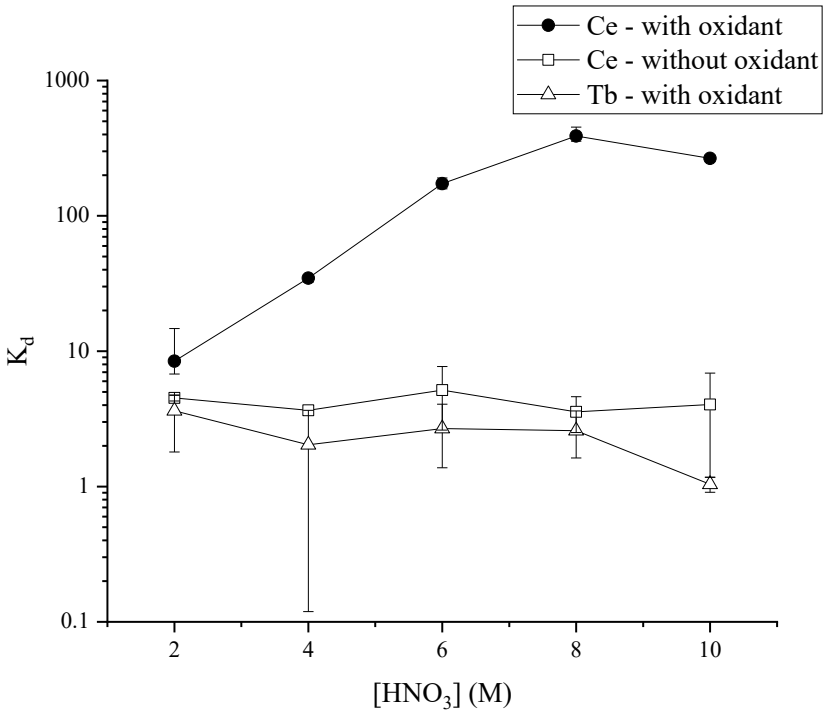

Figure B.1 – Maximum, minimum and mean distribution coefficients (K_d) of Tb(III), Ce(III) and Ce(IV) on UTEVA extraction chromatography resin across a range of HNO_3 concentrations (linked to Figure 3.1).

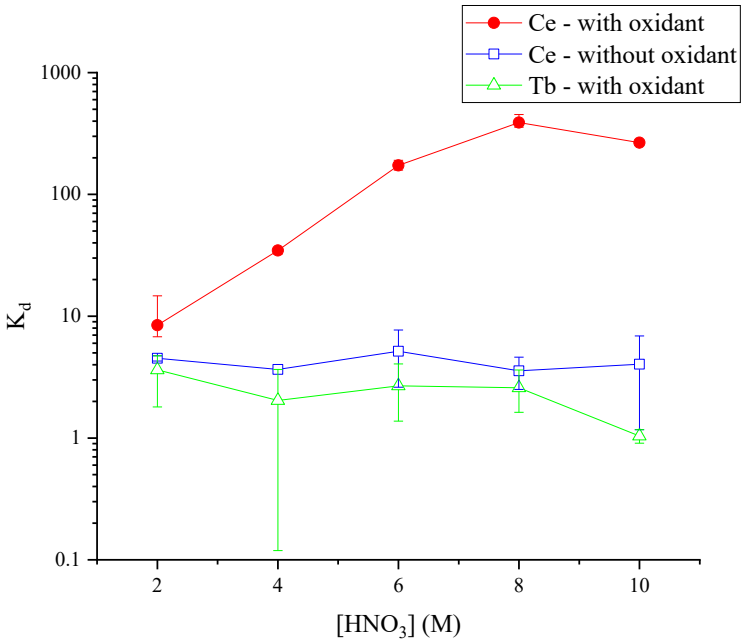

Figure B.2 – Duplicate of Figure B.1 with colour to show maximum and minimum K_d values more clearly.

Appendix C – Data to accompany Figure 3.2

*Table C.1 – Distribution coefficient values (K_d) for **cerium** on AG1 ion-exchange resin across a nitric acid concentration range in the presence of an oxidising agent, $NaBrO_3$.*

HNO_3 (M)	*Repeat 1 (K_d)*	*Repeat 2 (K_d)*	*Repeat 3 (K_d)*	*Mean K_d*
2	-0.37	-0.16	3.90	**1.12**
4	5.02	19.06	24.82	**16.30**
6	35.64	165.77	140.50	**113.97**
8	79.33	340.67	261.62	**227.21**
10	183.25	553.66	341.66	**359.52**

*Table C.2 – Distribution coefficient values (K_d) for **terbium** on AG1 ion-exchange resin across a nitric acid concentration range in the presence of an oxidising agent, $NaBrO_3$.*

HNO_3 (M)	*Repeat 1 (K_d)*	*Repeat 2 (K_d)*	*Repeat 3 (K_d)*	*Mean K_d*
2	-1.09	-0.44	2.26	**0.24**
4	2.17	-0.01	3.02	**1.73**
6	3.28	1.07	0.70	**1.69**
8	3.29	2.66	0.49	**2.15**
10	4.03	5.05	3.29	**4.12**

*Table C.3 – Distribution coefficient values (K_d) for **cerium** on TEVA extraction chromatography resin across a nitric acid concentration range in the presence of an oxidising agent, $NaBrO_3$.*

HNO_3 (M)	*Repeat 1 (K_d)*	*Repeat 2 (K_d)*	*Repeat 3 (K_d)*	*Mean K_d*
2	62.84	237.11	238.88	**179.61**
4	158.37	572.23	1232.90	**654.50**
6	436.91	437.79	624.50	**499.73**
8	594.41	404.93	414.00	**471.11**
10	329.82	363.28	420.88	**371.33**

*Table C.4 – Distribution coefficient values (K_d) for **terbium** on TEVA extraction chromatography resin across a nitric acid concentration range in the presence of an oxidising agent, $NaBrO_3$. # denotes the K_d value which was plotted onto Figure 3.2 and Figure C.1 instead of the mean K_d value. This was needed where the 'mean K_d' value was negative.*

HNO_3 (M)	*Repeat 1 (K_d)*	*Repeat 2 (K_d)*	*Repeat 3 (K_d)*	*Mean K_d*
2	2.06	3.25	1.30	**2.20**
4	5.13	1.69	2.03	**2.95**
6	1.73	-1.42	4.05	**1.45**
8	-4.20	**0.06 #**	-1.42	-1.85
10	**0.29 #**	0.14	-1.21	-0.26

*Table C.5 – Distribution coefficient values (K_d) for **cerium** on TK100 extraction chromatography resin across a nitric acid concentration range in the presence of an oxidising agent, $NaBrO_3$.*

HNO_3 (M)	*Repeat 1 (K_d)*	*Repeat 2 (K_d)*	*Mean K_d*
2	26.86	120.70	**73.78**
4	63.16	307.45	**185.31**
6	79.80	321.06	**200.43**
8	299.27	436.36	**367.81**
10	568.87	713.01	**640.94**

*Table C.6 – Distribution coefficient values (K_d) for **terbium** on TK100 extraction chromatography resin across a nitric acid concentration range in the presence of an oxidising agent, $NaBrO_3$.*

HNO_3 (M)	*Repeat 1 (K_d)*	*Repeat 2 (K_d)*	*Mean K_d*
2	0.79	1.99	**1.39**
4	4.82	2.19	**3.51**
6	10.72	0.79	**5.75**
8	1.85	2.89	**2.37**
10	2.54	-0.40	**1.07**

*Table C.7 – Distribution coefficient values (K_d) for **cerium** on UTEVA extraction chromatography resin across a nitric acid concentration range in the presence of an oxidising agent, $NaBrO_3$. * denotes a sample for which the K_d value could not be calculated. In this case, the aqueous phase was not successfully isolated at the end of the batch separation due to it being absorbed by the filter paper.*

HNO_3 (M)	*Repeat 1 (K_d)*	*Repeat 2 (K_d)*	*Repeat 3 (K_d)*	*Mean K_d*
2	14.71	6.78	3.81	**8.433**
4	36.52	32.3	35.16	**34.66**
6	158.50	190.71	170.52	**173.24**
8	452.79	356.29	357.72	**388.93**
10	253.94	*	278.34	**266.14**

*Table C.8 – Distribution coefficient values (K_d) for **terbium** on UTEVA extraction chromatography resin across a nitric acid concentration range in the presence of an oxidising agent, $NaBrO_3$. * denotes a sample for which the K_d value could not be calculated. In this case, the aqueous phase was not successfully isolated at the end of the batch separation due to it being absorbed by the filter paper.*

HNO_3 (M)	*Repeat 1 (K_d)*	*Repeat 2 (K_d)*	*Repeat 3 (K_d)*	*Mean K_d*
2	4.74	4.35	1.80	**3.63**
4	3.66	2.33	0.12	**2.04**
6	2.61	1.38	4.06	**2.68**
8	2.51	3.62	1.63	**2.58**
10	1.17	*	0.91	**1.04**

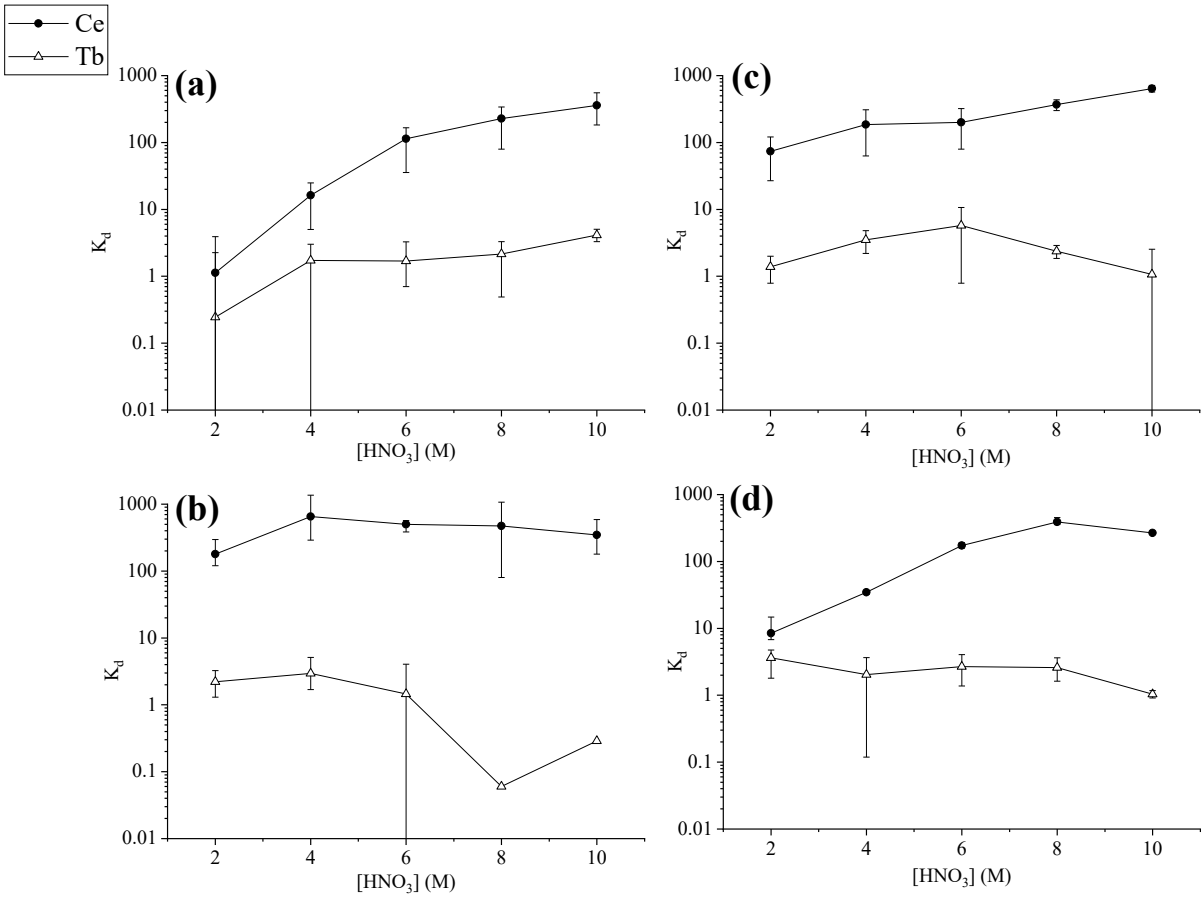

*Figure C.1 - Maximum, minimum and mean distribution coefficients (K_d) of Tb (III) and Ce(IV) across a range of HNO_3 concentrations on **(a)** AGI ion exchange resin, **(b)** TEVA resin, **(c)** TK100 resin, **(d)** UTEVA resin. (linked to Figure 3.2)*

*Table C.9 – Separation factors (SF) between terbium and cerium on the different studies resins at defined HNO_3 concentrations (mean K_d(Ce)/mean K_d(Tb), see equation 2.2). *denotes when the highest positive value was used out of the repeats, due to negative mean K_d for terbium.*

HNO_3 (M)	*AG1*	*TEVA*	*TK100*	*UTEVA*
2	4.61	45.92	53.16	2.32
4	9.45	153.41	52.84	17.02
6	67.59	3635.08	34.84	64.58
8	105.67	13375.31*	199.34	107.53
10	87.21	1722.78*	64.09	227.09

Appendix D – Data to accompany Figure 3.4

*Table D.1 – Summary of the blank and dilution corrected ICP-MS measurement (CPS) of **cerium** at m/z 140 in fractions collected from the stepwise chemical separation using a UTEVA cartridge. 1 mL fractions were collected throughout. (see Figure 3.4 and Figure 3.5 for the elution profile and method, respectively)*

Fraction Number	*Repeat 1 (CPS)*	*Repeat 2 (CPS)*	*Repeat 3 (CPS)*	*Mean Ce CPS*
1	680.05	4520.85	2870.41	2690.44
2	3677.28	5671.27	3383.84	4244.13
3	3893.97	3753.95	4000.70	3882.87
4	1500.14	210.01	7148.54	2952.90
5	4207.41	1170.10	2780.37	2719.29
6	956.74	263.35	2563.67	1261.25
7	6568.27	203.34	2563.67	3111.76
8	2140.24	253.35	2680.36	1691.32
9	1580.17	286.68	2730.39	1532.42
10	8622.62	223.35	2847.06	3897.7
11	2333.61	253.35	3167.13	1918.03
12	1746.85	376.70	2963.76	1695.77
13	17072.71	1536.87	2967.08	7192.22
14	39911.98	1503.48	5164.43	15526.63
15	81750.36	2376.96	7121.84	30416.39
16	125769.48	6014.73	10256.98	47347.06
17	199353.93	13562.80	17209.60	76708.78
18	259281.72	17770.37	25821.06	100957.72
19	306811.98	27644.06	36447.88	123634.64
20	382010.34	39033.74	50032.84	157025.64
21	572037.91	49832.72	79945.11	233938.58
22	11541110.25	77079.19	3736311.19	5118166.87
23	15042912.28	12932505.63	22949318.82	16974912.24
24	129716.47	11209643.97	149600.41	3829653.62
25	18591.61	45016.06	45643.81	36417.16
26	7190.06	29136.92	9129.68	15152.22
27	5301.64	14607.26	7198.63	9035.84

28	3841.03	12391.98	5844.66	7359.23
29	2790.67	12952.40	5357.77	7033.62
30	2363.89	9166.45	4500.84	5343.72
31	1550.31	6931.85	3813.98	4098.71
32	2163.82	5201.13	3377.17	3580.71
33	1713.72	7048.57	2930.40	3897.56
34	750.15	4717.62	2420.29	2629.35
35	486.77	13556.23	2183.59	5408.86
36	1073.54	14613.77	1463.48	5716.93
37	346.73	3280.50	2276.95	1968.06
38	380.08	3153.83	2020.24	1851.38
39	286.71	3447.20	2070.28	1934.73
40	506.75	1643.52	1930.24	1360.17

*Table D.2 – Summary of the blank and dilution corrected ICP-MS measurement (CPS) of **terbium** at m/z 159 in fractions collected from the stepwise chemical separation using a UTEVA cartridge. 1 mL fractions were collected throughout. (see Figure 3.4 and Figure 3.5 for the elution profile and method, respectively)*

Fraction Number	*Repeat 1 (CPS)*	*Repeat 2 (CPS)*	*Repeat 3 (CPS)*	*Mean Tb CPS*
1	133.34	413.36	76.67	207.79
2	613068.46	305112.78	203622.32	373934.52
3	2361237.41	1904592.06	2005052.42	2090293.96
4	2958161.62	2459204.81	2676931.00	2698099.14
5	2958111.00	2593847.77	2803616.32	2785191.70
6	3030350.58	2606336.21	2817291.83	2817992.87
7	3035649.54	2616439.96	2836179.75	2829423.08
8	3059237.35	2565676.57	2861839.53	2828917.82
9	3012025.37	2628092.51	2846971.72	2829029.87
10	2966616.83	2532099.23	2878475.37	2792397.14
11	2823615.48	2523006.94	2855866.31	2734162.91
12	2621346.63	2470427.05	2722030.89	2604601.52
13	385394.87	1844245.65	821870.37	1017170.30
14	46981.41	223108.11	113855.13	127981.55
15	33114.37	105512.83	63383.01	67336.74
16	32533.15	91701.30	58756.12	60996.86
17	32840.40	110113.75	64935.34	69296.49
18	31905.14	96796.52	62108.05	63603.24
19	30305.33	92667.51	61840.23	61604.36
20	31474.40	92170.10	58869.66	60838.05
21	33895.94	85934.10	64631.41	61487.15
22	33668.65	95781.30	64440.42	64630.12
23	12832.26	95791.29	32696.79	47106.78
24	580.03	27280.08	1293.44	9717.85
25	1240.10	296.68	1763.50	1100.10
26	466.70	240.01	563.37	423.36
27	366.68	233.35	586.71	395.58
28	203.34	140.01	213.35	185.57
29	170.01	223.35	246.68	213.35

30	276.68	136.67	283.35	232.24
31	300.02	163.34	256.68	240.01
32	253.35	133.34	213.34	200.01
33	326.69	213.35	190.01	243.35
34	143.34	136.67	273.35	184.46
35	143.34	313.36	206.68	221.12
36	310.02	276.68	366.69	317.80
37	176.68	80.00	456.70	237.79
38	166.68	120.01	296.68	194.46
39	216.68	103.34	300.02	206.68
40	256.68	116.67	176.67	183.34

Table D.3 – A summary of the information used to calculate the elemental recovery of terbium and cerium in the main terbium fractions (1-15) after separation using a UTEVA column. Counts per second (CPS) reported in this table value were calculated by summing the mean values of relevant fractions. Uncertainties are based on standard deviation between repeats (n=3).

	Ce	*Tb*
Fractions 1-15 (CPS)	84733.10 ± 81222.63	28529404.17 ± 1265848.91
Total (CPS)	26859866.52 ± 2123235.81	29100801.01 ± 995646.93
Mean elemental recovery (%)	**0.30 ± 0.28**	**98.25 ± 1.00**

*Table D.4 – Summary of the blank and dilution corrected ICP-MS measurement (CPS) of **cerium** at m/z 140 in fractions collected from the stepwise chemical separation using a TEVA cartridge. 1 mL fractions were collected throughout. (see Figure 3.4 for the elution profile)*

Fraction Number	*Repeat 1 (CPS)*	*Repeat 2 (CPS)*	*Repeat 3 (CPS)*	*Mean Ce CPS*
1	1181.10	1833.08	1233.55	1415.91
2	2545.44	2711.54	781.72	2012.90
3	1008.79	359.53	144.14	504.15
4	1524.26	1184.62	37.91	915.60
5	1239.36	1199.46	274.45	904.42
6	834.12	-120.65	719.49	477.66
7	1978.77	794.11	739.75	1170.87
8	2521.36	1223.72	1823.51	1856.20
9	2277.74	2378.85	667.81	1774.80
10	1182.89	680.70	1893.51	1252.37
11	1216.51	334.84	477457.57	159669.64
12	34937.29	750781.41	1136296.53	640671.74
13	354932.44	1658686.39	1124572.60	1046063.81
14	202508.39	1112388.79	1000022.00	771639.72
15	171571.93	729274.26	833978.05	578274.75
16	167432.37	638589.73	706109.69	504043.93
17	147215.61	600914.30	701866.68	483332.20
18	119078.40	518291.64	688829.65	442066.56
19	142534.52	531012.36	629375.67	434307.52
20	144257.22	691154.87	1921942.19	919118.09
21	372439.23	1283244.58	21247171.98	7634285.26
22	2108837.99	2449281.42	707901.36	1755340.26
23	2294398.30	1700382.69	75711.34	1356830.77
24	2377079.57	1117214.86	23404.40	1172566.28
25	2066378.48	1034672.28	12091.37	1037714.04
26	1839880.19	1311705.84	7488.16	1053024.73
27	1800500.55	1288619.52	6987.14	1032035.74
28	1824005.46	1546761.30	4628.56	1125131.77
29	1554894.48	1654995.63	4831.81	1071573.97
30	1302555.32	876524.63	3696.19	727592.05

31	1259578.81	840136.84	3131.19	700948.95
32	1151122.84	764645.29	3108.11	639625.41
33	1020343.83	662932.27	2679.77	561985.29
34	827211.10	695334.96	2455.07	508333.71
35	759638.33	504802.50	2186.98	422209.27
36	681679.67	439831.10	2851.06	374787.28
37	696081.24	409575.81	3489.60	369715.55
38	575261.37	344059.82	3206.42	307509.21
39	388666.04	*	*	388666.04
40	416253.90	*	*	416253.90

*Table D.5 – Summary of the blank and dilution corrected ICP-MS measurement (CPS) of **terbium** at m/z 159 in fractions collected from the stepwise chemical separation using a TEVA cartridge. 1 mL fractions were collected throughout. (see Figure 3.4 for the elution profile)*

Fraction Number	*Repeat 1 (CPS)*	*Repeat 2 (CPS)*	*Repeat 3 (CPS)*	*Mean Tb CPS*
1	51456.23	687280.80	1537890.84	758875.96
2	2640930.72	3401452.95	4003022.18	3348468.62
3	4081238.74	4036152.29	4006488.41	4041293.15
4	4423205.77	3674870.51	4548517.90	4215531.39
5	3780346.56	3825742.49	3966193.29	3857427.45
6	3670794.96	3636318.75	3785525.22	3697546.31
7	3701122.70	3683303.22	4228908.02	3871111.31
8	3685275.74	3732412.65	3804506.60	3740731.66
9	3733474.03	3578826.35	4196823.03	3836374.47
10	3684005.98	3397832.82	4163030.61	3748289.80
11	4382705.25	3516243.94	809659.98	2902869.72
12	1589318.51	943814.24	24945.38	852692.71
13	30317.88	11681.86	11948.51	17982.75
14	17089.39	7856.41	9645.20	11530.33
15	16486.34	9386.19	8772.77	11548.44
16	16407.03	9579.86	8599.01	11528.63
17	43569.15	6807.67	9535.04	19970.62
18	15036.98	9287.70	9141.42	11155.37
19	16540.25	6397.22	8505.05	10480.84
20	14768.08	8946.34	8659.10	10791.18
21	16011.55	6615.22	6587.31	9738.03
22	2397.67	-69.58	781.85	1036.65
23	-619.66	868.23	1179.92	476.17
24	-641.56	514.99	474.78	116.07
25	-691.94	602.65	1158.31	356.34
26	-554.78	505.04	329.47	93.25
27	-412.33	502.30	289.25	126.41
28	-606.49	705.98	580.17	226.55
29	-846.11	303.10	269.46	-91.19
30	-856.84	501.37	233.04	-40.81

31	-681.91	193.86	786.25	99.40
32	-637.09	430.46	582.38	125.25
33	-674.81	403.23	517.74	82.05
34	-784.54	480.65	244.63	-19.75
35	-851.13	283.62	317.15	-83.46
36	-877.67	371.95	277.90	-75.94
37	-621.95	200.38	823.10	133.84
38	-1084.33	198.49	594.13	-97.24
39	-1192.17	*	*	-1192.17
40	-1004.40	*	*	-1004.40

Table D.6 – A summary of the information used to calculate the elemental recovery of terbium and cerium in the main terbium fractions (1-15) after separation using a TEVA cartridge. Counts per second (CPS) reported in this table value were calculated by summing the mean values of relevant fractions. Uncertainties are based on standard deviation between repeats (n=3).

	Ce	*Tb*
Fractions 1-15 (CPS)	3208604.54 ± 2107933.35	38912274.08 ± 692888.63
Total (CPS)	28110989.00 ± 2820228.77	38987670.16 ± 717412.83
Mean elemental recovery (%)	**11.27 ± 7.29**	**99.81 ± 0.08**

Appendix E – Data to accompany Figure 4.3 and Figure 4.4

*Table E.1 – Distribution coefficient values (K_d) for **europium** on LN resin across a nitric acid concentration range. # denotes the* K_d *value which was plotted onto Figure 4.3 and Figure D.1 instead of the mean K_d value. This was needed where the 'mean K_d' value was skewed by an outlying value.*

HNO_3 (M)	*Repeat 1 (K_d)*	*Repeat 2 (K_d)*	*Repeat 3 (K_d)*	*Mean K_d*
0	1244.79	943.22	759.50	982.50
0.007	4832.73	3485.54	3799.40	4039.22
0.010	37060.23	19818.32	10235.77	22371.44
0.050	53524.06	23262.34	25628.82	34138.41
0.100	3887.99	3594.80	3674.98	3719.26
0.198	339.16	316.91	242.19	299.42
0.500	11.16	16.80	12.44	11.80
0.801	2.42	5.08	6.06	4.52
1.001	2.18	1.23	1.45	1.62
1.987	0.51 #	-2.45	1.01	-0.31

*Table E.2 – Distribution coefficient values (K_d) for **gadolinium** on LN resin across a nitric acid concentration range. # denotes the* K_d *value which was plotted onto Figure 4.3 and Figure D.1 instead of the mean K_d value. This was needed where the 'mean K_d' value was skewed by an outlying value.*

HNO_3 (M)	*Repeat 1 (K_d)*	*Repeat 2 (K_d)*	*Repeat 3 (K_d)*	*Mean K_d*
0	1016.67	634.57	715.81	789.02
0.007	4453.44	1973.99	2271.57	2899.66
0.010	20402.61	4457.54	10412.85	11757.67
0.050	27233.71	44088.12	31441.64	34254.49
0.100	5750.88	6767.63	4386.83	5635.12
0.198	510.49	517.99	593.02	540.50
0.500	24.35	22.36	16.28	21.00
0.801	5.36	1.29	4.84	3.83
1.001	2.53	4.89	3.83	3.75
1.987	0.32 #	0.44	-0.72	0.02

*Table E.3 – Distribution coefficient values (K_d) for **terbium** on LN resin across a nitric acid concentration range.*

HNO_3 (M)	*Repeat 1 (K_d)*	*Repeat 2 (K_d)*	*Repeat 3 (K_d)*	*Mean K_d*
0	554.00	971.02	914.30	813.11
0.007	2486.53	2384.09	2531.21	2467.28
0.010	4166.64	4435.43	6236.20	4946.09
0.050	78163.66	35318.99	83382.32	65621.66
0.100	26283.38	23618.34	27624.59	25842.10
0.198	683.91	2563.07	3140.51	2129.16
0.500	131.61	114.39	172.84	139.61
0.801	26.42	17.91	17.26	20.53
1.001	11.92	22.19	12.89	15.67
1.987	1.99	0.69	1.69	1.46

*Table E.4 – Distribution coefficient values (K_d) for **dysprosium** on LN resin across a nitric acid concentration range. * denotes a sample for which the K_d value could not be calculated. In this case, the aqueous phase was not successfully isolated at the end of the batch separation due to it being absorbed by the filter paper.*

HNO_3 (M)	*Repeat 1 (K_d)*	*Repeat 2 (K_d)*	*Repeat 3 (K_d)*	*Mean K_d*
0	792.68	644.41	580.07	672.38
0.007	1770.87	2831.73	2476.61	2359.74
0.010	3515.25	2228.95	4612.88	3452.36
0.050	31756.91	51653.87	48485.22	43965.33
0.100	65411.13	48594.21	49156.97	54387.43
0.198	7481.26	8263.57	8469.74	8071.52
0.500	371.58	*	397.21	384.40
0.801	76.58	74.46	72.71	74.58
1.001	35.40	34.13	34.13	34.55
1.987	4.06	0.80	3.29	2.72

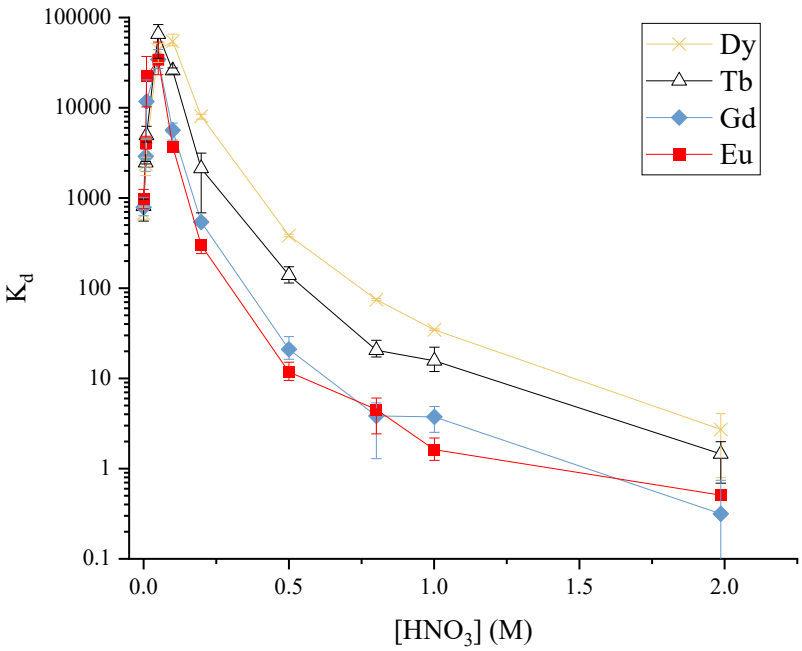

Figure E.1 – Maximum, minimum and mean distribution coefficients (K_d) of Eu, Gd, Tb and Dy across a range of HNO_3 concentrations on LN resin (50 – 100 µm). (linked to Figure 4.3)

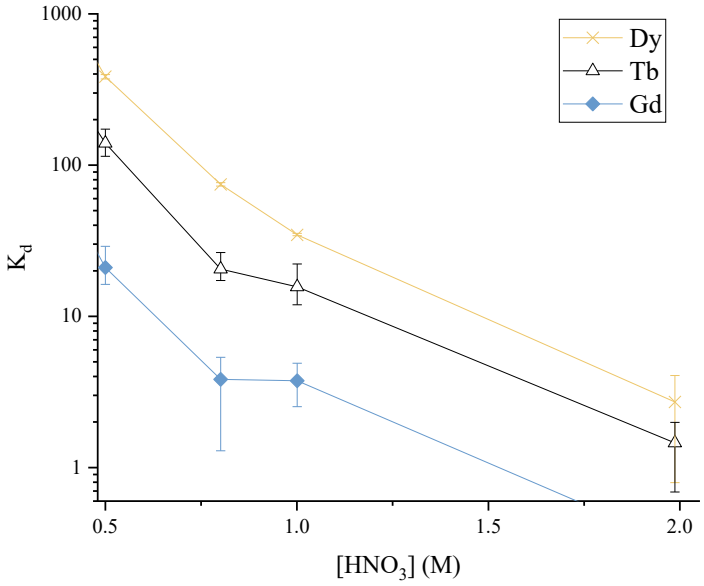

Figure E.2 – Maximum, minimum and mean distribution coefficients (K_d) of Gd, Tb and Dy across a range of HNO_3 concentrations on LN resin (50 – 100 µm) – zoomed in to highlight conditions which were used in initial column-based separation studies. (linked to Figure 4.4)

Appendix F – Data to accompany Figure 4.11

Figure F.1 – Summary of the calculated elemental recovery (%) values for the stepwise separation of gadolinium, terbium and dysprosium on an LN resin at a mobile phase flow rate of 1.0 mL/min. 1mL fraction were collected throughout. This data was used to collate Figure 4.11 (left).

Fraction Number	*Gd (%)*	*Tb (%)*	*Dy (%)*
1	0.00	0.00	0.00
2	0.00	0.00	0.00
3	0.00	0.00	0.00
4	0.00	0.00	0.00
5	0.00	0.00	0.00
6	0.00	0.00	0.00
7	0.19	0.00	0.00
8	2.02	0.00	0.00
9	7.20	0.00	0.00
10	16.63	0.00	0.00
11	22.43	0.00	0.00
12	18.43	0.00	0.00
13	11.34	0.00	0.00
14	6.56	0.00	0.00
15	4.75	0.00	0.00
16	3.40	0.00	0.00
17	2.59	0.00	0.00
18	2.01	0.00	0.00
19	1.46	0.00	0.00
20	1.14	0.00	0.00
21	1.01	0.00	0.00
22	0.78	0.00	0.00
23	0.54	0.01	0.00
24	0.37	0.07	0.00
25	0.21	0.27	0.00
26	0.13	0.90	0.00
27	0.10	2.48	0.00
28	0.06	4.50	0.00
29	0.04	7.68	0.00
30	0.03	10.83	0.00
31	0.03	12.77	0.00
32	0.02	13.50	0.00
33	0.01	11.81	0.00
34	0.02	10.52	0.00
35	0.01	6.78	0.00
36	0.01	4.36	0.00
37	0.00	2.61	0.00
38	0.00	1.50	0.00
39	0.01	0.85	0.01
40	0.00	0.57	0.05
41	0.01	0.25	0.42

42	0.01	0.09	2.52
43	0.01	0.04	10.31
44	0.00	0.02	23.60
45	0.00	0.01	29.14
46	0.00	0.01	19.75
47	0.00	0.00	8.08
48	0.00	0.00	1.94
49	0.00	0.00	0.29
50	0.00	0.00	0.07
51	0.00	0.00	0.02
52	0.00	0.00	0.01
53	0.00	0.00	0.01
54	0.00	0.00	0.01
55	0.00	0.00	0.01
56	0.00	0.00	0.00
57	0.00	0.00	0.00
58	0.00	0.00	0.00
59	0.00	0.00	0.00
60	0.00	0.00	0.00

Figure F.2 – Summary of the calculated elemental recovery (%) values for the stepwise separation of gadolinium, terbium and dysprosium on an LN resin at a mobile phase flow rate of 0.5 mL/min. 1mL fraction were collected throughout. This data was used to collate Figure 4.11 (right).

Fraction Number	*Gd (%)*	*Tb (%)*	*Dy (%)*
1	0.01	0.00	0.00
2	0.00	0.00	0.00
3	0.01	0.00	0.00
4	0.02	0.00	0.00
5	0.01	0.00	0.00
6	0.01	0.00	0.00
7	0.41	0.00	0.00
8	9.00	0.00	0.00
9	25.26	0.00	0.00
10	27.00	0.00	0.00
11	15.69	0.00	0.00
12	8.48	0.00	0.00
13	4.49	0.00	0.00
14	2.28	0.00	0.00
15	1.17	0.00	0.00
16	0.58	0.00	0.00
17	0.33	0.00	0.00
18	0.17	0.00	0.00
19	0.08	0.00	0.00
20	0.05	0.00	0.00
21	0.03	0.01	0.00
22	0.02	0.06	0.00

23	0.02	0.18	0.00
24	0.02	0.64	0.00
25	0.01	2.11	0.00
26	0.02	5.05	0.00
27	0.01	8.87	0.00
28	0.01	13.59	0.00
29	0.01	16.97	0.00
30	0.01	15.56	0.00
31	0.00	11.88	0.00
32	0.01	7.47	0.00
33	0.01	4.25	0.00
34	0.00	2.33	0.00
35	0.01	0.95	0.00
36	0.00	0.34	0.00
37	0.01	0.14	0.00
38	0.01	0.06	0.00
39	0.01	0.03	0.00
40	0.01	0.02	0.01
41	0.00	0.01	0.01
42	0.01	0.01	0.03
43	0.01	0.01	0.06
44	0.03	0.01	0.76
45	0.01	0.01	8.45
46	0.01	0.01	35.37
47	0.00	0.01	38.62
48	0.00	0.00	12.04
49	0.00	0.00	1.18
50	0.00	0.00	0.08
51	0.00	0.00	0.02
52	0.00	0.00	0.01
53	0.00	0.00	0.01
54	0.00	0.00	0.00
55	0.00	0.00	0.00
56	0.00	0.00	0.00
57	0.00	0.00	0.01
58	0.00	0.00	0.00
59	0.00	0.00	0.00
60	0.00	0.00	0.00

Appendix G – Data to accompany 'simulant ^{xxx}Tb' separations

*Table G.1 – Summary of the calculated **elemental recovery (%)** values for the 'simulant ^{149}Tb' solution, containing caesium, barium, neodymium, samarium, europium, gadolinium, and terbium, after it had undergone chemical separation using the method summarised in Table 4.4. The raw ICP-MS data was blank, and dilution corrected before the elemental recovery was calculated using equation 2.3. 1 mL fractions were collected throughout (see Figure 4.12 for the elution profile). Cause(s) of the negative values were unknown, but could be due to contamination of blank samples, contamination of the instrument introduction system, uncorrected instrumental drift and/or the unrecorded use of different grade acids (i.e., analytical-grade vs. trace-grade).*

Fraction Number	*Cs (%)*	*Ba (%)*	*Nd (%)*	*Sm (%)*	*Eu (%)*	*Gd (%)*	*Tb (%)*
1	0.00	0.05	0.00	0.00	0.00	0.00	0.00
2	0.00	0.11	0.00	0.00	0.00	0.00	0.00
3	1.23	2.43	0.00	0.00	0.00	0.00	0.00
4	59.39	57.33	17.97	0.00	0.01	-0.01	0.03
5	17.08	17.64	50.46	4.81	0.00	0.02	0.07
6	8.43	9.54	12.45	42.72	0.40	0.00	0.02
7	4.53	5.07	8.07	28.00	14.13	0.03	0.01
8	2.15	2.55	3.53	9.87	35.78	1.29	0.01
9	1.17	1.42	1.96	5.32	25.86	12.12	0.00
10	0.53	0.78	0.87	2.44	9.89	26.02	0.00
11	0.25	0.36	0.48	1.42	4.86	27.25	0.00
12	0.11	0.21	0.23	0.62	2.27	14.45	0.00
13	0.03	0.11	0.07	0.29	1.27	7.17	0.00
14	-0.01	0.06	0.01	0.15	0.65	3.37	0.00
15	-0.02	0.04	-0.01	0.09	0.39	1.92	0.00
16	-0.02	0.11	-0.02	0.03	0.22	1.12	0.00
17	-0.02	0.05	-0.02	0.02	0.12	0.66	0.00
18	-0.02	0.21	-0.03	0.01	0.06	0.41	0.00
19	-0.02	0.51	-0.02	0.00	0.03	0.23	0.00
20	-0.02	0.05	-0.02	0.00	0.01	0.15	0.00
21	-0.03	0.00	-0.03	0.00	0.01	0.07	0.00
22	-0.03	0.02	-0.02	0.00	0.00	0.04	0.00
23	-0.02	0.05	-0.02	0.00	0.00	0.01	0.00
24	-0.02	0.01	-0.02	0.00	0.00	0.01	0.00
25	-0.02	-0.02	-0.03	0.00	0.00	0.01	0.00
26	-0.02	0.03	-0.03	0.00	0.00	0.01	0.03
27	-0.02	0.01	-0.03	0.00	0.00	0.00	0.31
28	-0.02	0.01	-0.03	0.00	0.00	0.01	1.53
29	-0.02	0.04	-0.03	0.00	0.00	0.01	4.93
30	-0.02	-0.04	-0.03	0.00	0.00	0.01	9.91
31	-0.03	0.03	-0.02	0.00	0.00	0.00	15.55
32	-0.03	0.00	-0.03	0.00	0.00	0.01	18.16
33	-0.02	0.02	-0.02	0.00	0.00	0.01	17.49
34	-0.02	0.01	-0.02	0.00	0.00	0.01	13.31
35	-0.02	0.03	-0.02	0.00	0.00	0.00	8.27
36	-0.02	0.03	-0.02	0.00	0.00	-0.01	4.36

37	-0.02	0.04	-0.02	0.00	0.00	0.00	1.92
38	-0.02	0.03	-0.02	0.00	0.00	0.00	0.80
39	-0.03	0.06	-0.03	0.00	0.00	-0.02	0.25
40	-0.02	0.01	-0.03	-0.01	0.00	-0.02	0.08
41	-0.02	0.02	-0.02	0.00	0.00	0.00	0.03
42	-0.02	0.02	-0.02	0.00	0.00	-0.01	0.01
43	-0.02	0.01	-0.02	0.00	0.00	0.00	0.00
44	-0.02	0.01	-0.02	0.00	0.00	0.01	0.01
45	-0.02	-0.01	-0.03	0.00	0.00	0.01	0.01
46	-0.02	0.03	-0.03	0.00	0.00	0.01	0.00
47	-0.02	0.04	-0.02	0.00	0.00	0.00	0.00
48	-0.02	0.01	-0.02	0.00	0.00	0.00	0.00
49	-0.02	0.02	-0.03	-0.01	0.00	-0.01	-0.01
50	-0.02	0.01	-0.02	-0.01	0.00	0.00	-0.01
51	-0.03	0.12	-0.02	0.00	0.00	0.00	-0.01
52	-0.02	0.02	-0.02	0.00	0.00	0.00	-0.01
53	-0.02	0.07	-0.02	0.00	0.00	0.00	-0.01
54	-0.02	0.02	-0.02	0.00	0.00	0.00	-0.01
55	-0.03	0.03	-0.02	0.00	0.00	-0.03	-0.01
56	-0.03	0.47	-0.01	0.00	0.00	-0.02	-0.01
57	-0.02	0.01	-0.03	0.00	0.00	0.00	-0.01
58	-0.02	-0.01	-0.03	0.00	0.00	0.00	-0.01
59	-0.03	0.04	-0.01	0.00	-0.01	-0.02	-0.01
60	-0.03	-0.01	-0.01	0.00	-0.01	-0.01	-0.01
Total	93.78	99.93	95.06	95.76	95.93	96.28	96.99

Table G.2 – Summary of the elemental recovery and elemental proportion information within the main terbium fractions for the 'simulant ^{149}Tb' separation.

**elemental proportion for barium, europium, gadolinium, and terbium would be 0.36%, 0.02%, 0.16% and 99.46%, respectively, if the negative values were assumed to be zero (i.e., barium, europium and gadolinium impurities and terbium purity).*

	Cs	*Ba*	*Nd*	*Sm*	*Eu*	*Gd*	*Tb*
Elemental recovery in fractions 21-40 (%)	-0.49	0.35	-0.50	-0.01	0.02	0.15	96.90
*Elemental proportion in fractions 21-40 (%) **	-0.51	0.37	-0.52	-0.01	0.02	0.16	100.49

*Table G.3 – Summary of the calculated **elemental recovery (%)** values for the 'simulant ^{152}Tb' solution, containing caesium, barium, cerium, samarium, europium, gadolinium, terbium, and dysprosium, after it had undergone chemical separation using the method summarised in Table 4.4. The raw ICP-MS data was blank, and dilution corrected before the elemental recovery was calculated equation 2.3. 1 mL fractions were collected throughout (see Figure 4.13 for the elution profile). Cause(s) of the negative values and inaccurate total elemental recovery values were unknown.*

Fraction Number	*Cs (%)*	*Ba (%)*	*Ce (%)*	*Sm (%)*	*Eu (%)*	*Gd (%)*	*Tb (%)*	*Dy (%)*
1	-0.01	0.18	-0.03	0.00	-0.04	0.01	0.00	0.00
2	-0.01	-0.09	-0.03	0.00	-0.04	0.00	0.00	0.00
3	-0.01	-0.03	-0.03	0.00	-0.03	0.00	0.00	0.00
4	30.41	33.91	2.60	0.00	-0.03	0.03	0.00	0.00
5	46.02	44.12	35.66	0.04	-0.03	0.28	0.01	0.00
6	20.24	20.72	24.60	16.93	-0.03	0.17	0.00	0.02
7	10.49	11.01	12.28	54.12	2.66	0.10	0.00	0.06
8	5.98	6.37	7.38	25.53	27.69	0.21	0.00	0.03
9	3.75	4.10	5.45	11.76	45.50	5.23	0.00	0.01
10	2.38	2.63	4.09	6.78	24.55	24.79	0.00	0.01
11	1.57	1.85	3.43	4.44	11.45	39.48	0.00	0.00
12	0.87	0.94	2.31	2.33	5.24	23.80	0.00	0.00
13	0.62	0.68	2.15	1.89	3.73	13.93	0.00	0.00
14	0.37	0.31	1.73	1.27	2.44	7.05	0.00	0.00
15	0.24	0.20	1.55	0.90	1.79	4.53	0.00	0.00
16	0.13	-0.02	1.14	0.42	0.99	2.47	0.00	0.00
17	0.10	-0.05	1.15	0.28	0.69	1.90	0.00	0.00
18	0.06	-0.06	1.00	0.17	0.39	1.25	0.00	0.00
19	0.05	-0.13	1.04	0.13	0.25	0.84	0.00	0.00
20	0.03	-0.15	0.91	0.08	0.13	0.47	0.00	0.00
21	0.02	-0.15	0.86	0.06	0.09	0.27	0.00	0.00
22	0.01	-0.14	0.85	0.05	0.05	0.20	0.00	0.00
23	0.01	-0.10	0.76	0.03	0.02	0.13	0.01	0.00
24	0.00	-0.17	0.74	0.02	0.01	0.08	0.05	0.00
25	0.00	-0.18	0.60	0.02	0.00	0.07	0.21	0.00
26	0.00	-0.16	0.62	0.01	-0.01	0.05	0.98	0.00
27	0.00	-0.18	0.62	0.01	-0.02	0.04	3.34	0.00
28	0.00	-0.21	0.54	0.01	-0.02	0.03	6.87	0.00
29	-0.01	-0.21	0.54	0.00	-0.03	0.03	12.98	0.00
30	0.00	-0.14	0.55	0.01	-0.03	0.01	19.21	0.00
31	0.00	-0.23	0.50	0.00	-0.03	0.01	21.58	0.00
32	-0.01	-0.23	0.42	0.00	-0.03	0.02	18.51	0.00
33	-0.01	-0.08	0.42	0.00	-0.03	0.01	16.37	0.00
34	0.00	-0.25	0.39	0.00	-0.03	0.01	10.97	0.00
35	-0.01	-0.24	0.41	0.00	-0.03	0.01	6.92	0.00
36	-0.01	-0.23	0.45	0.00	-0.04	0.00	4.19	0.00
37	-0.01	-0.25	0.32	0.00	-0.04	0.01	1.56	0.00
38	-0.01	-0.24	0.33	0.00	-0.04	0.01	0.78	0.00
39	-0.01	-0.18	0.32	0.00	-0.04	0.01	0.37	0.00
40	-0.01	-0.27	0.32	0.00	-0.04	0.01	0.16	0.00

41	-0.01	-0.24	0.26	0.00	-0.03	0.01	0.07	0.00
42	-0.01	-0.25	0.26	0.00	-0.03	0.01	0.05	0.00
43	-0.01	-0.27	0.28	0.00	-0.03	0.01	0.03	0.01
44	-0.01	-0.27	0.28	0.00	-0.03	0.00	0.03	0.09
45	-0.01	-0.24	0.25	0.00	-0.04	0.01	0.03	0.82
46	-0.01	-0.27	0.23	0.00	-0.04	0.01	0.02	6.28
47	-0.01	-0.22	0.21	0.00	-0.03	0.00	0.01	23.57
48	-0.01	-0.25	0.18	0.00	-0.03	0.00	0.01	39.71
49	-0.01	-0.22	0.21	0.00	-0.03	0.02	0.01	38.34
50	-0.01	-0.22	0.16	0.00	-0.03	0.00	0.00	9.93
51	0.00	0.10	0.00	0.00	-0.01	0.00	0.00	0.00
52	0.00	0.12	0.00	0.00	-0.01	0.00	0.00	0.00
53	0.00	0.00	0.18	0.00	0.00	0.00	0.00	0.04
54	0.00	0.14	0.17	0.00	0.00	0.00	0.00	0.02
55	0.00	-0.01	0.15	0.00	0.00	0.01	0.00	0.01
56	0.00	0.04	0.20	0.00	0.00	0.01	0.00	0.01
57	0.00	0.00	0.12	0.00	0.00	0.01	0.00	0.00
58	0.00	0.00	0.13	0.00	0.00	0.00	0.00	0.00
59	0.00	-0.02	0.13	0.00	0.00	0.00	0.00	0.00
60	0.00	-0.01	0.13	0.00	0.00	0.00	0.00	0.00
Total	123.17	120.55	122.45	127.32	126.66	127.64	125.32	118.98

Table G.4 – Summary of the elemental recovery and elemental proportion information within the main terbium fractions for the 'simulant ^{152}Tb' separation.

[#] elemental recovery was estimated by normalising the elemental recovery fraction and total to a maximum 100% by using equation 2.4.

**elemental proportion for cerium, samarium, gadolinium and terbium would be 7.88 %, 0.16 %, 0.71 % and 91.25 %, respectively, if the negative values were assumed to be zero (i.e., cerium, samarium and gadolinium impurity and terbium purity).*

	Cs	*Ba*	*Ce*	*Sm*	*Eu*	*Gd*	*Tb*	*Dy*
*Estimated elemental **recovery** in fractions 21-40 (%) [#]*	-0.03	-3.21	8.61	0.18	-0.23	0.78	99.78	0.00
*Elemental **proportion** in fractions 21-40 (%) **	-0.03	-3.03	8.13	0.17	-0.22	0.74	94.24	0.00

*Table G.5 – Summary of the calculated **elemental recovery (%)** values for the 'simulant ^{155}Tb' solution, containing lanthanum, cerium, praseodymium, europium, gadolinium, terbium and dysprosium, after it had undergone chemical separation using the method summarised in Table 4.4. The raw ICP-MS data was blank, and dilution corrected before the elemental recovery was calculated using equation 2.3. 1 mL fractions were collected throughout (see Figure 4.14 for the elution profile). Cause(s) of the negative values were unknown.*

Fraction Number	*La (%)*	*Ce (%)*	*Pr (%)*	*Eu (%)*	*Gd (%)*	*Tb (%)*	*Dy (%)*
1	0.01	0.02	0.00	0.00	0.04	0.00	0.00
2	0.01	0.00	0.00	-0.01	0.02	0.00	0.00
3	0.00	0.00	0.00	0.00	0.06	0.00	0.00
4	0.01	0.01	0.00	0.00	0.06	0.00	0.00
5	0.00	0.00	0.00	0.00	0.05	0.00	0.00
6	0.00	0.02	0.00	0.00	0.07	0.00	0.00
7	0.02	0.02	0.00	0.00	0.06	0.00	0.00
8	12.97	1.00	0.25	0.00	0.04	0.00	0.00
9	27.22	23.00	19.39	0.01	0.08	0.00	0.00
10	15.50	19.47	24.24	0.00	0.10	0.00	0.00
11	9.95	11.83	13.85	0.00	0.09	0.00	0.00
12	7.53	8.67	9.42	-0.01	0.07	0.00	0.00
13	5.17	6.26	6.72	0.00	0.08	0.00	0.00
14	4.16	5.10	4.97	0.00	0.06	0.00	0.00
15	3.05	3.91	3.79	0.11	0.08	0.00	0.00
16	2.36	3.03	2.89	1.01	0.08	0.00	0.00
17	1.92	2.59	2.32	5.28	0.06	0.00	0.00
18	1.21	1.77	1.53	12.23	0.04	0.00	0.00
19	0.94	1.36	1.11	15.85	0.06	0.00	0.00
20	0.68	1.11	0.88	13.88	0.13	0.00	0.00
21	0.61	0.98	0.67	10.98	0.58	0.00	0.00
22	0.42	0.75	0.54	7.70	1.77	0.00	0.00
23	0.31	0.61	0.39	5.24	4.80	0.00	0.00
24	0.23	0.47	0.29	3.97	9.35	0.00	0.00
25	0.17	0.42	0.21	3.21	13.20	0.00	0.00
26	0.13	0.34	0.18	2.92	17.46	0.00	0.00
27	0.10	0.25	0.12	2.44	16.25	0.00	0.00
28	0.06	0.20	0.08	1.75	12.77	0.00	0.00
29	0.07	0.17	0.06	1.20	8.25	0.00	0.00
30	0.05	0.15	0.04	0.77	5.10	0.00	0.00
31	0.03	0.13	0.04	0.42	3.03	0.00	0.00
32	0.02	0.09	0.03	0.20	1.67	0.00	0.00
33	0.02	0.08	0.03	0.09	0.86	0.00	0.00
34	0.02	0.06	0.01	0.04	0.51	0.00	0.00
35	0.01	0.06	0.01	0.05	0.20	0.00	0.00
36	0.01	0.05	0.01	0.03	0.10	0.00	0.00
37	0.01	0.05	0.01	0.01	0.06	0.00	0.00
38	0.01	0.04	0.01	0.01	0.03	0.00	0.00
39	0.01	0.04	0.00	0.01	0.06	0.00	0.00
40	0.01	0.03	0.00	0.01	0.03	0.00	0.00

41	0.00	0.03	0.00	0.02	0.03	0.00	0.00
42	0.00	0.03	0.00	0.01	0.02	0.00	0.00
43	0.00	0.01	0.00	0.01	0.03	0.00	0.00
44	0.01	0.02	0.00	0.00	0.02	0.00	0.00
45	0.01	0.04	0.00	0.01	0.04	0.01	0.00
46	0.00	0.03	0.00	0.00	0.04	0.13	0.00
47	0.00	0.02	0.00	0.00	0.03	2.29	0.00
48	0.00	0.01	0.00	0.00	0.03	21.48	0.00
49	0.00	0.02	0.00	0.00	0.01	49.88	0.01
50	0.00	0.01	0.00	0.00	0.01	20.05	0.01
51	0.00	0.01	0.00	0.00	0.02	1.70	0.00
52	0.00	0.01	0.00	0.00	0.01	0.13	0.01
53	0.00	0.02	0.00	0.00	0.00	0.03	0.01
54	0.00	0.01	0.00	0.00	0.00	0.01	0.30
55	0.00	0.01	0.00	0.00	0.01	0.00	3.64
56	0.00	0.01	0.00	0.00	0.00	0.01	18.05
57	0.00	0.00	0.00	0.00	0.01	0.00	33.52
58	0.00	0.01	0.00	0.00	0.02	0.00	27.01
59	0.00	0.01	0.00	0.00	0.01	0.00	10.55
60	0.00	0.01	0.00	0.01	0.01	0.00	1.98
Total	95.05	94.45	94.14	89.45	97.76	95.73	95.12

Table G.6 – Summary of the elemental recovery and elemental proportion information within the main terbium fractions for the 'simulant ^{155}Tb' separation.

	La	*Ce*	*Pr*	*Eu*	*Gd*	*Tb*	*Dy*
*Elemental **recovery** in fractions 41-50 (%)*	0.02	0.21	0.01	0.04	0.25	93.83	0.02
*Elemental **proportion** in fractions 41-50 (%) **	0.02	0.23	0.02	0.05	0.27	99.40	0.02

Appendix H – Data to accompany Table 4.5

Table H.1 – Summary of the caesium, barium and neodymium data used in the calculation of the terbium recovery and terbium purity for the 'simulant ^{149}Tb' chemical separation. Elemental recovery was calculated using equation 2.4. Uncertainties are based on counting statistics only (n=10).

	Cs	*Ba*	*Nd*
Fractions 41-50 (CPS)	380.06 ± 116.18	2163.48 ± 198.48	-26.70 ± 55.70
Total (CPS)	1816161.02 ± 29059.27	70532.49 ± 564.68	122346 ± 978.77
Elemental recovery in fractions 41-50 (%)	0.02 ± 0.01	3.07 ± 0.28	-0.02 ± 0.05

Table H.2 – Summary of the samarium, europium and gadolinium data used in the calculation of the terbium recovery and terbium purity for the 'simulant ^{149}Tb' chemical separation. Elemental recovery was calculated using equation 2.4. Uncertainties are based on counting statistics only (n=10).

	Sm	*Eu*	*Gd*
Fractions 41-50 (CPS)	90.00 ± 34.64	-23.34 ± 141.67	360.01 ± 81.86
Total (CPS)	95017.65 ± 855.21	293913.23 ± 4114.93	107469.72 ± 1074.70
Elemental recovery in fractions 41-50 (%)	0.09 ± 0.04	-0.01 ± 0.05	0.33 ± 0.08

Table H.3 – Summary of the terbium data used in the calculation of the terbium recovery and terbium purity for the 'simulant ^{149}Tb' chemical separation. Elemental recovery was calculated using equation 2.4. Uncertainties are based on counting statistics only (n=10).

	Tb
Fractions 41-50 (CPS)	678599.34 ± 11709.23
Total (CPS)	674665.04 ± 6072.05
Elemental recovery in fractions 41-50 (%)	100.58 ± 1.96
Terbium purity in fractions 41-50 (%)	96.65 ± 2.82

Table H.4 – Summary of the caesium, barium and samarium data used in the calculation of the terbium recovery and terbium purity for the 'simulant ^{152}Tb' chemical separation. Elemental recovery was calculated using equation 2.4. Uncertainties are based on counting statistics only (n=10).

	Cs	*Ba*	*Sm*
Fractions 41-50 (CPS)	-150.00 ± 135.81	1573.44 ± 192.26	13.32 ± 36.97
Total (CPS)	1791641.38 ± 25084.39	71848.13 ± 647.74	95034.05 ± 1140.41
Elemental recovery in fractions 41-50 (%)	-0.01 ± 0.01	2.19 ± 0.27	0.01 ± 0.04

Table H.5 – Summary of the europium, gadolinium and dysprosium data used in the calculation of the terbium recovery and terbium purity for the 'simulant ^{152}Tb' chemical separation. Elemental recovery was calculated using equation 2.4.Uncertainties are based on counting statistics only (n=10).

	Eu	*Gd*	*Dy*
Fractions 41-50 (CPS)	73.35 ± 94.85	516.70 ± 89.38	63.32 ± 52.36
Total (CPS)	289382.67 ± 4051.85	108385 ± 1083.85	166380.71 ± 1830.48
Elemental recovery in fractions 41-50 (%)	0.03 ± 0.03	0.48 ± 0.08	0.04 ± 0.03

Table H.6 – Summary of the terbium data used in the calculation of the terbium recovery and terbium purity for the 'simulant ^{152}Tb' chemical separation. Elemental recovery was calculated using equation 2.4. Uncertainties are based on counting statistics only (n=10).

	Tb
Fractions 41-50 (CPS)	673671.89 ± 19180.84
Total (CPS)	680516.50 ± 6125.04
Elemental recovery in fractions 41-50 (%)	98.99 ± 2.96
Terbium purity in fractions 41-50 (%)	97.31 ± 4.29

Table H.7 – Summary of the lanthanum, cerium and praseodymium data used in the calculation of the terbium recovery and terbium purity for the 'simulant ^{155}Tb' chemical separation. Elemental recovery was calculated using equation 2.4. Uncertainties are based on counting statistics only (n=10).

	La	*Ce*	*Pr*
Fractions 41-50 (CPS)	176.64 ± 110.60	1383.39 ± 122.21	146.67 ± 91.31
Total (CPS)	856612.52 ± 8566.36	649309.19 ± 8441.77	1000121.34 ± 8001.06
Elemental recovery in fractions 41-50 (%)	0.00 ± 0.00	0.21 ± 0.02	0.01 ± 0.01

Table H.8 – Summary of the europium, gadolinium and dysprosium data used in the calculation of the terbium recovery and terbium purity for the 'simulant ^{155}Tb' chemical separation. Elemental recovery was calculated using equation 2.4. Uncertainties are based on counting statistics only (n=10).

	Eu	*Gd*	*Dy*
Fractions 41-50 (CPS)	176.65 ± 78.32	373.33 ± 57.14	46.66 ± 24.29
Total (CPS)	398063.71 ± 5573.08	149116.67 ± 1391.21	220913.71 ± 2430.14
Elemental recovery in fractions 41-50 (%)	0.04 ± 0.02	0.25 ± 0.04	0.02 ± 0.01

Table H.9 – Summary of the terbium data used in the calculation of the terbium recovery and terbium purity for the 'simulant ^{155}Tb' chemical separation. Elemental recovery was calculated using equation 2.4. Uncertainties are based on counting statistics only (n=10).

	Tb
Fractions 41-50 (CPS)	918239.33 ± 6140.16
Total (CPS)	978578.34 ± 8807.30
Elemental recovery in fractions 41-50 (%)	93.83 ± 1.05
Terbium purity in fractions 41-50 (%)	99.40 ± 1.59

Appendix I – Data to accompany Figure 4.16

*Table I.1 – Summary of the calculated **elemental recovery (%)** values for the 'simulant ^{155}Tb' solution, containing lanthanum, cerium, praseodymium, europium, gadolinium, terbium and dysprosium, after it had undergone chemical separation using the method summarised in Table 4.6. The raw ICP-MS data was blank, dilution and internal standard corrected before the elemental recovery was calculated using equation 2.3. 0.5 mL fractions were collected throughout (see Figure 4.16 for the elution profile). Cause(s) of the negative values were unknown.*

Fraction Number	*La (%)*	*Ce (%)*	*Pr (%)*	*Eu (%)*	*Gd (%)*	*Tb (%)*	*Dy (%)*
1	5.39	3.39	2.64	0.00	0.32	0.00	0.00
2	6.64	4.20	3.27	0.01	0.62	0.00	0.00
3	40.69	37.37	35.57	0.53	1.98	0.03	0.04
4	41.62	40.58	45.16	4.36	0.62	0.00	0.00
5	4.33	9.14	12.29	18.30	3.00	0.00	0.00
6	0.47	1.38	0.54	40.33	14.32	0.00	0.00
7	0.33	0.95	0.38	28.56	33.52	0.00	0.00
8	0.06	0.48	0.08	5.43	44.50	0.08	0.00
9	0.04	0.43	0.04	0.29	7.55	0.50	0.00
10	0.04	0.43	0.05	0.09	-0.87	2.32	0.00
11	0.04	0.41	0.04	0.08	-1.68	7.30	0.01
12	0.01	0.20	0.01	0.05	0.16	72.88	4.19
13	0.01	0.16	0.00	0.01	-1.02	14.78	22.43
14	0.00	0.15	0.00	0.01	-0.79	0.33	43.17
15	0.01	0.13	0.00	0.00	-0.96	0.09	23.94
TOTAL	99.66	99.41	100.08	98.06	101.27	98.32	93.78

Table I.2 – Summary of the elemental recovery and elemental proportion information within the main terbium fractions for the 'simulant ^{155}Tb' separation on a smaller column.

**elemental proportion for lanthanum, cerium, praseodymium, europium, terbium and dysprosium would be 0.04 %, 0.63 %, 0.04 %, 0,11 %, 77.46 % and 21.72%, respectively, if the negative value was assumed to be zero (i.e., lanthanum, cerium, praseodymium, europium and dysprosium impurity and terbium purity).*

	La	*Ce*	*Pr*	*Eu*	*Gd*	*Tb*	*Dy*
Elemental recovery in fractions 11-13 (%)	0.05	0.77	0.05	0.14	-2.55	94.96	26.62
*Elemental proportion in fractions 11-13 (%) **	0.05	0.64	0.04	0.11	-2.12	79.10	22.18

Appendix J – Data to accompany Figure 5.1

Table J.1 – Summary of the data showing the variation of distribution coefficient (K_d) with an increasing concentration of gadolinium per unit volume of LN resin (50-100 μm). Repeat 1 of 3.

Repeat 1	*mg Gd/mL resin*	*K_d*
	3.73	28562.65
	7.99	6099.67
	10.85	1180.99
	15.19	84.82
	20.48	27.99

Table J.2 – Summary of the data showing the variation of distribution coefficient (K_d) with an increasing concentration of gadolinium per unit volume of LN resin (50-100 μm). Repeat 2 of 3.

Repeat 2	*mg Gd/mL resin*	*K_d*
	3.60	65855.91
	7.42	6217.55
	10.54	1560.17
	16.21	50.04
	20.55	28.84

Table J.3 – Summary of the data showing the variation of distribution coefficient (K_d) with an increasing concentration of gadolinium per unit volume of LN resin (50-100 μm). Repeat 3 of 3.

Repeat 3	*mg Gd/mL resin*	*K_d*
	3.67	41593.83
	6.90	8512.74
	12.65	380.70
	15.79	48.63
	17.78	38.25

Table J.4– Summary of the data showing the variation of distribution coefficient (K_d) with an increasing concentration of gadolinium per unit volume of LN resin (50-100 μm). Mean and standard deviation between repeats (n=3) is shown.

Mean	*mg Gd/mL resin*	*K_d*
	3.67 ± 0.07	45337.46 ± 18926.38
	7.44 ± 0.54	6943.32 ± 1360.43
	11.35 ± 1.14	1040.62 ± 602.13
	15.73 ± 0.51	61.16 ± 20.50
	19.61 ± 1.58	31.69 ± 5.70

Appendix K – Data to accompany Table 5.3

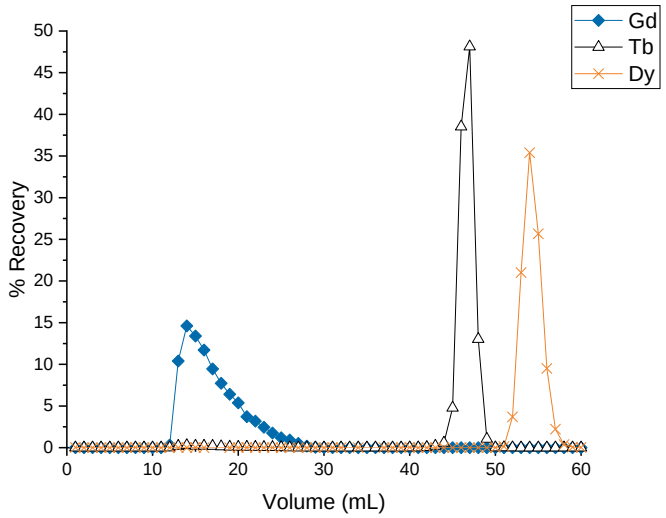

*Figure K.1 - Elution profile illustrating the separation of bulk quantities of gadolinium (**10 mg** Gd_2O_3) from trace quantities of terbium and dysprosium (1 µg) on an LN resin column (50-100 µm particle size, 7×200 mm column dimensions). (Repeat #1 only)*

Table K.1 – Summary of the internal standard, blank and dilution corrected ICP-MS data for the separation of 1 µg terbium from 10 mg gadolinium and 1 µg dysprosium (Repeat #1 only).

Fraction Number	*Gd (CPS)*	*Tb (CPS)*	*Dy (CPS)*
1	1.72E+05	0	4.00E+03
2	1.32E+05	4.03E+03	0
3	1.51E+05	0	0
4	1.31E+05	0	0
5	1.55E+05	1.99E+03	0
6	1.18E+05	2.03E+03	0
7	1.91E+05	2.01E+03	0
8	2.01E+05	0	4.02E+03
9	1.51E+05	2.04E+03	0
10	1.80E+05	1.99E+03	0
11	1.74E+05	0	0
12	3.55E+08	6.11E+03	0
13	1.18E+10	1.46E+05	0
14	1.66E+10	2.10E+05	0
15	1.52E+10	1.51E+05	4.08E+03
16	1.33E+10	1.50E+05	0
17	1.07E+10	1.41E+05	-2.03E+03
18	8.78E+09	1.04E+05	-2.03E+03
19	7.28E+09	6.96E+04	0
20	6.11E+09	6.43E+04	0
21	4.22E+09	6.10E+04	4.07E+03

22	3.61E+09	5.11E+04	0
23	2.78E+09	4.04E+04	0
24	2.00E+09	4.42E+04	2.01E+03
25	1.35E+09	2.89E+04	0
26	1.05E+09	1.01E+04	0
27	5.84E+08	2.07E+03	0
28	2.02E+08	2.05E+03	0
29	4.95E+07	0	0
30	1.61E+07	0	0
31	7.98E+06	0	2.03E+03
32	5.76E+06	0	2.07E+03
33	5.05E+06	2.12E+03	-2.02E+03
34	3.88E+06	-2.02E+03	2.23E+03
35	3.26E+06	0	-2.10E+03
36	2.97E+06	0	-2.10E+03
37	1.81E+06	2.05E+03	0
38	1.60E+06	0	0
39	1.46E+06	4.08E+03	0
40	1.22E+06	6.11E+03	6.11E+03
41	9.04E+05	1.22E+04	0
42	7.91E+05	4.59E+04	0
43	6.93E+05	1.51E+05	0
44	6.13E+05	4.20E+05	0
45	1.05E+06	3.47E+06	0
46	1.72E+06	2.79E+07	0
47	1.57E+06	3.49E+07	6.07E+01
48	1.24E+06	9.44E+06	0
49	8.41E+05	7.53E+05	0
50	6.70E+03	6.37E+03	0
51	3.83E+05	2.17E+04	2.29E+04
52	2.59E+05	8.54E+03	6.05E+05
53	1.91E+05	4.33E+03	3.44E+06
54	1.36E+05	2.14E+03	5.79E+06
55	1.01E+05	1.79E+03	4.20E+06
56	7.90E+04	9.52E+02	1.56E+06
57	5.98E+04	6.80E+02	3.63E+05
58	5.05E+04	6.22E+02	6.09E+04
59	4.02E+04	6.49E+02	9.63E+03
60	3.95E+04	2.57E+02	3.51E+03
Initial	1.14E+11	7.24E+07	1.64E+07

Table K.2 – Summary of the normalised elemental recovery data for the separation of 1 μg terbium from 10 mg gadolinium and 1 μg dysprosium. Calculated using equation 2.4 (Repeat #1 only).

Fraction Number	*Gd (%)*	*Tb (%)*	*Dy (%)*
1	0.00	0.00	0.02
2	0.00	0.01	0.00
3	0.00	0.00	0.00
4	0.00	0.00	0.00
5	0.00	0.00	0.00
6	0.00	0.00	0.00
7	0.00	0.00	0.00
8	0.00	0.00	0.02
9	0.00	0.00	0.00
10	0.00	0.00	0.00
11	0.00	0.00	0.00
12	0.33	0.01	0.00
13	11.13	0.19	0.00
14	15.65	0.27	0.00
15	14.34	0.19	0.03
16	12.54	0.19	0.00
17	10.12	0.18	-0.01
18	8.27	0.13	-0.01
19	6.86	0.09	0.00
20	5.76	0.08	0.00
21	3.98	0.08	0.03
22	3.40	0.07	0.00
23	2.62	0.05	0.00
24	1.88	0.06	0.01
25	1.27	0.04	0.00
26	0.99	0.01	0.00
27	0.55	0.00	0.00
28	0.19	0.00	0.00
29	0.05	0.00	0.00
30	0.02	0.00	0.00
31	0.01	0.00	0.01
32	0.01	0.00	0.01
33	0.00	0.00	-0.01
34	0.00	0.00	0.01
35	0.00	0.00	-0.01
36	0.00	0.00	-0.01
37	0.00	0.00	0.00
38	0.00	0.00	0.00
39	0.00	0.01	0.00
40	0.00	0.01	0.04
41	0.00	0.02	0.00
42	0.00	0.06	0.00
43	0.00	0.19	0.00
44	0.00	0.54	0.00
45	0.00	4.42	0.00

46	0.00	35.58	0.00
47	0.00	44.46	0.00
48	0.00	12.04	0.00
49	0.00	0.96	0.00
50	0.00	0.01	0.00
51	0.00	0.03	0.14
52	0.00	0.01	3.76
53	0.00	0.01	21.39
54	0.00	0.00	36.03
55	0.00	0.00	26.14
56	0.00	0.00	9.68
57	0.00	0.00	2.26
58	0.00	0.00	0.38
59	0.00	0.00	0.06
60	0.00	0.00	0.02

Table K.3 – A summary of the repeat data for the separation of 1 μg terbium from 10 mg gadolinium and 1 μg dysprosium.

	Repeat 1	*Repeat 2*	*Repeat 3*	*Mean*
Tb purity	54.22%	50.57%	55.98%	53.59%
Gd impurity	45.77%	49.42%	44.00%	46.40%
Tb recovery	106.40%	121.97%	85.71%	104.69%
Normalised Tb recovery	98.28%	98.35%	98.38%	98.34%
Gd/Tb ratio (initial)	10000	10000	10000	10000
Gd/Tb ratio (41-50)	0.84	0.98	0.79	0.87
Decontamination factor	1.21E+04	1.04E+04	1.29E+04	1.18E+04

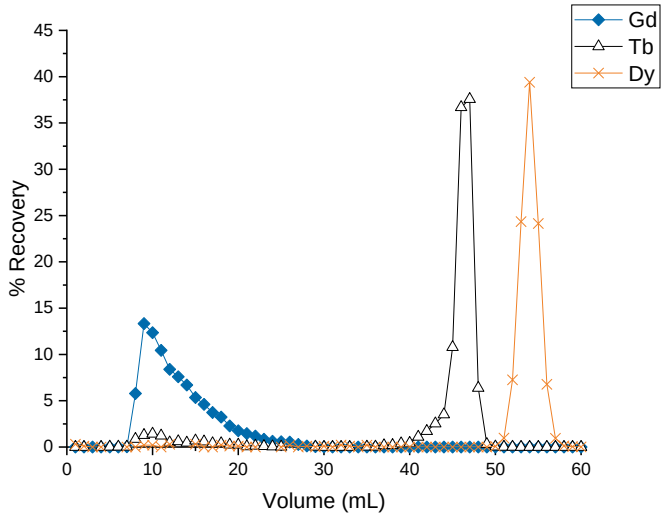

*Figure K.2 - Elution profile illustrating the separation of bulk quantities of gadolinium (**50 mg** Gd_2O_3) from trace quantities of terbium and dysprosium (1 μg) on an LN resin column (50-100 μm particle size, 7×200 mm column dimensions)*

Table K.4 – Summary of the internal standard, blank and dilution corrected ICP-MS data for the separation of 1 μg terbium from 50 mg gadolinium and 1 μg dysprosium.

Fraction Number	*Gd (CPS)*	*Tb (CPS)*	*Dy (CPS)*
1	-1.36E+07	0	5.94E+04
2	2.50E+05	0	1.98E+04
3	-1.35E+07	-2.02E+04	0
4	-1.45E+07	3.03E+02	0
5	-1.29E+07	1.94E+04	-3.99E+04
6	-1.09E+07	2.01E+04	-3.99E+04
7	1.05E+08	2.02E+04	0
8	3.09E+10	7.77E+05	0
9	7.13E+10	1.15E+06	3.91E+04
10	6.61E+10	1.28E+06	3.87E+04
11	5.59E+10	1.09E+06	0
12	4.49E+10	4.35E+05	5.68E+04
13	4.06E+10	5.51E+05	-3.87E+04
14	3.59E+10	4.11E+05	-1.92E+04
15	2.86E+10	6.16E+05	5.77E+04
16	2.47E+10	5.23E+05	0
17	2.00E+10	3.52E+05	0
18	1.73E+10	3.49E+05	4.11E+04
19	1.22E+10	2.18E+05	1.99E+04
20	9.41E+09	2.17E+05	1.97E+04
21	7.78E+09	6.23E+04	0
22	6.30E+09	1.18E+05	0
23	4.49E+09	8.04E+04	-2.01E+04
24	3.35E+09	4.05E+04	-2.01E+04

25	3.08E+09	2.07E+04	0
26	2.85E+09	-1.99E+04	3.98E+04
27	1.53E+09	-2.04E+04	0
28	6.17E+08	-4.06E+04	1.99E+04
29	2.05E+08	2.04E+04	0
30	5.82E+07	0	1.99E+04
31	1.86E+07	0	0
32	5.67E+06	0	4.05E+04
33	1.14E+07	-6.25E+02	2.00E+04
34	4.47E+06	-2.06E+04	0
35	3.08E+06	1.99E+04	3.98E+04
36	8.83E+05	1.99E+04	0
37	2.43E+06	1.60E+05	0
38	1.58E+06	1.82E+05	0
39	5.95E+05	3.41E+05	0
40	-1.93E+06	3.87E+05	0
41	3.66E+06	9.81E+05	1.99E+01
42	3.19E+06	1.54E+06	0
43	2.81E+06	2.26E+06	0
44	2.51E+06	3.14E+06	0
45	4.41E+06	9.63E+06	0
46	7.42E+06	3.28E+07	2.03E+01
47	7.73E+06	3.35E+07	6.00E+01
48	5.91E+06	5.70E+06	0
49	4.11E+06	2.69E+05	4.10E+02
50	2.72E+06	3.67E+04	1.29E+04
51	1.87E+06	1.45E+04	1.85E+05
52	1.39E+06	6.73E+03	1.39E+06
53	9.12E+05	3.62E+03	4.67E+06
54	6.99E+05	2.45E+03	7.56E+06
55	5.12E+05	1.74E+03	4.63E+06
56	4.10E+05	7.73E+02	1.30E+06
57	3.08E+05	7.34E+02	1.80E+05
58	2.41E+05	5.11E+02	2.40E+04
59	1.93E+05	4.45E+02	7.17E+03
60	1.58E+05	1.17E+02	2.89E+03
Initial	5.35E+11	8.93E+07	1.92E+07

Table K.5 – Summary of the normalised elemental recovery data for the separation of 1 μg terbium from 50 mg gadolinium and 1 μg dysprosium. Calculated using equation 2.4.

Fraction Number	*Gd (%)*	*Tb (%)*	*Dy (%)*
1	0.00	0.00	0.29
2	0.00	0.00	0.10
3	0.00	-0.02	0.00
4	0.00	0.00	0.00
5	0.00	0.02	-0.20
6	0.00	0.02	-0.20
7	0.02	0.02	0.00
8	6.34	0.78	0.00
9	14.61	1.16	0.19
10	13.53	1.29	0.19
11	11.45	1.10	0.00
12	9.20	0.44	0.28
13	8.32	0.56	-0.19
14	7.35	0.41	-0.09
15	5.86	0.62	0.28
16	5.06	0.53	0.00
17	4.09	0.36	0.00
18	3.54	0.35	0.20
19	2.50	0.22	0.10
20	1.93	0.22	0.10
21	1.59	0.06	0.00
22	1.29	0.12	0.00
23	0.92	0.08	-0.10
24	0.69	0.04	-0.10
25	0.63	0.02	0.00
26	0.58	-0.02	0.20
27	0.31	-0.02	0.00
28	0.13	-0.04	0.10
29	0.04	0.02	0.00
30	0.01	0.00	0.10
31	0.00	0.00	0.00
32	0.00	0.00	0.20
33	0.00	0.00	0.10
34	0.00	-0.02	0.00
35	0.00	0.02	0.20
36	0.00	0.02	0.00
37	0.00	0.16	0.00
38	0.00	0.18	0.00
39	0.00	0.34	0.00
40	0.00	0.39	0.00
41	0.00	0.99	0.00
42	0.00	1.55	0.00
43	0.00	2.27	0.00
44	0.00	3.17	0.00
45	0.00	9.70	0.00

46	0.00	33.01	0.00
47	0.00	33.80	0.00
48	0.00	5.74	0.00
49	0.00	0.27	0.00
50	0.00	0.04	0.06
51	0.00	0.01	0.91
52	0.00	0.01	6.85
53	0.00	0.00	22.98
54	0.00	0.00	37.20
55	0.00	0.00	22.79
56	0.00	0.00	6.40
57	0.00	0.00	0.89
58	0.00	0.00	0.12
59	0.00	0.00	0.04
60	0.00	0.00	0.01

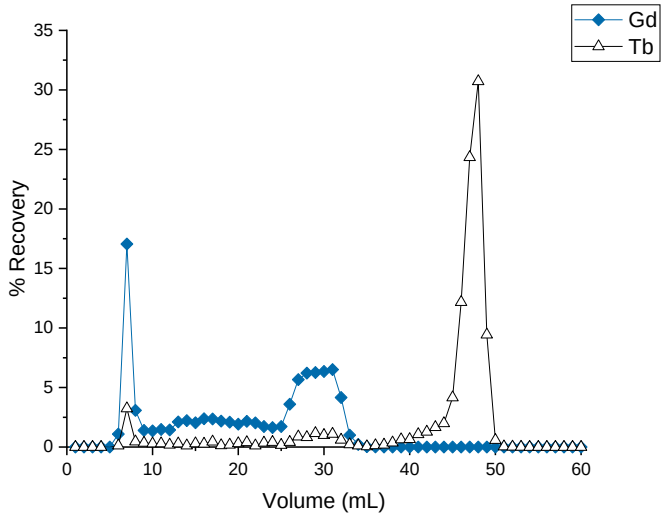

*Figure K.3 - Elution profile illustrating the separation of bulk quantities of gadolinium (**100 mg** Gd_2O_3) from trace quantities of terbium (1 μg) on an LN resin column (50-100 μm particle size, 7×200 mm column dimensions)*

Table K.6 – Summary of the internal standard, blank and dilution corrected ICP-MS data for the separation of 1 μg terbium from 100 mg gadolinium and 1 μg dysprosium.

Fraction Number	*Gd (CPS)*	*Tb (CPS)*	*Dy (CPS)*
1	1.12E+07	0	0
2	5.55E+06	0	0
3	7.34E+05	0	0
4	-2.24E+07	0	2.10E+04
5	-1.27E+07	-2.15E+04	0
6	8.10E+09	1.01E+05	0
7	1.26E+11	2.73E+06	0
8	2.28E+10	3.80E+05	0
9	1.03E+10	2.90E+05	0
10	1.00E+10	2.43E+05	0
11	1.09E+10	2.46E+05	0
12	1.07E+10	1.61E+05	2.02E+04
13	1.56E+10	2.39E+05	0
14	1.64E+10	1.00E+05	0
15	1.51E+10	2.48E+05	0
16	1.76E+10	2.26E+05	0
17	1.75E+10	3.72E+05	4.13E+04
18	1.62E+10	1.19E+05	0
19	1.55E+10	1.60E+05	0
20	1.42E+10	2.61E+05	0
21	1.60E+10	3.30E+05	0
22	1.50E+10	9.73E+04	0
23	1.28E+10	2.99E+05	-2.00E+04
24	1.21E+10	3.50E+05	-2.00E+04
25	1.28E+10	1.40E+05	0

26	2.66E+10	3.54E+05	0
27	4.20E+10	7.37E+05	2.05E+04
28	4.60E+10	6.95E+05	0.00E+00
29	4.64E+10	9.80E+05	3.92E+04
30	4.71E+10	8.40E+05	0
31	4.82E+10	9.28E+05	0
32	3.09E+10	5.11E+05	0
33	7.40E+09	1.83E+05	0
34	1.61E+09	9.71E+04	0
35	2.53E+08	3.93E+04	0
36	5.32E+07	1.18E+05	0
37	2.14E+07	1.62E+05	0
38	1.47E+07	3.07E+05	0
39	2.91E+06	5.37E+05	0
40	-2.13E+06	5.48E+05	0.
41	1.63E+07	9.00E+05	1.87E+01
42	1.20E+07	1.08E+06	-2.03E+01
43	1.09E+07	1.40E+06	0
44	9.25E+06	1.68E+06	0
45	1.28E+07	3.51E+06	0
46	2.21E+07	1.02E+07	9.77E+01
47	2.16E+07	2.05E+07	1.21E+02
48	1.87E+07	2.59E+07	1.37E+02
49	1.18E+07	7.95E+06	9.24E+02
50	8.23E+06	4.93E+05	1.22E+04
51	5.71E+06	3.75E+04	1.18E+05
52	3.81E+06	1.39E+04	6.46E+05
53	2.73E+06	5.66E+03	2.14E+06
54	1.93E+06	2.85E+03	4.20E+06
55	1.36E+06	1.75E+03	4.61E+06
56	1.04E+06	1.48E+03	2.72E+06
57	8.22E+05	1.13E+03	7.70E+05
58	6.00E+05	6.37E+02	1.15E+05
59	4.71E+05	4.88E+02	1.63E+04
60	4.06E+05	4.28E+02	4.94E+03
Initial	7.41E+11	8.42E+07	1.47E+07

Table K.7 – Summary of the normalised elemental recovery data for the separation of 1 μg terbium from 100 mg gadolinium and 1 μg dysprosium. Calculated using equation 2.4.

Fraction Number	*Gd (%)*	*Tb (%)*	*Dy (%)*
1	0.00	0.00	0.00
2	0.00	0.00	0.00
3	0.00	0.00	0.00
4	0.00	0.00	0.14
5	0.00	-0.02	0.00
6	1.17	0.12	0.00
7	18.24	3.11	0.00
8	3.30	0.43	0.00
9	1.49	0.33	0.00
10	1.45	0.28	0.00
11	1.58	0.28	0.00
12	1.54	0.18	0.13
13	2.26	0.27	0.00
14	2.37	0.11	0.00
15	2.18	0.28	0.00
16	2.54	0.26	0.00
17	2.52	0.42	0.27
18	2.34	0.14	0.00
19	2.24	0.18	0.00
20	2.05	0.30	0.00
21	2.31	0.38	0.00
22	2.17	0.11	0.00
23	1.85	0.34	-0.13
24	1.75	0.40	-0.13
25	1.84	0.16	0.00
26	3.85	0.40	0.00
27	6.06	0.84	0.13
28	6.65	0.79	0.00
29	6.69	1.12	0.25
30	6.79	0.96	0.00
31	6.96	1.06	0.00
32	4.45	0.58	0.00
33	1.07	0.21	0.00
34	0.23	0.11	0.00
35	0.04	0.04	0.00
36	0.01	0.13	0.00
37	0.00	0.18	0.00
38	0.00	0.35	0.00
39	0.00	0.61	0.00
40	0.00	0.62	0.00
41	0.00	1.02	0.00
42	0.00	1.23	0.00
43	0.00	1.59	0.00
44	0.00	1.91	0.00
45	0.00	3.99	0.00

46	0.00	11.67	0.00
47	0.00	23.35	0.00
48	0.00	29.46	0.00
49	0.00	9.05	0.01
50	0.00	0.56	0.08
51	0.00	0.04	0.77
52	0.00	0.02	4.18
53	0.00	0.01	13.84
54	0.00	0.00	27.18
55	0.00	0.00	29.83
56	0.00	0.00	17.59
57	0.00	0.00	4.98
58	0.00	0.00	0.75
59	0.00	0.00	0.11
60	0.00	0.00	0.03

Appendix L – Data to accompany Table 5.8

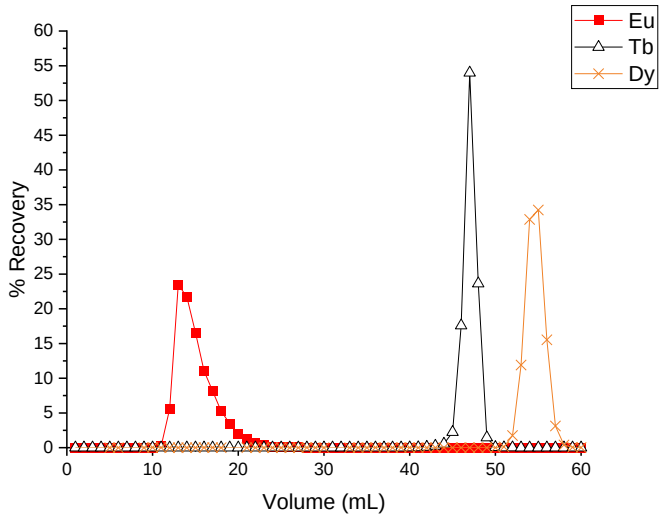

*Figure L.1 - Elution profile illustrating the separation of bulk quantities of europium (**10 mg** Eu_2O_3) from trace quantities of terbium and dysprosium (1 µg) on an LN resin column (50-100 µm particle size, 7×200 mm column dimensions)*

Table L.1 – Summary of the internal standard, blank and dilution corrected ICP-MS data for the separation of 1 µg terbium from 10 mg europium and 1 µg dysprosium.

Fraction Number	*Eu (CPS)*	*Tb (CPS)*	*Dy (CPS)*
1	-5.52E+04	0	-2.00E+03
2	3.06E+04	4.23E+03	-2.00E+03
3	3.04E+04	4.13E+03	-2.04E+03
4	-1.05E+05	0	-2.04E+03
5	-1.79E+05	-2.12E+03	0
6	-1.70E+05	-2.12E+03	0
7	-7.86E+04	1.93E+03	-4.41E+03
8	-2.05E+04	4.03E+03	-4.39E+03
9	6.49E+04	-2.10E+03	0
10	1.01E+07	-2.10E+03	6.21E+03
11	3.18E+08	4.17E+03	2.09E+03
12	8.78E+09	0	0
13	3.67E+10	0	0
14	3.40E+10	6.07E+03	0
15	2.59E+10	0	0
16	1.73E+10	0	4.00E+03
17	1.28E+10	-2.01E+03	2.05E+03
18	8.22E+09	-2.01E+03	0
19	5.44E+09	-4.12E+03	-2.06E+03
20	3.02E+09	-4.12E+03	-2.06E+03
21	1.86E+09	4.29E+03	0

22	9.56E+08	0	0
23	5.27E+08	-2.00E+03	0
24	2.65E+08	-3.88E+01	0
25	1.52E+08	2.00E+03	0
26	1.01E+08	0	0
27	4.52E+07	0	0
28	2.23E+07	0	4.07E+03
29	1.03E+07	0	0
30	5.33E+06	0	0
31	4.15E+06	0	-1.91E+03
32	3.09E+06	2.05E+03	-3.95E+03
33	2.14E+06	2.46E+01	0
34	1.82E+06	6.40E+01	0
35	1.34E+06	3.98E+03	0
36	9.25E+05	2.08E+03	2.08E+03
37	9.31E+05	0	0
38	7.49E+05	0	0
39	1.45E+06	4.07E+03	2.03E+03
40	6.05E+05	1.23E+04	4.11E+03
41	6.25E+05	3.53E+04	0
42	5.51E+05	9.63E+04	6.00E+01
43	4.84E+05	2.21E+05	2.01E+01
44	4.42E+05	4.78E+05	4.04E+01
45	6.06E+05	1.97E+06	2.01E+01
46	9.99E+05	1.55E+07	2.05E+01
47	1.21E+06	4.76E+07	2.23E+01
48	9.92E+05	2.08E+07	4.21E-01
49	6.96E+05	1.29E+06	1.56E+02
50	4.72E+05	5.93E+04	7.28E+02
51	3.58E+05	1.68E+04	2.46E+04
52	2.56E+05	8.63E+03	3.49E+05
53	1.88E+05	4.77E+03	2.37E+06
54	1.43E+05	2.33E+03	6.55E+06
55	1.05E+05	1.74E+03	6.82E+06
56	8.35E+04	1.09E+03	3.10E+06
57	6.95E+04	7.00E+02	6.21E+05
58	5.43E+04	5.15E+02	7.74E+04
59	6.21E+04	5.58E+02	1.15E+04
60	8.31E+04	2.05E+02	4.58E+03
Initial	1.74E+11	8.59E+07	2.07E+07

Table L.2 – Summary of the normalised elemental recovery data for the separation of 1 μg terbium from 10 mg europium and 1 μg dysprosium. Calculated using equation 2.4.

Fraction Number	*Eu (%)*	*Tb (%)*	*Dy (%)*
1	0.00	0.00	-0.01
2	0.00	0.00	-0.01
3	0.00	0.00	-0.01
4	0.00	0.00	-0.01
5	0.00	0.00	0.00
6	0.00	0.00	0.00
7	0.00	0.00	-0.02
8	0.00	0.00	-0.02
9	0.00	0.00	0.00
10	0.01	0.00	0.03
11	0.20	0.00	0.01
12	5.61	0.00	0.00
13	23.44	0.00	0.00
14	21.75	0.01	0.00
15	16.58	0.00	0.00
16	11.05	0.00	0.02
17	8.17	0.00	0.01
18	5.25	0.00	0.00
19	3.47	0.00	-0.01
20	1.93	0.00	-0.01
21	1.19	0.00	0.00
22	0.61	0.00	0.00
23	0.34	0.00	0.00
24	0.17	0.00	0.00
25	0.10	0.00	0.00
26	0.06	0.00	0.00
27	0.03	0.00	0.00
28	0.01	0.00	0.02
29	0.01	0.00	0.00
30	0.00	0.00	0.00
31	0.00	0.00	-0.01
32	0.00	0.00	-0.02
33	0.00	0.00	0.00
34	0.00	0.00	0.00
35	0.00	0.00	0.00
36	0.00	0.00	0.01
37	0.00	0.00	0.00
38	0.00	0.00	0.00
39	0.00	0.00	0.01
40	0.00	0.01	0.02
41	0.00	0.04	0.00
42	0.00	0.11	0.00
43	0.00	0.25	0.00
44	0.00	0.54	0.00
45	0.00	2.24	0.00

46	0.00	17.60	0.00
47	0.00	53.98	0.00
48	0.00	23.63	0.00
49	0.00	1.46	0.00
50	0.00	0.07	0.00
51	0.00	0.02	0.12
52	0.00	0.01	1.75
53	0.00	0.01	11.90
54	0.00	0.00	32.86
55	0.00	0.00	34.23
56	0.00	0.00	15.54
57	0.00	0.00	3.12
58	0.00	0.00	0.39
59	0.00	0.00	0.06
60	0.00	0.00	0.02

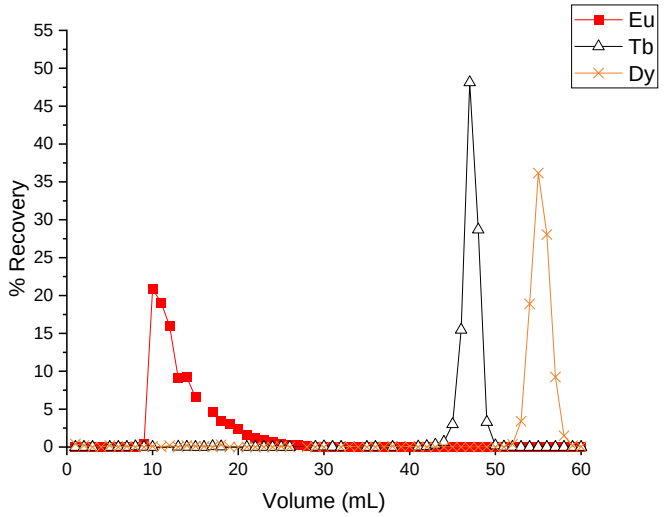

Figure L.2 - Elution profile illustrating the separation of bulk quantities of europium (50 mg Eu_2O_3) from trace quantities of terbium (1 μg) on an LN resin column (50-100 μm particle size, 7×200 mm column dimensions)

Table L.3 – Summary of the internal standard, blank and dilution corrected ICP-MS data for the separation of 1 μg terbium from 50 mg europium and 1 μg dysprosium.

Fraction Number	*Eu (CPS)*	*Tb (CPS)*	*Dy (CPS)*
1	-3.18E+06	0	8.38E+04
2	-3.19E+06	0	4.32E+04
3	-3.04E+06	4.84E+02	0
4	-2.90E+06	-2.11E+04	0
5	-3.22E+06	0	4.19E+04
6	-3.28E+06	0	0
7	-2.77E+06	0	2.02E+04
8	1.46E+06	6.31E+04	0
9	2.74E+09	2.08E+04	0
10	1.49E+11	0	2.07E+04
11	1.36E+11	-4.23E+04	0
12	1.14E+11	-4.23E+04	4.11E+04
13	6.48E+10	2.11E+04	0
14	6.55E+10	2.08E+04	4.16E+04
15	4.70E+10	0	2.09E+04
16	-3.33E+06	0	2.04E+04
17	3.26E+10	8.02E+04	0
18	2.42E+10	6.07E+04	6.07E+04
19	2.18E+10	-1.98E+04	0
20	1.70E+10	-4.03E+04	0
21	1.10E+10	0	0
22	8.37E+09	0	0
23	6.38E+09	0	0
24	4.43E+09	0	0
25	2.88E+09	0	2.07E+04

26	2.23E+09	0	0
27	1.57E+09	-2.08E+04	-2.08E+04
28	9.86E+08	-2.08E+04	5.21E+01
29	4.66E+08	2.08E+04	0
30	2.28E+08	6.02E+04	0
31	9.24E+07	2.07E+04	-2.08E+04
32	4.91E+07	0	-2.53E+02
33	3.45E+07	-2.07E+04	2.04E+04
34	2.44E+07	-2.07E+04	0
35	1.59E+07	0	0
36	1.23E+07	0	0
37	8.87E+06	-4.16E+04	0
38	6.94E+06	-6.30E+01	2.08E+04
39	4.56E+06	-2.06E+04	0
40	3.99E+06	-4.09E+04	2.00E+04
41	4.82E+06	4.01E+04	-2.04E+01
42	3.92E+06	9.94E+04	-6.12E+01
43	3.31E+06	2.58E+05	0
44	2.85E+06	5.96E+05	0
45	3.90E+06	2.68E+06	2.06E+01
46	5.16E+06	1.38E+07	0
47	6.17E+06	4.30E+07	-2.17E+00
48	5.15E+06	2.57E+07	-1.77E+00
49	3.76E+06	2.95E+06	1.93E+01
50	2.99E+06	1.83E+05	-2.11E+01
51	2.16E+06	2.56E+04	2.22E+03
52	1.71E+06	1.24E+04	7.44E+04
53	1.07E+06	6.58E+03	7.01E+05
54	1.07E+06	3.38E+03	3.88E+06
55	6.39E+05	2.32E+03	7.43E+06
56	5.15E+05	1.50E+03	5.76E+06
57	4.00E+05	8.87E+02	1.90E+06
58	3.18E+05	2.73E+02	3.08E+05
59	2.58E+05	5.93E+02	3.85E+04
60	2.14E+05	2.21E+02	8.49E+03
Initial	8.12E+11	8.00E+07	1.96E+07

Table L.4 – Summary of the normalised elemental recovery data for the separation of 1 μg terbium from 50 mg europium and 1 μg dysprosium. Calculated using equation 2.4.

Fraction Number	*Eu (%)*	*Tb (%)*	*Dy (%)*
1	0.00	0.00	0.41
2	0.00	0.00	0.21
3	0.00	0.00	0.00
4	0.00	-0.02	0.00
5	0.00	0.00	0.20
6	0.00	0.00	0.00
7	0.00	0.00	0.10
8	0.00	0.07	0.00
9	0.39	0.02	0.00
10	20.84	0.00	0.10
11	19.08	-0.05	0.00
12	15.94	-0.05	0.20
13	9.10	0.02	0.00
14	9.20	0.02	0.20
15	6.59	0.00	0.10
16	-	0.00	0.10
17	4.58	0.09	0.00
18	3.40	0.07	0.30
19	3.06	-0.02	0.00
20	2.39	-0.05	0.00
21	1.54	0.00	0.00
22	1.17	0.00	0.00
23	0.89	0.00	0.00
24	0.62	0.00	0.00
25	0.40	0.00	0.10
26	0.31	0.00	0.00
27	0.22	-0.02	-0.10
28	0.14	-0.02	0.00
29	0.07	0.02	0.00
30	0.03	0.07	0.00
31	0.01	0.02	-0.10
32	0.01	0.00	0.00
33	0.00	-0.02	0.10
34	0.00	-0.02	0.00
35	0.00	0.00	0.00
36	0.00	0.00	0.00
37	0.00	-0.05	0.00
38	0.00	0.00	0.10
39	0.00	-0.02	0.00
40	0.00	-0.05	0.10
41	0.00	0.04	0.00
42	0.00	0.11	0.00
43	0.00	0.29	0.00
44	0.00	0.67	0.00
45	0.00	3.00	0.00

46	0.00	15.48	0.00
47	0.00	48.13	0.00
48	0.00	28.70	0.00
49	0.00	3.30	0.00
50	0.00	0.20	0.00
51	0.00	0.03	0.01
52	0.00	0.01	0.36
53	0.00	0.01	3.41
54	0.00	0.00	18.89
55	0.00	0.00	36.17
56	0.00	0.00	28.06
57	0.00	0.00	9.24
58	0.00	0.00	1.50
59	0.00	0.00	0.19
60	0.00	0.00	0.04

Appendix M – ICP-QQQ-MS measurement interference at m/z 175 caused by high gadolinium concentration

Table M.1 – The internal standard, blank and dilution corrected CPS values present in the main gadolinium fractions (fractions 11-30) where no terbium was expected. The percentage contamination in the m/z 175 signal was calculated to comment on the impact of gadolinium polyatomic species and tailing on terbium measurement. Repeats 1-3 were taken from the experimental data from the separation of 1 μg terbium from 10 mg gadolinium and 1 μg dysprosium

In fractions 11-30	*Repeat 1*	*Repeat 2*	*Repeat 3*
CPS at m/z 173	1.10E+11	1.06E+11	1.27E+11
CPS at m/z 175	1.65E+06	1.28E+06	1.44E+06
Proportion of m/z 173 signal at m/z 175	0.00150%	0.00121%	0.00114%

Table M.2 – The internal standard, blank and dilution corrected CPS values present in the main gadolinium fractions (fractions 11-30) where no terbium was expected. Repeat 4 was taken from the experimental data from the separation of 1 μg terbium from 50 mg gadolinium and 1 μg dysprosium. Repeat 5 was taken from the experimental data from the separation of 1 μg terbium from 100 mg gadolinium and 1 μg dysprosium.

In fractions 11-30	*Repeat 4*	*Repeat 5*	***Mean (n=5)***
CPS at m/z 173	3.20E+11	4.27E+11	**2.18E+11**
CPS at m/z 175	5.02E+06	6.95E+06	**3.27E+06**
Proportion of m/z 173 signal at m/z 175	0.00157%	0.00163%	**0.00141%**

Appendix N – Webster et.al. (2018)

B. Webster, P. Ivanov, S. Collins, B. Russell, A. Robinson, D. Read, Purification of Tb-155 produced at CERN-MEDICS for applications in nuclear medicine. In: Annual Congress of the European Association of Nuclear Medicine, 13-17 October 2018, Dusseldorf, Germany, *EJNMMI*, 2018, **45**, 1-844

OP-692

Purification of ^{155}Tb produced at CERN-MEDICIS for applications in nuclear medicine

B. Webster[1,2], P. Ivanov[2], S. Collins[2], B. Russell[3], A. Robinson[2,3,4], D. Read[1,2]; [1]University of Surrey, Guildford, UNITED KINGDOM, [2]National Physical Laboratory, Teddington, UNITED KINGDOM, [3]The Christie NHS Foundation Trust, Manchester, UNITED KINGDOM, [4]University of Manchester, Manchester, UNITED KINGDOM.

Introduction: A quartet of terbium isotopes (^{149}Tb, ^{152}Tb, ^{155}Tb and ^{161}Tb) has been identified as promising isotopes for use in therapeutic, diagnostic or theranostic nuclear medicine. Terbium-161 can be produced by neutron irradiation of a ^{160}Gd target followed by its subsequent beta decay[1]. The other terbium isotopes are mainly produced at the CERN-MEDICIS facility by proton-induced spallation of a tantalum target followed by the mass-separation and isolation of desired radionuclides[2-4]. Gamma-emitting polyatomic impurities, such as ^{139}Ce^{16}O in a ^{155}Tb sample, are produced but not separated in this process which emphasises the need for further radiochemical separation before their application in nuclear medicine. The aim of this study was to develop a rapid and effective separation scheme that is capable of successfully isolating the desired terbium from the cerium impurities. **Methods:** Separation of terbium from cerium impurities has been studied using stable element standards in nitric acid on various ion-exchange (AG1, Bio-Rad) and extraction chromatography resins (UTEVA, TK100 and TEVA, Triskem International). The effect of cerium oxidation with sodium bromate has been studied to encourage selective adsorption of the tetravalent Ce(IV) impurity over the desired Tb(III) product. The rate of adsorption to the resin and the rate of cerium oxidation have also been studied in order to find the optimum conditions for rapid separation. Inductively coupled plasma mass spectrometry (ICP-MS) and HPGe gamma-spectrometry have been used to quantify the quality of the separations achieved. **Results and Conclusions:** The process has been optimised to provide a rapid radiochemical separation to afford a high radiochemical yield. All resins performed best at high nitric acid concentrations and separation was dependent on the selective oxidation of cerium from Ce(III) to Ce(IV). Separation using a mixed resin bed (AG1, UTEVA and TEVA) successfully removed a 31% cerium-139 impurity with an excellent terbium-155 recovery (>90%). This method allows for radiologically pure ^{155}Tb solutions to be prepared which are suitable for pre-clinical applications, SPECT phantom studies and primary standardisation. **References:** 1. S. Lehenberger et al., ***Nucl. Med. Biol.***, 2011, **38**, 917-924. 2. C. Müller et al., ***Nucl. Med. Biol.***, 2014, **41**, e58-e65. 3. C. Müller et al., ***J. Nucl. Med.***, 2012, **53**, 1951-1959. 4. B.J. Allen et al., ***Appl. Radiat. Isot.***, 2001, **54**, 53-58.

Appendix O – Webster *et al.* (2019)

B. Webster, P. Ivanov, B. Russell, S. Collins, T. Stora, J. P. Ramos, U. Köster, A. P. Robinson and D. Read, Chemical Purification of Terbium-155 from Pseudo-Isobaric Impurities in a Mass Separated Source Produced at CERN, *Sci. Rep.*, 2019, **9**, 10884[86]

SCIENTIFIC REPORTS

OPEN

Chemical Purification of Terbium-155 from Pseudo-Isobaric Impurities in a Mass Separated Source Produced at CERN

Received: 24 April 2019
Accepted: 11 July 2019
Published online: 26 July 2019

Ben Webster[1,2], Peter Ivanov[1], Ben Russell[1], Sean Collins[1], Thierry Stora[3], Joao Pedro Ramos[3,4], Ulli Köster[5], Andrew Paul Robinson[1,6,7] & David Read[1,2]

Four terbium radioisotopes ($^{149, 152, 155, 161}$Tb) constitute a potential theranostic quartet for cancer treatment but require any derived radiopharmaceutical to be essentially free of impurities. Terbium-155 prepared by proton irradiation and on-line mass separation at the CERN-ISOLDE and CERN-MEDICIS facilities contains radioactive ^{139}Ce^{16}O and also zinc or gold, depending on the catcher foil used. A method using ion-exchange and extraction chromatography resins in two column separation steps has been developed to isolate ^{155}Tb with a chemical yield of ≥95% and radionuclidic purity ≥99.9%. Conversion of terbium into a form suitable for chelation to targeting molecules in diagnostic nuclear medicine is presented. The resulting ^{155}Tb preparations are suitable for the determination of absolute activity, SPECT phantom imaging studies and pre-clinical trials.

Four terbium isotopes (^{149,152,155,161}Tb) have been identified as having suitable physical properties (i.e. half-life ($T_{1/2}$); emission type and quantity of emitted radiation) for use in cancer treatment and diagnosis. (Table 1)[1–3]. Initial pre-clinical trials[1] have highlighted all four isotopes as being theranostic candidates using a folate-receptor derivative, cm09. Terbium isotopes form stable complexes with DOTA-containing targeting agents which show favourable *in-vivo* stability, emphasising their suitability for clinical use[1,4,5]. Terbium-155 ($T_{1/2}$ = 5.32 d[3]) offers promise as an imaging tracer in single photon emission computed tomography (SPECT), with initial pre-clinical studies indicating excellent image quality even at low doses[4]. The administration of ^{155}Tb alongside a therapeutic terbium isotope would give a theranostic pair with identical chemical properties; this is particularly advantageous as it facilitates the application of personalised medicine.

Terbium-161 can be generated via neutron activation of a ^{160}Gd target and subsequent decay of the ^{161}Gd product to give the desired ^{161}Tb (^{160}Gd(n,γ)^{161}Gd (β^-) ^{161}Tb)[5]. The other isotopes (^{149,152,155}Tb) have been produced mainly via a proton-induced spallation reaction on a tantalum target combined with on-line mass separation at the CERN-ISOLDE facility[6–8]. A high percentage of the 1.4 GeV protons delivered by the proton synchrotron booster do not interact with the ISOLDE targets and therefore, the CERN-MEDICIS facility was established to produce isotopes for medical applications by inducing spallation reactions in a secondary target. At CERN-MEDICIS, off-line mass separation is applied to isolate isotopes of the same A/q value[6,7]. Terbium-155 sources used in this study were collected after mass-separation by implantation of the ion beam (155 A/q) into zinc-coated gold foils. Further chemical separation is still required as mass separation is unable to differentiate between isobaric and pseudo-isobaric species. Removal of the foil matrix is also required.

Alternative methods of producing these isotopes have been investigated (Table 2)[8–15]. However, full-scale production at a radionuclide purity sufficient for clinical studies has not yet been demonstrated.

All lanthanides, especially neighbouring elements, have similar chemical properties due to small differences in their ionic size/charge ratio, making the isolation of high purity individual lanthanide solutions challenging[16].

[1]National Physical Laboratory, Teddington, TW11 0LW, UK. [2]Department of Chemistry, University of Surrey, Guildford, GU2 7XH, UK. [3]CERN - European Organization for Nuclear Research, Esplanade des Particules 1, 1217, Meyrin, Switzerland. [4]KU Leuven, Institute for Nuclear and Radiation Physics, Celestijnenlaan 200D, 3001, Heverlee, Belgium. [5]Institut Laue-Langevin, 38042, Grenoble, France. [6]Christie Medical Physics and Engineering (CMPE), The Christie NHS Foundation Trust, Manchester, M20 4BX, UK. [7]University of Manchester, Manchester, M13 9PL, UK. Correspondence and requests for materials should be addressed to P.I. (email: peter.ivanov@npl.co.uk)

Isotope	$T_{1/2}$	Decay mode (branching ratio)	Energy of particle radiation	Energy of main γ and X-ray emissions (keV)	Application			
					α therapy	PET	SPECT	β/auger therapy
^{149}Tb	4.12 h	α (16.7%) β^+ (7.1%)	E_α = 3.967 MeV $E_{\beta^+ max}$ = 730 keV	352 (29%) 165 (26%)	x	x		
^{152}Tb	17.5 h	β^+ (17%)	$E_{\beta^+ max}$ = 1.080 MeV	344 (64%)		x		
^{155}Tb	5.32 d	EC (100%)	—	43 (86%) 49 (20%) 87 (32%) 105 (25%)			x	
^{161}Tb	6.89 d	β (100%)	$E_{\beta max}$ = 154 keV	26 (23%) 45–46 (18%) 49 (17%) 75 (10%)			x	x

Table 1. Physical properties of four terbium isotopes and their applications in nuclear medicine[1,2]. EC – electron capture; PET – positron emission tomography; SPECT – single photon emission computed tomography.

Isotope	Nuclear reactions	Production facility	Incident particle energy	References
^{149}Tb	Ta(p,sp)^{149}Tb	Synchrotron	1.4 GeV (CERN)	Allen *et al.*[8]
	^{151}Eu(^{3}He, 5n)^{149}Tb	Cyclotron	40–70 MeV	Zagryadskii *et al.*[14]
^{152}Tb	Ta(p,sp)^{152}Tb	Synchrotron	1.4 GeV (CERN)	Allen *et al.*[8]
	^{nat}Gd(p,4n)^{152}Tb	Cyclotron	39 MeV	Steyn *et al.*[9]
^{155}Tb	Ta(p,sp)^{155}Tb	Synchrotron	1.4 GeV (CERN)	Allen *et al.*[8]
	^{nat}Gd(p,n)^{155}Tb	Cyclotron	11 MeV	Vermeulen *et al.*[13]
	^{155}Eu(α,n)^{155}Tb	Cyclotron	28 MeV	Kazakov *et al.*[12]
^{161}Tb	^{160}Gd(n,γ)^{161}Gd -> ^{161}Tb	Nuclear reactor	(flux = 8×10^{14} neutrons cm^{-2} s^{-1})	Lehenberger *et al.*[3]

Table 2. Established and alternative production methods for the four terbium isotopes.

They exist predominately in the III+ oxidation state under aqueous conditions. The exceptions are europium, which can be selectively reduced to Eu(II) under strongly reducing conditions, and cerium, which can be easily oxidised to Ce(IV). Changes in oxidation state markedly influence chromatographic behaviour and this can be exploited when developing separation methods.

A well-known method of separating lanthanide elements utilises cation-exchange chromatography with α-hydroxyisobutyric acid (α-HIBA) eluent and provides good separation even from neighbouring elements[1,5,8]. However, the process is slow and requires precise control of chemical conditions (pH and α-HIBA concentration) to give optimal yield and purity. Attempts to accelerate separation tend to compromise terbium recovery.

A significant ^{139}Ce ($T_{1/2}$ = 137.6 d[17]) impurity exists in ^{155}Tb sources from CERN-ISOLDE and CERN-MEDICIS owing to formation of the pseudo-isobaric species, ^{139}Ce^{16}O, which cannot be removed by mass separation. Given its half-life, it constitutes an increasing proportion of overall source activity during transport and storage. In this study, we present a simple method for producing radiologically pure terbium preparations in a chemical form suitable for chelation to targeting molecules as well as for absolute activity measurements and phantom imaging studies. Our aim was to develop a robust, efficient and rapid method capable of isolating terbium from the foil matrix as well as from ^{139}Ce by selective oxidation. Therefore, ion-exchange and extraction chromatography resins were chosen based on their selectivity for tetravalent over trivalent species.

Results

Chemical separation. *Batch separation.* In the presence of an oxidant (sodium bromate, $NaBrO_3$) and in HNO_3 solutions commercial UTEVA, TEVA and TK100 extraction resins (*Triskem International*) and AG1 anion exchange resin (*BioRad*) all showed pronounced cerium adsorption selectivity over terbium (Fig. 1). The results imply oxidation of cerium to Ce(IV) was achieved, with terbium remaining in the trivalent state (Tb(III)).

High Ce adsorption (K_d = 100–1,000) was observed at high HNO_3 concentrations (8–10 M) on all four resins, whilst terbium adsorption remained minimal (K_d = 0.1–10) across the concentration range (Fig. 2). The best separation resolutions (Equation (2), SR > 100) were obtained using TEVA and UTEVA resins at high HNO_3 concentrations; further studies were conducted on these resins using pre-packed cartridges.

Kinetic studies. UTEVA extraction chromatography resin was chosen to demonstrate kinetic behaviour with the rate of cerium adsorption studied in 10 M HNO_3/0.1 M $NaBrO_3$ solutions; rapid adsorption (<60 s) was observed (Fig. 3a). The rate of cerium oxidation was also studied in 10 M HNO_3/0.1 M $NaBrO_3$ solutions. Solutions were filtered under vacuum after a minimum of 60 s in contact with the resin. Rapid oxidation (<90 s) of cerium was observed (Fig. 3b).

Neither the rate of adsorption nor the rate of oxidation were limiting factors in the separation, suggesting that rapid column separation is achievable under these conditions.

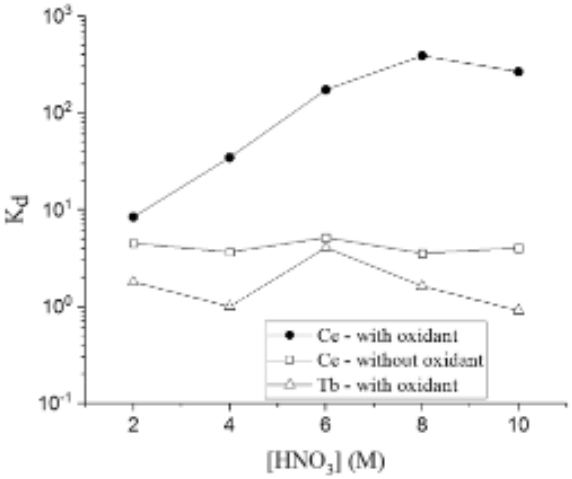

Figure 1. Distribution coefficients (K_d) for Ce(IV), Ce(III) and Tb(III) in HNO_3 solutions on UTEVA extraction chromatography resin. (N = 3).

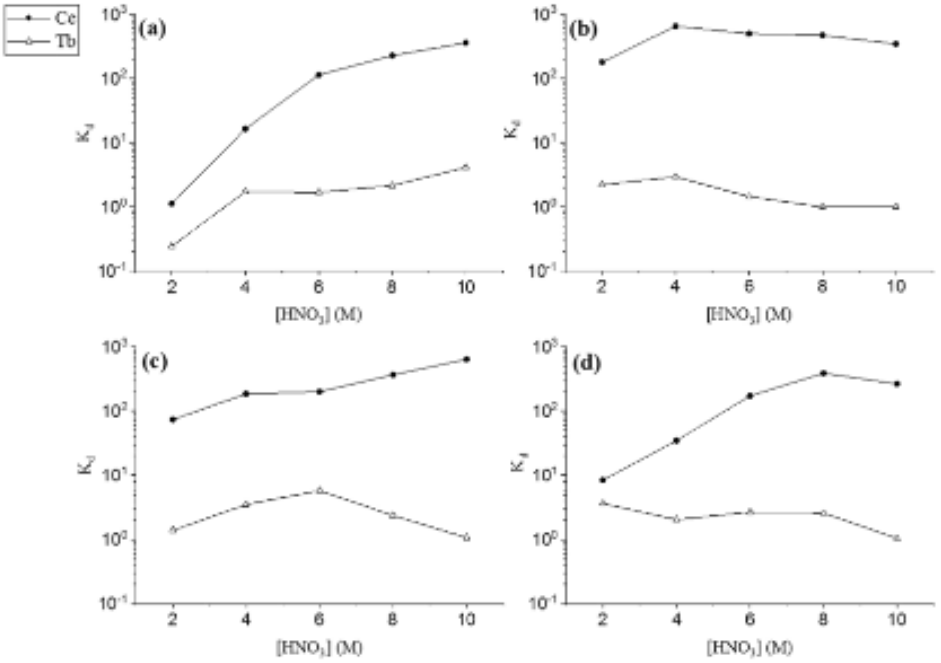

Figure 2. Distribution coefficients (K_d) of Ce(IV) and Tb(III) in HNO_3 solutions on (**a**) AG1 ion exchange resin, (**b**) TEVA resin, (**c**) TK100 resin, (**d**) UTEVA resin. (N = 3).

Column studies. Column-based separation using a commercially available pre-packed UTEVA cartridge (2 mL) provided effective isolation of terbium from cerium impurities. The elution profile (Fig. 4) shows that terbium (>99%) was removed in the load solution (10 mL, 8 M HNO_3) and the subsequent wash solution (10 mL, 8 M HNO_3) with minimal cerium impurities remaining (<0.002%). Cerium was successfully recovered by elution from the cartridge in hydrochloric solution (<10 mL, 0.1 M). The column-based separation was repeated using a pre-packed TEVA cartridge (2 mL); however, the separation achieved was less successful as ~0.1% Ce was detected in the Tb fraction under similar conditions (Fig. 4).

These column studies allowed the development of a separation scheme for the removal of ^{155}Tb from both ^{139}Ce isotopic impurities and the zinc-plated gold catcher foil matrix (Fig. 5).

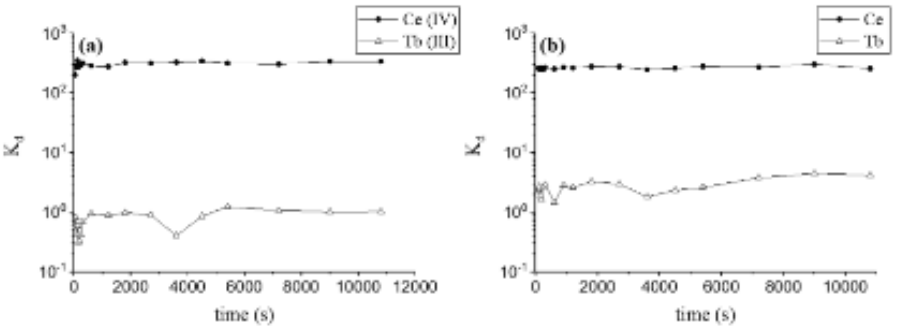

Figure 3. Kinetics of (**a**) the adsorption of Ce(IV) and Tb(III) onto UTEVA resin, and (**b**) the oxidation of cerium using sodium bromate. Measured as the distribution coefficient (K_d) as a function of time.

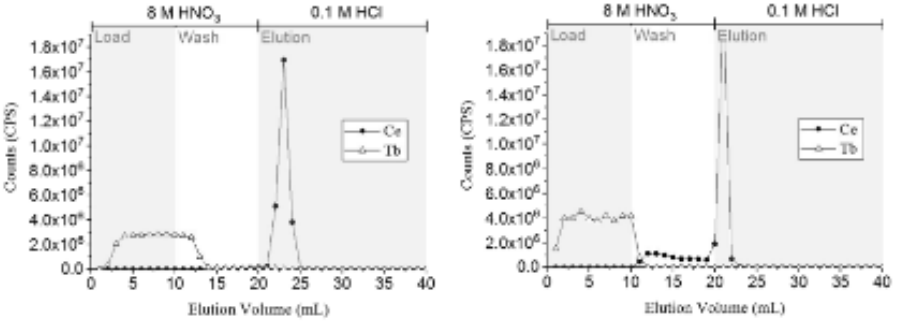

Figure 4. Elution profiles (N = 3) for Tb and Ce from a pre-conditioned 2 mL UTEVA cartridge (left) and a pre-conditioned 2 mL TEVA cartridge (right). Approximate flow rate = 0.3 mL/min.

Validation with active ^{155}Tb. The method has been validated on three sources (nominal ^{155}Tb activity Bq – MBq) over a two year period. A mass separated source received from CERN-ISOLDE in 2017 (EOB - 07/09/2017 18:42:00) contained a significant ^{139}Ce impurity ($A_0(^{139}Ce)/A_0(^{155}Tb) = 0.30 \pm 0.02$), Table 3). The scheme detailed in Fig. 5 removed ^{139}Ce to the level of the Compton continuum background ($D_{1,0}(^{139}Ce)/A_0(^{155}Tb) = 0.00021$). Total terbium fraction recovery, $R_{0,1}(^{155}Tb)/R_{0,2}(^{155}Tb)$, was 0.973+/− 0.038 with a radiochemical purity of 99.98% (Table 3). This was consistent for all validation experiments.

Discussion

In many cases, it is essential that suitable radiochemical methods are available to provide radionuclides in sufficient quantities with relatively high specific activity, radionuclidic and chemical purity to facilitate accurate pre-clinical and clinical study. The method described is able to produce high radiological purity ^{155}Tb sources, suitable for absolute activity, nuclear data and ionisation chamber measurements. The sources are also suitable for bioconjugation, molecular chelation and SPECT imaging studies. Although the ^{139}Ce impurity discussed here does not possess significant biological toxicity[18], it is radioactive and, if not removed, would result in an unnecessary additional dose to the patient.

Currently, proton-induced spallation is the main route for producing ^{155}Tb at CERN for (pre)-clinical studies. The chemical purification method proposed here (Fig. 5) allows the quantitative separation of ^{155}Tb from a zinc and/or gold matrix and from ^{139}Ce impurities produced by spallation at the CERN-ISOLDE and CERN-MEDICIS facilities. The method is rapid, simple and can also be used to recover a high purity ^{139}Ce source; a useful standard in gamma spectrometry ($E_\gamma = 165.86$ keV, 79.90%)[17].

The method has not yet been validated for the removal of other stable (e.g. $^{139}La^{16}O^+$, $^{155}Gd^+$) or longer-lived, radioactive (e.g. $^{155}Eu^+$) isobaric impurities; as with $^{139}Ce^{16}O$, they would not be removed by mass separation. Such impurities might not pose a significant toxicological risk if they were to enter the body[19,20] but nevertheless, would form stable complexes with DOTA ($\log K > 22$)[21] and DOTA-containing targeting molecules[4] and could compete with the target terbium isotope(s), reducing their efficacy.

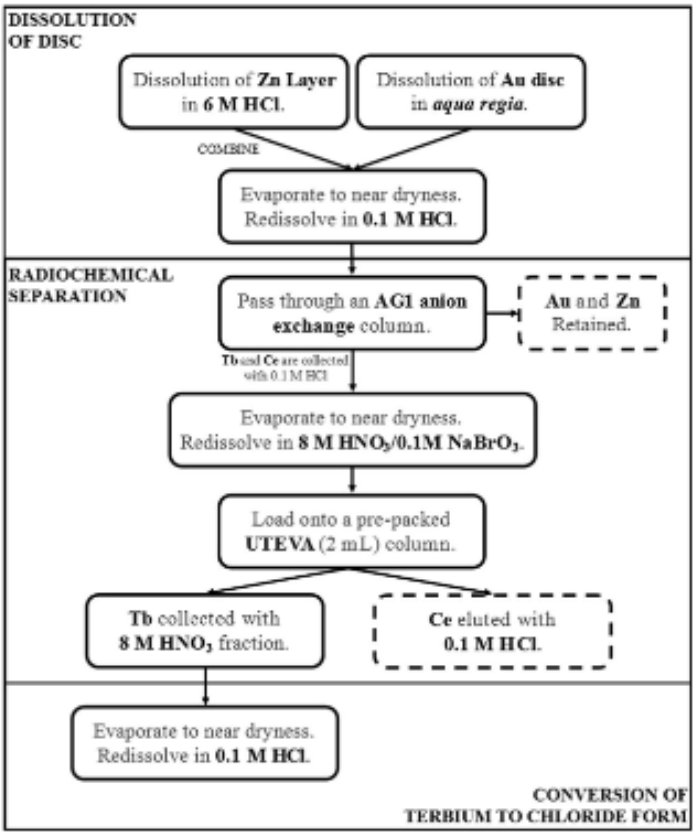

Figure 5. Final ^{155}Tb separation scheme for CERN-ISOLDE and CERN-MEDICIS sources with an additional ^{139}Ce recovery step.

Isotope	$T_{1/2}$	Activity of material supplied (MBq)	Activity following separation
^{139}Ce	136.7 d	2.79 ± 0.068	<1.90 kBq
^{155}Tb	5.32 d	9.28 ± 0.63	9.03 ± 0.049 MBq

Table 3. Radioisotopic composition of a ^{155}Tb source received from CERN-ISOLDE before and after chemical separation (reference time 2017-09-29 12:00 UTC).

Materials and Methods

Chemicals. Standard element solutions at starting concentrations of 1000 ppm were purchased from Johnson Matthey and Fluka Analytical (Tb and Ce, respectively). Mixed standard solutions were prepared in HNO_3 (Trace Analysis Grade, Fisher Scientific) and diluted to the required concentration with ultrapure water (ELGA PURELAB Flex, Veolia Water, Marlow, UK, 18 MΩ cm, <5 ppb Total Organic Carbon). Anion exchange resin (Bio Rad AG1-X8, 100–200 mesh) and extraction chromatography resins (TEVA, TK100 and UTEVA, Triskem International 100–150 μm) were used throughout.

The ^{155}Tb source was provided by CERN-ISOLDE and CERN-MEDICIS in the form of a zinc-coated gold foil. HCl (Trace Analysis Grade, Fisher Scientific) and HNO_3 were used for foil dissolution and $NaBrO_3$ (Alfa Aesar) for cerium oxidation.

Inductively coupled plasma mass spectrometry (ICP-MS). Measurement of stable ^{140}Ce and ^{159}Tb was carried out using a tandem ICP-MS/MS (Agilent 8800) equipped with a collision-reaction cell positioned between two quadrupole mass filters. The instrument was run in Single Quad mode, with only the second mass filter operating. The instrument is fitted with a quartz double-pass spray chamber and a MicroMist nebuliser (Glass Expansion, Melbourne, Australia) and nickel sample and skimmer cones (Crawford Scientific, South Lanarkshire, UK). It was tuned daily using a mixed 1 ppb standard solution (Ce, Co, Li, Mg, Tl and Y in 2% v/v HNO_3). No

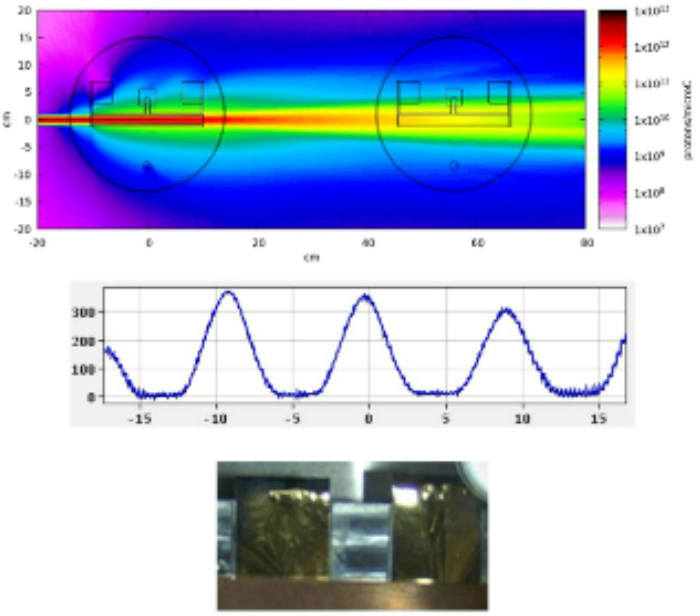

Figure 6. Top: Fluka simulation[25,26] showing the incoming proton beam on an ISOLDE target (3.5 g/cm^2 UC_x for the purpose of the simulation) and intercepting the MEDICIS target downstream. Middle: Screenshot taken with the beam scanner, located before the implantation chamber. Beams at A/q = 154,155,156 are seen (153, 157 partly visible). The collected beam is centred on A/q = 155, while isotopes present at other masses are physically removed from the implantation using mechanical slits located ahead of the foil. The horizontal scale is in mm. Bottom: Two zinc-coated gold foils in the collection chamber seen from the rear. The collection takes place on the foil located on the left.

additional terbium-specific tuning was carried out. A ^{209}Bi (10 ppb solution in 2% v/v HNO_3) internal standard was used to monitor and correct for instrumental drift during longer runs. Blank HNO_3 (2% v/v) solutions were monitored regularly to ensure no Ce or Tb cross-contamination during a run.

Gamma-ray spectrometry. An n-type HPGe γ-ray spectrometer with a resolution (FWHM) of 1.79 keV at 1.33 MeV and relative efficiency 28% was used to determine the ^{139}Ce/^{155}Tb activity ratio. The detection system set-up and full-energy peak efficiency calibration is described in detail by Collins *et al.*[22].

The nuclear data (half-lives and γ-ray emission intensities) used to determine the activities of ^{155}Tb and ^{139}Ce were taken from the evaluated database of ENSDF and the DDEP, respectively[3,17]. As ^{139}Ce could not be observed after the chemical separation, the activity ratio of the ^{139}Ce/^{155}Tb in the chemically separated solution was estimated from the detection limit of the detector for ^{139}Ce[23].

Irradiation conditions and mass separation. Terbium-155 sources used in this study were produced at the CERN-ISOLDE and CERN-MEDICIS facilities. Three ^{155}Tb sources were produced and provided to NPL for chemical separation between 2017 and 2018. The irradiation conducted at CERN-MEDICIS was as follows:

A high purity Ta metal target (*Ta647M*) made of 12 rolls of Ta foil (99.95% purity, 12 μm thick, 15 mm wide, 2 cm diameter) with a total mass of 357 g was arranged in a 20 cm long Ta tube coupled to a rhenium surface ion source. The target was irradiated with 1.4 GeV protons delivered by the Proton Synchrotron Booster accelerator (CERN, Geneva). The CERN-MEDICIS irradiation target is located in the High Resolution Separator (HRS) beam dump position at ISOLDE (Fig. 6), and receives a fraction of the scattered 1.8×10^{18} protons downstream from a primary HRS target (*623SiC*, ISOLDE physics program). The irradiation was scheduled within the MED004 approved experiment and took place from 27th September to 1st October 2018. The irradiated target was then moved to the CERN-MEDICIS isotope mass separator in order to release and extract ion species selected at mass-to-charge ratio of 155[6]. The separated ions were collected on a zinc-plated gold foil and removed on 3rd October. The following isotopes were implanted upon sample retrieval: ^{139}Ce (implanted as $^{139}Ce^{16}O^+$): 6.9 MBq; ^{155}Dy: 3.6 MBq; ^{155}Tb: 20 MBq. Upon reception at NPL, ^{155}Dy had decayed below the detection limit ($D_{L,0}$ (^{155}Dy) = 1.75 kBq).

Chemical separation. *Batch separation studies.* The adsorption of Tb and Ce onto ion exchange (AG1, BioRad) and extraction chromatography resins (TEVA, UTEVA and TK100, Triskem International) was studied over a range of HNO_3 solution concentrations (2–10 M). Nitric acid solutions (2 mL) containing a mixture of 100 ppb stable Ce and Tb were prepared. An aliquot was taken from each solution for ICP-MS measurement. The

remaining solution was added to 0.1 g of resin (UTEVA, TEVA, TK100 or AG1). Sodium bromate (0.1 M, 0.03 g) was added to identical samples to assess changes in adsorption to the resin as a result of selective oxidation of Ce. In all cases, the samples were shaken and left to equilibrate for 24 h. After equilibration, the solutions were filtered to isolate the aqueous phase (Whatman 41 ashless filter paper, 20–25 µm pore size). An aliquot was taken from each sample, diluted with 2% HNO_3 (2% v/v) and analysed by ICP-MS.

The adsorption of Tb and Ce onto each resin was quantified by calculating the distribution coefficient (K_d) using Eq. (1)[24].

$$k_d = \left(\frac{(CPS)_0 - (CPS)_t}{(CPS)_t}\right) \times \left(\frac{V}{m}\right) \quad (1)$$

Where $(CPS)_0$ and $(CPS)_t$ are the concentrations of analyte in the aqueous phase before and after equilibration, respectively, V is the volume of solution (mL) and m is the mass of resin used (g).

The separation achievable in the different HNO_3 solutions was quantified by calculating the separation factor using Eq. (2).

$$SF = \left(\frac{k_d(Tb)}{k_d(Ce)}\right) \quad (2)$$

Kinetic studies. In order to determine the rate at which Ce(IV) and Tb(III) are adsorbed onto UTEVA, a HNO_3 (10 M) solution containing 100 ppb Ce, 100 ppb Tb and sodium bromate (0.1 M) was left for 24 h to allow for the oxidation of Ce(III) to Ce(IV). Aliquots (2 mL) were added to vials containing UTEVA resin (0.1 g) and were left in static conditions before being filtered to isolate the aqueous phase at regular time intervals under vacuum (60 seconds–180 minutes).

Likewise, to determine the rate at which Ce is oxidised, an excess of sodium bromate (0.1 M, 0.03 g) was added to a HNO_3 solution (2 mL, 10 M) containing 100 ppb Ce, 100 ppb Tb and 0.1 g of UTEVA resin. Repeat samples were left in static conditions before being filtered to isolate the aqueous phase at regular time intervals under vacuum (90 seconds - 180 minutes).

An aliquot of each filtrate was diluted with HNO_3 (2% v/v) before analysis by ICP-MS. Distribution coefficients were calculated using Eq. (1).

Column studies. Column-based separation was studied using a pre-packed 2 mL UTEVA cartridge (50–100 µm, *Triskem International*). The resin was pre-conditioned with 8 M HNO_3 (20 mL). A HNO_3 solution (10 mL, 8 M) containing 0.1 M $NaBrO_3$, 100 ppb Tb and 100 ppb Ce was loaded onto the resin. A wash solution of 10 mL 8 M HNO_3 was added to ensure removal of all Tb from the cartridge. Subsequent elution of Ce was achieved using 20 mL 0.1 M HCl. This separation method was also repeated using a pre-packed 2 mL TEVA cartridge (50–100 µm, *Triskem International*).

Throughout the separations, 1 mL fractions were collected, diluted with HNO_3 (2% v/v) and analysed by ICP-MS in order to compile an elution profile. Column separations were carried out under gravity (approximate flow rate = 0.3 mL/min).

Method validation with active sample. Three zinc-coated gold foils containing ^{155}Tb and ^{139}Ce were received at NPL from CERN-ISOLDE and CERN-MEDICIS. The radionuclides were leached by dissolving the zinc layer in 20 mL 6 M HCl and the gold foil in 20 mL *aqua regia*. Both layers were dissolved in order to maximise the yield of terbium from the sources received. The combined solution was evaporated gently on a hot plate (~150 °C) to incipient dryness and re-dissolved in a 10 mL 8 M HNO_3/0.1 M $NaBrO_3$ solution. An ampoule was prepared for HPGe gamma spectrometry in order to quantify the activity of ^{155}Tb and ^{139}Ce present. After analysis, the portion was recombined with the bulk solution.

A pre-packed 2 mL UTEVA cartridge (*Triskem International*, 50–100 µm) was conditioned with 20 mL 8 M HNO_3. The 10 mL sample was then loaded onto the column and the fraction collected under gravity. The column was washed with 10 mL 8 M HNO_3. This fraction was collected, under gravity, and combined with the load fraction. The combined fractions were evaporated gently on a hot plate (~150 °C) to incipient dryness and re-dissolved in 20 mL 0.1 M HCl.

An ampoule of the combined terbium fractions was prepared and analysed by HPGe gamma spectrometry in order to assess the resultant purity of the ^{155}Tb source after separation. The terbium recovery was calculated as follows:

$$\frac{R_{0,2}}{R_{0,1}} = \frac{\frac{N_2}{\Delta t_{L,2} \cdot m_2} \cdot e^{-\lambda \Delta t_2} \frac{\Delta t_2 \cdot \lambda}{(1 - e^{-\lambda \Delta t_2})} \cdot m_E}{\frac{N_1}{\Delta t_{L,1} \cdot m_1} \cdot e^{-\lambda \Delta t_1} \frac{\Delta t_1 \cdot \lambda}{(1 - e^{-\lambda \Delta t_1})} \cdot m_D} \quad (3)$$

where $R_{0,1}$ and $R_{0,2}$ are the count rates of the 105 keV gamma-ray emission before and after separation of the ^{139}Ce, respectively at the reference time 2017-09-29 12:00 UTC. N_1 and N_2 are the net peak areas of the 105 keV full-energy peak measured before and after separation, $\Delta t_{L,1}$ and $\Delta t_{L,1}$ are the measurement live times, m_1 and m_2 are the measured active masses of solution, m_D and m_E are the total mass of solution used to dissolve the Zn layer of the target and eluent used in the chemical separation, respectively, λ is the decay constant of ^{155}Tb, t_1 and t_2 are the time elapsed since the reference time and Δt_1 and Δt_2 are the measurement real times.

Conclusion

A novel method has been developed for the isolation of ^{155}Tb from sources produced at CERN-ISOLDE and CERN-MEDICIS, currently the main producers of the isotope. A high purity ^{155}Tb preparation was successfully recovered from a zinc-coated gold matrix and from ^{139}Ce impurities using a chromatography-based system. The method was shown to be capable of separating 100 ppb Tb and Ce in a 10 mL solution, equivalent to ~6 GBq ^{155}Tb and ~0.25 GBq ^{139}Ce. The radiologically pure ^{155}Tb preparation was subsequently used for absolute activity measurements and ion chamber measurements. The preparations are also suitable for phantom imaging and pre-clinical studies.

Data Availability

The data generated and analysed during this study are available, upon reasonable request, from the corresponding author.

References

1. Müller, C. *et al.* A unique matched quadruplet of terbium radioisotopes for PET and SPECT and for α- and β⁻ radionuclide therapy: An *in vivo* proof-of-concept study with a new receptor-targeted folate derivative. *J. Nucl. Med.* **53**, 1951–1959, https://doi.org/10.2967/jnumed.112.107540 (2012).
2. Sonzogni, A., Brookhaven National Laboratory. Evaluated nuclear structure data file search and retrieval (ENSDF), https://www.nndc.bnl.gov/ensdf/ (2018).
3. BIPM. *Monographie BIPM-5 – Table of Radionuclide*, Seven Volumes, CEA/LNE-LNHB, 91191 Gif-sur-Yvette, France and BIPM, Pavillon de Breteuil, 92312 Sevres, France, http://www.nucleide.org/DDEP.htm (2004).
4. Müller, C. *et al.* Future prospects for SPECT imaging using the radiolanthanide terbium-155 – production and preclinical evaluation in tumour-bearing mice. *J. Nucl. Med.* **41**, e58–e65, https://doi.org/10.1016/j.nucmedbio.2013.11.002. (2014).
5. Lehenberger, S. *et al.* The low-energy β⁻ and electron emitter ^{161}Tb as an alternative to ^{177}Lu for targeted radionuclide therapy. *J. Nucl. Med.* **38**, 917–924, https://doi.org/10.1016/j.nucmedbio.2011.02.007 (2010).
6. Formento Cavaier, R., Haddad, F., Sounalet, T., Stora, T. & Zahi, I., the MEDICIS-PROMED collaboration. Terbium radionuclides for theranostics applications: A focus on MEDICIS-PROMED. *Phys. Procedia* **90**, 157–163, https://doi.org/10.1016/j.phpro.2017.09.053 (2017).
7. dos Santos Augusto, R. M. *et al.* CERN-MEDICIS(medical isotopes collected from ISOLDE): A new facility. *Appl. Sci.* **4**, 265–281, https://doi.org/10.3390/app4020265 (2014).
8. Allen, B. *et al.* Production of terbium-152 by heavy ion reactions and proton induced spallation. *Appl. Radiat. Isotopes* **54**, https://doi.org/10.1016/S0969-8043(00)00164-0 (2001).
9. Steyn, G. F. *et al.* Cross sections of proton-induced reactions on ^{152}Gd, ^{155}Gd and ^{159}Tb with emphasis on the production of selected Tb radionuclides. *Nucl. Instrum. Methods Phys. Res. B* **319**, 128–140, https://doi.org/10.1016/j.nimb.2013.11.013 (2014).
10. Duchemin, C., Guertin, A., Haddad, F., Michel, N. & Métivier, V. Deuteron induced Tb-155 production, a theranostic isotope for SPECT imaging and auger therapy. *Appl. Radiat. Isotopes* **118**, 281–289, https://doi.org/10.1016/j.apradiso.2016.09.030 (2016).
11. Tárkányi, F. *et al.* Activation cross-sections of deuteron induced reactions on ^{nat}Cd up to 50 MeV. *Appl. Radiat. Isotopes* **83**, 25–35, https://doi.org/10.1016/j.apradiso.2013.10.010 (2014).
12. Kazakov, A. G., Aliev, R. A., Bodrov, A. Y., Priselkova, A. B. & Kalmykov, S. N. Separation of radioisotopes of terbium from a europium target irradiated by 27 MeV α-particles. *Radiochim. Acta* **106**, https://doi.org/10.1515/ract-2017-2777 (2017).
13. Vermeulen, C. *et al.* Cross sections of proton-induced reactions on ^{nat}Cd with special emphasis on the production possibilities of ^{152}Tb and ^{155}Tb. *Nucl. Instrum. Methods Phys. Res. B* **275**, 24–32, https://doi.org/10.1016/j.nimb.2011.12.064 (2012).
14. Zagryadskii, V. A. *et al.* Measurement of terbium isotope yield in irradiation of ^{151}Eu targets by ^{3}He nuclei. *At. Energy* **123**, 55–58, https://doi.org/10.1007/s10512-017-0299-8 (2017).
15. Szelecsényi, F., Kovács, Z., Nagatsu, K., Zhang, M.-R. & Suzuki, K. Investigation of deuteron-induced reactions on ^{nat}Cd up to 30 MeV: possibility of production of medically relevant ^{155}Tb and ^{161}Tb. *J. Radioanal. Nucl. Chem.* **307**, 1877–1881, https://doi.org/10.1007/s10967-015-4528-0 (2016).
16. Moeller, T. Atomic structure and its consequences – the dawn of understanding in *The chemistry of the lanthanides* (eds Sisler, H. H. & Van der Werf, C. A.) 18–21 (1963).
17. Martin, M. J. ENSDF: The evaluated nuclear structure data file. *AIP Conf. Proc.* **146**, 10–13, https://doi.org/10.1063/1.35876 (1986).
18. U.S. Environmental Protection Agency. Toxicological review of cerium oxide and cerium compounds: In support of summary information on the Integrated Risk Information System (IRIS), https://cfpub.epa.gov/ncea/iris/iris_documents/documents/toxreviews/1018tr.pdf (2009).
19. Rim, K. T., Koo, K. H. & Park, J. S. Toxicological evaluations of rare earths and their health impacts to workers: a literature review. *Saf. Health Work* **4**, 12–26, https://doi.org/10.5491/SHAW.2013.4.1.12 (2013).
20. Collon, S. A. Scandium, Yttrium & the Lanthanides: Inorganic & Coordination Chemistry in *Encyclopaedia of Inorganic Chemistry* (ed. King, R. B.) 1–40 (2006).
21. Cacheris, W. P., Nickle, S. K. & Sherry, A. D. Thermodynamic study of lanthanide complexes of 1,4,7-triazacyclononane-N,N′,N″-triacetic acid and 1,4,7,10-tetraazacyclododecane-N,N′,N″,N‴-tetraacetic acid. *Inorg. Chem.* **26**, 958–960, https://doi.org/10.1021/ic00253a038 (1987).
22. Collins, S. M. *et al.* The potential radio-immunotherapeutic α-emitter 227Th – part II: Absolute γ-ray emission intensities from the excited levels of 223Ra. *Appl. Radiat. Isot.* **145**, 251–257, https://doi.org/10.1016/j.apradiso.2018.10.023 (2019).
23. Currie, L. A. Limits for qualitative detection and quantitative determination. *Application to radiochemistry. Anal. Chem.* **40**, 586–593, https://doi.org/10.1021/ac60259a007 (1968).
24. Horwitz, E. P., McAlister, D. R. & Dietz, M. L. Extraction Chromatography Versus Solvent Extraction: How Similar are They? *Sep. Sci. Technol.* **41**, 2163–218, https://doi.org/10.1080/01496390600742492 (2006).
25. Böhlen, T. T. *et al. The FLUKA Code: Developments and Challenges for High Energy and Medical Applications Nuclear Data Sheets* **120**, 211–214, https://doi.org/10.1016/j.nds.2014.07.049 (2014).
26. Ferrari, A., Sala, P. R., Fasso, A. & Ranft, J. CERN-2005-10, INFN/TC_05/11, SLAC-R-773 (2005).

Acknowledgements

B.W.'s participation was facilitated by a PhD studentship co-sponsored by the University of Surrey and the National Physical Laboratory. The National Physical Laboratory is operated by NPL Management Ltd, a wholly-owned company of the Department for Business, Energy and Industrial Strategy (BEIS). We gratefully recognise Chris Gilligan of AWE plc. for useful discussions regarding the chemical separation of the lanthanide elements. T.S. would like to thank the team involved in the preparation, operation and shipping of the isotope collection at CERN-MEDICIS. U.K. would also like to thank the team involved in the preparation, operation and shipping

of the isotope collection at CERN-ISOLDE and the ISOLDE RILIS team who provided the smooth operation of the laser ion source. The collections at CERN-ISOLDE were supported by the European Union's Horizon 2020 research and innovation programme under *grant agreement* No. 654002 (ENSAR2 project).

Author Contributions

B.W., P.I. and B.R. contributed the overall ideas and towards the design of the chemical separation procedure. B.W. wrote the majority of text in this manuscript and compiled the figures and tables. S.C. provided information and spectra associated with gamma spectrometry analysis. B.R. provided information with regard to ICP-MS analysis and both B.R. and P.I. assisted with active experimental work. T.S., J.P.R. and U.K. provided information regarding the production process at CERN-MEDICIS including Figure 6. All authors reviewed the manuscript and helped with editorial input.

Additional Information

Competing Interests: The authors declare no competing interests.

Publisher's note: Springer Nature remains neutral with regard to jurisdictional claims in published maps and institutional affiliations.

Appendix P – Russell *et al.* (2020)

B. Russell, P. Ivanov, B. Webster and D. Read, *Agilent Application Note: Characterization of Rare Earth Elements used for Radiolabeling Applications by ICP-QQQ*, 2020[204]

Application Note
Materials, Nuclear, Pharmaceutical

Agilent
Trusted Answers

Characterization of Rare Earth Elements used for Radiolabeling Applications by ICP-QQQ

Analysis of radiogenic REE isotopes in bulk REE matrices

Authors

B. Russell[1], P. Ivanov[1]
B. Webster[1,2], D. Read[1,2]

[1]Nuclear Metrology Group, National Physical Laboratory, Teddington, UK
[2]School of Chemistry and Chemical Engineering, University of Surrey, Guildford, UK

Verified for Agilent 8900 ICP-QQQ

Introduction

Radiolabeling refers to a technique where a compound or substance is labeled (or tagged) with a radioactive isotope of an element. The labeled material can then be used for controlled delivery of the radiation emitted by the active isotope, or detected and traced from the radioactivity of the isotopic label.

The use of radiolabeled materials is growing steadily, with the market for radiolabeled pharmaceutical compounds expected to be worth over 5 billion US dollars by 2024 (*1*). Elements that can form useful radioisotopes include the lanthanides – also known as rare earth elements (REEs). Radio-lanthanide compounds are used in pharmaceutical and imaging applications.

To meet the rising demand for radio-lanthanides, there is a critical need for analytical techniques to support the production of traceable, high purity, labeled lanthanides (*2*). Production scale chemical purification and labeling of

radio-lanthanides is challenging though, because all the lanthanides have similar chemical properties and tend to behave as a consistent group. To prepare a pure radio-lanthanide, it is necessary to accurately characterize the chemical composition of the non-radioactive natural or isotopically enriched starting material used. Before a candidate starting material can be used for routine radionuclide production, each batch must be tested and validated to ensure that radionuclide yields will be of the desired quantity and quality (*3*). To carry out this level of quality assurance (QA), accurate analytical procedures are needed, particularly to determine the level of trace lanthanide contaminants in the pure lanthanide starting material. Since any impurities need to be removed, the QA data is also useful to guide the design of robust, reproducible chemical separation methods (*4*). Determining the type and quantity of impurities present in the starting material also helps manufacturers predict whether unwanted radioactive side-products will be produced during irradiation.

Table 1 lists several radio-lanthanide product isotopes that have chemical and radioactive decay properties that make them suitable for applications in radiolabeling. In most of these examples, the starting material is a different element to the intended radio-lanthanide product isotope. This avoids the radio-lanthanide product isotope being affected by high concentrations of a stable isotope of the same element in the irradiated target, which cannot be removed by subsequent chemical separation. Typically, the radionuclides are produced by irradiating a lanthanide or lanthanide oxide starting material target at a nuclear reactor or cyclotron facility. For example, terbium-155 can be produced from gadolinium (III) oxide (Gd_2O_3) starting material in a cyclotron. The stable isotope ^{155}Gd is converted to the radioisotope ^{155}Tb via a (p, n) reaction, where a proton enters the nucleus and a neutron leaves the nucleus simultaneously.

Table 1. Starting materials and production route for radio-lanthanides used in labeling applications.

Radio-lanthanide	Starting Material*	Possible Nuclear Reaction Production Route**
^{153}Sm	^{152}Sm	^{152}Sm(n, γ) → ^{153}Sm
^{149}Tb	^{151}Eu	^{151}Eu(^{3}He, 5n) → ^{149}Tb
^{155}Tb	^{155}Gd	^{155}Gd(p, n) → ^{155}Tb
^{161}Tb	^{160}Gd	^{160}Gd(n, γ)^{161}Gd → ^{161}Tb + β-
^{166}Ho	^{164}Dy	^{164}Dy(n, γ)^{165}Dy(n, γ)^{166}Dy → ^{166}Ho + β-
^{169}Er	^{168}Er	^{168}Er(n, γ) → ^{169}Er
^{177}Lu	^{176}Yb	^{176}Yb(n, γ)^{177}Yb → ^{177}Lu + β-

** Starting materials are often isotopically enriched targets.*
***n (neutron), p (proton), γ (gamma), ^{3}He (helium-3).*

The accurate characterization of REE materials is challenging for conventional single quadrupole ICP-MS. The REEs form hydride (MH^+), oxide (MO_x^+), and hydroxide (MOH^+) polyatomic ions in the plasma or during ion extraction, and these polyatomic ions can overlap the measured isotopes of other REEs. High intensity REE matrix element peaks can also cause peak tail overlaps on trace REE isotopes measured at adjacent masses. This peak tailing effect, known as the abundance sensitivity (AS), is different for different types of mass spectrometer. On commercial single quadrupole ICP-MS instruments, the AS is typically 10^{-7}, which means that every 10 million counts at a high intensity peak contributes one count to the adjacent masses. This AS performance means that an intense major element peak can cause peak tailing overlaps on trace analytes at adjacent masses when measured by single quadrupole ICP-MS.

Compared to single quadrupole ICP-MS, Agilent triple quadrupole ICP-MS (ICP-QQQ) instruments offer superior resolution of polyatomic interferences using reactive cell gases. This performance improves accuracy in complex sample types, including analysis of trace REEs in geological samples and materials applications (*5, 6*). Also, Agilent ICP-QQQ instruments use a tandem mass spectrometer configuration (MS/MS) with two full-sized quadrupole mass analyzers, Q1 and Q2, both housed in high vacuum regions. Two mass filtering steps reduce peak tail overlaps, as the overall AS in MS/MS is the product of the AS of the two quadrupoles, so 10^{-7} x 10^{-7}, or 10^{-14} (*7*).

Previous studies suggest that ICP-QQQ methods can improve the accuracy of analysis of trace impurities in the lanthanide starting materials/targets used for radio-lanthanide production. Also, assessment of the concentration of impurities in the starting material recovered after chemical separation of the radioisotope could allow for re-use of the recovered material.

The chemical separation methods used to purify radio-lanthanide isotopes can be designed and optimized using stable isotopes of each lanthanide, rather than the radioactive material. ICP-QQQ can be used to measure the intended lanthanide product element at trace (ppt) levels in the presence of a high concentration (ppm level) of the bulk target material. This capability enables realistic testing of the separation scheme while using cheap, safe, and readily available natural REE materials.

In this study, several pairs of trace REE analytes and adjacent mass neighboring REE matrix elements relevant to radio-lanthanide production were measured by ICP-QQQ. The samples included materials that are typically used as

irradiation targets for radio-lanthanide production. The use of ICP-QQQ for optimizing radiochemical separation of target lanthanides, and for measuring REE impurities in irradiated targets, was also demonstrated. The developed methods will enable end users to compile a REE impurity profile of materials of relevance to the production of radionuclides for labeling applications.

Experimental

Sample preparation

For the detection limit (DL) study, calibration standards from 1 ppt to 100 ppb were prepared for each trace REE in solutions containing 10 ppm of the neighboring REE matrix element. All solutions were stabilized with 2% HNO_3. These bulk-trace lanthanide pairs are summarized in Table 2. Similar solutions were prepared to test the extraction chromatography-based chemical separation procedures.

Table 2. Pairs of natural REE matrix elements and trace REE analytes used for preparation of calibration standard sets to test resolution of adjacent mass interferences.

Bulk REE Matrix (Isotopic abundance, %)	Trace REE Analyte (Isotopic abundance, %)
^{139}La (99.91)	^{140}Ce (88.45)
^{140}Ce (88.45)	^{141}Pr (100)
^{159}Gd (24.84)	^{159}Tb (100)
^{164}Dy (28.18)	^{165}Ho (100)
^{165}Ho (100)	^{166}Er (33.61)
^{168}Er (26.78)	^{169}Tm (100)
^{174}Yb (31.83)	^{175}Lu (97.41)

The performance of the ICP-QQQ MS/MS method with O_2 cell gas was investigated using analysis of Tb in the presence of a Gd matrix. Gadolinium (III) oxide powder (Gd_2O_3, 99.999 % purity) was gently dissolved in 8 M HNO_3, evaporated to dryness, and then redissolved in 2% HNO_3 to give a final concentration of 10 ppm Gd.

Irradiated Gd_2O_3 targets were dissolved in concentrated HNO_3. To determine the target radio-lanthanide activity levels and any other radionuclides produced, an aliquot was taken for measurement by gamma spectrometry. Following this analysis the sample was left for enough time to allow short-lived radionuclides to decay, after which the stable REE impurities were determined by ICP-QQQ.

Instrumentation

An Agilent 8800 ICP-QQQ was used in this study. The 8800 was equipped with a standard sample introduction system comprising a glass concentric nebulizer, a quartz spray chamber, a quartz torch with 2.5 mm i.d. injector, and nickel-tipped interface cones. The general instrument operating conditions are summarized in Table 3.

Table 3. ICP-QQQ operating parameters.

Parameter	Setting
Scan Mode	MS/MS
Plasma Conditions	Low matrix
RF Power (W)	1550
Extract 1 (V)	0
Extract 2 (V)	–175
Reaction Cell Gas	Oxygen
Oxygen Flow Rate (mL/min)	0.3 (30% of full-scale)
Octopole Bias (V)	–5.0
Energy Discrimination (V)	–7.0
Octopole RF (V)	200

Results and discussion

Instrument sensitivity and interference removal

To remove the matrix element hydride and peak tailing interferences for each of the trace REE analytes investigated, the 8800 ICP-QQQ was operated in MS/MS mode with O_2 cell gas. To compare the performance of single quadrupole ICP-MS, the measurements were also performed using the 8800 in single quad mode, where Q1 does not perform any mass selection.

Using the example of trace Tb analysis in a Gd matrix, Tb was measured as the product ion $^{159}Tb^{16}O^+$ at *m/z* 175 using mass shift. In single quad mode, the $^{158}Gd^1H$ and ^{158}Gd tailing interferences were not effectively avoided using O_2 cell gas. A 10 ppm Gd standard gave a signal at *m/z* = 175 of approximately 1.3×10^6 counts per second (cps). This high background meant Tb could not be measured at concentrations below 100 ppt.

Using MS/MS mode with Q1 and Q2 set to *m/z* = 159 and 175, respectively, the *m/z* 175 background signal in the 10 ppm Gd matrix was reduced to ~4,400 cps, which enabled accurate low-level Tb measurement. Using MS/MS, a detection limit of 2.1 ppt was achieved for Tb in the 10 ppm Gd matrix with background subtraction (Figure 1).

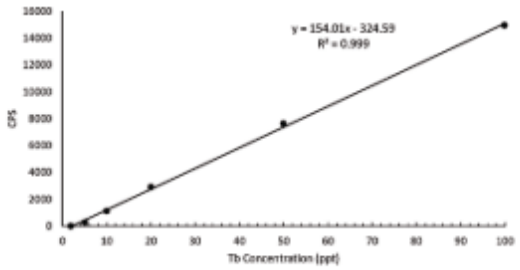

Figure 1. Calibration for Tb in the presence of 10 ppm ^{159}Gd. Tb measured as $^{159}Tb^{16}O^+$ by ICP-MS/MS in O_2 mass-shift mode.

A similar trend was seen for the other trace lanthanides listed in Table 4. Operating the 8800 in MS/MS with on-mass or mass-shift mode using O_2 cell gas, DLs in the low ppt range were achieved for most analytes. Only Ho (measured at *m/z* 165) in a Dy (164) matrix and Er (166) in a Ho (165) matrix showed higher DLs, up to 1.1 ppb in the case of Ho in Dy. The ppt level DLs are equivalent to purity levels of up to 2.1×10^{-7} relative to the 10 ppm concentration of each respective matrix element. This sensitivity is significantly better than the purity information currently provided by the manufacturers of lanthanide powders. The purity analysis also provides valuable information about possible radionuclides that may be formed from contaminants during irradiation of the lanthanide starting material powders.

The single O_2 cell gas mode used for this study gave acceptable data for all trace lanthanides studied. The DLs for some REEs, e.g., trace Ho in Dy, could be improved by further optimizing the cell conditions or using an alternative reaction gas such as N_2O or NH_3 (*6*).

Table 4. Detection limits achieved by 8800 ICP-QQQ for trace REEs in REE matrices. Analysis based on measurement of natural, stable isotope elemental standards.

Trace Element (Measured isotope)	Q1 / Q2	Matrix Element (10 ppm)	DL of Trace Element (ppt)
Ce (140)	140/156	^{139}La	12.2
Pr (141)	141/157	^{140}Ce	11.9
Tb (159)	159/175	^{158}Gd	2.1
Ho (165)	165/181	^{164}Dy	1100
Er (166)	166/182	^{165}Ho	186
Tm (169)	169/185	^{168}Er	2.3
Lu (175)	175/191	^{174}Yb	9.3

Measurement of lanthanide oxide samples

The concentrations of trace lanthanides in a solution containing 10 ppm Gd_2O_3 powder were determined using the 8800 ICP-QQQ with O_2 cell gas. As shown in Figure 2, most REEs were measured on-mass. Only ^{159}Tb, ^{172}Yb, and ^{175}Lu were measured as oxide product ions in mass-shift mode to avoid interferences from $^{158}Gd^1H$ at *m/z* 159, $^{156}Gd^{16}O$ at *m/z* 172, and $^{158}Gd^{16}O^1H$ at *m/z* 175 (Figure 2).

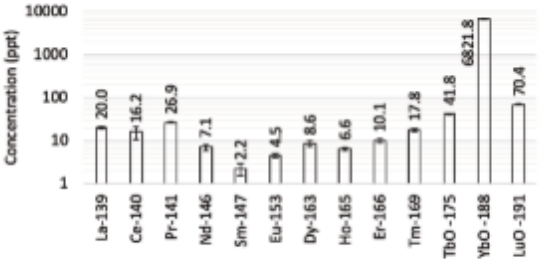

Figure 2. Impurity profile and ICP-MS measurement uncertainties (2σ) of Gd_2O_3 powder used for irradiation.

Elemental standard solutions are used to test chemical separation procedures, so the same ICP-QQQ method was used to measure impurities in a Gd single-element ICP standard. The results are shown in Figure 3. The relatively high measured concentration of YbO in the powder and ICP standard suggests that the interference from $^{156}Gd^{16}O$ and $^{156}Gd^{16}O_2$ on ^{172}Yb and $^{172}Yb^{16}O$, respectively, were not fully resolved. Yb is also not very reactive with oxygen cell gas, leading to low sensitivity for the YbO^+ product ion. The method could potentially be improved through further optimizing the cell conditions or using an alternative cell gas such as N_2O or NH_3 (*6*, *7*).

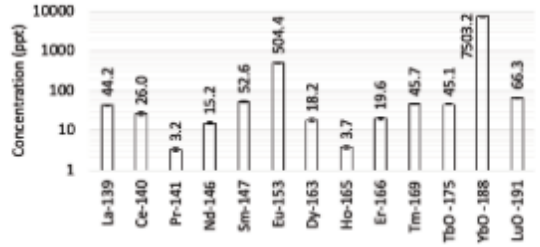

Figure 3. Impurity profile and ICP-MS measurement uncertainties (2σ) of a Gd ICP standard using 8800 ICP-QQQ in MS/MS mode with O_2 cell gas.

Chemical separation results

Operating the 8800 in MS/MS mode with O_2 cell gas and using stable element analogs in place of short-lived radioactive samples enables the optimization of separation procedures under realistic conditions. Realistic conditions refer to the separating of a trace level target lanthanide in the presence of high concentrations of a neighboring lanthanide. This approach enables the development of robust radiochemical procedures before testing with active samples. It also avoids the cost and safety issues of handling active materials during method development.

In this study, Tb was separated from Gd using an extraction chromatography column packed with a LN (lanthanide) resin (50–100 µm particle size, Triskem International). Figure 4 shows an elution profile for Gd and Tb at a 4.5×10^4 excess of Gd. Gd was expected to elute with 0.75 M HNO_3, while Tb was expected to be retained until conditions were switched to 1.0 M HNO_3 (*8*). To check if the separation scheme had been effective, each 1 mL fraction was collected and measured using ICP-MS/MS in O_2 mass-shift mode. The results showed that a small amount of ^{159}Tb was recovered in the ^{158}Gd fraction.

The effectiveness of the ICP-QQQ method to resolve Tb from Gd has been demonstrated using trace Tb standards in a Gd matrix. This performance gives confidence that the signal at *m/z* 159 seen in the Gd fraction was due to trace ^{159}Tb eluting together with the Gd, rather than an interference from $^{158}Gd^1H$. Also, based on the starting concentration of Tb added to the column, the total Tb recovery was <100%, suggesting little or no contribution from Gd to the measured Tb signal.

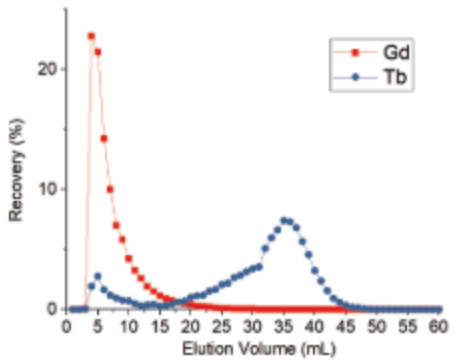

Figure 4. Elution profile for Tb and Gd.

Measurement of impurities in irradiated samples

A compacted Gd_2O_3 powder target was irradiated to produce ^{155}Tb (half-life of 5.32 days). The irradiated target was then dissolved in concentrated HNO_3 and an aliquot was used to measure the activity level of ^{155}Tb and other short-lived radionuclides by gamma spectrometry. After leaving the sample enough time for the radioisotopes to decay, the stable REE isotopes remaining in the Gd_2O_3 sample were measured using ICP-QQQ.

Lanthanum and Ce were the only REE contaminants detected in the final sample at concentrations of ~13.1 and 3.5 ppm, respectively. However, the concentration of both La and Ce was reduced to below background levels after chemical separation. The detection of La and Ce in the irradiated Gd_2O_3 powder shows the potential for stable and long-lived radionuclide impurities to be formed during irradiation. The findings illustrate the importance of chemical separation in the production of high purity radio-lanthanides.

The ICP-QQQ method can be used for post-separation analysis of the final radio-lanthanide product to assess the concentration of stable impurities still present, and to help assess the effectiveness of the chemical separation. Depending on the application, enriched or recycled target materials may be used that contain lanthanides at non-natural abundances, which will affect the level of impurities that can be measured. The measurement of such impurities is important as a QA measure, as high concentrations of impurities can lead to competition for the chelating agent used, which can reduce the radiolabeling efficiency.

Conclusion

The use of radio-lanthanides is of increasing interest in pharmaceutical and imaging applications. Preparation of high purity radio-lanthanides often requires separation of the low concentration target isotope from the high concentration stable REE matrix. To check the purity of the starting REE materials, the Agilent 8800 ICP-QQQ was operated in MS/MS mode with O_2 cell gas to measure all REE impurities in high-purity REE matrices. The ICP-QQQ method was much more effective at removing REE matrix-based polyatomic and peak tailing interferences compared to single quadrupole ICP-MS.

The measurement of trace levels of Tb in the presence of bulk Gd was used as an example. The results obtained from analyzing stable element standards showed that the method was useful for a range of radio-lanthanides.

Overall, the ICP-MS/MS method improved accuracy and confidence of the measurements needed for a complete REE impurity profile of materials used in the production of radionuclides for pharmaceutical and imaging applications. The study has shown that the method is suitable for:

- The measurement of REE impurities in the starting powders used for irradiation.
- Optimizing chemical separation conditions using stable element analogs.
- Assessing the REE impurities present in the irradiated target material post-irradiation.

References

1. Markets and Markets, Nuclear Medicine/ Radiopharmaceuticals Market by Type (Diagnostic (SPECT - Technetium, PET- F-18), Therapeutic (Beta Emitters – I-131, Alpha Emitters, Brachytherapy – Y-90)), Application (Oncology, Cardiology) - Global Forecast to 2024, accessed online August 2020, https://www.marketsandmarkets.com/Market-Reports/radiopharmaceuticals-market-417.html
2. M. Van de Voorde *et al.* Radiochemical processing of nuclear-reactor-produced radio lanthanides for medical applications. *Coordination Chemistry Reviews* **2019**, 382 (1), 103–125
3. The International Pharmacopoeia, Ninth Edition. https://apps.who.int/phint/en/p/docf/
4. B. Webster *et al.* Chemical Purification of Terbium-155 from Pseudo-Isobaric Impurities in a Mass Separated Source Produced at CERN, *Nature Scientific Reports* **2019**, 9, 1–9
5. N. Sugiyama, Removal of hydride ion interferences (MH^+) on Rare Earth Elements using the Agilent 8800 Triple Quadrupole ICP-MS, Agilent publication, 5991-1481EN
6. N. Sugiyama and G. Woods, Direct measurement of trace rare earth elements (REEs) in high-purity REE oxide using the Agilent 8800 Triple Quadrupole ICP-MS with MS/MS mode. Agilent publication, 5991-0892EN
7. N. Sugiyama, Direct Analysis of Ultratrace Rare Earth Elements in Environmental Waters by ICP-QQQ, Agilent publication, 5994-1785EN
8. F. Monroy-Guzman and E. J. Salinas, Separation of Micro-Macrocomponent Systems: Ho-Dy and Lu-Yb by Extraction Chromatography, *J. Mex. Chem. Soc.*, **2015**, 59, 143–150

www.agilent.com/chem

RA.673587963

Printed in the USA, October 23, 2020
5994-2389EN

Agilent
Trusted Answers

Appendix Q – Trinder *et al.* (2020)

R. R. Trinder, T. Kokalova, D. J. Parker, C. Wheldon, B. Phoenix, P. Ivanov, B. Russel, B. Webster, P. Regan, A. Robinson, D. Cullen, S. Pells, R. Allen, S. Pirrie, A. Turner and P. Santa Rita, in *Journal of Physics: Conference Series*, IOP Publishing Ltd, 2020, vol. 1643, p. 12209.[117]

27th International Nuclear Physics Conference (INPC2019) IOP Publishing
Journal of Physics: Conference Series **1643** (2020) 012209 doi:10.1088/1742-6596/1643/1/012209

Theragnostics - Alternative production of terbium isotopes at the University of Birmingham using an MC40 cyclotron

R. R. Trinder[1], Tz. Kokalova[1], D. J. Parker[1], C. Wheldon[1], B. Phoenix[1], P. Ivanov[2], B. Russel[2], B. Webster[2], P. Regan[2,3], A. Robinson[2], D. Cullen[4], S. Pells[4], R. Allen[1], S. Pirrie[1], A. Turner[1], P. Santa Rita[1]

[1]University of Birmingham, UK, [2]National Physical Laboratory, UK, [3]University of Surrey, UK, [4]University of Manchester, UK

E-mail: rrt313@student.bham.ac.uk

Abstract. In this work alternative methods for the production of terbium isotopes, and in particular ^{152}Tb and ^{155}Tb, have been investigated. These isotopes, which could be used for theragnostics, have been produced using an alpha and a proton beam incident on europium and gadolinium targets, respectively. The experimental results have been compared with the predicted cross-sections, calculated using TALYS and PACE4 code.

1. Introduction

Over time the diagnosis and treatment tools used to identify and remove cancer growths in patients have evolved. New ideas and techniques are continuously being investigated to improve the treatment of cancer. Table 1 lists some of the currently employed techniques to diagnose and treat cancer.

Table 1. Currently used techniques to treat and diagnose cancer.

Treatment	Diagnostic Imaging
Surgery	X-ray
Internal and External Radiation therapy	CT (Computerised Tomography)
Chemotherapy	MRI (Magnetic resonance imaging)
Immunotherapy	PET (Positron Emission Tomography)
Hormone therapy	Gamma Camera/SPECT (Single Photon Emission Computed Tomography)
Stem cell transplant	Ultrasound
Targeted therapy	Mammography

Internal radiotherapy, PET (Positron Emission Tomography) and SPECT (Single Photon Emission Computed Tomography) imaging are techniques classified under 'Nuclear medicine'.

Nuclear medicine works by introducing radioactive isotopes into the body and using the different forms of decay to either perform therapy or diagnostic imaging of a patient.

Therapy can be performed by using either beta or alpha emitting isotopes. The beta or alpha particles ionise the neighbouring cells causing damage to the DNA, often leading to either single- or double-strand breakages, respectively. Positron emitting isotopes are used to perform diagnostic PET imaging and isotopes which predominantly emit gammas are used for diagnostic SPECT imaging.

In nuclear medicine, cancer cells are located by attaching the radioactive nuclide to a biological targeting agent. For example, a glucose molecule can be replicated and modified such that a ^{18}F atom is attached to form FDG (fluorodeoxyglucose), see figure 1 . In this case the biological targeting agent reacts in the body as glucose does. Glucose is drawn into cells which are using up energy in metabolic processes i.e. the cells will break-down the glucose molecule to release energy for the cell's use. FDG will behave in the same way as glucose and will thus concentrate in areas of high activity, e.g. active areas of the brain and cancer lesions. It is the higher concentration of FDG in these areas which will be highlighted in a PET and SPECT images.

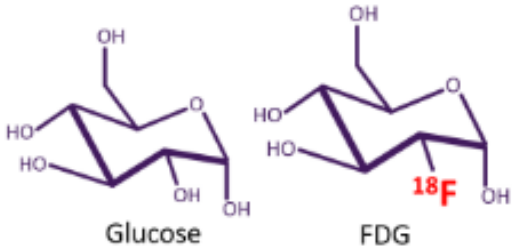

Figure 1. Molecular diagrams of Glucose and FDG (fluorodeoxyglucose)

A more specific method of cancer targeting is to use proteins (peptides). Cancer cells will have specifically shaped proteins on their outer membranes. If a complementary (i.e. fits like a glove over a hand) peptide is made, this will only attach to that specific cancer protein. A radioactive nuclide can then be attached to this complementary peptide using a chelator (linker) as shown in figure 2. This can be a more direct and tailored method of targeting cancer lesions.

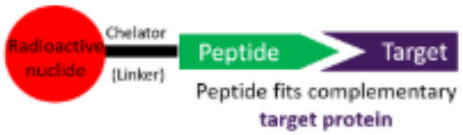

Figure 2. Schematic diagram of a radioactive nuclide attached to a peptide targeting molecule

It is the combination of **thera**py and dia**gnostic** imaging (**theragnostics**) which aims to provide a more tailored treatment to cancer. By monitoring therapy with diagnostic imaging the effectiveness of the treatment can be seen and changed according to need. The radiation dose received by a patient during treatment can also be monitored. Currently, a combination of Lu and Ga is commonly used in hospitals for β^-therapy and PET diagnostic imaging, respectively. These nuclei are different elements, hence, they will not necessarily chemically interact the same within the body. This provides uncertainty in the comparing diagnostic imaging to therapy,

which in turn provides doubt to the reliability of a theragnostic treatment. A way of resolving this issue would be to use different isotopes of the same element to perform the therapy and diagnostic imaging. Scandium, copper, arsenic and terbium are a few examples of proposed elements which have suitable properties for medical use. Some of the main properties to consider are half-life and energy of emitted radiation. The half-life of a medical isotope must be of reasonable length, so that it can be produced, transported, undergo radiochemical procedures and pass regulation tests before being administered to the patient. There must then be enough activity for the treatment or diagnostic imaging to be carried out effectively. However, the half-life must also be short enough that the isotope is not providing an unnecessarily large dose to the patient and their surroundings. In addition to the half-life requirements, the energies of the emitted radiation must also be suitable for the task. For example, a SPECT isotopes would ideally only emit gammas of a low energy (100-200 keV) which lie within a region of high efficiency for the gamma detectors; ideal PET isotopes would emit solely positrons and no gamma-rays other than 511 keV gammas from positron annihilation. In addition to this, for isotopes to be practical for hospital use, they should be able to be produced locally if not within the hospital. Hospital cyclotrons predominantly accelerate proton beams up to 17 MeV. This limits the type of isotopes that can be produced and is important to consider when developing new production methods.

Production of terbium by ISOLDE (Isotope Separator On Line DEtector) and MEDICIS (Medical Isotopes Collected from ISOLDE) [1] at CERN led to promising clinical trials over the past 8 years carried out by C. Müller et al. [2, 3, 4, 5] Consequently, these trials have motivated research into alternative production methods.

Table 2. The decay modes and most intense gamma transitions of the terbium isotopes used in theragnostics and their medical purpose. Here, E_α is the energy of the emitted α particle, E_β is the energy of the emitted β particle, E_γ is the energy of the emitted γ-ray and I_γ is the branching ratio of each γ-ray.

Isotope	Decay mode (Branching ratio)	Half life	E_α *(MEV)* / Average E_β (MEV)	E_γ (keV)	I_γ (%)	Use
149	α(16.7%) β^+ (7.1%)	4.12 h	***3.967(3)***	165.98(2)	26.4(8)	α therapy
				352.24(2)	29.4(9)	
			0.730(4)	388.57(2)	18.4(6)	
				652.12(2)	16.2(5)	
152	β^+ (20.3%)	17.5 h	1.140(13)	271.09(7)	9.53(21)	PET imaging
				344.278(1)	63.5(17)	
				586.27(7)	9.21(21)	
				778.904(2)	5.54(13)	
155	EC (100%)	5.32 d	N/A	86.55(3)	32.0(18)	SPECT imaging
				105.318(3)	25.1	
				180.169(9)	7.5(4)	
				262.27(1)	5.3(3)	
161	β^- (100%)	6.89 d	0.154(19)	25.6514	23.2(15)	β^- or Auger therapy
				48.9153	17.0(9)	
				57.1917(3)	1.79(10)	
				74.5667	10.2(5)	

The "quadruplet" of terbium isotopes (^{149}Tb, ^{152}Tb, ^{155}Tb and ^{161}Tb) proposed for theragnostic use possess the suitable properties for medical isotopes. These isotopes can be

used for all four aspects of nuclear medicine, α therapy, PET imaging, SPECT imaging and β^- therapy, respectively. Table 2 lists the half-lifes and energies of the emitted radiation from each isotope. Both the half-lifes and emitted energies for each isotope are suitable for medical purposes.

Looking at table 2, the terbium isotopes can be paired according to their half-lifes. Both the ^{149}Tb and ^{152}Tb have similar half-lifes of hours and ^{155}Tb and ^{161}Tb have similar half-lifes of days. The similar half-lifes of these pairs means that each pair can be used together to perform a more accurate form of theragnositcs for patient dose calculations.

Medical studies carried out by C. Muller, et al [2, 3, 4, 5] have provided the evidence required to further the investment into terbium production techniques. Their studies suggest that all four of the terbium isotopes would perform well for each of their designed functions. In addition to this, there is strong evidence [5] that, for example, in the case of prostate cancer ^{161}Tb will out perform ^{177}Lu because ^{161}Tb emits a β^- with a lower energy and thus has shorter range in tissue than ^{177}Lu so can target a more localised region.

2. Production

The MC40 cyclotron at the University of Birmingham is capable of accelerating proton and alpha particles up to 40 MeV and ^{3}He nuclei and deuteron particles can also be accelerated for isotope production. With these capabilities it is possible to produce ^{152} Tb and ^{155}Tb and potentially ^{149} Tb and ^{161}Tb [1].

The initial research focus was the production of the diagnostic imaging isotopes. The cross-section of interaction depends on energy. By varying the energy of the proton or alpha beam incident on the target the ratios of products produced changed. In order to create Tb isotopes, targets of either gadolinium or europium were used. Terbium isotopes can then be separated from the irradiate target using radio-chemical techniques being developed and NPL (National Physics Laboratory) [6].

For initial tests natural europium and gadolinium targets were used to identify which terbium isotopes could be produced using the MC40 cyclotron.

2.1. Europium target

The reaction mechanism for the production of ^{152}Tb and ^{155}Tb using and alpha beam on an natural europium target is as follows,

$$^{151}Eu(\alpha, 3n)^{152}Tb$$
$$^{153}Eu(\alpha, 2n)^{155}Tb$$

Initial investigations were done by looking at the PACE4 (Projection Angular-momentum Couples Evaporation Monte Carlo code) [7, 8] cross-section calculations for the interaction of alpha on a natural europium target (see figure 3(b)). The alpha beam energy was chosen by selecting the energy where the cross-section was a maximum for ^{152}Tb production. The irradiated Eu target was then place in front of a HPGe (High Purity Germanium) detector to identify products made using the emitted gammas. A small section of the gamma spectrum collected is shown in figure 4. Looking at this section alone, it can be observed that ^{154}Tb and ^{153}Tb were identified but more importantly ^{152}Tb in the ground state and excited isomer state were also identified. The isomeric state has a half life of 4 minutes compared to 17.5hrs for the ground state. Thus when gamma spectra were collected an hour later the purely isomeric ^{152}Tb states were no longer visible.

Although PACE4 was used for the initial investigation, the code does not differentiate between different isomers of terbium. An alternative code, TALYS (nuclear reaction code) [9] can differentiate between isomeric states. Comparing the PACE4 and TALYS cross-section (see

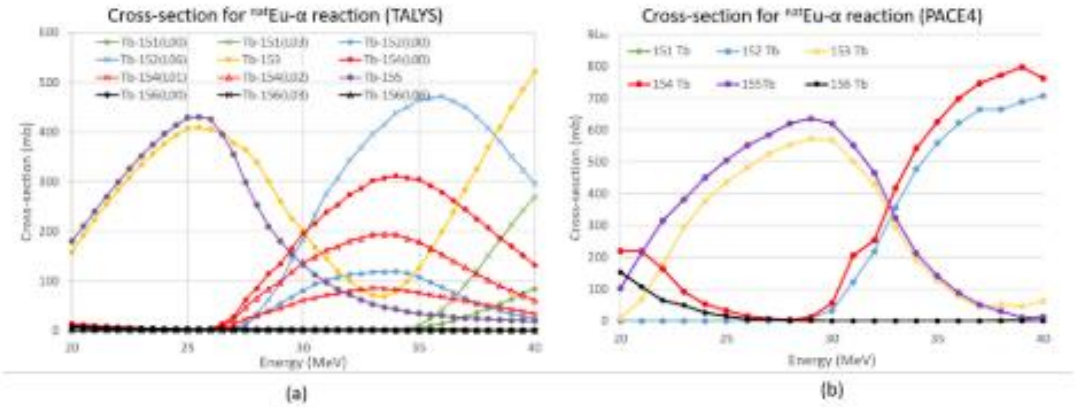

Figure 3. Cross-sections of interaction vs. energy of alpha beam on an natural Eu target (a)TALYS calculation (b)PACE4 calculation

figure 3(a)) there is a discrepancy between which alpha energy will produce the maximum cross-section for ^{152}Tb production. TALYS predicts a maximum cross-section at 34-36 MeV and PACE4 at 40 MeV. In the energy region for the initial production, TALYS predicts a much higher cross-section for the production of ^{153}Tb compared to PACE4. This was reflected in the gamma spectra data collected in figure 4 which displays the presence of ^{153}Tb. Therefore, for future investigation TALYS was used to calculate cross-sections to predict suitable beam energies.

An investigation to measure the cross-section of interaction for the production of terbium using an alpha beam incident on a europium target has begun. Preliminary results are currently being analysed.

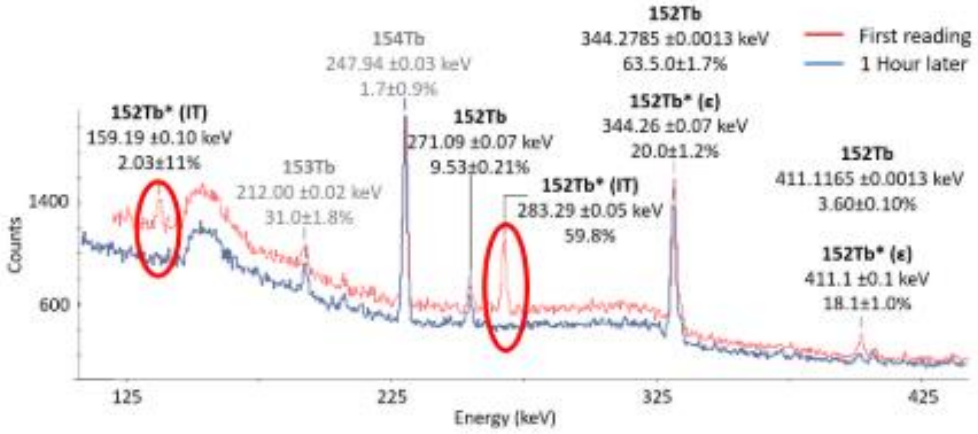

Figure 4. Calibrated section between 125 keV and 425 keV of the irradiated natural Eu foil gamma spectra, labelled with identified gamma energies and isotopes responsible for energy peaks

2.2. Gadolinium target

To identify which terbium isotopes could be produced using a proton beam incident on a gadolinium target, a natural gadolinium target was used. There are seven natural isotopes of gadolinium compared to the two of europium. This increases the complexity of production when comparing cross-section of interaction. The energy of the proton beam was selected using TALYS cross-section calculations. The energy select was to ideally produce a high yield of ^{155}Tb. A preliminary analysis of the gamma spectra collected of the target (see figure 5) revealed that ^{155}Tb was produced. The quantity of ^{155}Tb produced and the identification of the other isotopes present require further study.

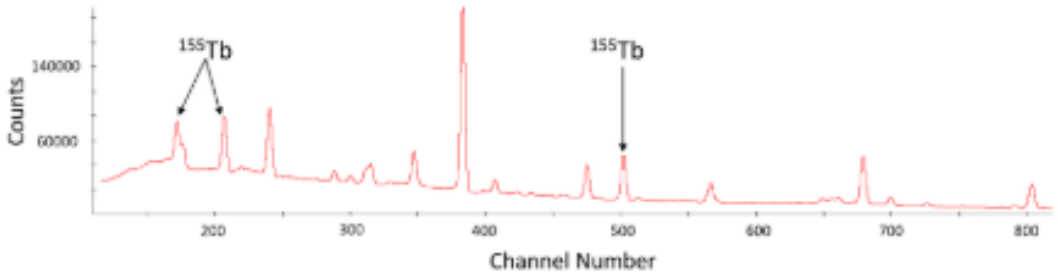

Figure 5. Preliminary identification of ^{155}Tb in an irradiated natural Gd foil

Summary

This preliminary study proved that the ^{152}Tb isotope can successfully be produced at the MC40 cyclotron using an alpha beam on a europium target, and the ^{155}Tb isotope could also be produced using a proton beam on a gadolinium target. The cross-section for the the production of terbium in each of these cases will be calculated from the spectra collected and compared to the predicted cross-section made by PACE4, TALYS and EMPIRE [10].

The optimal beam energy for the production of each isotope will then be determined from the cross-sections. Enriched targets will be used to gain a higher yield of the desired isotope and reduce other terbium isotope contaminants which can not be removed by radio-chemical separation at NPL.

References

[1] Formento Cavaier R and et al 2017 *Physics Procedia* **90** 157–163
[2] Müller C and et al 2012 *J Nucl Med* **53** 1951–1959
[3] Müller C and et al 2014 *J. High Energy Phys.* Nuclear Medicine and Biology **40** e58–e65
[4] Müller C and et al 2016 *EJNMMI Research* **35** 1–10
[5] Müller C and et al 2019 *EJNMMI Research* **49** 1919–1930
[6] Webster B and et al 2019 *Nature Scientific Reports* **9** 10884
[7] Tarasov O and Bazin D 2008 *NIM B* **266** 4657–4664
[8] Gavron A 1980 *Phys.Rev.* **C 21** 230–236
[9] Koning A, Hilaire S and Duijvestijn M 2008 *EDP Sciences* 211–214
[10] Herman M, Capote R, Carlson B, Obložinský P, Sin M, Trkov A, Wienke H and Zerkin V 2007 *Nucl. Data Sheets* **108** 2655

Appendix R – Duchemin *et al.* (2021)

C. Duchemin, J. P. Ramos, T. Stora, … P. Ivanov, … B. Russell, … B. Webster et al., CERN-MEDICIS: A Review Since Commissioning in 2017, Front. Med., 2021, **8**, 693682, 1-11[219]

frontiers in Medicine

ORIGINAL RESEARCH
published: 15 July 2021
doi: 10.3389/fmed.2021.693682

OPEN ACCESS

Edited by:
Jean-Pierre Pouget, Institut National de la Santé et de la Recherche Médicale (INSERM), France

Reviewed by:
Valery Radchenko, TRIUMF, Canada
Pierre Delahaye, UPR3266 Grand Accélérateur National d'Ions Lourds (GANIL), France

***Correspondence:**
Charlotte Duchemin
charlotte.duchemin@cern.ch

Specialty section:
This article was submitted to Nuclear Medicine, a section of the journal Frontiers in Medicine

Received: *11 April 2021*
Accepted: *15 June 2021*
Published: *15 July 2021*

Citation:
Duchemin C, Ramos JP, Stora T, Ahmed E, Aubert E, Audouin N, Barbero E, Barozier V, Bernardes A-P, Bertreix P, Boscher A, Bruchertseifer F, Catherall R, Chevallay E, Christodoulou P, Chrysalidis K, Cocolios TE, Comte J, Crepieux B, Deschamps M, Dockx K, Dorsival A, Fedosseev VN, Fernier P, Formento-Cavaier R, El Idrissi S, Ivanov P, Gadelshin VM, Gilardoni S, Grenard J-L, Haddad F, Heinke R, Juif B, Khalid U, Khan M, Köster U, Lambert L, Lilli G, Lunghi G, Marsh BA, Palenzuela YM, Martins R, Marzari S, Menaa N, Michel N, Munos M, Pozzi F, Riccardi F, Riegert J, Riggaz N, Rinchet J-Y, Rothe S, Russell B, Saury C, Schneider T, Stegemann S, Talip Z, Theis C, Thiboud J, van der Meulen NP, van Stenis M, Vincke H, Vollaire J, Vuong N-T, Webster B, Wendt K, Wilkins SG and the CERN-MEDICIS collaboration (2021) CERN-MEDICIS: A Review Since Commissioning in 2017. Front. Med. 8:693682. doi: 10.3389/fmed.2021.693682

CERN-MEDICIS: A Review Since Commissioning in 2017

***Charlotte Duchemin*[1,2*], *Joao P. Ramos*[1,2], *Thierry Stora*[1], *Essraa Ahmed*[2], *Elodie Aubert*[1], *Nadia Audouin*[3], *Ermanno Barbero*[1], *Vincent Barozier*[1], *Ana-Paula Bernardes*[1], *Philippe Bertreix*[1], *Aurore Boscher*[1], *Frank Bruchertseifer*[4], *Richard Catherall*[1], *Eric Chevallay*[1], *Pinelopi Christodoulou*[1], *Katerina Chrysalidis*[1], *Thomas E. Cocolios*[2], *Jeremie Comte*[1], *Bernard Crepieux*[1], *Matthieu Deschamps*[1], *Kristof Dockx*[2], *Alexandre Dorsival*[1], *Valentin N. Fedosseev*[1], *Pascal Fernier*[1], *Robert Formento-Cavaier*[1,3], *Safouane El Idrissi*[1], *Peter Ivanov*[5], *Vadim M. Gadelshin*[1,6], *Simone Gilardoni*[1], *Jean-Louis Grenard*[1], *Ferid Haddad*[3], *Reinhard Heinke*[1,2], *Benjamin Juif*[1], *Umair Khalid*[1,7], *Moazam Khan*[1,7], *Ulli Köster*[8], *Laura Lambert*[1], *G. Lilli*[1], *Giacomo Lunghi*[1], *Bruce A. Marsh*[1], *Yisel Martinez Palenzuela*[2], *Renata Martins*[1], *Stefano Marzari*[1], *Nabil Menaa*[1], *Nathalie Michel*[3], *Maxime Munos*[1], *Fabio Pozzi*[1], *Francesco Riccardi*[1], *Julien Riegert*[1], *Nicolas Riggaz*[1], *Jean-Yves Rinchet*[1], *Sebastian Rothe*[1], *Ben Russell*[5], *Christelle Saury*[1], *Thomas Schneider*[1], *Simon Stegemann*[1,2], *Zeynep Talip*[9], *Christian Theis*[1], *Julien Thiboud*[1], *Nicholas P. van der Meulen*[9], *Miranda van Stenis*[1], *Heinz Vincke*[1], *Joachim Vollaire*[1], *Nhat-Tan Vuong*[1], *Benjamin Webster*[5], *Klaus Wendt*[6], *Shane G. Wilkins*[1] *and the CERN-MEDICIS collaboration*

[1] *Organisation Européenne pour la Recherche Nucléaire (CERN), Geneva, Switzerland,* [2] *Katholieke Universiteit (KU) Leuven, Institute for Nuclear and Radiation Physics, Leuven, Belgium,* [3] *Groupement d'Intérêt Public ARRONAX, Nantes, France,* [4] *European Commission, Joint Research Centre, Nuclear Safety and Security, Karlsruhe, Germany,* [5] *National Physical Laboratory, Teddington, United Kingdom,* [6] *Johannes Gutenberg University, Mainz, Germany,* [7] *Pakistan Institute of Nuclear Science and Technology, Islamabad, Pakistan,* [8] *Institut Laue Langevin, Grenoble, France,* [9] *Paul Scherrer Institute, Villigen, Switzerland*

The CERN-MEDICIS (MEDical Isotopes Collected from ISolde) facility has delivered its first radioactive ion beam at CERN (Switzerland) in December 2017 to support the research and development in nuclear medicine using non-conventional radionuclides. Since then, fourteen institutes, including CERN, have joined the collaboration to drive the scientific program of this unique installation and evaluate the needs of the community to improve the research in imaging, diagnostics, radiation therapy and personalized medicine. The facility has been built as an extension of the ISOLDE (Isotope Separator On Line DEvice) facility at CERN. Handling of open radioisotope sources is made possible thanks to its Radiological Controlled Area and laboratory. Targets are being irradiated by the 1.4 GeV proton beam delivered by the CERN Proton Synchrotron Booster (PSB) on a station placed between the High Resolution Separator (HRS) ISOLDE target station and its beam dump. Irradiated target materials are also received from external institutes to undergo mass separation at CERN-MEDICIS. All targets are handled via a remote handling system and exploited on a dedicated isotope separator beamline. To allow for the release and collection of a specific radionuclide of medical interest, each target is heated to temperatures of up to 2,300°C. The created ions are extracted and accelerated to an energy up to 60 kV, and the beam steered through an off-line sector field magnet mass separator. This is followed by the extraction of the radionuclide of interest through mass separation and its subsequent implantation into a collection foil.

In addition, the MELISSA (MEDICIS Laser Ion Source Setup At CERN) laser laboratory, in service since April 2019, helps to increase the separation efficiency and the selectivity. After collection, the implanted radionuclides are dispatched to the biomedical research centers, participating in the CERN-MEDICIS collaboration, for Research & Development in imaging or treatment. Since its commissioning, the CERN-MEDICIS facility has provided its partner institutes with non-conventional medical radionuclides such as Tb-149, Tb-152, Tb-155, Sm-153, Tm-165, Tm-167, Er-169, Yb-175, and Ac-225 with a high specific activity. This article provides a review of the achievements and milestones of CERN-MEDICIS since it has produced its first radioactive isotope in December 2017, with a special focus on its most recent operation in 2020.

Keywords: CERN, MEDICIS, medical, radionuclides, mass separation

INTRODUCTION

Since the publication of the first official use of radionuclides administered to a patient to treat cancer in the 1930s, huge progress has been made. Several radionuclides are currently widely available as radiopharmaceuticals and mainly used to either diagnose or treat cancer. Research in nuclear medicine is ongoing with a growing interest in personalized treatment and diagnosis, the so-called theranostics approach. Adapting the treatment to each patient's pathology requires to have a large panel of approved radiopharmaceuticals available in order to give access to novel and diverse treatment modalities. The big advantage of personalized and targeted treatment is that individual pathologies can be taken into account and the destruction of the surrounding healthy tissue can be minimized by careful selection of the adequate radionuclide. In order to obtain such radiopharmaceuticals, one needs to produce a specific radionuclide with the highest isotopic and chemical purities within a standardized workflow and in sufficient quantities. These radionuclides can be created via the irradiation of a stable target material in particle accelerators or in nuclear reactors. However, additional processes are usually needed to reach the purity level necessary for the preclinical experiments and clinical trials. Depending on the radionuclide of interest, such purification can be attained either by means of chemical separation or by combining mass and chemical separation. Based on the strong expertise in mass separation of radioisotopes existing for more than 50 years at CERN's Isotope Separator On-Line DEvice facility (ISOLDE) (1), a project dedicated to medical applications has been initiated by CERN in 2010. The idea behind this new and unique facility is to produce non-conventional radionuclides having the required properties for both imaging and treatment as well as to expand the range of radionuclides available for the medical research in hospitals and in research centers across Europe. The facility has been funded with contributions from the CERN Knowledge Transfer Fund, private foundations and partner institutes, as well as benefitting from a European Commission Marie Skłodowska-Curie training grant titled MEDICIS-Promed. After the ground-breaking in September 2013 this new facility (see **Figure 1**), baptized MEDICIS (MEDical Isotopes Collected from ISolde), entered its commissioning phase in autumn 2017 (2). In Europe, a number of facilities producing radioactive beams by online isotope mass separation (ISOL) are currently operating such as ISOLDE at CERN, ALTO at IJC-Lab and SPIRAL-1 at GANIL, while ISAC at TRIUMF in Canada is also exploiting ISOL rare-isotope beams. While these facilities can technically produce isotopes for medical applications, their research activities are focused on fundamental and applied studies in nuclear physics with pure exotic radioactive beams through mass separation. Currently, CERN-MEDICIS is the only European facility which dedicates its full program to the production and delivery of medical isotopes for research in radiopharmaceutical science, operating in batch isotope mass separation mode. CERN-MEDICIS is also at the heart of a new European project called PRISMAP which is a consortium of 23 institutes in order to translate the emerging radionuclides into medical diagnosis and treatment, in which isotope mass separation plays an important role to achieve appropriate specific activities or radionuclidic purities. In the future, the SPES facility in Italy and the ISOL@MYRRHA facility in Belgium also aims to produce pure exotic radioactive beams and medical isotopes.

THE MEDICIS COLLABORATION AND ITS RESEARCH PROJECTS: FROM ITS BEGINNINGS TO THE PRESENT

CERN-MEDICIS produced its first radionuclides for medical research after an off-line mass separation on the 12th of December 2017. Tb-155 was the first radionuclide collected at MEDICIS, of the four terbium radioisotopes that are highly promising for cancer diagnosis and treatment. After this successful and promising commissioning phase, CERN-MEDICIS formally became a collaboration the year after, with the signature of the Memorandum of Understanding and the first collaboration board meeting held at CERN. The members of the collaboration (3) are experts in medical radionuclide production, nuclear medicine, radiochemistry and nuclear research. They hail from research institutes, hospitals and universities: GIP ARRONAX (France), CHUV (Switzerland), EANM (Europe), FABIS (Spain), HUG (Switzerland), ILL (France), IST (Portugal),

FIGURE 1 | The CERN-MEDICIS building completed in 2017.

TABLE 1 | MEDICIS collaboration boards, number of institutes taking part in the MEDICIS collaboration, number of submitted projects and list of radionuclides of interest.

Board number	Date	Number of institutes in the collaboration	Number of projects	Radionuclide(s) of interest
1	21/02/2018	12	13	C-11, Sc-43, Sc-44, Sc-47, Cu-67, Xe-131m, Xe-133m, Tb-149, Tb-152, Tb-155, Er-169
2	03/10/2018		3	Sc-44, Sc-47, Tb-149, Tb-155
3	20/03/2019		7	Fe-52, Fe-59, Tb-149, Tb-152, Tb-155, Tm-167, Er-169, Yb-175, Pt-191, Pt-193m, Pt-195m
4	18/09/2019		1	Ac-225, Ac-227
5	20/02/2020		1	Sm-153
6	17/09/2020		2	Cu-64, Ac-225
7	11/03/2021	14	4	Ba-128/Cs-128, Ce-134/La-134, Tb-149, Tb-152, Ac-225

JGU Mainz (Germany), JRC Karlsruhe (Germany), KU Leuven (Belgium), NPL (UK), PSI (Switzerland), PAEC (Pakistan), RTU-LU (Latvia). PAEC and RTU-LU officially joined the MEDICIS collaboration in 2021 (see **Table 1**). Biomedical projects are regularly submitted to the collaboration board, which evaluates the needs of the community as well as the technical feasibility and provides recommendations. In that way, the CERN-MEDICIS scientific program and list of radionuclides are defined. Since 2018, 31 projects have been submitted to the collaboration board in the biannual collaboration meetings that have already taken place (see **Table 1**). Through the list of approved projects (3), one can see strong interest in lanthanides and particularly terbium radioisotopes including the alpha emitter Tb-149 (4), the positron emitter Tb-152 (5) and the gamma and Auger emitter Tb-155 (6). The medical and scientific community also identified some scandium radioisotopes, such as Sc-44 for Positron Emission Tomography (PET) (7) and Sc-47 for use in both therapy and Single Photon Emission Computed Tomography (SPECT) (8). Cu-67 is a radionuclide being proposed among the projects that would be well-suited for theranostic applications (9). CERN-MEDICIS focuses also on the delivery of mass-separated Sm-153, Tm-167, Er-169, Yb-175, Hg-191/Pt-191 and the alpha emitter Ac-225. From the first year of operation in 2018 to the end of 2020, MEDICIS has provided nine different external research institutes or hospitals with 41 batches of high specific-activity radionuclides. This has been done within the framework of 12 approved projects. Since 2017, production and mass separated isotopes at CERN-MEDICIS support ongoing research programs by providing high purity products which are not accessible in cyclotrons or reactors without mass separation. Even though some of the above-mentioned radionuclides can be efficiently produced in reactors or cyclotrons, they are produced with isotopic impurities that can only be removed by going through a mass separation process. For example, Ac-227 will be a co-product of Ac-225 and some isotopes such as Tb-153, Tb-154, Tb-156 will be generated as contaminants of Tb-155. High Specific Activity (HSA) radionuclides from neutron activated targets can also be provided, such as HSA Er-169 which is otherwise not achievable.

MEDICIS' MODES OF OPERATION FOR RADIONUCLIDE PRODUCTION

One of the main features of CERN-MEDICIS is that it can profit from several irradiation possibilities to produce its isotopes before proceeding to the off-line mass separation of the radionuclide of medical interest (10). The facility has the opportunity to irradiate targets at CERN in the ISOLDE primary area. Every target unit is compatible with both, the ISOLDE and MEDICIS facilities, and is composed of an aluminum water-cooled vacuum vessel. The latter encloses a tubular tantalum oven inside of which a target material, ready for irradiation, is placed. This oven is connected to an ion source via a transfer line [more details can be found in (11)]. The MEDICIS target is installed for irradiation behind one of the ISOLDE's target station (HRS) and before the beam dump via an automatic rail conveyor system (RCS). The MEDICIS target can be:

FIGURE 2 | The MEDICIS robot about to transfer a target from the RCS to the target station.

- directly irradiated by the 1.4 GeV proton beam delivered by the CERN Proton Synchrotron Booster (12);
- indirectly irradiated by the fraction of the primary proton beam (>65%) which did not interact with the HRS target, as well as by its secondary particle showers [see more details in (10)] – so-called parasitic mode.

Once the MEDICIS target has been irradiated, it is transported back to a decay point via the same RCS. From this point onward a dedicated robot, from the KUKA® company, handles the target (see **Figure 2**) and is used to safely connect the target to the MEDICIS target station to subsequently start with the collection of the radionuclide of interest. It should be noted that with this mode of operation and since the full target unit is subjected to the proton and secondary particle fluences, not only the target material located inside the target oven is activated but the full unit is. In 2017 and 2018, 11 targets were irradiated and used for mass separation at CERN-MEDICIS, with some of them irradiated up to five times.

However, since the start-up of the Large Hadron Collider (LHC), accelerator operation at CERN is intermitted by extended upgrade and maintenance periods called Long Shutdowns (LS). During these periods the full accelerator chain is stopped and no protons can be delivered to the various CERN experiments. The first LS took place from February 2013 to mid-2014, followed by the second from January 2019 to mid-2021. CERN-MEDICIS is one of the very few facilities at CERN which was still operating during the second Long Shutdown (LS2). During the years 2019 and 2020, CERN-MEDICIS performed off-line mass separation of medically important radionuclides from materials irradiated at external partner institutes. This operation mode is being exploited since the first successful feasibility test carried out in 2018 with the mass separation and the collection of 18 MBq of Er-169 from naturally abundant Er-168, irradiated in the reactor of ILL in Grenoble (France) (13, 14). Each externally irradiated material to be mass separated is shipped to CERN-MEDICIS and it arrives either in sealed quartz vials or inside a dedicated

FIGURE 3 | PVD set-up with zinc filled molybdenum boat (picture on the left) with **(A)** the shutter, **(B)** the Molybdenum crucible with Zinc granulates and **(C)** the High Voltage lines – Zinc-coated gold foils (picture on the right).

FIGURE 4 | Dose rate measurement on the first collection of Tb-155 at CERN-MEDICIS.

sample holder, developed at CERN in 2019. It is a tight fit made of a tantalum cylinder with an inner part rhenium foil lining, coming with its plexiglass protection. The latter has been designed to prevent any contamination of the transport container and to guarantee an easy, rapid and safe transfer of the externally irradiated sample into the empty oven of the target unit. It was made to avoid any risk of dispersion and contamination as well as to limit the radiation exposure of the operator. All the externally irradiated materials imported to CERN-MEDICIS in 2020 were received inside this new piece of equipment and no contamination incident has been reported to date. In the case of reception of sealed quartz vials, the decontamination, opening and transfer into the target's empty oven were performed at CERN-MEDICIS using a dedicated automatic transfer system. Once the target unit is loaded with the radioactive material, it is handed over to the robot which couples it onto the MEDICIS target station in view of the mass separation and collection. It should be noted that in the case of externally irradiated material and in contrast to the mode of operation that involves the irradiation with protons at CERN in the ISOLDE target area, there is no activation of the target unit itself.

In 2019 and 2020, CERN-MEDICIS received and used 34 externally irradiated target materials. These radioactive samples were provided by the GIP ARRONAX in Nantes (France), ILL in Grenoble (France), JRC in Karlsruhe (Germany), PSI in Villigen (Switzerland) and SCK CEN in Mol (Belgium).

Regardless of the irradiation conditions and modes utilized, each target unit, once coupled to the target station by the robot, is heated up to very high temperatures to allow for the diffusion and effusion of the isotopes of interest. Even though the optimal temperature differs for each target material and radionuclide to be mass separated, these temperatures often reach more than 2,000°C. The isotopes pass through an ion source, where they are ionized and subsequently accelerated to be sent through a mass separator (dipole magnet) as Radioactive Ion Beams (RIBs). More information regarding the MEDICIS beam line can be found in (15). Furthermore, the MELISSA laser laboratory (16, 17) helps to increase the separation efficiency and the selectivity. The

TABLE 2 | Predicted activity gains from a direct irradiation in comparison to the indirect mode.

Target material	Titanium		Tantalum		ThO_2	
Radionuclide	Sc-44	Sc-47	Tb-149	Tb-152	Tb-155	Ac-225
Activity ratio $\frac{\text{Direct}}{\text{Indirect}}$	15	13	14	13	12	15

extracted radionuclides are usually implanted onto thin zinc-coated gold foils. The foils are prepared under high vacuum using 99.995% pure zinc granulate thermally heated in a molybdenum boat and evaporated onto the 0.25 mm thick gold substrates (**Figure 3**). With the assistance of a build-in INFICON thickness sensor the layer thickness is determined to 500 nm in this Physical Vapor Deposition (PVD) process. Preparation and cleaning of the gold plates (surface roughening and ultrasonic cleaning) is crucial for the zinc adherence and layer uniformity.

After the implantation, the foils are safely retrieved from the collection chamber and transported to a shielded fume hood by using a shielded trolley. This is followed by their shipment to one of CERN-MEDICIS' partner institutes.

MEDICIS' OPERATION FROM DECEMBER 2017 TO DECEMBER 2020: A REVIEW

2017: The First Radioactive Beam

The 10th of November 2017 marked the beginning of CERN-MEDICIS' operation with the start of hardware commissioning (power converters) and the polarization at 30 kV of the ion source platform for secondary ion beam generation. It was followed by the extraction of the first stable isotope beam 5 days later. The first target, containing 250 g of tantalum rolls as material inside the target oven, was irradiated for 24 h on the 5th of December 2017. One month later, the commissioning of the facility was completed with the first collection of Tb-155 (18) (see **Figure 4**). One Tb-155 sample was also shipped to the IST Lisboa (Portugal).

2018: A Full Year of Operation With the CERN Proton Beam

The year 2018 began with a technical stop of several months and stable beam tests, before CERN's proton beams were available again. In May 2018, CERN-MEDICIS was ready again to operate with irradiated targets and launch its first operation year. Beamtime was devoted to nine different approved projects through the year. It included several developments within the MEDICIS-Promed European Commission Marie Sklodowska-Curie innovative training program with, as examples, the successful separation of Er-169 from externally irradiated Er-168 (13, 14) as feasibility tests in preparation for LS2, as well as promising C-11 diffusion studies (19). In total, 5.5×10^{19} protons have been directed to the ISOLDE HRS target station in 2018, among which 44% could be exploited for the MEDICIS program (i.e., 2.4×10^{19} protons). It includes 6.0E18 protons (11%) that have been directly sent to the MEDICIS irradiation point by deflecting the proton beam below the upstream ISOLDE target while the latter was being set up for physics runs. This direct

TABLE 3 | Summary of the collections performed at CERN-MEDICIS in 2018, 2019 and 2020.

Year	Irradiation modes	Medical isotopes	Collected activity (MBq)	Maximum collection efficiency[a] (%)	Number of batches delivered	Number of projects concerned	Number of new targets
2018	CERN PSB & external irradiations	C-11, Tb-149, Tb-152, Tb-155, Tm-165, Er-169	235	1.6	4	2	12
2019	External irradiations	Tb-155, Er-169, Yb-175, Pt-195m	870	6.0	15	5	8
2020	External irradiations	Sm-153, Tb-155, Tm-167, Ac-225	540	22.5 (53% separated[b])	16	5	3

[a]*Calculated as the ratio between the total activity measured on the collection foils at the end of the collection and the activity present inside the target container at start of the collection.* [b]*An efficiency of 53% has been measured by the on-line γ-spectrometer but due to sputtering effects, part of the activity has been lost on the foils' support and inside the collection chamber.*

irradiation mode allows for considerably increasing the activity, which can be produced in the MEDICIS targets. Based on FLUKA Monte Carlo (20, 21) simulations (CERN version 4.1), a study performed on the radionuclide production in such a target being either directly or indirectly irradiated (see scenarios presented in section MEDICIS' Modes of Operation for Radionuclide Production) has been carried out (22). It focused on the activity of several radionuclides of interest for CERN-MEDICIS produced after different irradiation times ranging from 1 h to several days, in combination with 1 h of cooling time. For the indirect irradiation scenario, a UCx target has been placed upstream of the MEDICIS target. As a result, the gain in the activity produced using the direct irradiation mode ranges on average between 12 and 15 for Ac-225, Sc and Tb radioisotopes (see **Table 2**).

It should be noted that the high activity levels after the retrieval of the target units did not allow for quantitative activity measurements by gamma-ray spectroscopy. Dose rate measurements of the full target units have been carried out which confirm an expected notable gain in activation levels after direct irradiation. For example, a comparison of the previously described scenario yielded a ratio of 10 in the case of Ta target units. However, one should keep in mind that this value should be understood as an indication as it is based on measurements of the full target unit and not of a specific radionuclide.

Five radionuclides of medical interest were collected in 2018: Er-169, Tb-149, Tb-152, Tb-155 and Tm-165, a generator of the Auger electron emitter Er-165. The collected activities ranged from 1 to 137 MBq with separation efficiencies up to 1.6% (10). Two research institutes, the Centre Hospitalier Universitaire Vaudois (CHUV) in Lausanne (Switzerland) and the National Physical Laboratory (NPL) in Teddington (UK), respectively, received batches of Tb-149 and Tb-155. Within this framework, MEDICIS successfully showed its capability to collect and deliver the short half-life radionuclide Tb-149 ($T_{1/2}$ = 4.1 h) with a delay between the end of the target irradiation and the shipment departure of less than two half-lives. A total of 1.7 GBq of activity was handled in 2018, including the activity coming from isobars/impurities. Out of this value, 235 MBq could be exploited for medical applications. Twelve target units, including prototypes, were used for the CERN-MEDICIS program in 2018. Some of these targets were irradiated up to five times. This mode of operation significantly reduces the amount of generated radioactive waste and the costs. Including machine development runs, 220 h were devoted to the collection of radionuclides in 2018. CERN-MEDICIS profited from 20 irradiations slots and could proceed with 15 collection campaigns (see summary in **Table 3**). Although typically performed on zinc-coated gold foils, preliminary tests have been performed with the implantation of radionuclides in KNO_3 salt layer deposited on thin aluminum foils. The latter has been done within preliminary radiochemistry developments performed at CERN-MEDICIS and in view of simplifying the post-implantation radiochemistry process by recovery of the implanted activity in buffered aqueous solutions.

After a second collaboration board meeting on the 3rd of October 2018 (see **Table 1**), additional irradiation slots on the MEDICIS irradiation point were approved to extend the so-called ISOLDE nuclear physics winter program. Long-lived radionuclides were further extracted at the beginning of CERN's shutdown period, with Be-7 and radium monofluoride molecule beams, producing one of the ISOLDE physics result highlights (23).

After the last proton beam delivered at CERN on the 12th of November 2018, CERN-MEDICIS entered its technical stop period for maintenance and upgrade.

2019: A Year Without Protons at CERN Compensated by the Use of Externally Irradiated Target Materials

CERN-MEDICIS' second year of operation started with a 6 months technical stop dedicated to maintenance and upgrade, followed by a commissioning phase. Notably, in February the MEDICIS target storage shelves became fully operational (see **Figure 5**).

It was followed by the successful commissioning of the shielded fume hood in March into which the collection foils can be safely removed from their support, and where radiochemistry developments can be performed. Another milestone was reached in 2019 when the MELISSA laboratory (16, 17) became fully operational in April. The installed laser setup consisted of two Z-cavity Ti:sapphire lasers of the Mainz University/CERN design pumped by two 10 kHz pulsed Nd:YAG lasers InnoLas Nanio 532-18-Y (see **Figure 6**). Using intra-cavity frequency, doubling blue beams required for two-step resonant ionization

FIGURE 5 | The shielded storage shelves and the robot.

of rare-earth elements could be generated by this setup. The operating principle of MELISSA setup is identical to that of the ISOLDE resonance ionization laser ion source (RILIS) system (24). Since then, all collections performed at CERN-MEDICIS have profited from the added value and selectivity provided by MELISSA. The laser resonance ionization scheme for actinium (25, 26) is given as an example in **Figure 6**. A regularly updated compilation of laser schemes applied at RILIS systems can be found at http://riliselements.web.cern.ch/.

In June 2019, the CERN-MEDICIS target station was back in operation after the complete replacement of a defective extraction electrode on the MEDICIS beamline. The first collection of radionuclides started on the 2nd of July. The externally irradiated enriched Er-168 containing Er_2O_3 target was imported from ILL (France), from which 79 MBq of Er-169 was collected for shipment to PSI (Switzerland). CERN-MEDICIS operated in 2019 with target materials irradiated either at the nuclear research reactor of ILL or at the GIP ARRONAX cyclotron (France) until the end of the year.

Er-169, Yb-175 and Pt-195m have been produced in the reactor of ILL by neutron capture on enriched Er-168, Yb-174, and Pt-194, respectively. Due to the high quantity of stable isotopes present in the samples after neutron irradiation, mass separation allows to significantly increase the specific activity of the radionuclide of interest. An activity of 92 MBq of Pt-195m was shipped to the Hopitaux Universitaires de Genève (HUG) in Switzerland for preliminary tests prior to future mass separation. Throughout the year 2019, a total of 350 MBq of mass separated Er-169 was provided to PSI, together with 520 MBq of mass separated Yb-175 for radiochemical separation, quality control and proof-of-concept preclinical experiments (27).

ARRONAX provided its first sample containing Tb-155 at the beginning of August 2019, to be mass separated. It was produced by irradiating natural gadolinium foils by the 30 MeV proton beam on target delivered by its cyclotron (28). The sample was shipped to CERN-MEDICIS to separate the Tb-155 in mass from the stable gadolinium target atoms as well as from the other produced terbium isotopes. Three additional externally irradiated samples were provided by ARRONAX throughout the year 2019. Given the difficulties in extracting terbium isotopes from the irradiated gadolinium material, several weeks of stable beam tests have been dedicated to the operation optimization and laser scheme developments. In addition, post-irradiation radiochemistry had been performed at ARRONAX in order to reduce the proportion of gadolinium atoms in the sample and increase the mass separation efficiency. Two batches of mass separated Tb-155 were delivered to the National Physical Laboratory in the UK and to KU Leuven/SCK CEN in Belgium for radiochemical studies, detector calibration and isotope qualification.

The year 2019 can be summarized as 16 collection campaigns carried out within 922 h of operation (not including the weeks of operation devoted to stable beam tests). A total of 870 MBq of mass separated activity were delivered to the institutes with the addition of 92 MBq of Pt-195m. Four institutes and five different approved research projects could profit from these radionuclides. Eight target units were used throughout the year, with some of them used up to three times. Moreover, collection efficiencies up to 6% (for Yb-175) could be achieved which represents a significant improvement in comparison with the operation year 2018 (see **Table 3**). Last but not least CERN-MEDICIS welcomed 1400 visitors during CERN's Open Days on the 14th and 15th of September 2019.

2020: Record Separation Efficiencies Achieved With Externally Irradiated Target Materials

From January to March 2020 CERN-MEDICIS entered into a new technical stop for maintenance and upgrade. It included, among other works, the delicate replacement of a defective extraction electrode (a highly contaminated part) and the installation of a new gas injection system compatible with the use of chloride gas in view of producing molecular beams in the near future. Another improvement of the facility during the first semester 2020 was the integration of a compact Cadmium Zinc Telluride (CZT) γ-detector from Kromek® for the on-line monitoring of the collected activity being implanted onto the collection foils (see **Figure 7**) (29). The activity being accumulated during a collection can thus be monitored together with the radionuclidic purity of the beam impinging on the foil. Monitoring the implantation rate has helped in the daily operation and allowed for a notable increase in the separation efficiency, as shown in the following.

During the 5th collaboration board meeting, a new project regarding the mass separation of Sm-153 from externally irradiated targets of Sm-152 was proposed (see **Table 1**) (3). The project was approved by the board members with high priority for 2020.

The technical stop ended at the beginning of March, followed by its commissioning. It included software and stable beam tests until the 16th of March 2020. From that day onwards all CERN installations suspended their activities due to the Covid-19 sanitary crisis. In total, CERN-MEDICIS' operation was stopped for 10 weeks. During that time the official CERN-MEDICIS

FIGURE 6 | MELISSA laser set-up operational since April 2019 (picture on the left) and laser resonance ionization scheme for actinium (picture on the right).

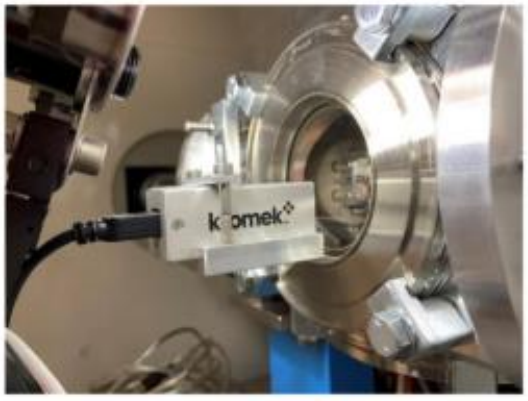

FIGURE 7 | CZT γ-ray detector installed in front of the window of the collection chamber and performing the on-line measurement of the activity being implanted on the foils.

website has been created as a portal for public outreach as well as exchange of information of the collaboration (3).

The operation of the facility restarted on the 25th of May, with the successful conditioning of the newly installed electrode, at voltages up to 65 kV. In parallel, an additional laser, provided by Mainz University, has been received and installed in MELISSA (see section 2019: A Year Without Protons at CERN Compensated by the Use of Externally Irradiated Target Materials). It is a grating-tunable Ti:sapphire cavity that considerably aids the scheme developments. Motorized etalon mounts and a laser beam stabilization system were installed to improve the long-term stability of the laser ion source. A beam imaging system was implemented to enable remote monitoring and diagnosis of the setup. These upgrades, combined with the additional laser system, allowed for improving the performance and reliability of the laser ion source during radionuclide collections as well as for increasing the number of elements for which the ion source can operate. In preparation of the near future mass separation of Sm-153, Tb-155 and Tm-167, the CERN-MEDICIS facility has dedicated several weeks of stable beam tests in synergy with MELISSA. From the use of an evaporated solution of Tb-159 (in 5% HNO_3) deposited on a rhenium foil, 3% of terbium separation efficiency has been achieved with target temperatures above 2,200°C. Tests performed with stable samarium have shown a separation efficiency of up to 31% with an optimal operation temperature found around 1,700°C. This temperature has subsequently been confirmed during the radioactive samarium collections by monitoring the optimum implantation rate with the online CZT detector. In addition, thulium separation efficiency measurements were performed. A solution of natural thulium was deposited and evaporated on natural Er_2O_3, in order to better reproduce the operation conditions with the irradiated material. Efficiencies ranging from 65% (pure thulium) to 60% (thulium with erbium oxide surplus) were achieved and dedicated systematic measurements on the influence of the presence of contaminants on the laser ionization efficiency were

performed by using different elements and ion source materials [more details can be found in (30)].

During the last week of June 2020 and after a successful, intensive and conclusive period of commissioning and stable beam production, the CERN-MEDICIS facility received the authorization to operate again with radioactive beams. The facility received its first externally irradiated target material of the year on 26th of June 2020. Radioactive ion beams have been produced at the end of June 2020 until the 9th of December 2020. The scientific program of the year focused on the mass separation, collection and delivery of four radionuclides of medical interest. It included the mass separation of Sm-153 ($t_{1/2}$ = 46.5 h), which is a β^- emitter having the advantage of a γ-emission at 103 keV that is detectable by external imaging devices. Sm-153 was initially produced from enriched Sm-152 targets and neutron capture reactions at the SCK CEN BR2 reactor (31). Additional batches of mass-separated Tb-155 were provided by CERN-MEDICIS to two partner institutes. This radionuclide had been initially produced at ARRONAX and shipped to CERN-MEDICIS for further processing. Moreover, the therapeutic radionuclide Tm-167 was produced from natural erbium targets irradiated by 22.8 MeV protons, at the Paul Scherrer Institute (30). Two samples of Ac-225 were provided to CERN-MEDICIS by JRC Karlsruhe in order to perform preliminary studies on separation efficiency and optimal operation temperatures within the framework of a project proposal approved at the 4th MEDICIS collaboration board. The study of the mass separation of this radionuclide was performed one time with Ac-225 being only deposited and dried on a rhenium foil and a second time with Ac-225 being deposited on a sample of thorium oxide as potential future irradiation target material.

The two extractions of Ac-225, with Ac-225 alone and Ac-225 deposited on a sample of ThO_2, led to separation efficiencies of 12.5 and 9.8%, respectively. Both were performed using surface and laser ionization. In the first scenario 1,900°C was found to be the optimal temperature, whereas temperatures above 2,300°C were necessary to extract the Ac-225 from ThO_2. These results represent important foundations for the operation in 2021 and provide input to the mass separation of Ac-225 from ThO_2 targets irradiated by the 1.4 GeV proton beam delivered by the CERN PS Booster. From the eight Sm-153 collection campaigns, the mass separated activities were ranging from 20 to 130 MBq. Depending on the initial activity present inside the target container at the start of the collection efficiencies of up to 12.7% were encountered. Separation efficiencies ranging between 1 and 6% were achieved during the four Tb-155 collections performed that year, to produce batches of mass separated Tb-155 with activities up to 20 MBq. By considering the activity given by the CZT γ-spectrometer which is monitoring the activity being implanted on the foils inside the collection chamber (see **Figure 7**), a maximum separation efficiency of 53% has been reached at CERN-MEDICIS that year, for the mass separation of Tm-167. However, during the three Tm-167 collection campaigns, sputtering effects of the implantation layer led to a loss of the activity on the frame of the foils' support as well as inside the collection chamber. From the activities measured after removal of the foils, a maximum efficiency value of 22.5% was observed (see **Table 3**). This figure is computed from the total activity measured on the collection foils during one collection campaign as a function of the activity which was present inside the target at the start of the collection on each foil (ranging from 75 to 120 MBq). The Tm-167 optimal operation temperature window was determined using progressing heating steps and found to be between 1,900 and 2,200°C. A detailed description is given in (30).

In 2020 a total of 17 collections have been performed with 16 batches shipped to four European partner institutes (PSI, SCK CEN/KU Leuven, CHUV and NPL). This corresponds to a total of 720 h of collection time. Only three new targets have been built for operation in 2020. Among these targets, one has been used 8 times and is still considered to be re-used in 2021 since no obvious sign of failure or decreased efficiency could be observed. In addition, three targets have been reutilized from 2019. Five approved projects could profit from high purity radionuclides delivered by CERN-MEDICIS in 2020 with a total of 530 MBq collected and shipped to our partners.

The radiochemistry activities have also progressed, starting from 2018. In 2020 the separation of the implanted isotopes from the zinc layer could take place at CERN-MEDICIS itself. Based on an ion-exchange chromatography, a method has been developed for the separation of the lanthanides collected in 2020 and has been tested for low activity levels, below 1 LA [Limite d'Autorisation according to the Swiss regulations (32)]. The parameters have been optimized specifically for three radiolanthanides, namely samarium, terbium and thulium. An automated system is also being developed to separate higher radioactivity levels. Irradiated metallic Pt-194 targets were converted into $PtCl_2$ at the partner institute PINSTECH (Islamabad, Pakistan) for the MED-022 project and will be used either directly or for Pt separation tests. In addition, the treatment of concentrated liquid radioactive acidic waste was performed in order to transform it into easily disposable solid waste.

MEDICIS IN 2021 AND BEYOND

Since its commissioning in December 2017, CERN-MEDICIS has shown its capability to deliver non-conventional radionuclides to its partner institutes with a gradual and continuous improvement of its capabilities. Despite the global public health crisis, the year 2020 brought important technical, operational and scientific results, partly reflected in other manuscripts of this topical issue (15, 27, 30, 31). It has been a successful year for the MEDICIS facility as well as for the new European Medical Isotope program—PRISMAP—which has been selected for funding (33). PRISMAP, backed by a consortium of 23 institutes, was approved for funding by the Research Infrastructures program INFRA-2-2020 of Horizon 2020 of the European Commission, in which isotope mass separation has been identified as an important step in the production of radiopharmaceuticals. PRISMAP aims to federate European key stakeholders for the translation of emerging radionuclides into medical diagnosis

and treatment. It has been initiated in May 2021, with mass separation and the CERN-MEDICIS facility at the center of the project.

The operation of the facility is stopped between January and May 2021 due to the construction of a new laboratory for the safe research and development of actinide nanomaterials as new target materials, which is being built as an annex to the CERN-MEDICIS laboratory. CERN-MEDICIS will continue providing its external partners with high specific activity radionuclides from June 2021 onward. Targets irradiated at CERN as well as externally irradiated materials will be exploited. The irradiation possibilities are foreseen to be extended thanks to a second irradiation station installed behind the second ISOLDE General Purpose Separator (GPS) target station. The results collected from the three past years of operation, together with the approved scientific program, have been used to set priorities on options for the upgrade of the facility. This notably includes studies to adapt the implantation layer to avoid sputtering, modification of the collection chamber for ion beam rasterizing and the possibility to collect multiple isotope beams in parallel. While the LHC injector upgrade (LIU) is coming to completion, proton beams from the PSB using the new Linac 4 injector will be available for the next 4 years. The next CERN Long Shutdown (LS3) will take place from the end of 2024 onward during which operation with external sources provided by the partner institutes, and produced in cyclotrons or reactors, will again become possible.

Within the CERN-MEDICIS collaboration and the PRISMAP European project, the list of isotopes will continue to be extended according to the needs of the community. By gaining experience during every year of operation, progressively larger activities will be produced and delivered to the research institute. With the aim to achieve a sustainable production scheme, which is among the goals of PRISMAP, further evolution could take place. This should be seen in the context of CERN's upgrade plans such as proton energy increases to 2 GeV or higher beam intensities that could further extend the present reach of the facility.

DATA AVAILABILITY STATEMENT

The original contributions presented in the study are included in the article/supplementary material, further inquiries can be directed to the corresponding author/s.

ETHICS STATEMENT

Written informed consent was obtained from the individual(s) for the publication of any potentially identifiable images or data included in this article.

AUTHOR CONTRIBUTIONS

TSt: project leader. CD and JPR: project coordination. CD: initial and final draft manuscript. All authors manuscript review and contribution to MEDICIS operation since 2017. CD and TSt: final approval of the version to be submitted. All authors contributed to the article and approved the submitted version.

FUNDING

Funding was also acknowledged through the CERN & Society Foundation, the Flanders Research Foundation (FWO), the CERN Knowledge Transfer fund and the European Commission (MEDICIS-Promed, H2020 contract #642889). The GIP ARRONAX acknowledges support from Equipex, Arronax-Plus n°ANR-11-EQPX-0004, Labex IRON n°ANR-11-LABX-18-01 and ISITE NExT n°ANR-16-IDEX-007.

ACKNOWLEDGMENTS

The authors would like to thanks all colleagues involved in the development and operation of the facility, notably from EN-CV, EN-SMM, SY-BI, SY-EPC, SY-STI, EN-HE, EN-DHO, HSE-RP, BE-OP, TE-VSC groups and the collaborating institutes. We wish to thank all the members of the CERN-MEDICIS collaboration for their commitment, support and advice.

REFERENCES

1. Catherall R, Andreazza W, Breitenfeldt M, Dorsival A, Focker GJ, Gharsa TP, et al. The ISOLDE facility. *J Physics G Nuclear Particle Phys.* (2017) 44:094002. doi: 10.1088/1361-6471/aa7eba
2. Dos Santos Augusto RM, Buehler L, Lawson Z, Marzari S, Stachura M, Stora T, et al. CERN-MEDICIS (MEDical Isotopes Collected from ISolde): a new facility. *Appl Sci.* (2014) 4:265–81. doi: 10.3390/app4020265
3. *CERN-MEDICIS Official Website, List of Collaborating Institutes and Approved Projects.* Available online at: https://medicis.cern/ (accessed April 7, 2021).
4. Müller C, Vermeulen C, Köster U, Johnston K, Türler A, Schibli R, et al. Alpha-PET with terbium-149: evidence and perspectives for radiotheragnostics. *EJNMMI Radiopharm Chem.* (2016) 1:5. doi: 10.1186/s41181-016-0008-2
5. Müller C, Singh A, Umbricht CA, Kulkarni HR, Johnston K, Benešová M, et al. Preclinical investigations and first-in-human application of 152Tb-PSMA-617 for PET/CT imaging of prostate cancer. *EJNMMI Res.* (2019) 9:68. doi: 10.1186/s13550-019-0538-1
6. Webster B, Ivanov P, Russell B, Collins S, Stora T, Ramos JP, et al. Chemical purification of terbium-155 from pseudo-isobaric impurities in a mass separated source produced at CERN. *Sci Rep.* (2019) 9:10884 doi: 10.1038/s41598-019-47463-3
7. Huclier-Markai S, Alliot C, Kerdjoudj R, Mougin-Degraef M, Chouin N, Haddad F. Promising scandium radionuclides for nuclear medicine: a review on the production and chemistry up to in vivo proofs of concept. *Cancer Biother Radiopharm.* (2018) 33:316–29. doi: 10.1089/cbr.2018.2485
8. Müller C, Bunka M, Haller S, Köster U, Groehn V, Bernhardt P, et al. Schibli. Promising prospects for 44Sc-/47Sc-based theragnostics: application of 47Sc for radionuclide tumor therapy in mice. *J Nucl Med.* (2014) 55:1658–64. doi: 10.2967/jnumed.114.141614
9. Biggin C, Harris M, Hedt A, Jeffer C. Radiological properties of next generation theranostics (Cu-64/Cu-67). *J Nucl Med.* (2017) 58:1014.
10. Duchemin C, Ramos JP, Stora T, Aubert E, Audouin N, Barbero E, et al. CERN-MEDICIS: a unique facility for the production of non-conventional radionuclides for the medical research. In: *11th International Particle Accelerator Conference.* Caen: JACoW Publishing. (2020). p. 75–9.

11. Köster U. ISOLDE target and ion source chemistry. *Radiochim Acta.* (2001) 89:749. doi: 10.1524/ract.2001.89.11-12.749
12. Hanke K. Past and present operation of the CERN PS booster. *Int J Modern Phys A.* (2013) 28:1330019. doi: 10.1142/S0217751X13300196
13. Formento-Cavaier R, Köster U, Crepieux B, Gadelshin VM, Haddad F, Stora T, et al. Very high specific activity erbium 169Er production for potential receptor targeted therapy. *Nuclear Instruments Methods Phys Res Section B.* (2020) 463:468–71. doi: 10.1016/j.nimb.2019.04.022
14. Köster U, Calzavara Y, Fuard S, Samuel M, Dorrer H, Zhernosekov K, et al. Radioisotope production at the high-flux reactor of Institut Laue Langevin. *Radiother Oncol.* (2012) 102:S169–70. doi: 10.1016/S0167-8140(12)70279-7
15. Martinez Palenzuela Y, Barozier V, Chevallay E, Cocolios TE, Duchemin C, Fernier P, et al. *The CERN-MEDICIS Isotope Separator Beam Line.* (2020).
16. Gadelshin VM, Barozier V, Cocolios TE, Fedoseev VN, Formento-Cavaier R, Haddad F, et al. MELISSA: laser ion source setup at CERN-MEDICIS facility. *NIMB.* (2020) 463:460–3. doi: 10.1016/j.nimb.2019.04.024
17. Gadelshin VM, Wilkins S, Fedosseev VN, Barbero E, Barozier V, Bernardes AP, et al. First laser ions at the CERN-MEDICIS facility. *Hyperfine Interact.* (2020) 241:55. doi: 10.1007/s10751-020-01718-y
18. CERN press release of the 12th of December 2017. *New CERN Facility Can Help Medical Research Into Cancer* (2017). Available online at: https://home.cern/news/press-release/cern/new-cern-facility-can-help-medical-research-cancer (accessed April 07, 2021).
19. Stegemann S, Cocolios TE, Dockx K, Leinders G, Popescu L, Ramos JP, et al. Production of intense mass separated ^{11}C beams for PET-aided hadron therapy. *Nuclear Instruments Methods Section B.* (2020) 463:403–7. doi: 10.1016/j.nimb.2019.04.042
20. Battistoni G, Boehlen T, Cerutti F, Chin PW, Esposito LS, Fassò A, et al. Overview of the FLUKA code. *Ann Nuclear Energy.* (2015) 82:10–18. doi: 10.1016/j.anucene.2014.11.007
21. Bohlen TT, Cerutti F, Chin MPW, Fassò A, Ferrari A, Ortega PG, et al. The FLUKA code: developments and challenges for high energy and medical applications. *Nuclear Data Sheets.* (2014) 120:211–4. doi: 10.1016/j.nds.2014.07.049
22. Duchemin C. *Radionuclide Production Estimate at CERN-MEDICIS, CERN Technical Note EDMS* (2021). p. 2478044.
23. Garcia Ruiz R, Berger R, Billowes J, Binnersley CL, Bissell ML, Breier AA, et al. Spectroscopy of short-lived radioactive molecules. *Nature.* (2020) 581:396–400. doi: 10.1038/s41586-020-2299-4
24. Fedosseev VN, Chrysalidis K, Goodacre TD, Marsh BA, Rothe S, Seiffert C, et al. Ion beam production and study of radioactive isotopes with the laser ion source at ISOLDE. *J. Phys G Nucl Particle Phys.* (2017) 44:084006. doi: 10.1088/1361-6471/aa78e0
25. Ferrer R, Barzakh A, Bastin B, Beerwerth R, Block M, Creemers P, et al. Towards high-resolution laser ionization spectroscopy of the heaviest elements in supersonic gas jet expansion. *Nat Commun.* (2017) 8:14520. doi: 10.1038/ncomms14520
26. Raeder S, Dombsky M, Heggen H, Lassen J, Quenzel T, Sjödi M, et al. In-source laser spectroscopy developments at TRILIS—towards spectroscopy on actinium and scandium. *Hyperfine Interact.* (2013) 216:33–9. doi: 10.1007/s10751-013-0832-7
27. Talip Z, Borgna F, Müller C, Ulrich J, Duchemin C, Ramos JP, et al. Production of mass separated Er-169 towards the first preclinical in vitro. *Front Med.* (2021) 8:643175. doi: 10.3389/fmed.2021.643175
28. Haddad F, Ferrer L, Guertin A, Carlier T, Michel N, Barbet J, et al. ARRONAX, a high energy and high intensity cyclotron for nuclear medicine. *Eur J Med Mol Imaging.* (2008) 35:1377–87. doi: 10.1007/s00259-008-0802-5
29. Christodoulou P. *An in-situ Gamma-Spectrometry System for the Characterization of Non-Conventional Radionuclides for Medical Research* (Master Thesis). Erasmus Mundus Joint Master Degree in Nuclear Physics (2020).
30. Heinke R, Chevallay E, Chrysalidis K, Cocolios TE, Duchemin C, Fedosseev VN, et al. Efficient production of high specific activity 167Tm at PSI and CERN-MEDICIS. *Front Med.* (2021).
31. Van de Voorde M, Duchemin C, Heinke R, Cocolios TE, Cardinaels T, Ponsard B, et al. Production of Sm-153 with very high specific activity for targeted radionuclide therapy. *Front Med.* (2021).
32. *Ordonnance sur la radioprotection (ORaP) suisse*, du 26 avril 2017 (Etat le 1er janvier 2021), Office Federal de la Sante Publique (OFSP), RO (2017). p. 4261.
33. PRISMAP - The European medical isotope programme. *Five Projects Coordinated by CERN, Submitted to H2020 Research Infrastructure Calls, Approved for Funding.* Available online at: https://cerneu.web.cern.ch/five-projects-approved (accessed March 28, 2021).

Conflict of Interest: The authors declare that the research was conducted in the absence of any commercial or financial relationships that could be construed as a potential conflict of interest.